Frequency Hopping Techniques for Digital Mobile Radio

Simon C. Rockliff, B.Sc., B.E. (Hons.)

Department of Electrical and Electronic Engineering
The University of Adelaide
Adelaide, South Australia.

A thesis submitted for the degree of Doctor of Philosophy.

May 1990.

Contents

Abstract

A fast-frequency-hopping, DPSK cellular mobile radio system is examined. The results both independently confirm and extend earlier work, and provide new results for isolated and multiple cells. All analysis and modelling is subject to common assumptions, ensuring comparisons between alternative receivers are valid.

Previous results for the performance of an orthogonally coded FH-DPSK system using a linear receiver, in correlated Rayleigh fading and white Gaussian noise, have been extended to investigate the use of spatial diversity techniques. Better results are obtained from conventional combining schemes than from an alternative diversity scheme proposed in the literature.

If user interference is modelled as a series of independent Gaussian tone interferers in individual channels of the target user's frequency hopping sequence, simulation confirms analytic results from other authors showing the linear receiver performs poorly. A receiver which makes hard decisions on every code bit before decoding and a non-linear receiver which operates on the normalized received complex envelope on each channel are investigated as better alternatives. Use of the "normalizing" receiver is found to produce considerable performance improvements over the other receivers when tone interferers are present, with slight degradation over the linear receiver in Rayleigh fading and AWGN alone. Problems are revealed with the use of Hadamard orthogonal coding in tone interference, with one solution shown to be reasonably effective in averaging out variations in user bit error rates which otherwise occur. Simulation of isolated and multiple cells indicates that around 70-80 active users per cell with a mean error rate of 10^{-3} may be achievable. Derivation and simulation of the optimum linear receiver for the FH-DPSK system show better results are possible if the interfering tones are recognized.

Other coding schemes are examined, with an improved analytical formulation of the hard decision bit error rate producing results in close agreement with simulation. Estimates of the system user capacity for several codes, with hard decision and

normalizing receivers and using random hopping sequences, are presented and some schemes tested by simulation. Better FH-DPSK system performance is predicted than that previously published by other authors.

Acknowledgements.

I would like to thank my supervisor, Dr. Bruce Davis, for informative and helpful discussions, and his clear explanations of aspects of communication theory. Many thanks are also due to Dr. Doug Gray of DSTO Salisbury, for his critical proof-reading and suggestions. The encouragement that both he and Dr. Ian Fuss gave me is highly appreciated. Discussions with Mr. John Asenstorfer and Dr. Mike Miller contributed to my understanding of coding theory, and Mr. Michael Liebelt did a superb job as computing system manager. The company of my fellow postgraduates was both instructive and enjoyable, and Mr. Michael Pope and Mr. Ian Dall were especially invaluable for their expert tips on debugging computing programs. The financial support of the Defence Science and Technology Organisation is gratefully acknowledged. Finally, special thanks go to my parents and in particular to my wife Sue, for the support and understanding that helped me through the difficult times.

S.C.R.

Declaration.

This thesis has been submitted to the Faculty of Engineering at the University of Adelaide for examination in respect of the Degree of Ph.D. in Engineering.

This thesis contains no material which has been accepted for the award of any other degree or diploma in any University, and to the best of the author's knowledge and belief contains no material previously published or written by another person, except where due reference is made in the text of the thesis.

The author hereby consents to this thesis being made available for photocopying and for loans as the University deems fitting, should the thesis be accepted for the award of the Degree.

Simon Rockliff

May 14, 1990

Chapter 1

Introduction

The use of spread spectrum (SS) transmission for civilian use has a relatively short history. While the military establishment has devoted much effort since World War II to the development of SS systems to exploit the obvious benefits of secrecy and antijam capability, very little research was performed in the civilian area until the mid-1970's. A notable exception is the use by America's NASA of direct sequence spread spectrum for communicating with deep space probes, using the coded signals for ranging [1]. In general, telecommunications companies and statuary authorities responsible for providing communications have not considered spread spectrum transmission for the civilian bands until the present, due to the nature of the services that were provided and complexity of the equipment required. The shift from analogue voice traffic to an increasing proportion of digital traffic has been catered for by adapting the frequency division multiplex (FDM) systems which have served the network well for many years.

Several factors have combined to stimulate an interest in the possibilities of using spread spectrum transmission in telecommunications networks. The first is the evolution of the Integrated Services Digital Network (ISDN) , in which all communications, both voice and data, are represented in digital form. This digital information representation is essential for all the practicable types of spread spectrum systems

that can be used to give multiple access.

The second factor is the growth of new services which operate in environments in which spread spectrum signals may have some advantage over conventional narrow-band modulation schemes. Thus three areas for which spread spectrum techniques look to hold some promise for are cellular mobile radio, indoor wireless communications and low-bit-rate satellite multiple access by small earth stations. It has also been suggested as a technique to help reduce the problem of adjacent satellite transmission interference caused by congestion in the geosynchronous orbit.

Another highly important development has been the advance of technology. Surface acoustic wave and charge-coupled devices which can perform complex filtering tasks are now available, and the wide range of miniature semiconductor products and custom design facilities make the complexity of spread spectrum transmission and reception far more manageable and at far less cost than before.

This thesis studies the application of a particular type of spread spectrum transmission, "fast frequency hopping", to a mobile radio system, concentrating on systems using differential phase shift keying modulation. "Mobile radio" in this context is a mobile telephony system, interconnected with the public switched telephone network, in which users can receive and initiate calls on units which may be vehicle mounted (the most common case) or portable such as a handheld or briefcase radiotelephone. The unit would be able to be used while in motion, up to speeds in excess of 100 km/hr.

To appreciate why spread spectrum is being considered for mobile radio use, one must look at the urban radio channel and the transmission problems faced by system designers. This is covered in the first section of this chapter. A brief description of cellular mobile radio concepts is then given, with reference to current implementation and proposals for new systems, including fast frequency hopping. The next part of the chapter is devoted to introducing and reviewing material specific to fast frequency hopping: the generation of hopping sequences and models for user interference. Finally, results already obtained by other authors are reviewed for frequency

hopping differential phase shift keyed (FH-DPSK) and multilevel frequency shift keyed (FH-MFSK) systems. The final section examines a FH minimum-shift-keyed system proposed by another author and gives a corrected treatment of this system.

1.1 Mobile Radio Systems

To place the suggested use of spread spectrum techniques for mobile radio transmission in context, an overview of the factors affecting transmission through the urban mobile radio channel will be reviewed, and the current options for mobile radio described.

1.1.1 The Urban Mobile Radio Channel

The urban mobile radio channel is subject to a number of degradations which make communication difficult. The factors of importance to this thesis will be briefly reviewed here. The models described for the signal variation on the urban mobile UHF radio channel will be used in later analysis and in particular, in the simulation of the channel. For more information about mobile radio propagation, a thorough coverage can be found in [2,3,4].

A radio signal travelling from the base station to the mobile (and vice versa, by reciprocity) may take a large number of different paths, being reflected and diffracted by buildings, vehicles, hills and other objects. The net sum of all the signals travelling by different paths to a particular location is a signal which exhibits a complicated mix of attenuation and fading. For convenience, this variation is often assumed to be caused by three main mechanisms, operating over different physical distances (or time in the case of relative motion between the receiver and transmitter).

Attenuation with Distance

The first mechanism, varying the most slowly of the three, is attenuation with distance. At a given distance d from the transmitter, the signal will suffer a mean power attenuation which follows an inverse power law as $d^{-\zeta}$, where ζ is an exponent which ranges from the case of 2 for free space to 4 for large distances across built-up terrain. Modifying factors include the heights and gains of both the base station and the mobile antennae, the "roughness" of terrain over which the signal passes, the dielectric constant of the earth's surface in the vicinity, and the ground slope at the mobile. For example, a formula often used to approximate the transmission power loss over plane earth, corresponding to the case of $\zeta = 4$, is

$$P_r = P_t g_b g_m \left(\frac{h_b h_m}{d^2}\right)^2 \tag{1.1}$$

where P_r is received power

P_t is transmitted power

g_b is the gain of base station antenna

g_m is the gain of mobile antenna

h_b is the height of the base station antenna

h_m is the height of mobile antenna

d is the distance from base to mobile.

The number and variability of parameters involved, and the departures in practice from the formulae being used, make the prediction of the attenuation quite a complicated procedure, highly dependent on the particular terrain and character of the city for which the service is being designed. Nevertheless, numerous models have been proposed to help estimate the attenuation. Good reviews of such models can be found in Jakes [2] and Lee [3], and more recently a fairly comprehensive comparison of several propagation models has appeared in a special issue of the IEEE Transactions in Vehicular Technology [4].

A convenient approximation to the real situation which does not rely on too many factors is a model proposed by Lee [3,4]. This model is valid to distances out to the radio horizon, and attenuation is computed in two parts. The first is an area-to-area component, dependent on 3 parameters. At a distance of d kilometers, the area-to-area path loss is given by

$$L_f = L_0 + \gamma \log d + F_0 \qquad \text{dB} \tag{1.2}$$

where L_0 is the median transmission loss in dB at 1km

γ is the coefficient of attenuation with distance in dB/decade

F_0 is an adjustment for changes from default, *eg* for a higher antenna.

Values of L_0 and γ obtained experimentally for different environments are given in table 1.1.1, where they are given for a frequency of 900MHz, base station height of 30m and a mobile antenna height of 3m. Path loss is predicted by choosing appropriate values from the table for the environment having similar characteristics to the area in question.

Environment	L_0 (dB at 1 km)	γ
Free Space	91.3	20
Open Area	91.3	43.5
Suburban	104.0	38.5
Philadelphia	112.8	36.8
Newark	106.3	43.1
Tokyo	128.0	30

Table 1.1: Propagation Parameters (from [4])

This value is then corrected to obtain a point-to-point path loss by introducing a term for the effective base station height h_e, which is dependent on the relative height of the mobile with respect to the base station and the ground slope in the vicinity of the mobile. This may be greater or less than the actual base station height. For flat terrain, (which will be the case considered later), the effective height of the base

station is equal to the real height. The point-to-point loss is then given by

$$L'_f = L_f + 20\log(h_e/30) \tag{1.3}$$

The value of the received power at a particular distance from the transmitter, averaged over the surrounding neighbourhood (of the order of hundreds of metres), is known as the area mean m_d, and is given by the attenuation of transmitted power:

$$m_d = P_t - L'_f \qquad \text{(dB)} \tag{1.4}$$

Shadow Fading

The attenuation determines the mean for a second level of signal variation. This variation is known as "shadow fading", and is due to the local large scale topography, such as the presence of large buildings or hills which cause a signal "shadow". The extent over which a shadow fading cycle will occur is determined by this topography, but has been found in urban areas to have some correspondence with city block spacings, and hence is termed a "slow" fading effect. It is typically modelled as following a lognormal distribution. Expressed in decibels, the signal envelope, averaged over distances of the order of tens of metres, is Gaussian distributed with mean m_d and variance σ dB. Typically, σ varies from 6–12 dB, increasing with the amount of urbanisation. The density function is therefore

$$p(\bar{s}_d) = \frac{1}{\sigma\sqrt{2\pi}} \exp\left(-\frac{(\bar{s}_d - m_d)^2}{2\sigma^2}\right) \tag{1.5}$$

The signal $\bar{s} = 10^{\bar{s}_d/20}$ forms the local mean of the received signal envelope over these short distances, where another level of fading acts.

Fast Fading

The final form of fading is known as "fast fading" due to the large number of fluctuations that the envelope will undergo in a distance of several metres. It is

often modelled as following a Rayleigh distribution, such that the envelope has a probability density function given by

$$p(s) = \frac{\pi s}{2\bar{s}^2} \exp\left(-\frac{s^2\pi}{4\bar{s}^2}\right) \tag{1.6}$$

with mean $\mathbf{E}[s] = \bar{s}$ and mean square value $\mathbf{E}[s^2] = 4\bar{s}^2/\pi$.
The probability distribution of the phase of the received signal is uniformly distributed on $[0, 2\pi)$, as the phase will vary slowly over time with the fading. To see how this fast fading arises, and some of the properties associated with it, a common model for the formation of the fading will be outlined.

The diversity of routes that a signal may take from the transmitter to the receiver results in phenomena known as multipath and time delay spread. Consider a signal sent through the channel at time $t - \tau$ and received at time t. The time dependent impulse response of the channel may be written as

$$h(t,\tau) = \sum_{i=1}^{\infty} a_i(t)\delta(\tau - \tau_i(t)) \tag{1.7}$$

which reflects the sum of the component signals arriving with an amplitude a_i and the path time delay τ_i. In general, a_i and τ_i are independently distributed functions of time t, and vary as the vehicle moves. The "delay spread" is a measure of the how tightly bunched the paths delays are. The τ_i usually (although not always) follow an exponential distribution [2], *i.e.*

$$p(\tau_i) = \frac{1}{T_d} e^{-\frac{\tau_i}{T_d}} \qquad 0 \leq \tau_i < \infty \tag{1.8}$$

Measurements taken in New York city [5,3] have shown that in urban areas, average delay spread T_d is about 1.3μs, and in suburban areas of New Jersey, a typical value for T_d is 0.5μs. Maximum delay spreads of up to 10μs have been recorded heavily built-up areas, such as in New York [5], and in some mountainous areas such as Switzerland, where large echos off surrounding hills lead to significant signal components being received at delays of up to 30μs [6]. At a particular location, the contributing time delayed components (with associated phase) sum to a received signal vector which exhibits severe amplitude and phase fluctuations over short distances. For example, a car on a street would receive signal contributions from

a number of significant sources. reflected from the surrounding buildings and other cars, as shown in figure 1.1.1.

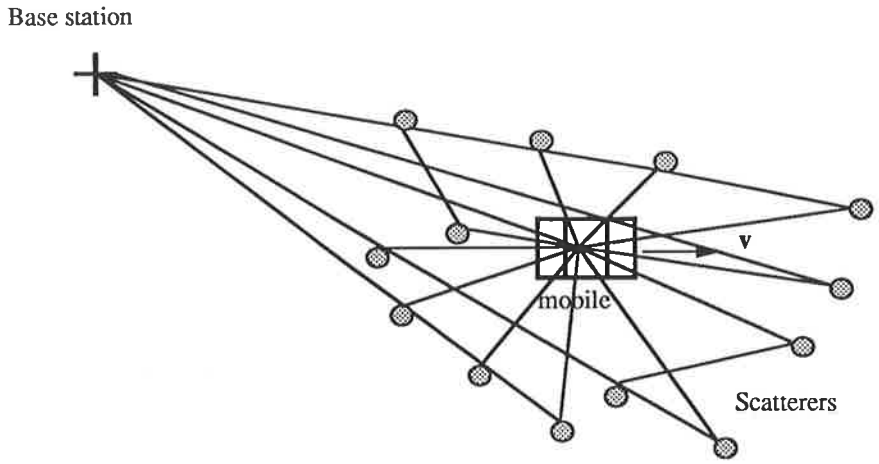

Figure 1.1: Illustration of multipath caused by scatterers in the vicinity of a moving vehicle.

If a signal $e^{j2\pi ft}$ is applied to the channel then the output is

$$\begin{aligned} v_0(t) &= \sum_i a_i(t) e^{j2\pi f(t-\tau_i(t))} \\ &= \left[\sum_i a_i(t) e^{-j2\pi f\tau_i(t)}\right] e^{j2\pi ft} \\ &= H(f,t) e^{j2\pi ft} \end{aligned}$$

where $H(f,t)$ is the time dependent frequency response

$$\begin{aligned} H(f,t) &= \int_{-\infty}^{\infty} h(\tau,t) e^{-j2\pi f\tau} d\tau \\ &= \sum_i a_i(t) e^{-j2\pi f\tau_i(t)} \end{aligned}$$

For a large number of scatterers, the central limit theorem states that $H(f,t)$ will converge to a complex Gaussian process:

$$H(f,t) = x(f,t) + jy(f,t) \tag{1.9}$$

$$= \sum_i a_i(t)\cos(2\pi f\tau_i(t)) - j\sum_i a_i(t)\sin(2\pi f\tau_i(t)) \tag{1.10}$$

If the time delay spread is much larger than $1/f$, then $x(f,t)$ and $y(f,t)$ are uncorrelated and hence independent :

$$\mathbf{E}[x(f,t)y(f,t)] = -\mathbf{E}\left[\sum_i \sum_k a_i a_k \sin(2\pi f\tau_i)\cos(2\pi f\tau_k)\right]$$

$$
\begin{aligned}
&= -\mathbf{E}\left[\sum_i a_i^2 \sin(2\pi f\tau_i)\cos(2\pi f\tau_i)\right] \\
&\quad -\mathbf{E}\left[\sum_i \sum_{k\neq i}(a_i a_k)[\sin 2\pi f\tau_i \cos 2\pi f\tau_k]\right] \\
&= -(1/2)\sum_i \mathbf{E}[a_i^2]\,\mathbf{E}[\sin(4\pi f\tau_i)]
\end{aligned}
$$

assuming a_i, a_k, τ_i and τ_k are independent.

As the range of values that τ_i may take is typically much greater than $1/f$, such that the distribution of $(2\pi f\tau_i) \bmod 2\pi$ is essentially uniform, the expectation $\mathbf{E}[\sin(4\pi f\tau_i)] = 0$ and hence the cross-correlation of $x(f,t)$ and $y(f,t)$ is zero. For the two independent and identically distributed Gaussian random variables x and y, the envelope of the faded signal formed by the operation $\alpha = \sqrt{x^2+y^2}$ will have a Rayleigh density function as previously described.

A further complicating factor in this fast fading model is the vehicle motion. Clarke's model [7] assumes the scatterers are uniformly distributed around the vehicle, which is travelling with a velocity v. The channel is assumed to be wide-sense stationary. Incoming plane waves from different angles with respect to the vehicle experience a Doppler shift commensurate with the angle subtended to the direction of motion. By the same argument using the central limit theorem, the fading can be written as a complex exponential process as the number of scatterers increases towards infinity. For an omnidirectional antenna such as a vertical whip, receiving power equally from all directions around the vehicle, the power spectrum of the received radio frequency electric field has been derived as [2]

$$
S_{E_z}(f) = \frac{b_0}{\pi f_D}\left[1-\left(\frac{f-f_0}{f_D}\right)^2\right]^{-1/2} \qquad |f-f_0| < f_D \tag{1.11}
$$

where b_0 is the average received power

f_0 is the carrier frequency

f_D is the maximum Doppler shift

The equivalent baseband power spectral density is

$$S_b(f) = \frac{b_0}{\pi f_D}\left[1 - \left(\frac{f}{f_D}\right)^2\right]^{-1/2} \qquad |f| < f_D \tag{1.12}$$

The normalized autocovariance function for the received envelope magnitude is

$$\rho_{|E_z|}(\tau) = J_0(2\pi f_D \tau) \tag{1.13}$$

The inphase and quadrature moments of the complex fading envelope have also been derived, leading to the correlation functions:

$$R_{x_1x_2}(\tau) = R_{y_1y_2}(\tau) = b_0 J_0(2\pi f_D \tau) \tag{1.14}$$

$$R_{x_1y_2}(\tau) = R_{y_1x_2}(\tau) = 0 \tag{1.15}$$

where the subscripts $1, 2$ refer to times $t_1, t_2 = t_1 - \tau$ respectively. The corresponding power spectral densities for the quadrature components are

$$S_x(f) = S_y(f) = \frac{b_0}{\pi f_D \sqrt{1 - (f/f_D)^2}} \qquad |f| < f_D \tag{1.16}$$

For two signals separated in frequency by Δf, it has also been shown that the correlation between the Gaussian components of the envelope at the different frequencies are given by :

$$\mathbf{E}[y_1y_2] = \mathbf{E}[x_1x_2] = \frac{b_0}{1 + (\Delta f/B_c)^2} \tag{1.17}$$

$$\mathbf{E}[x_1y_2] = -\mathbf{E}[x_2y_1] = \frac{b_0 \Delta f/B_c}{1 + (\Delta f/B_c)^2} \tag{1.18}$$

$$\mathbf{E}[x_1^2] = \mathbf{E}[x_2^2] = \mathbf{E}[y_1^2] = \mathbf{E}[y_2^2] = b_0 \tag{1.19}$$

where $B_c = (2\pi T_d)^{-1}$ is coherence bandwidth, (defined to be where the correlation between envelopes is 0.5).

One further point to be noted is that the Rayleigh fast fading distribution represents the worst case in which no direct signal component exists, such that the incident power flux is approximately uniform with angle. If a significant direct signal or specular component exists, the Rayleigh distribution will change to a Rician

distribution, which has much smaller fades and a probability density function

$$p(s) = \frac{2s}{s_0^2} \exp\left[-\frac{(s^2 + A^2)}{s_0^2}\right] I_0\left[\frac{2sA}{s_0^2}\right] \tag{1.20}$$

where A is the amplitude of the steady signal, s_0 is the rms value of s and $I_0(.)$ is the modified Bessel function of order zero.

Aside Other models have also been proposed for the transitional region between the fast-fading, small local area model (Rayleigh fading) and the wider area shadow fading model (lognormally distributed). The Weibull distribution is a more general distribution which has been proposed to fit measurements of fading. The probability density function is

$$p(s) = \frac{\xi c}{s_0}\left(\frac{cs}{s_0}\right)^{\xi-1} \exp\left[-\left(\frac{cs}{s_0}\right)^{\xi}\right] \tag{1.21}$$

where ξ is a shape parameter chosen to give a good fit to measured data, and $c = [(2/\xi)\Gamma(2/\xi)]^{1/2}$ is a normalization factor.

Another distribution is the Nakagami-m distribution, which has the probability density function

$$p(s) = \frac{2m^m s^{2m-1} e^{-(m/\Omega)s^2}}{\Gamma(m)\Omega^m} \tag{1.22}$$

where $\Omega = < s^2 >$ is the power of the received signal averaged over time,
and $m = < s^2 >^2 / < (s^2 - < s >^2)^2 >$.
The Nakagami-m distributions for increasing m may be recognised as the series of χ-distributions with even numbers $2m$ of Gaussian contributing elements. For $m = 1$ the Nakagami distribution becomes the Rayleigh distribution, and the Weibull distribution also assumes this form for the case of $\xi = 1/2$. Thus both of these distributions can be seen to be more flexible than the Rayleigh distribution. However, the choice of the parameters is conditioned on a knowledge of the statistics of the signal in a particular location and hence there are no general sets of parameters. The more complex forms of the distributions are also less convenient for analysis than that of the Rayleigh distribution. As a consequence, although these more general distributions have more parameters which may be chosen to give a better fit to measured data in many cases, the Rayleigh fast-fading/lognormal shadow fading distributions are still commonly used as models for urban mobile radio propagation.

1.1.2 Present and Future Mobile Radio Systems

Modern radio systems are arranged as cellular schemes, where the service area, such as a large city and suburban areas, is divided into cells. Each cell has its own base station or multiple base stations which serve the mobile units within its area. Current mobile radio systems use analogue frequency modulation, with the frequency deviation plus guard bands (to avoid adjacent channel interference) resulting in channel separations of 25–30 kHz.

A call is initiated by the mobile unit by requesting the dialled number on a special set-up channel common to all mobiles in the cell. If the call is successfully placed, the switching centre then assigns a channel pair to the mobile unit (one channel for transmission each way) for the duration of the call. As the mobile unit moves through different cells, "handoff" takes place whereby the mobile unit is passed from the control of the current base station and onto the next. This sequence is initiated when the signal level is too low for reasonable quality conversation, and utilises voice channel signalling. For incoming calls, the mobile unit is paged progressively throughout the cells in a given order until the mobile unit responds or is deemed not to be active. At the end of a call, voice channel signalling is used to acknowledge termination and the channels are cleared for further use.

The cellular approach works by re-using frequency channels in different cells. The total number of frequency channels available is divided up among the number of cells N in a cluster. The cluster size is determined by the distance separation necessary to keep the cochannel interference between two cells that use the same frequencies to an acceptable level. In an ideal situation, N is a number which enables an array of regular geometric shaped cells to form a complete cover over the entire service area, such as $N = 4, 7, 9, 12, 13, 16, 19$. Reuse distance is typically $\sqrt{3N}$ times the major radius (*ie* largest corner radius) of the cell. Cochannel interference decreases as N increases, but the available number of channels in each cell decreases.

In theory, by reducing the size of cells and the power transmitted, and main-

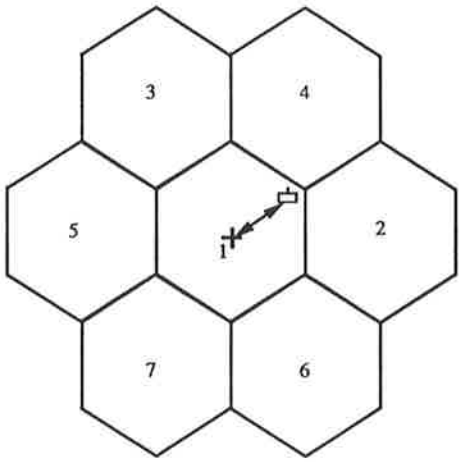

Figure 1.2: A cluster of 7 cells, where each cell has a non-overlapping subset of 1/7 of the total available number of frequency channels

taining frequency reuse at a certain cluster size, the same number of users may be accommodated in every cell and hence the number of users per element of area may be increased by subdivision of cells. This is only partly true in practice, as reuse distances vary with cell size due to changes in the propagation attenuation factor. Large cells typically have attenuation proportional to d^{-4}, which enables small clusters to be used. In small cells, the attenuation with distance approaches d^{-3}, which requires clusters of $N = 16$ or greater. Base stations also are expensive: hence there is a move toward sector illumination, whereby each base station has several directional antennae which may be arranged to increase the frequency reuse by each antenna illuminating only part of a cell.

For these systems, to hold the "blocking probability" (*ie* probability that all channels are in use) to a reasonable level such as 2%, the average number of channels in use must be no greater than a certain percentage of those available in the cell. This is the "trunking efficiency", which ranges from 60–80% depending on the number of channels available and the channel assignment strategy used.

To obtain higher capacity systems, another aspect that can be examined is to choose a modulation method which allows more channels per cell. Currently, narrow-

band FM systems are a contender, where the channel spacing is reduced to around 12–15kHz. Another possibility is single sideband amplitude modulation (SSB) transmission, where frequency companding and amplitude companding may be used to give voice channels with a 5 kHz spacing. A sounding tone must be sent to act as a reference for power control and frequency locking purposes. Frequency stability is seen as being a problem in this system, and it is not very well suited to digital data transfer. For digital systems, the current CCITT standard G.721 sets an encoded voice rate of 32kb/s using adaptive delta pulse code modulation which gives toll quality speech transmission. Future mobile radio systems (*eg* European GSM) will use 16kb/s or lower rate transmission as better prediction methods are developed.

All of the above narrowband schemes are badly affected by frequency selective fading, to the extent that up to 20 dB more transmitted power may be required over the non-fading situation. While coding can be used in a digital system to increase the resistance to fading, the amount of delay that can be incurred in the interleaving and decoding process is bounded by user tolerance levels to the overall delay and echo in the loop. In particular, any calls which involve satellite connections would be badly affected [8], and would have to be avoided. Space diversity using two antennae separated by more than a quarter of a carrier wavelength is a well known method of reducing the effects of frequency selective fading, but is costly to implement and is not suited to handheld use.

As an alternative, several systems using spread spectrum techniques have been proposed. The advantage that these systems enjoy over narrowband systems is that that at any particular time, the fading only appears in a small section of the bandwidth. By spreading the signal power over the entire bandwidth, the effect of fading is averaged out and the power necessary to be transmitted is reduced. Unfortunately, such a scheme also means that other users will interfere with a particular user's transmissions. The system must therefore be designed to cope with a degree of such interference. How these systems cope with the user interference, and the equivalent saving on frequency reuse that may be gained by such techniques, (*ie* the number of users possible) in a multiple cell system over a narrowband approach, is

of interest to telecommunications authorities. The topic of this thesis is the examination of a particular type of spread spectrum mobile radio system, in which fast frequency hopping and differential phase shift keyed (FH-DPSK) modulation are used.

1.2 Frequency Hopping Transmission

Spread spectrum transmission for cellular mobile radio was first proposed in 1977–78 [9] and immediately generated wide interest. The concept was seen as radical in suggesting that a wideband, interference-limited modulation scheme would enable a larger number of users to share the available bandwidth than conventional frequency division multiplexed FM. Since then, much effort has been expended in the mobile radio field on investigating frequency hopping systems. Attention has also been paid to the possibilities of direct sequence (pseudo-noise) systems. This aspect is not covered here and the reader is referred to references such as [10,11].

In a frequency hopping scheme, each user is assigned a unique frequency-time address sequence of n "chips". The sequence is designed for minimum cross-correlation with all other user sequences, thus minimising cochannel interference. Transmission takes place by the user modulating one or more channel symbols on to a carrier at a particular frequency, and then hopping to the next frequency in the cycle for the next transmission. If one or less code symbol is transmitted per hop, the scheme is commonly referred to as a "fast frequency hopping" system. Conversely, if more than one code symbol is transmitted per hop, the system is a "slow frequency hopping" scheme.

While in a non-fading additive white Gaussian noise channel or slow Rician fading environment, coherent systems may sometimes be employed to give maximum performance, the same does not apply in a fading environment such as the mobile radio channel where the fading may have Rayleigh statistics and a fading rate which cannot be assumed to be negligible with respect to the transmitted symbol rate. As

multipath and Doppler shift cause the phase of the received signal to vary randomly with time, coherent detection is generally regarded as impractical. Large phase transitions will cause the coherent tracking mechanism (such as a Costas or De Budas loop) to lose lock and hence the reference carrier extracted from the signal will always be unstable, leading to an unacceptable irreducible error rate [12]. Most proposed schemes therefore use non-coherent detection, or else assume that the phase variation between adjacent samples is small (a function of the Doppler shift due to vehicle motion) and hence differentially coherent modulation and detection may be used. Discriminator detection has also been proposed for FSK systems.

In a multilevel frequency shift keying (MFSK) system, a k bit data word is used to select a frequency from an $n = 2^k$ orthogonal set. This frequency is then used to modify a length L frequency address sequence to produce the sequence of tones to be transmitted The modulation used is on-off keying. This can be detected by a non-coherent envelope detector or a correlator and squarer. This system allows for a very large number of frequency channels to be used, as no memory is required in the system.

Alternatively, differential phase shift keying (DPSK) may be used to modulate the carrier. For this scheme, consecutive bits have a mutual phase shift of π radians if the code bit is 1 and zero phase shift for a data bit of 0 (or -1 depending on notation). This form of modulation requires the phase of the channel impulse response over the two symbols to be as close to identical as possible. This condition is generally met with enough precision for transmission on a single frequency at UHF. For slow frequency hopping, a packet of information would be transmitted on a particular frequency, with synchronization occurring at the start of every packet on a new frequency. The packets are very long compared to the propagation times and delay spreads involved and hence all users can be arranged to hop at effectively the same time with minimal packet overlaps at any frequency. For fast frequency hopping, synchronization is a more difficult problem. It has been commonly assumed that phase coherence could be maintained by using DPSK between chips of the same frequency in the hopping cycle. This would require using accurate clocks

and hopping frequencies which are separated by multiples of a particular frequency. Also, Lee and Miller [13] have gone one step further and assumed that techniques are available which allow phase coherence to be maintained between hops of different frequencies. This seems far more difficult to achieve in practice and has not been pursued.

A further modulation method which has been proposed is minimum shift keying (MSK). In the context of fast frequency hopping, little work has been performed on systems using this modulation method. Some problems with one analysis are examined in a following section. Interest in this modulation scheme, and other variants such as Gaussian filtered MSK, is mainly limited to slow frequency hopping schemes [14] which are currently the subject of much research.

The focus of this thesis has been on evaluating the performance of fast frequency hopped DPSK schemes. A review of this scheme and previously obtained results follows, and for comparison, two other fast frequency hopped schemes will also be briefly described. To aid in the understanding of the various models, a brief description of the allocation of hopping sequences and several common interference models will first be given.

1.3 Frequency Hopping Address Sequences

To minimise user interference, it is important for users to have frequency hopping sequences which coincide as little as possible. In an isolated cell situation with synchronous operation, such as base-to-mobile transmission, such a requirement is easy to accomplish, as any arbitrary patterns which do not overlap and make good use of the available frequencies (to minimise correlated fading due to a wide coherence bandwidth) are suitable.

However, this ideal situation is not likely to occur in a real system. Even in an isolated cell with synchronous transmission, time delay spread and timing errors

can cause other user's pulses to smear into the target user's time/frequency slots. More importantly, multiple cell schemes are used to increase the number of users that can be supported in a large area, and hence even where the base station can synchronise its transmissions, the signals from surrounding cells will arrive with variable propagation delays. Finally, for the case of mobile to base transmission, synchronism of the received user sequences can not be achieved even within an isolated cell, and hence each user's sequence has a random time shift with respect to any other user's sequence.

Therefore any two address sequences must have a uniformly low cross-correlation irrespective of their relative time shift. Several schemes with such properties have been developed. These schemes have focussed on producing sets of "one-coincidence" address vectors, utilising the theory of finite (Galois) fields [15]. Under these schemes, any two addresses can have at most one coincidence on an aperiodic basis when shifted relative to each other.

One such scheme is detailed in [9]. The generation of these sequences proceeds as follows:

1. Select a prime number p such that $q = p - 1$ is the number of channels, chosen as large as possible within the constraint

$$p \leq \frac{Wk}{R_b n} \tag{1.23}$$

   where the parameters and typical values which have been assumed by other authors are given in table 1.2.

   These parameter values lead to a choice of $q = 96$.

2. The smallest primitive root β of GF(p) is found. The powers of a primitive root will generate all q non-zero elements of the Galois Field GF(p).

3. Generate the vector of powers Π_p of the primitive root β. This is used to permute other vectors to form the address sequence.

$$\Pi_p = (1, \beta, \beta^2, \beta^3, \ldots, \beta^{q-1}) \tag{1.24}$$

Quantity	Symbol	Value Assumed
information bit rate	R_b	32 kbit/s
total one-way bandwidth	W	20 MHz
bits per frame	k	5
codeword length	n	32
number of hops in sequence	L	32
chip period	τ	4.88 μs

Table 1.2: Values initially assumed for transmission

4. Select an arbitrary starting permutation S^1 of the frequency set $\{1, 2, \ldots, q\}$

5. Operate on S^1 with Π_p $(q-1)$ times to form q sequences S^j, where the operation $S^j = \Pi_p S^{j-1}$ is

$$\begin{aligned} s^j_\beta &= s^{j-1}_1 \\ s^j_{\beta^2} &= s^{j-1}_\beta \\ &\vdots \quad \vdots \\ s^j_1 &= s^{j-1}_{\beta^{q-1}} \end{aligned}$$

Each new vector is produced by the element in position β^i of the previous vector being moved to position β^{i+1}. This produces q distinct sequences of length q. When considered aperiodically, there may be at most one coincidence between the two sequences. This is demonstrated in figure 1.3.

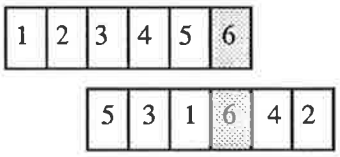

Figure 1.3: Correlation of two FH address sequences from [9]

When in repeated use, as in figure 1.4, there may be at most two coincidences per frame.

6. **Example** Consider the trivial case of $p = 7$.

Then the smallest primitive root is $\beta = 3$.

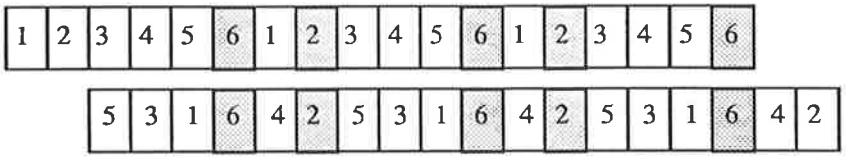

Figure 1.4: Repeated use of FH address sequence from [9]

Vector of powers of the primitive root: $\{\beta^0, \beta^1, \beta^2 \ldots . \beta^{q-1}\} = \{1, 3, 2, 6, 4, 5\}$
Arbitrarily choose a starting vector permutation of the 6 elements,
eg $S^1 = \{3, 2, 4, 6, 1, 5\}$.
Then the permutation operation will generate the following vectors:

$$\begin{aligned} S^2 &= \{1, 4, 3, 5, 6, 2\} \\ S^3 &= \{6, 3, 1, 2, 5, 4\} \\ S^4 &= \{5, 1, 6, 4, 2, 3\} \\ S^5 &= \{2, 6, 5, 3, 4, 1\} \\ S^6 &= \{4, 5, 2, 1, 3, 6\} \end{aligned}$$

7. The vectors are then subdivided into runs of L elements, where L is the number of channels in the frequency hopping cycle. There will then be $q[q/L]$ sequences available, where $[q/L]$ is the largest integer less than or equal to (q/L). These short sequences will also possess the same one-coincidence properties as the larger vectors, and it is possible that two sequences will never collide. For frame synchronous transmission, it is possible to obtain $[q/L]$ sets of q sequences such that the sequences within the set will never collide in any place when used frame synchronously, and sequences from any two sets will collide in at most one chip on an aperiodic basis. In this fashion, up to $[q/L]$ cells in a cluster could minimise interference by using a different set for base-to-mobile transmission.

Alternatively, Seay [16], Mersereau [17], Sarwate and Pursley [18,19] and Einarsson [20] have proposed frequency hopping patterns based on Reed-Solomon codes. For example, Einarsson gives the following formula for generating a FH-MFSK hopping pattern of L chips over a possible q frequencies, where q is either a prime

number or a power of a prime.

$$\mathbf{x}_j = a_j(1, 1, \ldots, 1) + d_j(1, \beta, \beta^2, \ldots, \beta^{L-1}) \tag{1.25}$$

where a_j is an element of GF(q), representing the unique address of the jth user, β is a primitive generator of GF(q), and d_j is the current data symbol for user j. For FH-DPSK use, the message data symbol is made equal to a constant: the message is encoded via DPSK between the successive chips at the same frequency in the cycle. These sequences have the property that two sequences may have at most one coincidence when shifted relative to one another by integral numbers of chips.

Lam and Sarwate [21] have developed these Reed-Solomon hopping patterns further, and produced a set of sequences which have at most one partial coincidence when used asynchronously. By this it is meant that when the sequences are used to direct the frequencies of chip periods in a frequency hopping cycle, if two sequences are displaced relative to one another by a time period which is not an integral number of chip periods, they will coincide in at most one part of a chip period. The sequences are defined:

$$x_j = a_j(1, 1, \ldots, 1) + \beta^b(1, \beta^V, \beta^{2V}, \ldots, \beta^{(L-1)V}) \tag{1.26}$$

where $V = (q-1)/L$ and $L < (q-1)$

q is a prime number or power of a prime

a_j is an arbitrary element of GF(q) representing the address of user j

b is an index which must be specified

As q may be a prime number or the power of a prime, these patterns may be generated to more closely match the number of channels that the coded bit rate allows in the total available bandwidth. However, it is found that not all values of b are suitable, and hence the number of sequences is reduced from that generated by the alternative methods.

When used synchronously, it is easy to minimise adjacent channel interference due to channel and timing imperfections by keeping the sequences well separated in

frequency. This is possible to do until the number of users equals half the available number of channels.

Haskell [22] has proposed a method of addressing for FH-MFSK based on each vector having a constant slope with respect to the time/frequency matrix. These "chirp" vectors also satisfy the "one-coincidence" property. However, when a complete set is used synchronously, they will always clash in one chip, and hence are not the best choice for any synchronous transmission arrangement. In addition, for wide coherence bandwidths, those vectors with small slopes will be badly affected by correlated fading which results in a much greater error rate than for the uncorrelated fading case. These vectors are not deemed as suitable for FH-DPSK transmission as the other methods.

1.4 Interference Models

1.4.1 White Gaussian Noise Interference Model

The additive white Gaussian noise (AWGN) interference model results from the the assumption that the signal power from many simultaneous users is spread uniformly across the entire available bandwidth. This approach can be argued on the following grounds: in an asynchronous system, the interference seen at the output of the bandpass filters of the receiver can be thought of as the sum of contributions from many in-band and adjacent channel interferers. For example, for a rectangular envelope multiplying the carrier signal, the fraction of interferer power seen at the output of a matched filter at frequency f from an interferer on the frequency f_j with a mismatch of a fraction ϵ of the chip period τ can be obtained as [23]

$$\frac{\sin^2(\pi\epsilon(f-f_j)\tau)}{[\pi(f-f_j)\tau]^2}$$

For a great number of these interferers, the contributions with random phase are assumed to sum to a zero mean Gaussian random variable by the central limit theorem. As the interferers are spread across the bandwidth in order to maximize the

processing gain and diversity of the system, it is assumed that to a close approximation, the power spectral density of the interference will be uniform across the total bandwidth, as shown in figure 1.5.

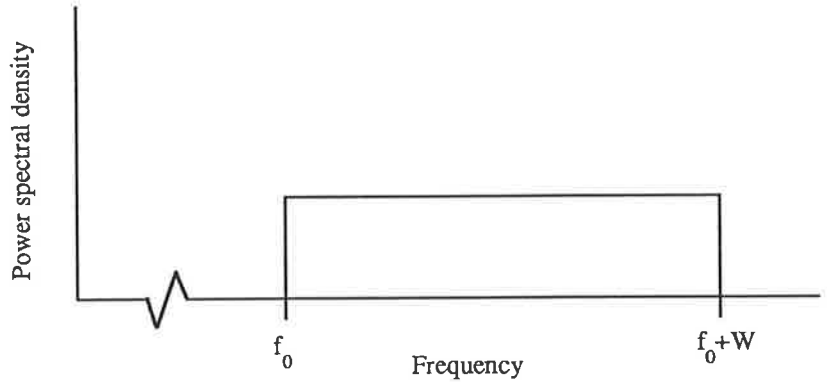

Figure 1.5: One-sided power spectral density of interference as assumed under the additive white Gaussian noise model.

Hence for $(J-1)$ interferers, a total bandwidth of W Hz, and a target signal power of S Watts, if all interferers are received at the base station with the same average power as the target signal, the interference one-sided power spectral density is given by [9,24,25]

$$I = (J-1)S/W \quad \text{Watts/Hz} \tag{1.27}$$

Under this model, background (thermal) noise is generally neglected as it is taken as being much less than the interference power.

Analysis and simulation under the assumption of this interference model is relatively straightforward, as the received signal on each time chip consists of the faded transmitted signal for that chip plus Gaussian noise, identically and independently distributed in each channel. Various analyses of the FH-DPSK system exist for this model [24,25], with the most rigorous treatments being [26,21].

Multiple cells are easily modelled under this approximation, as they simply contribute more noise. The magnitude of this noise can be estimated by integrating the power from all surrounding cells, using the mean power resulting after attenuation [9,25].

1.4.2 Tone Interferer Model

The tone interferer model results from recognizing that if a large tone interferer exists within the bandwidth of the bandpass filter of a particular chip frequency, it is a persistent effect (due to the frequency hopping cycle), which has far greater power than the noise variance assumed by the AGWN model.

For the purposes of analysis, two cases can be identified which are mathematically tractable for some receivers. Both assume that a certain degree of synchronism can be achieved, such that frequency tones which are orthogonal over the matched filters of a receiver can be successfully employed. This implies that no adjacent channel interference exists, and only co-channel interference need be considered.

The first case is that of frame synchronization of user frequency hopping sequences. In this case, user sequences can be assumed to be synchronised to minimize correlation, by being aligned in time, all hopping at the same instant. Such a situation is possible for base to mobile transmission in an isolated cell. Given the large number of frequencies and hopping sequences available, it is likely that for the number of users likely to be using the system, the hopping sequences could be arranged such that no clashes between users occur. This then represents the ideal situation, where every available channel may be utilized within a cell. With just background noise and fading to degrade the signal, the result is a considerable power saving over conventional frequency division multiplexing schemes. Of course, in a multiple cell scheme, interference from other cells will be non-synchronous due to propagation delays.

The second case is that of chip level synchronisation of user frequency hopping sequences, where all users hop at the same instant but their hopping sequences have a shift of a random number of chip periods. The frequency tones are chosen to be orthogonal over the matched filters, so that interference comes solely from users who share the exact frequency/time chip as the target signal. The probability of a clash or "hit" is dependent on the statistics of the addressing sequences used.

For addressing sequences with low cross correlation [9,21] a memoryless random addressing strategy may be used to upper bound the probability of a clash. From this, the number of users can be linked to the probability of error. For a power control assumption and an isolated cell, if an interferer is present in a frequency chip, it is represented as a Rayleigh fading tone of random phase with average power equal to the wanted signal. An example of a typical one-sided power spectral density of the entire one-way bandwidth (*ie* encompassing all uplink channels and users) is pictured in figure 1.6.

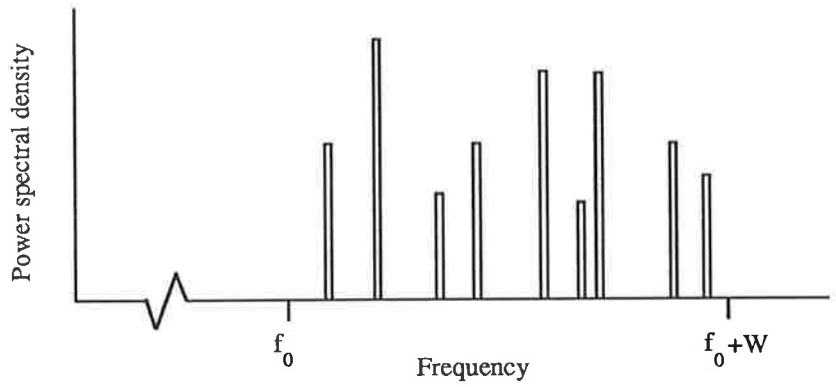

Figure 1.6: Power spectral density of interference as assumed under the tone interferer model, during a particular time chip.

If the transmitted signal is of the form

$$s(t) = \sum_{l=0}^{L-1} \sqrt{2S}\,\mathrm{rect}_\tau(t - l\tau)\cos(2\pi f_l t + \phi_l) \tag{1.28}$$

where

$$\mathrm{rect}_\tau(t) = \begin{cases} 1 & \text{if } 0 \le t \le \tau \\ 0 & \text{otherwise} \end{cases}$$

the contribution of the jth interferer to the wanted signal can then be represented as

$$i_j(t) = \sum_{l=0}^{L-1} \sqrt{2S}\,\mathrm{rect}_\tau(t - l\tau)\left[\xi_{jl}\cos(2\pi f_l t) + \eta_{jl}\sin(2\pi f_l t)\right] \tag{1.29}$$

where ξ_{jl} and η_{jl} are independent and identically distributed zero mean Gaussian random variables. Under the power control and chip synchronism assumptions, the variance $\gamma_{jl}/2$ is such that

$$\gamma_{jl} = \begin{cases} 1 & \text{if the } j\text{th interferer is present in the } l\text{th chip} \\ 0 & \text{otherwise} \end{cases}$$

The distribution of γ_{jl} is determined by the addressing algorithm, and by whether the shift between user sequences is random or deterministic (such as zero shift which is frame synchronous transmission). For the one-coincidence addressing schemes being used, it is a difficult problem to evaluate the large number of permutations of addresses and hence the γ_{jl}. A random addressing assumption is therefore usually made to facilitate analysis, and is discussed in a later chapter. Where no synchronism exists between user hopping sequences, the quantities γ_{jl} become continuously valued between 0 and 1, and depend on the amount of time overlap and frequency separation between two chips of different sequences (discussed in the previous section).

1.4.3 Partial Band Interference Model

The partial band interference model is commonly used in assessing jamming strategies in military communications. The assumption under this model is that a high level of Gaussian noise interference due to a jammer exists uniformly over a proportion of the bandwidth, as shown in figure 1.7. Both the proportion of the band and the actual power level emitted is determined by the way the jammer distributes its power. Worst case analyses always assume the total power budget, which in the mobile radio case would be $S(J-1)$ Watts, is spread uniformly across a fraction r of the band. Background noise (often neglected for simplicity) is assumed to present in the remaining portion of the band. It is assumed the target signal will use the whole

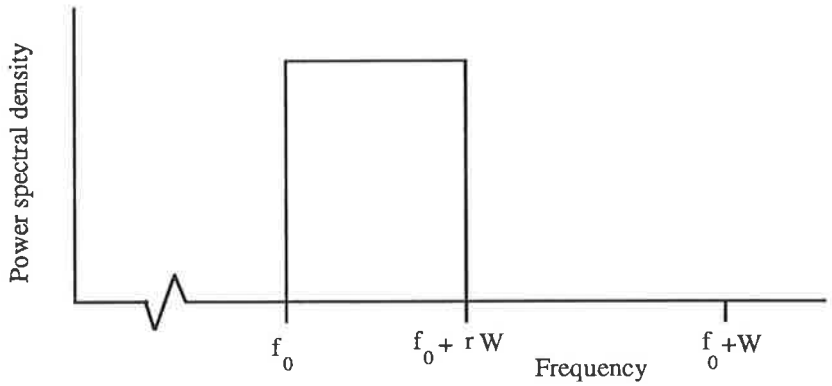

Figure 1.7: Power spectral density of interference as assumed under the partial band interference model.

bandwidth and therefore will receive interference proportionally. By maximizing the bit error rate with respect to r, a worst case estimate can be arrived at. However, this is not a very realistic situation for the case of friendly user interference. It is quite possible that the user will experience no interference. Conversely, the user may be simultaneously subject to several interfering sources in the one chip interval. This occurrence is not well explained by the partial band interferer model. For this reason, analyses of the FH-DPSK system have preferred the AGWN or tone interferer/random addressing models.

1.5 Frequency Hopping Differential Phase Shift Keying Schemes

A number of different proposals for FH-DPSK systems have been put forward. These vary widely in the models used for interference and the receiver structures, but all share a common modulation and coding approach, dating back to the first proposal for a frequency hopping mobile radio system using differential phase shift keying. Cooper and Nettleton [9] introduced a system which encoded the message bits using orthogonal coding and DPSK between chips in adjacent frequency cycles. The advantages claimed for this system were manifold. The intrinsic frequency diversity reduces the damaging effects of frequency selective fading. Call blocking as found in conventional schemes (*ie* no free channels) need not exist, as the effect of adding more users was claimed to be a gradually increasing error rate for all users; a feature known as "gradual degradation". This tolerance to interference was supposed to allow the reuse of all channels in the entire system bandwidth in all cells, thus allowing many more users than conventional frequency division multiplexing schemes. The unique frequency hopping sequence ensured a degree of message privacy and under Nettleton and Coopers' addressing scheme, allowed travel between cells without the necessity of switching channels at handoff.

However, frequency hopping does introduce some disadvantages. Power control

is necessary for maximum efficiency, to prevent the "near-far" problem where signals from sources close to the receiver overwhelm those from further away. The equipment is more complex than that required for conventional FDM, and some form of vehicle location technique is seen as required to manage power control and handoff between base stations.

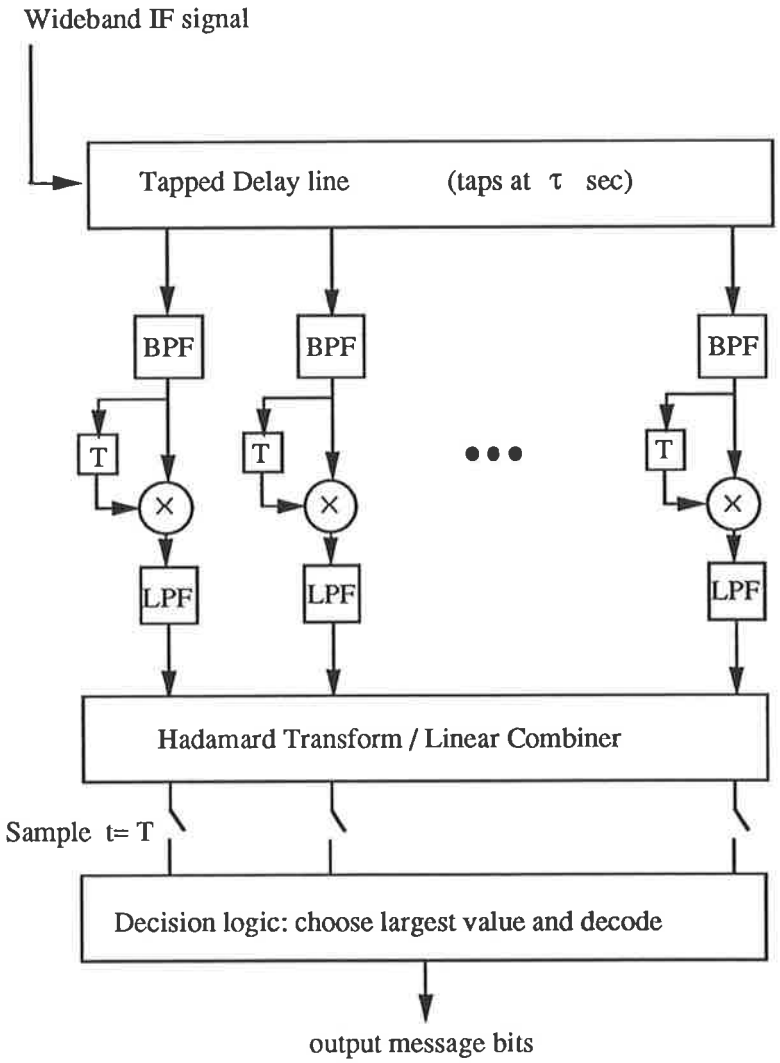

Figure 1.8: Schematic diagram of the linear FH-DPSK matched filter receiver

In the system suggested in [24], k message bits are encoded into a codeword constituted by a row of the $n \times n$ Hadamard matrix, where $n = 2^k$. Each of the n code bits (chips) is transmitted on its own unique frequency during the hopping sequence by differential phase shift keying the chip frequency using the same chip in the previous frame as the reference. A schematic diagram of the FH-DPSK receiver is shown in figure 1.8. The input bandpass filters are assumed to be matched to

the transmitted signal, which is a rectangular envelope modulating the phase of the carrier by 0 or π radians. The output of each bandpass filter is then multiplied by the previous output delayed by one frame, and then lowpass filtered to remove the double frequency terms. All lowpass filter outputs are then linearly combined by the Hadamard transform, and the n resulting outputs are then sampled and the largest value selected as that most likely representing the k message bits.

Cooper and Nettleton based their analysis on the assumption that the interferers can be represented as additive white Gaussian noise, as described in section 1.4.1. If the interference from other users is expected to look like white Gaussian noise, the product detector output produces a mixture of Gaussian and non-Gaussian noise terms. The resulting noise output from the Hadamard transform is therefore also a combination of noise with two different distributions, but to enable a solution to be found, Nettleton and Cooper [24] assume the noise is described purely by the non-Gaussian distribution, which in effect is the worst case estimate. The outputs of the linear combiner are assumed to independent due to the orthogonality of the Hadamard transform and the fact that the non-Gaussian noise distribution has a shape very similar to a Gaussian distribution.

The probability of the correct decision being made on the combiner outputs for a particular bit energy to noise ratio may then be expressed in an integral form as the probability that the correct combiner output is greater than all other combiner outputs. The probability of codeword error can then be averaged over all possible values of the Rayleigh fading coefficients. This is solved by Monte Carlo averaging, where the probability of error is computed a large number of times for fading variables generated with a Rayleigh distribution. The values of the phasor representing fading magnitude and phase are assumed not to change over the duration of a frequency hopping cycle. If the channels are assumed to fade independently, the Rayleigh fading coefficients for each channel are generated independently. If the effect of a wide coherence bandwidth is to be examined, the channel fading coefficients are correlated when generated by multiplying the real and imaginary Gaussian amplitude components by the appropriate transformation matrix, and then treating

the resulting Rayleigh magnitude components exactly as for the independent fading case.

An alternative formulation of the performance for the additive white Gaussian interference model is given by Henry [25]. He assumes that as the noise output of the linear combiner is composed of a large sum of terms, which are approximately Gaussian and uncorrelated (by the Hadamard transform), it can be represented by the central limit theorem as Gaussian. The probability of an error being made in a pairwise comparison between the correct combiner output and another combiner output can then be written as the probability of a signal plus Gaussian noise being less than zero, and the total probability of codeword error is upper bounded by the union bound of $(n-1)$ times the pairwise error probability. Hence a comparatively simple formulation can be obtained to predict the performance of the system when Rayleigh fading is either present or absent. This derivation produces results which are very close to those of Nettleton and Cooper for the non-fading case, and slightly more optimistic for the fading case.

Yue [27] applied a result from quadratic detector theory [28] to this model to obtain a set of analytic bounds for a number of different fading distributions. The characteristic function of a single product detector output, conditional on the independent fading on that channel, is raised to the power $n/2$ to obtain the characteristic function of the difference between the linear combiner outputs for two codewords. This characteristic function is then averaged over the probability distribution of the fading coefficients, and the pairwise codeword error probability P_p can be computed as the inverse Fourier transform of the characteristic function. Inversion of the complex Fourier integral may be achieved by the method of residues if a convenient analytical form of the integral exists. If this is not possible or is too complex, the curve of integration from $-\infty$ to $+\infty$ may be distorted to pass through a saddle-point on the imaginary axis and a Taylor series approximation integrated term by term [26,29]. The codeword error probability is then upper bounded by the union bound $(n-1)P_p$ and lower bounded by P_p. For Rayleigh fading, Yue obtained very similar results to those derived for error probability for binary FSK transmitted over

$n/2$ independent channels with square law detection [30,31,32]. The similarity of probability of error expression for binary FSK and DPSK is not surprising: it was pointed out by Stein [33] in his unified treatment of M-ary FSK on fading channels.

The results for this particular treatment of the problem can be summarised. For power control case, the interferers have average power equal to that of the wanted signal and shadow fading can be ignored. The probability of bit error is bounded by

$$\frac{n}{2(n-1)}P_p \leq P_b \leq \frac{n}{2}P_p \tag{1.30}$$

For the no-fading case

$$P_p = 2^{-n/2}\exp\left[-\frac{nE_c}{2N_0}\right]\sum_{l=0}^{(n/2)-1}\sum_{r=l}^{(n/2)-1}\frac{2^{-r}}{l!}\binom{(n/2)-1+r}{r-l}\left(\frac{nE_c}{2N_0}\right)^l \tag{1.31}$$

and for the case of Rayleigh fading:

$$P_p = \frac{1}{(2+4b_0(E_c/N_0))^{n/2}}\sum_{l=0}^{(n/2)-1}\binom{(n/2)-1-l}{l}\left(\frac{N_0+4E_cb_0}{2N_0+4E_cb_0}\right)^l \tag{1.32}$$

where b_0 is the parameter of the Rayleigh fading distribution

$$p(\alpha) = \frac{\alpha}{b_0}\exp\left(-\frac{\alpha^2}{2b_0}\right) \tag{1.33}$$

and with power control to combat shadow fading, $\mathbf{E}[\alpha^2] = 1$ and $b_0 = 1/2$. These results were also independently confirmed by Lam and Sarwate [21].

The assumption of interference appearing as white Gaussian noise is a common device which has more application in direct sequence spread spectrum analysis. While it serves as a convenient and relatively tractable starting point for analysis, it is an approximation. Work by Mazo [34] has indicated that this approximation leads to an estimate of the average performance of over all possible ways of assigning user sequences for a direct sequence system. He showed that if the user sequences in n-dimensional space have a cross-correlation magnitude as large as $(t/n)^{1/2}$, where $t > 1$ is a convenient parameter, then the number of simultaneous users is reduced by a factor of t compared to what the Gaussian approximation would predict. While this result was illustrated from a direct sequence perspective, it does point out the danger of arbitrarily assuming that interference may be represented as white

Gaussian noise over the entire bandwidth. The addressing system proposed by Nettleton and Cooper with overlapping frequencies resulting in cross-correlation of signals may not be well represented by the white Gaussian interference model.

Another point which must be made in relation to the white Gaussian interference model is that it assumes a stationary distribution of random AGWN interference over all the chips. However, because of the cyclic nature of the user and interferer hopping sequences, large interferers can be present within a chip and persist for the duration of the call (fading appropriately). These are not adequately represented by the AWGN approximation, but are better modelled as a cyclostationary type of process.

To this end, Yue [26,35,23] has produced an alternative analysis of the FH-DPSK system for an isolated cell using the tone interferer model (section 1.4.2) in which interferers are assumed either not to be present or to be allocated by random addressing with the interferers represented as in-phase and quadrature Gaussian signals. Each interferer is assumed to have an average power equivalent to that of the target signal and affects only one channel. An assumption in this model is that frame or chip synchronism is possible to achieve, and hence orthogonal tones (where the frequency separation results in zero adjacent channel interference at the output of a matched filter) can be used. This can be arranged in an isolated cell for base to mobile transmission, but is again an approximation for mobile to base transmission and multiple cells. It can be argued however [26] that the performance for asynchronous operation lies between the cases of frame synchronism and chip synchronism. For the case of chip synchronism and the linear receiver of figure 1.8, this approach leads to far worse performance results than those predicted by the AWGN interference model.

After noting that the proposed FH-MFSK systems which had a higher user capacity used hard decisions on each chip, Yue also extended these results to the case of hard decisions (± 1) being made on the output of the quadratic detectors, before combining. This is effectively hard decision decoding of the received signal.

For this case, an analytic formulation is relatively straightforward to derive, and under a random addressing assumption, the number of users possible in the system can be derived. Results for this case show that the capacity of the system is much improved at high bit-energy-to-noise ratios.

For the asynchronous addressing scheme of Cooper and Nettleton, Matsumoto and Cooper [36,37] have derived integral formulations of bit error rate for noiseless transmission with a tone interferer located within the main lobe of each of the bandpass filters of each of the chips. For the linear receiver from the original proposal, it was found that communication at a bit error rate of $P_b < 10^{-3}$ was possible even for quite large tone interferers. When a hard limiter was inserted after the bandpass filter and before the quadratic detector, further gains in performance were noted. However, some of the assumptions made in the analysis regarding the Gaussian nature and independence of variables used in the integral formulation are not obvious, and the results are questionable for low values of bit error rate due to inadequate numbers of variates being used in the Monte Carlo evaluation. The presence of background noise, ignored in their treatment, may lead to a significant degradation in performance. In addition, these results are not easily compared with results by other researchers, due to the different assumptions which have been made.

All the above analyses can be seen to have some assumptions inherent that do not represent the real situation. Chip synchronism is not a situation which is likely to occur in practice, owing to propagation delays and delay spread. The real situation would have reduced cochannel interference due to smaller overlap of two sequences, and include adjacent channel interference due to the non-orthogonality of the presence of an interferer in the adjacent channel for only part of the time. Addressing in a real system is not random, but each sequence is determined to have low cross-correlation properties under random time shifts. Shadow fading may be a real problem on a link with no power control *eg* a frame synchronous base-to-mobile link. The effects of multiple cells are not dealt with in a satisfactory manner. It is therefore clear that more research is required in these areas before a useful prediction of performance can be obtained. A useful start would be to assess the performance

of the different receivers under an identical set of assumptions.

A summary of the system capacity as estimated so far is given in the following tables, where the authors' names are given along with their estimate of usage at a bit error rate of $P_b = 10^{-3}$. The information bit rate is assumed to be 32 kbit/s and the total available one-way bandwidth is 20 MHz. Power control within the cell to counteract shadow fading is assumed.

1. AWGN Interference Model (linear receiver only)

   (a) Isolated Cell

Analysis	No. of users
Nettleton and Cooper [24]	45
Henry [25]	58
Yue [26]	65

   (b) Multiple Cells

   Calculations were done for the cell corners, and attenuation is assumed to obey a d^{-3}—d^{-4} power law, leading to a range of user numbers.

Analysis	Number of users
Henry [25]	16–31
Yue [26]	≥ 18

2. Random addressing, chip synchronous model, isolated cell

   Yue [26,35,38] analysed the linear receiver, the post-detection hard limiting receiver (hard decisions) and a receiver with a soft limiter after the quadratic detector. The number of users that the system can support at an average bit error rate of $P_b = 10^{-3}$ for a range of E_b/N_0 values is given below.

No. of users	E_b/N_0		
	30 dB	20 dB	15 dB
Soft Limiting	56	50	36
Hard Limiting	53	42	17
Linear	26	24	19

The larger increase in the number of users in moving from $E_b/N_0 = 15$ dB to 20 dB than from $E_b/N_0 = 20$ dB to 30 dB represents a shift from a noise dominated system to a mutual interference dominated system.

1.6 Frequency Hopping Multilevel Frequency Shift Keying Schemes

Frequency-Hopped Multilevel Frequency Shift Keying (FH-MFSK) was initially proposed by Viterbi [39] for low bit rate satellite multiple access. Consequently, several researchers at AT&T Bell Laboratories who had seen Cooper and Nettletons' paper on frequency hopping mobile radio, examined applying Viterbi's scheme to mobile radio [40,41,42]. This led to a series of papers attempting to predict the performance of such a system in the cellular mobile radio environment [43,44,45,46,47,48,22,49,50,51,52].

In this system, each user is allocated a particular L chip address sequence which is drawn from a set of $q = 2^k$ tones. The address sequence is modified by a k bit data word, forming a new L chip tone sequence to be transmitted. On-off keying is used to modulate the carrier at each time chip, with the pulse error probabilities for this type of modulation in a Rayleigh fading channel being well known [53]. By careful choice of address hopping patterns, the frequency overlap of chips transmitted by different users can be minimised, although even in a frame synchronous system, clashes will still occur due to the modification of the frequency address by the data. (Note that this is a different situation to FH-DPSK).

Varying results have been obtained for this form of transmission scheme. Initial results [40] were promising, with far greater capacity than that of FH-DPSK, but later papers have been less enthusiastic about its potential. It appears [43,44,45,46] that the number of users possible in an asynchronous, multicell environment is significantly less than that of an isolated cell, to the extent that the capacity is not significantly more than that of an equivalent FDM system. The cases of synchronous and asynchronous operation have been investigated for both isolated and multiple cells, and hence no further work on this system will be presented in this thesis. Results from other authors will be quoted for purposes of comparison.

1. Isolated Cell

Yue has analysed this system for the cases of the hard decision receiver, and his results substantially agree with those of Goodman *et al* [40]. He has also examined the performance with a linear receiver and a receiver with soft limiting of the energy detector outputs before linear combining [38]. The results for the numbers of users which result on average in a bit error rate of 10^{-3} for each user are given below. The information bit rate is 32 kbit/s and total available bandwidth is 20 MHz as for the FH-DPSK case.

No. of users	E_b/N_0 dB		
	30	20	15
Soft Limiter	238	156	91
Hard Limiter	188	115	56
Linear	10	9	6

Agusti *et al* [44] have performed an alternative analysis, modelling the interference as a Poisson point process, and taking in to account the effect of adjacent channel interference.

No. of users	E_b/N_0 dB			
	30	25	20	15
No adjacent channel interference	170	140	108	65
Adjacent channel interference	113	90	58	<30

2. Multiple Cells

This has been examined by Agusti *et al* [44,45,46] for the case of signal power attenuation with distance as $d^{-3.5}$ and standard deviation of the lognormal fading equal to 8 dB. Interference from cells surrounding the central cell was approximated as additive white Gaussian noise, and the intra-cell interference as a Poisson point process.

No. of users	E_b/N_0 dB			
	30	25	20	15
7 cells	16	15	14	10
37 cells	14	13	12	9

Further Monte Carlo simulation by Agusti *et al* gave slightly better results, indicating that the Gaussian approximation for intercell interference is pessimistic. It was also found that subdividing the channels into subsets for

allocation to cells in a cluster (as in a frequency division multiplexing system) gave worse results, due to a lack of frequency diversity available within a cell.

No. of users	E_b/N_0 dB			
	30	25	20	15
7 cells	34	33	30	22

3. Effect of lognormally distributed shadowing

   The effect of lognormal shadowing on capacity reduction has also been examined. Nguyen [52] gives the following number of users in the hard decision system, for Rayleigh fading without lognormal shadowing, and with lognormal fading and a standard deviation of 6 dB (at the low end of the typical range). Chip synchronism is assumed, therefore adjacent channel interference is not considered.

No. of users	E_b/N_0 dB		
	30	25	20
Rayleigh, $\sigma = 0$ dB	151	131	102
Rayleigh/Lognormal, $\sigma = 6$	115	85	56

   These results are substantially equivalent to those of Bakewell [54] and others [48].

4. Effect of Wide Coherence Bandwidths

   Similar capacity reduction has also been noted for wide coherence bandwidths. For the case of wide coherence bandwidths, results from [55] are given for synchronous base-mobile transmission in an isolated cell, and an average signal to noise ratio of 25 dB.

Coherence Bandwidth (MHz)	0	0.2	1.0
Number of users at $P_b = 10^{-3}$	167	115	83-100

It is clear that the presence of interference from adjacent channels and multiple cells has a severe effect on the error rate and capacity of the FH-MFSK systems. The levels of users predicted by Agusti are not dissimilar to those that Henry predicted for FH-DPSK under the AWGN model, and a linear receiver. It is therefore of interest to know if the performance of the FH-DPSK system for different receiver

structures will result in a capacity gain, and how the multiple cell situation may affect this.

Some further improvement is possible in the figures for the FH-MFSK system. By exploiting the structure of the addressing schemes, further decoding can be performed which could result in increases of up to 60% in the number of users which may use the system at an average bit error rate of 10^{-3} [22,41].

1.7 A Frequency Hopping, Minimum Shift Keying Proposal

While little has appeared in the literature on the use of fast frequency hopping minimum shift keying (FH-MSK), Elnoubi [56] has proposed a FH-MSK system which uses repeat coding of N chips to transmit one bit of data, and decodes using a majority decision of the N chip hard decisions. Interference, as in the case of Nettleton and Cooper, is assumed to be represented by additive white Gaussian noise, with intensity proportional to the number of current users. Very good results were claimed by Elnoubi; unfortunately his analysis apeears to contain some errors which completely change these results. The treatment below follows that of Elnoubi, with attention drawn to the inconsistencies in his paper.

The MSK modulator at the transmitter produces an output

$$s(t) = \cos\left[w_0 t + \theta(t)\right] \tag{1.34}$$

where

$$\theta(t) = x_k + \frac{\pi}{2T} v_k t \qquad kT \leq t \leq (k+1)T \tag{1.35}$$

and ω_0 is the carrier (centre) frequency, $v_k = \pm 1$ is the data and x_k is a phase offset such that the phase transition from the $(k-1)$th bit to the kth bit is continuous and $\theta(t)$ is a piecewise linear phase function of time. The differential detector uses the shift in phase $\theta(t) - \theta(t-T)$ during the bit interval to decide the polarity of the

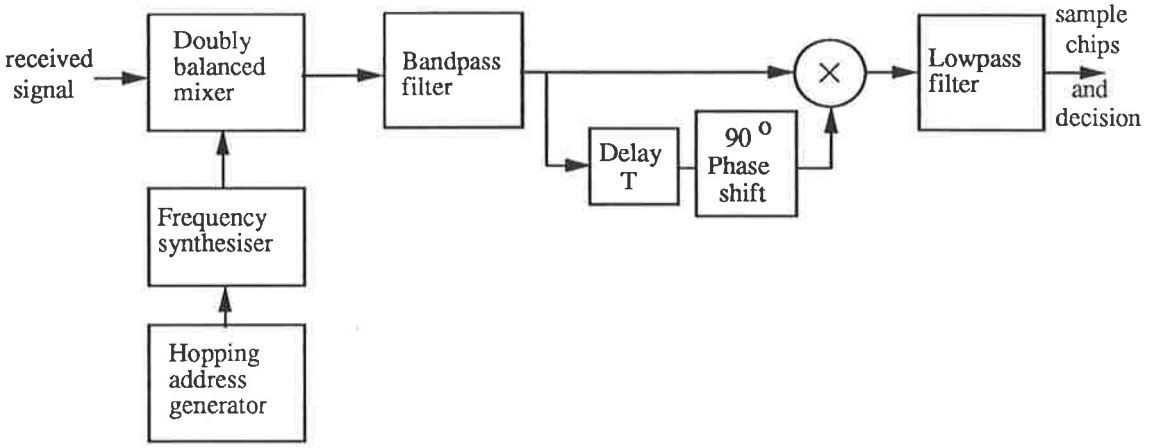

Figure 1.9: Schematic diagram of the FH-MSK receiver

transmitted bit. After being mixed with a frequency hopping carrier, the signal in a particular time chip l can be written as

$$s_l(t) = \cos\left[2\pi(f_0 + a_l f_1)t + \theta(t) + \phi_l\right] \qquad (l-1)\tau \leq t \leq l\tau \tag{1.36}$$

where a_l is the lth integer from the frequency hopping set, f_1 is the separation between the total number q of channels in the available bandwidth W, and ϕ_l is a phase constant associated with the lth channel.

The receiver for this modulation is shown in figure 1.9. It is assumed that the spacing between channels $f_1 = W/q$ is greater than the coherence bandwidth of the channel such that each channel fades independently, and that the bandwidth of the IF filter of main lobe width $2/\tau$ is less than the coherence bandwidth such that each channel experiences flat fading, *ie*

$$\frac{2}{\tau} < B_c < \frac{W}{q} \tag{1.37}$$

The following values are assumed:

$$\begin{aligned} W &= 20 \text{ MHz} \\ R_b &= 32 \text{ kb/s is the information bit rate} \\ T &= 1/R_b = N\tau = 31.25 \ \mu\text{s is the frame period} \end{aligned}$$

To satisfy both inequalities, $\tau \geq 2q/W = q \times 10^{-7}$ seconds, and $Nq < 312.5$ This differs from Elnoubi's paper where an incorrect figure of 32×10^3 is given.

After propagation through the fast Rayleigh fading channel, the dehopped received signal in the lth time chip is given by

$$\begin{aligned} r_l(t) &= z_{lc}(t)\cos\left[2\pi f_0 t + \theta(t) + \phi_l\right] - z_{ls}(t)\sin\left[2\pi f_0 t + \theta(t) + \phi_l\right] \\ &\quad + n_{lc}(t)\cos(2\pi f_0 t) - n_{ls}(t)\sin(2\pi f_0 t) \qquad (l-1)\tau \le t \le l\tau \end{aligned} \tag{1.38}$$

where z_{lc}, z_{ls} are i.i.d. zero mean Gaussian random variables representing the signal envelope, with variance σ_s^2

n_{lc}, n_{ls} are i.i.d. zero mean Gaussian variables representing interference and noise, with variance σ_n^2.

The power spectral density of z_{lc} and z_{ls} is

$$S_{z_{lc}}(f) = S_{z_{ls}}(f) = \begin{cases} \frac{\sigma_s^2}{\pi\sqrt{f_D^2 - f^2}} & |f| \le f_D \\ 0 & \text{otherwise} \end{cases} \tag{1.39}$$

where f_D is the maximum Doppler frequency.

The interference is assumed to appear as additive white Gaussian noise, with a power spectral density I resulting from the signal power of all other $(J-1)$ mobile users being uniformly spread across the entire bandwidth W. Assuming a power control scheme is in place whereby all signals are received with equal average power,

$$I = \frac{\sigma_s^2(J-1)}{W} \qquad \text{W/Hz} \tag{1.40}$$

Elnoubi assumes an ideal IF filter, rectangular in the frequency domain, with bandwidth $f_2 = 2/\tau$, equal to the main lobe of the $\sin(\pi f\tau)/(\pi f\tau)$ shaped spectrum of the signal. For this IF filter, centered on f_0, the transfer function is

$$H(f) = \begin{cases} 1 & |f - f_0| < |f_2/2| \\ 0 & |f - f_0| > |f_2/2| \end{cases} \tag{1.41}$$

and therefore the noise bandwidth is f_2 and $\sigma_n^2 = If_2$.

Using a result from [57] for differential detection of constant envelope FSK in Rayleigh fading, the probability of a hard decision chip error P_c is given by

$$P_c = \frac{1}{2}\left[\frac{1 - \Gamma\rho_s(T)}{\sqrt{(\Gamma+1)^2 - \rho_n^2(T)}}\right] \tag{1.42}$$

where $\Gamma \triangleq \sigma_s^2/\sigma_n^2 = q/(J-1)$ is the average signal to noise ratio

$\rho_n(\tau)$ is the autocorrelation of a quadrature noise component at time τ

$\rho_s(\tau)$ is the autocorrelation of the inphase signal envelope at time τ

The autocorrelations of the inphase signal component z_{Ic} and the inphase noise component n_{Ic} at time shift T are (equations (18) and (19) of [56])

$$\rho_s(T) = J_0(2\pi f_D T) \tag{1.43}$$

$$\rho_n(T) = \frac{\sin \pi f_2 T}{\pi f_2 T} = \frac{\sin \pi 2N}{\pi 2N} = 0 \tag{1.44}$$

The chip error probability is then

$$P_c = \frac{1}{2}\left[\frac{1 - \Gamma J_0(2\pi f_D T)}{(\Gamma + 1)}\right] \tag{1.45}$$

The probability of bit error for a given value of signal to noise ratio, for a simple repeat-N code is

$$P_b = \sum_{i=(N+1)/2}^{N} \binom{N}{i} P_c^i (1-P_c)^{N-i} \qquad N \text{ odd} \tag{1.46}$$

$$P_b = \frac{1}{2}\binom{N}{N/2} P_c^{N/2}(1-P_c)^{N/2} + \sum_{i=(N/2)+1}^{N} \binom{N}{i} P_c^i (1-P_c)^{N-i} \qquad N \text{ even} \tag{1.47}$$

and not simply equation (21) of [56], which is

$$P_b = \sum_{i=N/2}^{N} \binom{N}{i} P_c^i (1-P_c)^{N-i}$$

The resulting curve for a chip error probability versus signal to noise ratio is shown in figure 1.10.

Elnoubi displays separate curves for P_b versus Γ for $N = 12, 14, 15,$ and 16. Points taken from his curves are shown in figure 1.11. However, for a repeat coding system with hard decisions, the curve for P_b with $N = i$ and i odd, will always be exactly equal to the curve for P_b with $N = i + 1$. The distance of the code is N and therefore the error correction capability is t, where t is the largest integer less than

or equal to $(N-1)/2$. As Elnoubi's results show separate curves for successive odd and even values of N, it would seem that the results from Elnoubi are in error. The correct results from equations 1.46 and 1.47 are plotted in figure 1.11, and it can be seen that the bit error rates obtained for $N = 13, 14, 15, 16$ are higher than those predicted by Elnoubi for the range of signal to noise ratios shown.

The number of users that Elnoubi claims can be supported at a bit error rate of 10^{-3} in an isolated cell appears to be incorrect. He gives an example of using a $N = 14$ repeat code, which he claims requires a signal to noise ratio of $\Gamma = 0.8$. The maximum value of $q \leq [312.5/N] = 22$ channels. As each user requires 14 channels (each chip is sent on a different channel), this means that the target user will interfere heavily with any other user on the system. The chip period is $\tau = 2.2\mu$s, which is far too short to avoid serious degradation from typical delay spreads in urban areas. For this system, Elnoubi obtains a capacity of 60 users. In fact, assuming that the white Gaussian interference approximation holds for so few channels, the signal to noise ratio necessary for a $N = 14$ repeat code at $P_b = 10^{-3}$ is 4.0dB = 2.51 and hence the number of interferers would be $J - 1 = q/\Gamma \approx 8$.

For a comparison with a FH-DPSK system with white Gaussian interference assumed, let N take the values $N = 3, 5, 7$, resulting in the shortest chip period being 4.4μs. Then the signal to noise ratios required and the number of users $J = q/\Gamma + 1$ supported at $P_b = 10^{-3}$ are summarised in table 1.3.

Repeat N	signal-to-noise Γ dB	No. of users J
3	14.0	5
5	9.6	7
7	7.4	9

Table 1.3: Number of users at $P_b = 10^{-3}$ possible in FH-MSK system under white Gaussian interference model

The FH-DPSK system of Cooper and Nettleton, analysed by Henry [25], can

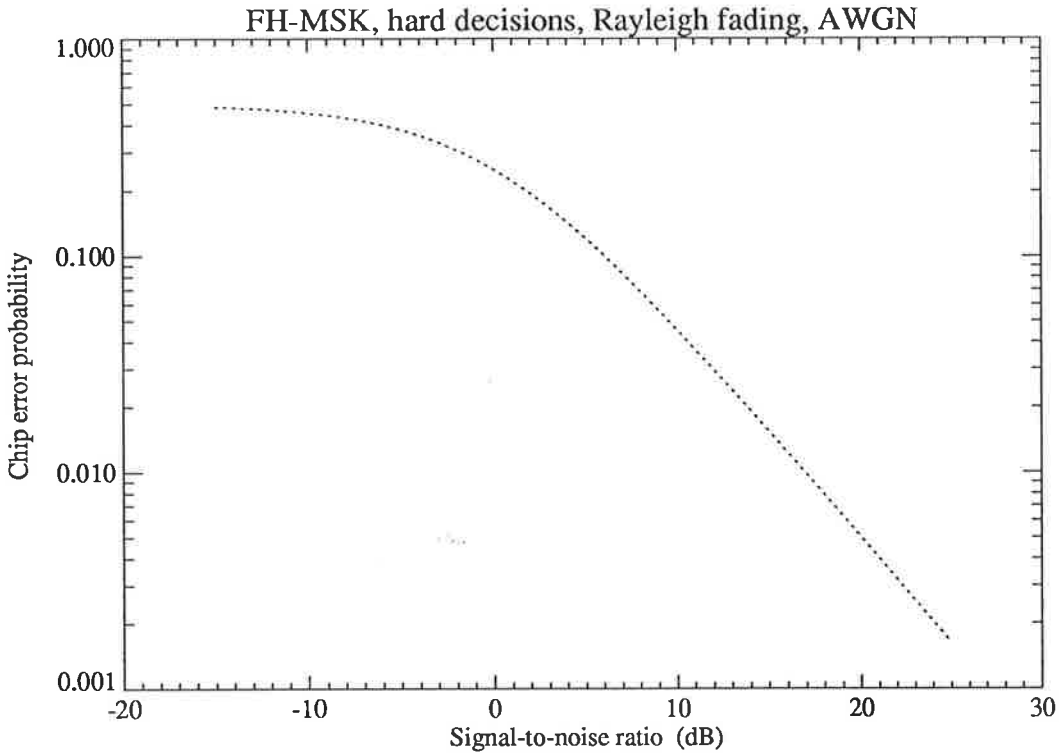

Figure 1.10: Chip error rate of the FH-MSK receiver, with ideal Rayleigh fading and AWGN.

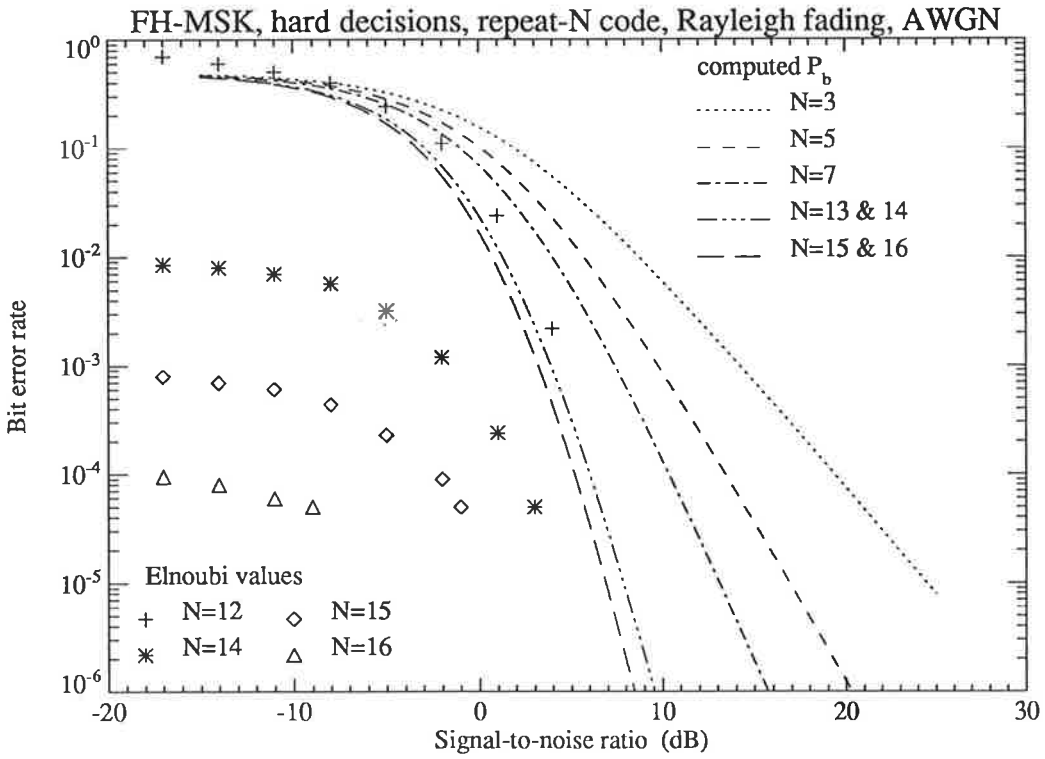

Figure 1.11: Bit error rate of the FH-MSK receiver, with ideal Rayleigh fading and AWGN, using repeat-N coding.

support 58 users under the white Gaussian noise model in an isolated cell with fast fading, and hence is far superior to this FH-MSK system. It is noted that the formula (1.45) for chip error simplifies to Voelcker's formula for differential detection of DPSK [58] which implies that for hard decisions, in fading and additive white Gaussian noise, FH-MSK and FH-DPSK will have similar performance, with the difference in performance dependent on the characteristics of the IF filter. However, later results will indicate that the performance which may be acheived for FH-DPSK with another receiver is far better than that derived here for FH-MSK.

Chapter 2

FH-DPSK Diversity in Fading and AWGN

This chapter considers the use of diversity for the FH-DPSK system using the linear receiver in a Rayleigh fading and additive white Gaussian interference environment. New results are obtained by applying several well-known diversity methods, the results of which are compared to those obtained from the form of diversity proposed by Nettleton and Cooper [24]. It is found that the conventional diversity approaches provide better performance, although extra complexity in the receiver would be required.

2.1 System Model

As signals in white Gaussian noise are being considered, the method of Nettleton and Cooper [9] was used. The approaches taken by Henry [25] and Yue [26] are not suitable for analysing correlated fading, as they rely on the independence of each frequency channel in the solution. On the other hand, the approach taken by Nettleton and Cooper is convenient to deal with because the correlated fading variables may be incorporated simply into the expression for the evaluation of probability of

error by Monte Carlo methods.

It is noted that the results of Nettleton and Cooper are somewhat pessimistic compared to those of Yue for the case of independent fading on each channel. This stems from the assumption that the combiner outputs are independent, whereas they are actually correlated. As the same procedure is used here, it is to be expected that the results may also be pessimistic for the case of correlated fading on each channel. However, the results derived in this section are useful as a guide to the relative performance of the different diversity systems. The results also suppose that the diversity schemes can be implemented, although this may be difficult to achieve in practice.

Consider a frequency hopping signal transmitted over $L = 2^k$ frequencies as:

$$s(t) = d(t)\sqrt{2S}\,\mathrm{rect}_\tau(t - l\tau)\cos(2\pi f_l t) \qquad l = 0, 1, \ldots, L-1 \tag{2.1}$$

where

$$L\tau = T \text{ is the frame period} \tag{2.2}$$

$$\mathrm{rect}_\tau(t) = \begin{cases} 1 & \text{if } 0 \le t \le \tau \\ 0 & \text{otherwise} \end{cases} \tag{2.3}$$

f_l is the lth frequency of the hopping pattern

The data is differentially encoded onto the signal with the mth word of k bits mapping to a corresponding codeword in the $L \times L$ Hadamard matrix $\boldsymbol{H}$ with elements $\{h_{ml}\} = \pm 1, \quad l = 0, \ldots, L-1$. The Hadamard matrix is specified by the relation

$$\boldsymbol{H}_k = \begin{bmatrix} \boldsymbol{H}_{k-1} & \boldsymbol{H}_{k-1} \\ \boldsymbol{H}_{k-1} & -\boldsymbol{H}_{k-1} \end{bmatrix} \qquad \text{with} \quad \boldsymbol{H}_1 = \begin{bmatrix} 1 & 1 \\ 1 & -1 \end{bmatrix} \tag{2.4}$$

This can be illustrated simply for the case of $k = 2$ as

$$\begin{matrix} \text{Data} \\ \begin{pmatrix} 00 \\ 01 \\ 10 \\ 11 \end{pmatrix} \end{matrix} \Rightarrow \begin{matrix} \boldsymbol{H} \\ \begin{pmatrix} 1 & 1 & 1 & 1 \\ 1 & -1 & 1 & -1 \\ 1 & 1 & -1 & -1 \\ 1 & -1 & -1 & 1 \end{pmatrix} \end{matrix} \tag{2.5}$$

Hence for the mth frame, the differential encoding is:

$$d_m(t) = \sum_{l=0}^{L-1} d_{ml}\,\mathrm{rect}_\tau(t - l\tau) \tag{2.6}$$

$$\text{and} \quad d_{ml} = d_{(m-1)l}h_{ml} \tag{2.7}$$

After fading through L Rayleigh channels, the received signal component is:

$$\hat{s}(t) = \sum_{l=0}^{L-1} \sqrt{2S} d_{ml} \alpha_l \text{rect}_\tau(t - l\tau) \cos(2\pi f_l t + \phi_l) \tag{2.8}$$

where ϕ_l is a phase angle uniformly distributed on $[0, 2\pi)$

α_l is a Rayleigh distributed random variable such that $\mathbf{E}[\alpha_l^2] = 1$, as power control is assumed to counteract shadow fading

The approach taken by Cooper and Nettleton was for the interference power to be distributed over the entire bandwidth as additive white Gaussian noise. For a total bandwidth W Hz and J users, the one-sided power spectral density due to the interference, neglecting the much smaller thermal noise, is therefore $N_0 = S(J-1)/W$.

The receiver is assumed to be a linear matched filter receiver, of the type shown in figure 1.8. After passing through the delay line, the received signal passes through matched bandpass filters, with impulse responses

$$h_l(t) = \frac{2}{\tau} \text{rect}_\tau(t) \cos 2\pi f_l(\tau - t) \tag{2.9}$$

The sum of the signal and white Gaussian noise, for the lth channel, can be written at the output of the matched bandpass filter as:

$$r_l(t) = \sqrt{2S}\beta(t)\alpha_l d_{ml} \cos(2\pi f_l t) + n_{l_c} \cos(2\pi f_l t) + n_{l_s} \sin(2\pi f_l t) \tag{2.10}$$

where

n_{l_c}, n_{l_s} are independent and identically distributed (i.i.d.) zero mean Gaussian random variables with variance σ_n^2

$\sigma_n^2 = N_0/\tau = \dfrac{S(J-1)}{W\tau}$ at sample time $t = \tau$

$\beta(t)$ is the periodic amplitude function resulting from the matched filter. At sample time τ, $\beta(\tau) = 1$

$$\beta(t) = \begin{cases} t/\tau & 0 \le t \le \tau \\ 2 - t/\tau & \tau \le t \le 2\tau \\ 0 & 2\tau < t < T \end{cases}$$

The phase and amplitude of the complex fading envelope are assumed to be unchanged over one frame, such that

$$\alpha_l(t) \approx \alpha_l(t - T) \tag{2.11}$$

Without loss of generality, it is assumed that the all-ones codeword x_0 is transmitted, and the demodulator output before the lowpass filter is

$$\begin{aligned} y_l'(t) &= r_l(t)r_l(t-T) \\ &= 2S\alpha_l^2\beta^2(t)\cos^2\omega_l t \\ &\quad + n_{l_c}(t)n_{l_c}(t-T)\cos^2\omega_l t + n_{l_s}(t)n_{l_s}(t-T)\sin^2\omega_l t \\ &\quad + \sqrt{2S}\alpha_l\beta(t)\left[n_{l_c}(t)+n_{l_c}(t-T)\right]\cos^2\omega_l t \\ &\quad + \sqrt{2S}\alpha_l\beta(t)\left[n_{l_s}(t)+n_{l_s}(t-T)\right]\sin\omega_l t\cos\omega_l t \\ &\quad + \left[n_{l_c}(t)n_{l_s}(t-T)+n_{l_s}(t)n_{l_c}(t-T)\right]\sin\omega_l t\cos\omega_l t \end{aligned} \tag{2.12}$$

After low pass filtering,

$$\begin{aligned} y_l(t) &= S\alpha_l^2\beta^2(t) + \frac{1}{2}\left[n_{l_c}(t)n_{l_c}(t-T)+n_{l_s}(t)n_{l_s}(t-T)\right] \\ &\quad + \sqrt{\frac{S}{2}}\alpha_l\beta(t)\left[n_{l_c}(t)+n_{l_c}(t-T)\right] \end{aligned} \tag{2.13}$$

with mean $\bar{y}_{l|\alpha}$ and variance $\sigma^2_{y_l|\alpha}$ given by

$$\bar{y}_{l|\alpha} = S\alpha_l^2\beta^2(t) \tag{2.14}$$

$$\begin{aligned} \sigma^2_{y_l|\alpha} &= \tfrac{1}{4}\left[2 < n_{l_c}^2(t) >^2\right] + S\alpha_l^2\beta^2(t) < n_{l_c}^2 > \\ &= \tfrac{1}{2}\sigma_n^4 + S\alpha_l^2\beta^2(t)\sigma_n^2 \end{aligned} \tag{2.15}$$

where the operation $< . >$ denotes time average.

Let $y(t)$ be the vector of L values of $y_l(t)$, and the vector of linear combiner outputs be $x(t)$. Now the linear combiner operation is defined as

$$x(t) = \boldsymbol{H}^T y(t) \tag{2.16}$$

$$x_j(t) = \sum_{l=0}^{L-1} y_l(t)h_{jl} \qquad j = 0,\ldots,L-1 \tag{2.17}$$

hence

$$\bar{x}_{j|\mathbf{F}} = S\beta^2(t)\sum_{l=0}^{L-1}\alpha_l^2 h_{jl} = S\beta^2(t)\boldsymbol{h}_j^T\boldsymbol{F} \tag{2.18}$$

$$\sigma^2_{x_j|\mathbf{F}} = \sum_{l=0}^{L-1}\sigma^2_{y_l|\mathbf{F}} = \frac{L}{2}\sigma_n^4 + S\beta^2(t)\sigma_n^2\boldsymbol{h}_o^T\boldsymbol{F} \tag{2.19}$$

where $\boldsymbol{F}^T = [\alpha_0^2,\ldots,\alpha_{L-1}^2]$ and $\boldsymbol{h}_j^T = [h_{j0},\ldots,h_{j(L-1)}]$.

The receiver decides which codeword was transmitted by choosing the largest value of x_j for $j = 0, \ldots, L-1$. At this point, Nettleton and Cooper make an assumption that the combiner outputs x_j are independent, as the noise terms from the quadratic detector outputs y_l are independent and have a distribution similar to a Gaussian distribution, and the combiner uses an orthogonal transformation to produce x_j. This has been shown by Yue [27] to be incorrect as the x_j are correlated, but produces an upper bound.

Letting $\Psi(x)$ be the normalized noise probability distribution, the expression for the pairwise probability of codeword error, conditional on the fading values on each channel, is:

$$\begin{aligned} P_{e_{0,j}|\mathbf{F},\mathbf{x_0}} &\approx 1 - \Psi\left\{\frac{x_0(t) - \bar{x}_{j|\mathbf{F}}}{\sigma_{x_{j|\mathbf{F}}}}\right\} \\ &= 1 - \Psi\left\{\nu + d(x_0, x_j|\boldsymbol{F})\right\} \end{aligned} \tag{2.20}$$

where

$$d(x_0, x_j|\boldsymbol{F}) \triangleq (\bar{x}_{0|\mathbf{F}} - \bar{x}_{j|\mathbf{F}})/\sigma_{x_{j|\mathbf{F}}} \tag{2.21}$$

$$\nu \triangleq (x_0(t) - \bar{x}_{0|\mathbf{F}})/\sigma_{x_{j|\mathbf{F}}} \tag{2.22}$$

The quantity $d(x_0, x_j|\boldsymbol{F})$ is the normalized distance between the mean value of x_0 and x_j, given a certain matrix $\boldsymbol{F}$ of squared fading coefficients on each channel.

$$d(x_0, x_j|\boldsymbol{F}) = \frac{S\beta^2(t)(\boldsymbol{h}_o - \boldsymbol{h}_j)^T\boldsymbol{F}}{\sqrt{\frac{L\sigma_n^4}{2} + S\beta(t)\sigma_n^2\boldsymbol{h}_o^T\boldsymbol{F}}} \tag{2.23}$$

Defining the average signal to noise ratio at sample time τ as Γ

$$\Gamma = S\beta^2(\tau)/\sigma_n^2 = S\tau/N_0 = \frac{E_b}{N_0} \times \frac{K}{2^K} \tag{2.24}$$

$$d(x_0, x_j|\boldsymbol{F}) = (\boldsymbol{h}_o - \boldsymbol{h}_j)^T\boldsymbol{F}\Gamma\sqrt{\frac{2}{L + 2\Gamma\boldsymbol{h}_o^T\boldsymbol{F}}} \tag{2.25}$$

With the assumption of independence of the x_j, the probability of error in any of the $(L-1)$ pairwise decisions can be derived as

$$P_{e|\mathbf{F}} = 1 - \int_{-\infty}^{\infty} p(\nu) \prod_{j=1}^{L-1} \Psi\{\nu + d(x_0, x_j|\boldsymbol{F})\} d\nu \tag{2.26}$$

The noise terms in the combiner outputs are

$$\sum_{i=0}^{L-1}\left(\frac{1}{2}[n_{l_c}(t)n_{l_c}(t-T)+n_{l_s}(t)n_{l_s}(t-T)]+\sqrt{\frac{S}{2}}\alpha_l\beta(t)[n_{l_c}(t)+n_{l_c}(t-T)]\right)$$

with variance

$$\sigma_x^2=\sum_{l=0}^{L-1}\sigma_{y|\mathbf{F}}^2=\sum_{l=0}^{L-1}\sigma_n^4(\tfrac{1}{2}+\Gamma\alpha_l^2) \tag{2.27}$$

For low signal-to-noise ratio Γ, the non-linear part of the noise, of form $\sum_{l=0}^{2L-1} n_{l_1}n_{l_2}$, dominates. For high values of Γ, the Gaussian part, of form $\sum_{l=0}^{2L-1} n_{l_c}$ dominates. Use of the non-Gaussian probability density results in a worst case estimate. The probability density function of the non-Gaussian part of the noise is known [59] (in error in [24])

$$\begin{aligned} p(\xi) &= \frac{\xi^{L-(1/2)}K_{L-(1/2)}(\xi)}{\sqrt{\pi}(L-1)!2^{L-(1/2)}} && \xi\geq 0 \\ &= p(-\xi) && \xi<0 \end{aligned} \tag{2.28}$$

where $K_{L-(1/2)}(\xi)$ is the modified Bessel function of the second kind of order $L-(1/2)$ [60]

$$K_{L-(1/2)}(\xi)=\sqrt{\frac{\pi}{2\xi}}e^{-\xi}\sum_{k=0}^{L-1}\frac{(L-1+k)!}{k!(L-1-k)!(2\xi)^k} \tag{2.29}$$

The distribution function $\Psi(a)$ is

$$\begin{aligned} \Psi(a) &= 1-\int_a^\infty p(\xi)d\xi \\ &= 1-\frac{1}{2^L(L-1)!}e^{-a}\sum_{r=0}^{L-1}\sum_{j=0}^{L-1-r}\frac{(L-1+r)!a^{L-1-r-j}}{r!(L-1-r-j)!2^r} \qquad a>0 \end{aligned} \tag{2.30}$$

The probability of codeword error can now be computed. For the non-fading case, the elements of the matrix $\boldsymbol{F}$ are always unity, and the equation 2.26 may be evaluated by numerical integration, as in [24].

For the fading case, the probability of error is conditional on the values of the fading coefficients. The codeword probability of error becomes

$$P_e=1-\int_0^\infty\int_0^\infty\cdots\int_0^\infty p(\alpha_0^2,\alpha_1^2,\ldots,\alpha_{L-1}^2)\left[1-P_{e|\mathbf{F}}\right]d\alpha_0^2,d\alpha_1^2\cdots d\alpha_{L-1}^2 \tag{2.31}$$

As this involves an L-fold integration, numerical integration by techniques such as Simpson's rule is not a realistic option. Instead, Monte Carlo averaging is carried

out, whereby a large number of variates with the appropriate distribution are generated and the probability of error evaluated repeatedly for the sequence of values. The average probability is then taken over all trials. For the case where the channels fade independently, the variables $\alpha_0^2, \ldots, \alpha_{L-1}^2$ are exponentially distributed and may be generated simply from a independent set of random variables $\{x_l\}$ distributed uniformly on $[0, 1)$.

$$\alpha_l^2 = -\ln x_l \tag{2.32}$$

$$p_{\alpha^2}(z) = e^{-z} \tag{2.33}$$

$$p_\alpha(\alpha) = 2\alpha e^{-\alpha^2} \tag{2.34}$$

From the codeword probability of error P_e, the bit error probability may be obtained as

$$P_b = \frac{2^{k-1}}{2^k - 1} P_e \tag{2.35}$$

Following the above procedure to obtain P_b produced the same results as those given in [24] (results for the no fading and Rayleigh fading cases are shown later for comparison with other results in figures 4.2 and 4.3).

2.2 Modelling Wide Coherence Bandwidth Fading

When the fading variables are not independent, it is necessary to generate sets of fading variables with the correct correlation. Consider the most general case, where two antennae are spaced a distance $\zeta = vt_0$ metres apart, where v is the vehicle speed. The correlation between the two envelopes as a function of frequency separation Δf and time shift t_0, or equivalently spatial shift ζ, is given by [2]

$$\rho(\Delta f, t_0) = \frac{J_0^2(2\pi f_D t_0)}{1 + 2\pi \Delta f T_d^2} = \frac{J_0^2(2\pi f_D \zeta / v)}{1 + (\Delta f / B_c)^2} \tag{2.36}$$

where T_d is the channel mean delay spread (assuming an exponential distribution)

$J_0(x)$is the Bessel function of the first kind, order zero

f_D is the maximum Doppler frequency

$B_c \triangleq [2\pi T_d]^{-1}$

is the coherence bandwidth, the frequency separation at which the correlation between envelope magnitudes is 0.5. Note that two definitions are commonly used for coherence bandwidth [2], and this version was chosen over the the alternative used in [24], where phase correlation is 0.5, as correlated amplitude fluctuations are the cause of high error rates, and not phase correlation.

Consider the case of envelopes at two frequencies f_1, f_2 and separation $\Delta f = f_1 - f_2$, with no time or spatial shift. *ie* from the same antenna. If $e^{j2\pi f_l t}$ is transmitted, from section 1.1.1 the received signal is (where $\Re$ denotes real part)

$$\begin{aligned} \Re\left[z_l(t)e^{j2\pi f_l t}\right] &= \Re\left[(x_l + jy_l)e^{j2\pi f_l t}\right] \\ &= \Re\left[\alpha_l(t)e^{j(2\pi f_l t+\theta_l)}\right] \end{aligned} \tag{2.37}$$

where $\alpha_l^2 = x_l^2+y_l^2$ and $\theta_l = \arg(x_l+jy_l)$. The variables α_l are Rayleigh distributed

$$p(\alpha) = \frac{\alpha}{b_0}e^{-\alpha^2/2b_0}$$

and θ_l is uniformly distributed on $[0, 2\pi)$.

The envelope magnitudes α_1, α_2 are required to be correlated in accordance with equations (1.17)–(1.19). Now

$$\begin{aligned} \mathbf{E}[\alpha_1^2\alpha_2^2] &= \mathbf{E}[(x_1^2 + y_1^2)(x_2^2 + y_2^2)] \\ &= \mathbf{E}[x_1^2x_2^2] + \mathbf{E}[x_1^2y_2^2] + \mathbf{E}[x_2^2y_1^2] + \mathbf{E}[y_1^2y_2^2] \end{aligned} \tag{2.38}$$

Expanding out terms

$$\begin{aligned} \mathbf{E}[x_1^2x_2^2] &= \mathbf{E}[x_1^2]\mathbf{E}[x_2^2] + 2\mathbf{E}[x_1x_2]\mathbf{E}[x_1x_2] \\ &= b_0^2\left(1 + \frac{2}{1+(\Delta f/B_c)^2}\right) \\ &= \mathbf{E}[y_1^2y_2^2] \end{aligned} \tag{2.39}$$

$$\begin{aligned}\mathbf{E}[x_1^2 y_2^2] &= \mathbf{E}[x_1^2]\mathbf{E}[y_2^2] + 2\mathbf{E}^2[x_1 y_2] \\ &= b_0^2\left(1 + 2\left(\frac{(\Delta f/B_c)}{1+(\Delta f/B_c)^2}\right)^2\right) \\ &= \mathbf{E}[x_2^2 y_1^2]\end{aligned} \tag{2.40}$$

Hence

$$\mathbf{E}[\alpha_1^2\alpha_2^2] = 4b_0^2\left(1 + \left(\frac{1+(\Delta f/B_c)^2}{(1+(\Delta/B_c)^2)^2}\right)\right) \tag{2.41}$$

The covariance of α_1^2 and α_2^2 is

$$\mathrm{Cov}(\alpha_1^2, \alpha_2^2) = \mathbf{E}[\alpha_1^2\alpha_2^2] - \mathbf{E}[\alpha_1^2]\mathbf{E}[\alpha_2^2] \tag{2.42}$$

$$\mathbf{E}[\alpha_1^2] = \mathbf{E}[\alpha_2^2] = 2b_0 \tag{2.43}$$

hence

$$\mathrm{Cov}(\alpha_1^2, \alpha_2^2) = (2b_0^2)\left(\frac{1+(\Delta f/B_c)^2}{(1+(\Delta f/B_c)^2)^2}\right) \tag{2.44}$$

$$= \frac{(2b_0)^2}{1+(\Delta f/B_c)^2} \tag{2.45}$$

The variables α_1^2, α_2^2 are exponentially distributed

$$p(\alpha^2) = \frac{e^{-\alpha^2/2b_0}}{2b_0} \tag{2.46}$$

and have a correlation coefficient

$$\rho_{\Delta f} = \frac{1}{1+(\Delta f/B_c)^2} \tag{2.47}$$

Let a set of complex Gaussian variables be defined as

$$z = \begin{bmatrix} x_0 + jy_0 \\ \vdots \\ x_{L-1} + jy_{L-1} \end{bmatrix} \tag{2.48}$$

The covariance matrix is

$$C = \mathbf{E}[zz^{*T}] = [c_{rs}] \tag{2.49}$$

where

$$\begin{aligned}c_{rs} &= \mathbf{E}[(x_r + jy_r)(x_s - jy_s)] \\ &= 2b_0\left[\frac{1}{1+(f_s-f_r)^2/B_c^2} + j\frac{(f_s-f_r)/B_c}{1+(f_r-f_s)^2/B_c^2}\right]\end{aligned} \tag{2.50}$$

Therefore

$$c_{rs} = \frac{2b_0}{1 + j(f_r - f_s)/B_c} \tag{2.51}$$

$\boldsymbol{C}$ is a positive definite Hermitian matrix as $c_{rs} = c_{sr}^*$ and can be factored into $\boldsymbol{C} = \boldsymbol{T}\boldsymbol{T}^{*T}$. Letting $\boldsymbol{z} = \boldsymbol{T}\boldsymbol{w}$, where the elements of $\boldsymbol{w}$ are independent complex Gaussian variables

$$\begin{aligned} \mathbf{E}[\boldsymbol{z}\boldsymbol{z}^{*T}] &= \mathbf{E}[\boldsymbol{T}\boldsymbol{w}\boldsymbol{w}^{*T}\boldsymbol{T}^{*T}] \\ &= \boldsymbol{T}\mathbf{E}[\boldsymbol{w}\boldsymbol{w}^{*T}]\boldsymbol{T}^{*T} \end{aligned} \tag{2.52}$$

If it is arranged such that $\mathbf{E}[\boldsymbol{w}\boldsymbol{w}^{*T}] = \boldsymbol{I}$ (identity matrix), then the complex Gaussian $w_i = u_i + jv_i$ is such that u_i and v_i are independent, and

$$\mathbf{E}[u_i] = \mathbf{E}[v_i] = 0 \tag{2.53}$$

$$\mathbf{E}[u_i^2] = \mathbf{E}[v_i^2] = 1/2 \tag{2.54}$$

The matrix $\boldsymbol{T}$ may be chosen to be lower triangular

$$\boldsymbol{T} = \begin{bmatrix} t_{00} & 0 & \cdots & 0 \\ t_{10} & t_{11} & 0 & \vdots \\ \vdots & & \ddots & \\ t_{(L-1)(L-1)} & \cdots & & t_{(L-1)(L-1)} \end{bmatrix} \tag{2.55}$$

Since $\boldsymbol{T}\boldsymbol{T}^{*T} = \boldsymbol{C}$, for the first row of $\boldsymbol{T}$

$$t_{00}^2 = c_{00} = 2b_0 \tag{2.56}$$

$$t_{00}t_{r0}^* = c_{0r} \quad \text{so} \quad t_{r0} = c_{r0}/t_{00} \quad \text{for} \quad r = 1, \ldots, L-1 \tag{2.57}$$

For the following rows, it can be shown that

$$t_{rs} = \frac{c_{rs} - \sum_{i=0}^{s-1} t_{si}^* t_{ri}}{t_{ss}} \qquad r = s+1, \ldots, L-1 \tag{2.58}$$

$$t_{ss} = \sqrt{c_{ss} - \sum_{i=0}^{s-1} |t_{si}|^2} \tag{2.59}$$

The procedure used to generate L correlated values of α_l^2 can be summarised as

1. Find $\boldsymbol{T}$ by above equations
2. Generate L pairs of independent, zero-mean Gaussian variables u_l, v_l each with variance $b_0 = 1/2$, to form w such that $w_l = u_l + jv_l$

3. Form the correlated complex Gaussian vector $\boldsymbol{z} = \boldsymbol{T}\boldsymbol{w}$

4. Form the L values of $\alpha_l^2 = |z_l|^2$

2.3 Diversity Systems

The form of diversity proposed by Nettleton and Cooper, which shall be referred to "alternate antenna/channel diversity", requires that adjacent frequency channels used by the receiver be fed from alternate antennae. If the separation between antennae is adequate, the correlation between the signal envelopes from each antenna will be negligible. The correlation between frequency channels an odd number of channels apart will therefore be effectively reduced by the correlation ρ_a between antennae, and hence may be made very small. This form of diversity was investigated by [24] and results were duplicated here for comparison with other forms of diversity.

In addition to the form of diversity proposed by [24], there exist several types of diversity which have been investigated for use in FM mobile radio systems.

1. Maximal ratio combining: signals from the branches fed by different antennae are co-phased, then weighted proportionally to their signal voltage to noise power ratio and summed before being demodulated.

2. Equal gain combining is a simpler form of diversity. Instead of maximising the output signal to noise ratio by adjusting the weighting on each branch, equal gains are used. Performance is not much worse than for maximal ratio combining, and no knowledge of the signal to noise ratio is required.

3. Selection diversity is where the signal to noise ratio of the M branches is monitored constantly and the signal is selected from the antenna with the best signal to noise ratio. In practice, signal strength is used a a guide to signal to noise ratio.

4. Switched diversity commonly uses two antennae. If the instantaneous signal envelope from the antenna under current use drops below a particular threshold, the receiver switches to signals from the other antenna. The probability of both antennae being in a fade simultaneously is very low. The performance is inferior to selection diversity.

The application of these diversity systems to the FH-DPSK system provides new results and may be compared with the results of Nettleton and Cooper to obtain a measure of the relative performance with correlated and uncorrelated fading. Practical implementation of some of the diversity schemes is likely to be quite complex. However, the modelling of such a system gives a guide to what performance improvements would be expected if such a system could be built. Modelling this situation can be achieved quite simply by an adaptation of the method of [9].

From previous discussions, the signal component envelopes at the output of two matched bandpass filters at a particular frequency l, corresponding to a two branch diversity scheme, are

$$r_{l_1}(t) = \sqrt{2S}\alpha_{l_1}\beta(t)$$
$$r_{l_2}(t) = \sqrt{2S}\alpha_{l_2}\beta(t)$$

Simulating switching diversity would require the values of fading used in the evaluation to be correlated in time as well as frequency. This is not possible to incorporate into the method being used here. Selection diversity is easily modelled: the two values of r_l are generated and the larger chosen – this corresponds to choosing the larger value of α_l. In practice, the system would require two sets of delay lines and matched filters. Both branch signals would have to be stored for a a complete frame in order to compare the phases for the differential decoding to function on switching, or else errors would result on cut-over. The program assumes that individual channels can be picked from each antenna, which is the best possible scenario.

For maximal ratio combining, the rule is that the two signals are co-phased and combined such that the resultant envelope magnitude on each channel is

$r = a_{l_1} r_{l_1} + a_{l_2} r_{l_2}$. The optimum value of a_{l_j} to maximise the signal to noise ratio is given by [2] $a_{l_j} = r_{l_j} / < n_{l_j}^2 >$, where $< n_l^2 >$ is the noise variance on the jth branch at the lth frequency. Assuming that the noise level on each branch at a particular frequency will be equal,

$$a_{l_j} = \frac{\sqrt{2S}\beta(t)\alpha_{l_j}}{\sigma_n^2} \tag{2.60}$$

Now the total signal to noise ratio of the maximal ratio combined signal is the sum of the component signal to noise ratios. Considering one frequency channel only, with the weights allocated to each of the inputs being a_1 and a_2,

$$\begin{aligned}
\text{Total SNR} &= \text{SNR}_1 + \text{SNR}_2 \\
&= \frac{r_1^2}{2\sigma_n^2} + \frac{r_2^2}{2\sigma_n^2} \\
&= \frac{(a_1 r_1 + a_2 r_2)^2}{2\sigma_n^2 (a_1^2 + a_2^2)} \\
&= \left(\frac{(a_1 r_1 + a_2 r_2)}{\sqrt{a_1^2 + a_2^2}} \right)^2 \left[2\sigma_n^2 \right]^{-1} \\
&= \frac{r_m^2}{2\sigma_n^2}
\end{aligned}$$

The effective envelope magnitude r_m used is

$$\begin{aligned}
r_m &= \frac{a_1 r_1 + a_2 r_2}{\sqrt{a_1^2 + a_2^2}} \\
&= \frac{a_1 r_1 \left(1 + (a_2 r_2)/(a_1 r_1)\right)}{a_1 \sqrt{1 + (a_2/a_1)^2}} \\
&= \frac{r_1 \left(1 + (\alpha_2/\alpha_1)^2\right)}{\sqrt{1 + (\alpha_2/\alpha_1)^2}} \\
&= r_1 \sqrt{1 + (\alpha_2/\alpha_1)^2} \\
&= \sqrt{2S}\beta(t)[\alpha_1^2 + \alpha_2^2]^{1/2}
\end{aligned}$$

Hence to model maximal ratio combining, it is sufficient to form α_1^2 and α_2^2 for each channel and to use the combined value $\alpha_m^2 = \alpha_1^2 + \alpha_2^2$ in the evaluation of equation (2.26).

For the case of equal gain combining, on each channel the envelope and SNR is

$$r_e = r_1 + r_2$$

$$\begin{aligned} \text{SNR} &= \frac{(r_1 + r_2)^2}{2(2\sigma_n^2)} \\ &= \frac{(\sqrt{2S}\beta(t))^2(\alpha_1 + \alpha_2)^2}{2(2\sigma_n^2)} \\ &= \frac{(\sqrt{2S}\beta(t))^2}{2\sigma_n^2}\left(\frac{\alpha_1 + \alpha_2}{\sqrt{2}}\right)^2 \end{aligned}$$

Hence α_1, α_2 are generated and the value

$$\alpha_e^2 = (\alpha_1 + \alpha_2)^2/2 \tag{2.61}$$

is used in the evaluation of probability of error.

The envelopes from the two antenna are assumed to have zero cross-correlation. This is the optimum situation, but is reasonably well approximated in practice, as the antennae on vehicles may be separated by several wavelengths of the carrier.

2.4 Results

Evaluation of the probability of error, given by equation 2.31, took place at points of bit-energy-to-noise-density ratio E_b/N_0 spaced 0.5 dB apart, with 100 iterations of the Monte Carlo evaluation of the probability of error being used to obtain a mean value. To speed up the program execution, the distribution function $\Psi(x)$ of the noise terms was computed once only and a cubic spline fitted and used in the program, with no significant loss of accuracy. Results were obtained for various coherence bandwidths, with the ratio of coherence bandwidth to total available bandwidth being set to $B_c/W = 0.01, 0.05, 0.1$. The case of $B_c/W \leq 0.01$ (shown as $B_c/W = 0.00$ in the figures) corresponds to the case where flat fading is assumed to occur over each channel and each channel fades independently: the ideal fading conditions used by [24] in the multiple narrowband model. The frequency channels were assumed to be separated by a bandwidth $\Delta f = W/L$.

These results are shown in figures 2.1–2.3. As the individual points on each curve exhibited a degree of uncertainty, owing to the finite number (100) of Monte

Carlo iterations used to obtain each point, a fourth order polynomial was fitted to the points by a weighted least mean squares technique. The weighting used on each point was inversely proportional to the variance of the point around its mean value, and effectively weighted each point by its reliability. The sensitivity of the fitted curves to fluctuations in results caused by different seeds is not great, as evidenced by the series of graphs, figures 2.4–2.6, of results for two seeds for the case of fading with no diversity and increasing coherence bandwidths. In addition, each of the simulations in the diversity comparison used the same initial seed for the random generator, so the performance of the diversity systems is simulated for an identical set of input conditions, and hence the interpolated curves can be expected to be positioned fairly accurately with respect to one another.

For the ideal fading case where each channel fades independently, the gain using the Nettleton and Cooper method is nil. The maximal ratio combining results are almost as good as for the case of reception with no fading and a single antenna. The equal gain combining and selection diversity performance results are progressively about half a decibel worse than the maximal ratio combining results at bit error rate of 10^{-3}. When the coherence bandwidth is increased to 5% of the total bandwidth, all the curves show a degradation in performance. The traditional diversity methods still produce better results than the ideal channel, no diversity case. The alternate antenna/channel diversity scheme does improve on the no-diversity results, but not by a large amount, and is significantly worse than the traditional diversity techniques. In particular, the use of selection diversity, which does not require co-phasing (which is likely to be very difficult to implement), can be seen to give better results. In system component terms, however, the alternate antenna/channel diversity schemes do make a significant improvement on the no-diversity with small hardware and implementation costs.

This trend is continued for the case where $B_c/W = 0.10$. It is obvious that wide coherence bandwidths do have a significant effect on the number of users that may use the system, as the required E_b/N_0 to maintain a $P_b = 10^{-3}$ is significantly increased. As frequency hopping transmission relies on the independence of the

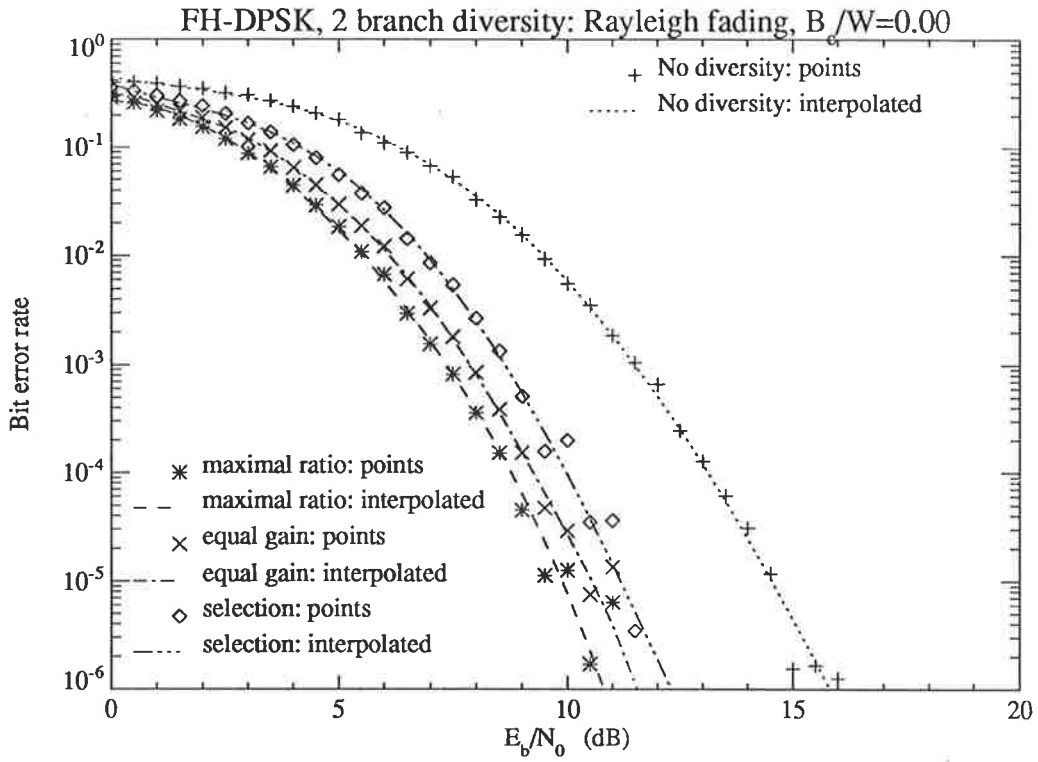

Figure 2.1: Bit error rates of the diversity schemes for two antennae, with uncorrelated Rayleigh fading on each channel.

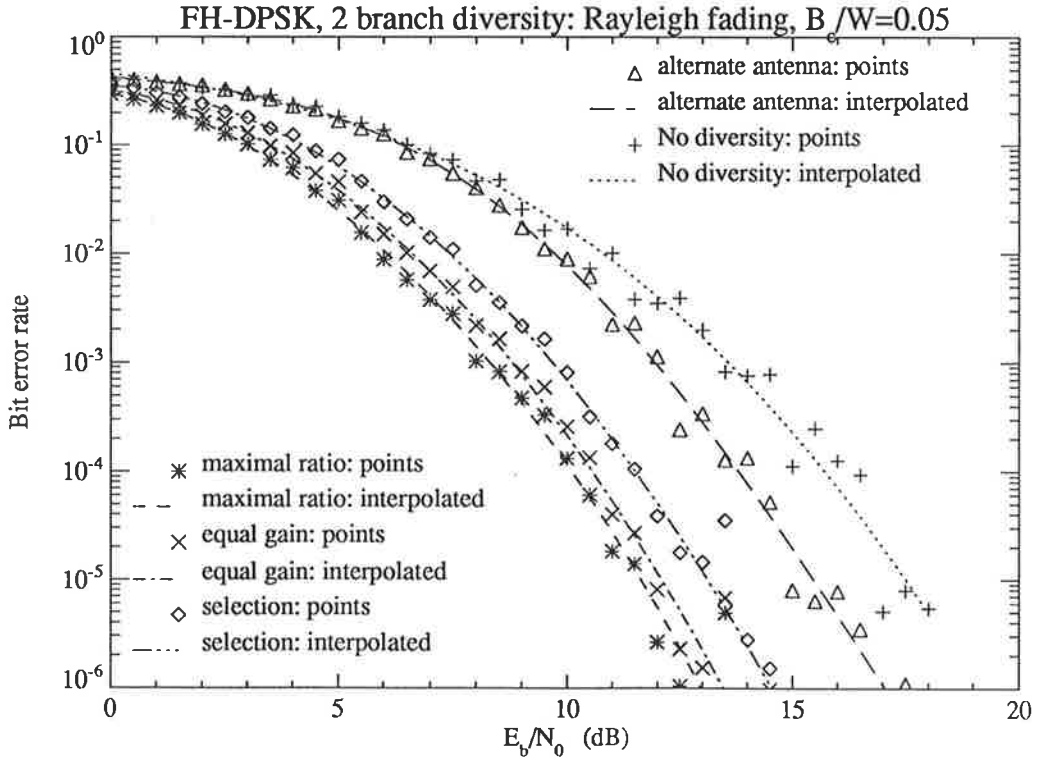

Figure 2.2: Bit error rates of the diversity schemes for two antennae, with correlated Rayleigh fading on each channel, $B_c/W = 0.05$.

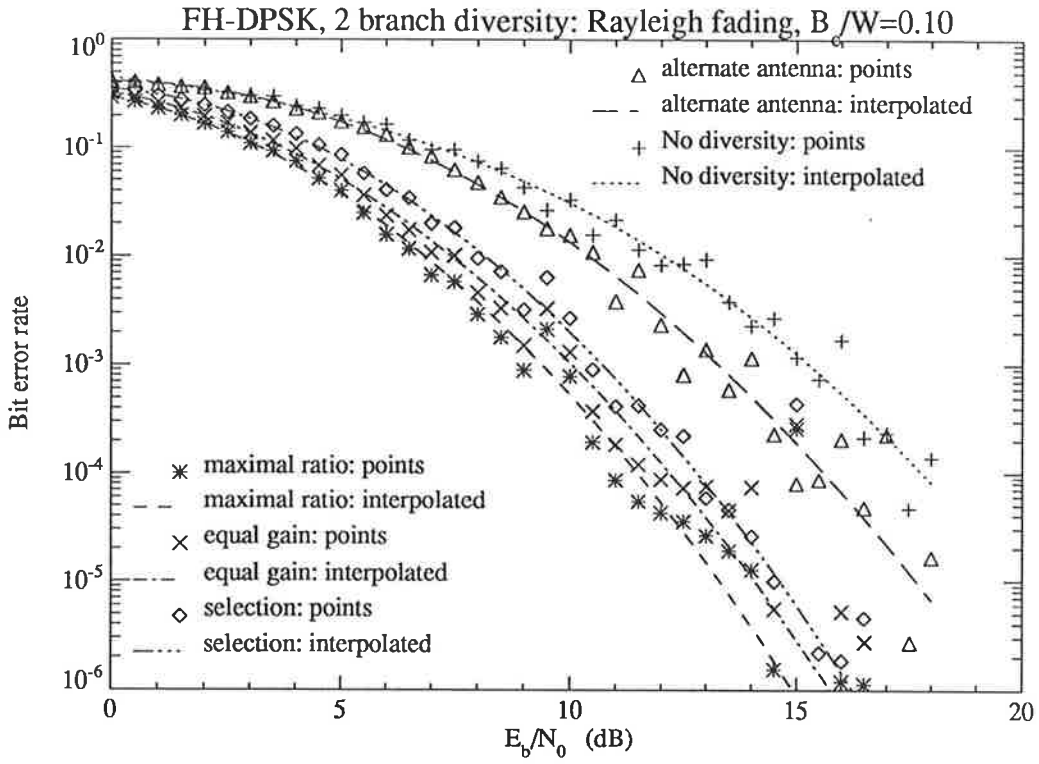

Figure 2.3: Bit error rates of the diversity schemes for two antennae, with correlated Rayleigh fading on each channel, $B_c/W = 0.10$.

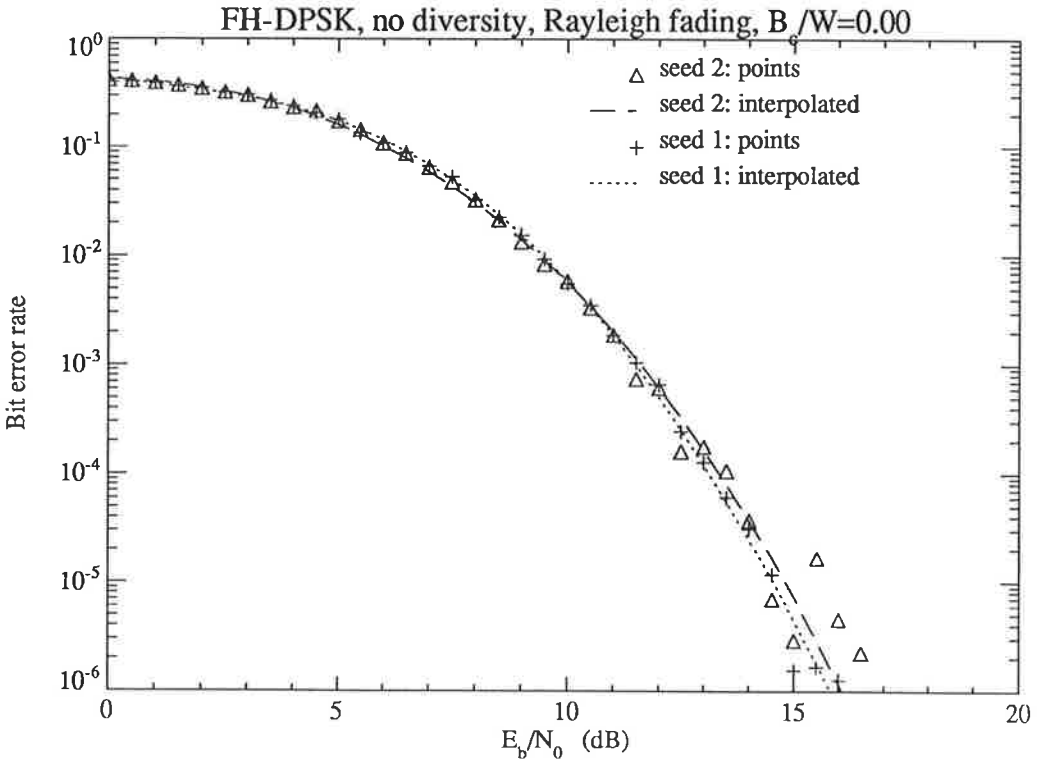

Figure 2.4: Bit error rates for two different random seeds, no diversity, with uncorrelated Rayleigh fading on each channel.

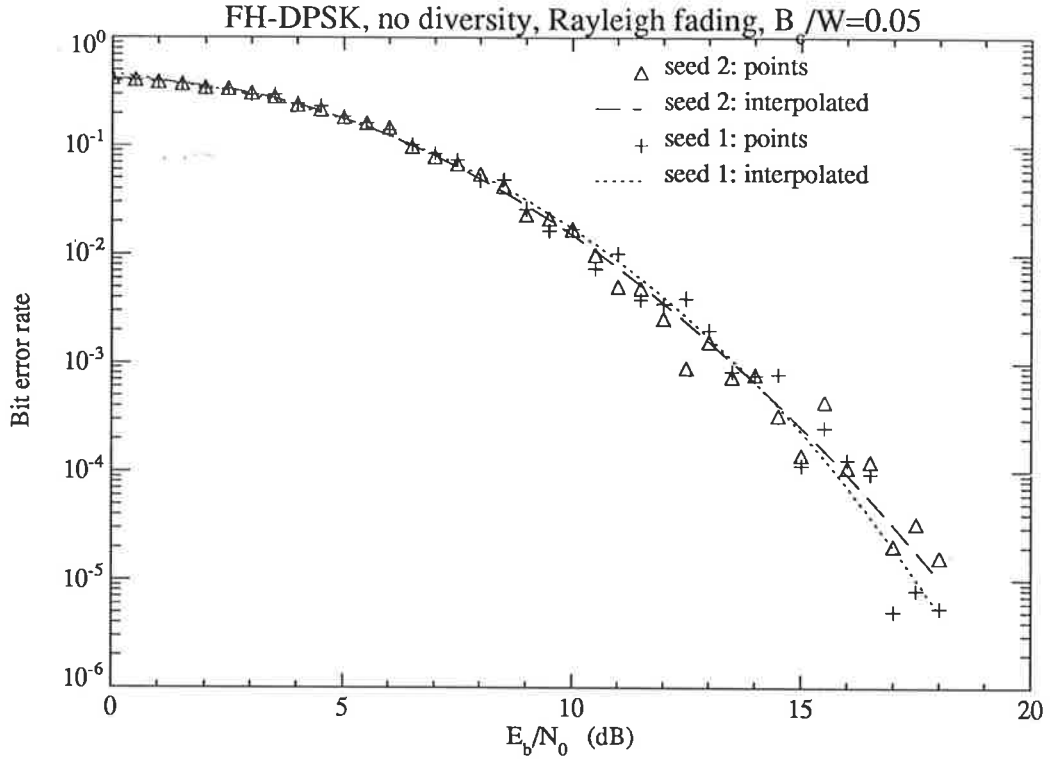

Figure 2.5: Bit error rates for two different random seeds, with correlated Rayleigh fading on each channel, $B_c/W = 0.05$.

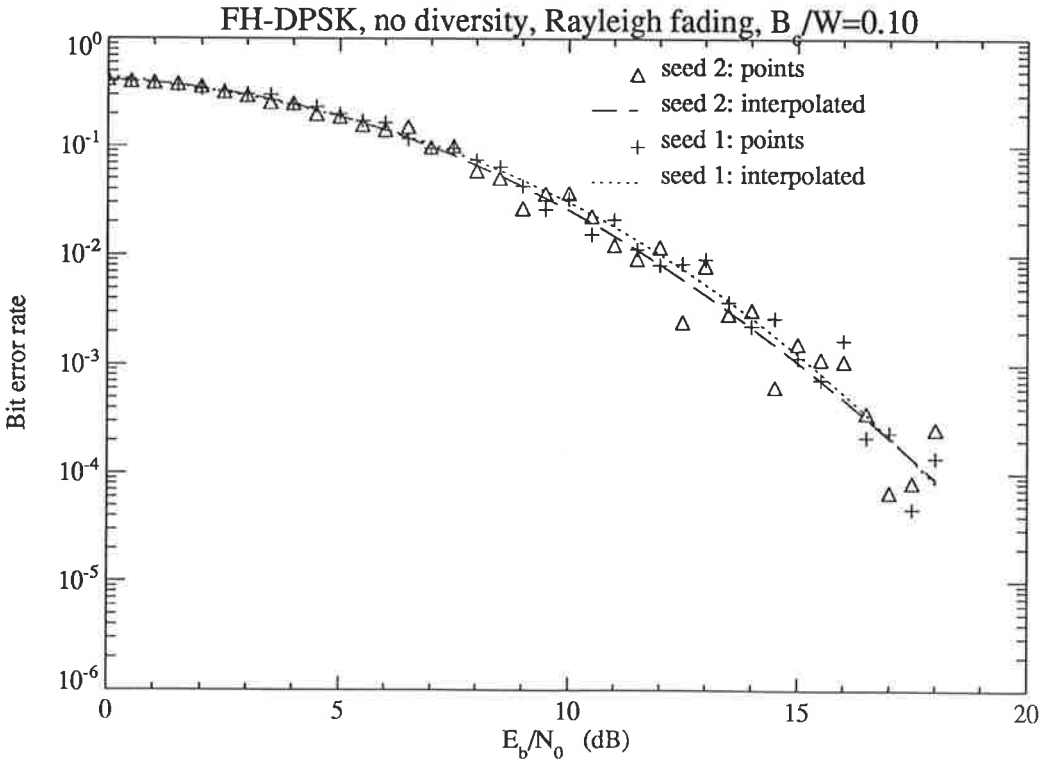

Figure 2.6: Bit error rates for two different random seeds, with correlated Rayleigh fading on each channel, $B_c/W = 0.10$.

channels to obtain frequency diversity, this is not unexpected, but it shows a need for diversity if full capacity is to be maintained and the fading channel is subject to wide coherence bandwidths. However, if diversity systems are to be considered, the performance improvements to frequency hopped transmission are far less than can be gained for conventional frequency division multiplexed systems, and involve much greater complexity.

As the above results are derived purely for transmission through fading channels with additive white Gaussian noise (in [24] the AWGN interference model was assumed), they can only be used as a guide to the best performance in the presence of tone interferers. Under the tone interferer model, the average E_b/N_0 at the receiver would be at least 15 dB which would give a very low error probability in the absence of interference. On the downlink (base to mobile), user sequences within a cell could be arranged to be orthogonal, and therefore be received without interference. The above results would apply to this situation.

The ultimate effect of very wide coherence bandwidths is equivalent to shadow fading, and the trend shows that large shadow fading variations will cause severe problems for reception. Of course, shadow fading is a comparatively long time scale effect, which extends over a large area. Diversity will only mitigate the effect of shadow fading very slightly. Other than power control, the only possible counter to shadow fading is by switching to another base station when the average signal strength drops below a threshold. Depending on the locations of the vehicle and the surrounding base stations, this may not improve the situation, and thus it can be seen that shadow fading is as much a problem for frequency hopping as for conventional FDM systems.

Chapter 3

Simulation Theory and Strategy

3.1 Why Simulation?

The analysis involved in frequency hopping schemes involves a great many variables, such as frequency, time delays and fading magnitude and phase for the desired signal, interferers and noise. To manage the complexity of the mathematics and obtain tractable expressions and hence results, it is necessary to make some approximations and assumptions as to the nature of quantities such as the sums and products of random variables. It may be thought that a large number of random variables would in fact enable better approximations to be made via the central limit theorem and other such devices. However, as has been pointed out in [26], the automatic assumption of Gaussian statistics can lead to results which are quite different to those produced by a truer estimate. Therefore in assessing the performance of different receivers in different fading environments, it is important to have a set of base assumptions which are common to all situations.

This has not been the case in the work published in FH-DPSK systems. In particular, the cases of hard-limited combining and band-pass hard-limiting are both claimed to give much better results than the linear receiver. While an analytic formulation for the receiver with hard decisions on each chip exists, the same is not

true for the situation where the receiver has hard-limiters after the bandpass filters and before the quadratic detectors, and linearly combines the detector outputs [37]. For this receiver, Matsumoto and Cooper derived a rather complex expression for the output for the hard limiter and then made some unsupported assumptions as to the Gaussian nature of the detector outputs and their independence. The result was an integral expression for the probability of bit error which still required Monte Carlo simulation to evaluate, using the assumed distributions for various parameters. The question that must be raised is how does this model compare with the hard decision decoding case? Matsumoto and Cooper assumed a noiseless system and overlapping frequency channels with single interferers appearing randomly somewhere within the main lobe of the channel bandpass filters. Due to the formulation of the problem, it is not easy to either compare the results or to obtain an estimate of the number of users who may use the system for the pre-detection hard-limiting receiver.

The advantage enjoyed by a direct simulation is the flexibility in modelling while maintaining a constant set of base assumptions. Small changes to the program are all that is necessary to model the different types of receiver. In addition, by including correlation between the consecutive samples of the complex fading envelope, it is possible to study if this is an important effect, as it has been found to cause an irreducible error rate for single channel DPSK transmission. This continuity in time means the burst error behaviour of the system can be observed. This is important if considering other coding schemes, such as convolutional or concatenated schemes. For these reasons, a series of simulation programs were written to model the reception of frequency hopping signals transmitted through the urban mobile radio channel. As each program is formulated in a reasonably modular fashion, a variety of coding schemes may be incorporated without too much effort.

Another use of the simulation is simply checking how close the analysis and derived upper bounds are to the real performance for the different models. The simulation can be extended to model as large a system as desired, (dependent on the amount of computing power and time available). In this fashion, new light can be shed on the performance of the different systems in a multiple cell context.

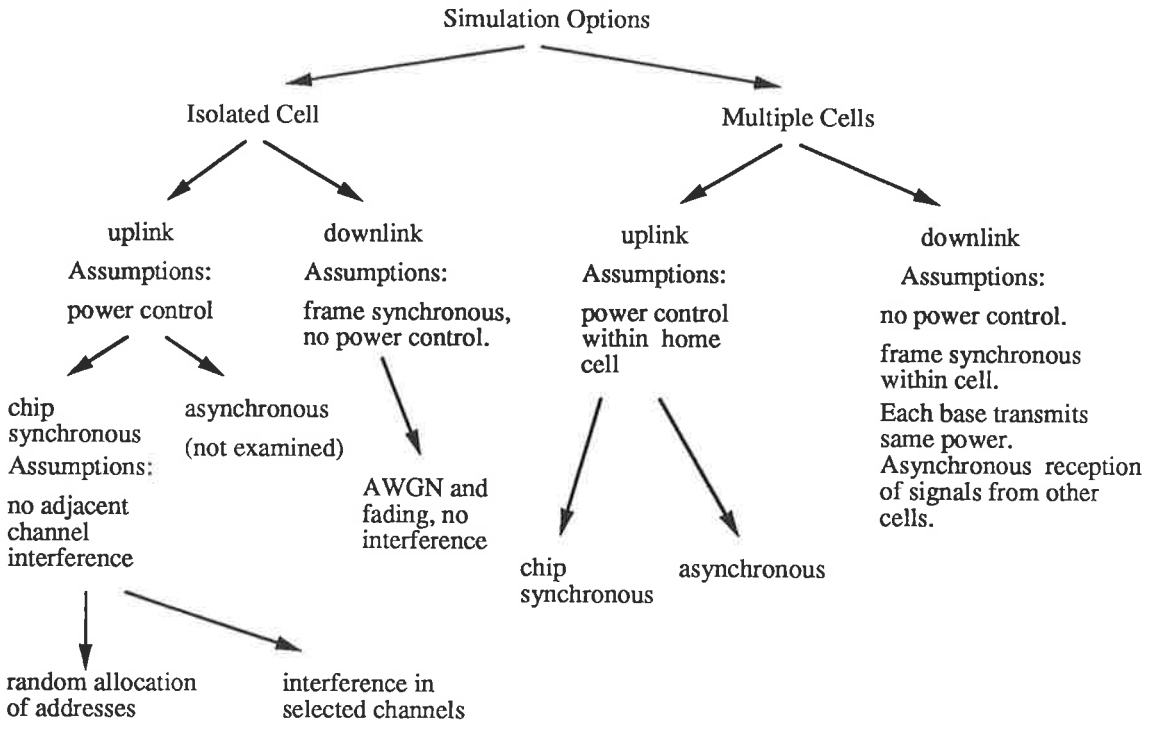

Figure 3.1: Simulation choices and assumptions in modelling the FH-DPSK mobile radio system.

3.2 Simulation Structure

The FH-DPSK system has many parameters which may be set independently, resulting in many system configurations available for simulation. However, some combinations of system variables are of more interest than others, and hence these cases were simulated. The system parameters and assumptions made with each choice are shown in figure 3.1. These assumptions determine what variables need to be simulated and how they are represented. For example, the assumption of uplink power control within a cell means that all transmissions from the mobile to the base are received with equal power, as the shadow fading and attenuation effects are counteracted. Thus within an isolated cell, attenuation and shadow fading on the uplink is set to a constant value of unity and can thus be ignored. Downlink transmission within isolated cell assumes that frame synchronism exists, implying that no interference from other users within the cell is recorded. (In fact, some will

exist due to delay spread, but this is ignored.) Hence only the effects of fading and additive white Gaussian noise are modelled; note that this is the situation assumed by the AWGN interference model.

For the case of multiple cells, it is assumed that power control exists on the uplink between users and their respective current base stations. Thus all transmissions from within a cell are received with the same power. If the users' transmissions are received asynchronously, such that an interfering chip has a fractional overlap of ϵ with respect to the target user's chip, it can be shown that [23] the envelope of the interfering signal is multiplied by ϵ in the case of co-channel interference, and by $[\sin(\pi\Delta f\epsilon\tau)]/(\pi\Delta f\epsilon\tau)$ in the case of interference from an adjacent channel located Δf away. Signals from outside the central cell are received with attenuation and shadow fading, adjusted to account for the power control within their respective home cells.

When dealing with a large number of channels and users as found in a frequency hopping multiple access scheme, it is important to model the parameters in the most efficient way. Failure to do so results in unrealistic run times, and even the most efficient code must run for a large amount of CPU time to get accurate Monte Carlo estimates of error rates around the level of $P_b = 10^{-4}$—10^{-5}. Techniques such as importance sampling [61] have been developed to speed up simulations. Unfortunately, while these techniques have found wide use in satellite and optical fibre transmission modelling, their use in a frequency hopping situation does not seem to be clearcut. The number of variables which interact in complex and sometimes non-linear ways mean that changing the variance of one or more parameters by a known amount (done to create more error events in a given time) has an unpredictable effect on the error rate. For this reason, this technique was not used in this simulation.

The method chosen to simulate the system is to consider the transmissions of a single user, modelling the complex envelopes of the de-hopped carriers at the output of the IF bandpass filters. Each channel is assumed to experience fast fading with independent Rayleigh statistics, with the local mean signal amplitude determined

by attenuation and shadow fading. As the local mean remains constant for the simulation duration, the Rayleigh envelope may be generated with unity average power and then multiplied by factors for signal-to-noise ratio and attenuation/shadow fading to give the correct signal magnitude. Interferers are modelled as independent Rayleigh fading tones located within a channel with their own shadow fading and with a hopping sequence timing overlap referred to that of the target user.

In this simulation program, only one sample per time chip is used to represent the signal. This corresponds to modelling the signal at the time of peak output from the matched bandpass filter of a the form of receiver described by Nettleton and Cooper, shown in figure 1.8. Alternatively, the signal can be viewed as being modelled at the sample times of a correlation receiver as shown in the next chapter, figure 4.1. As the program does not trace the waveform in each chip, ideal threshold detection and negligible intersymbol interference are assumed. It is also assumed that the user's transmissions can be acquired and symbol timing maintained. However, all analyses have assumed these properties. The issue of sample timing is discussed in [24], where it was concluded that the probability of threshold errors is at least an order of magnitude lower than the bit error rate and hence is not a significant source of error. Practical considerations also intervene here, as experience shows that only one sample per chip can be taken in order to have reasonable run times.

Each frequency channel used by the target user is treated as an independent entity. For each frequency therefore, a store of information is kept in a record structure consisting of the user number, slow fading envelope multiplier, and current fast fading generation coefficients. In addition, a pointer is kept to a linked list of other records corresponding to interferers present within that channel. This situation is pictured in figure 3.2.

The presence of other users in the system may be specified in two ways. For the isolated cell with the uplink being modelled and chip synchronism assumed, the case treated by Yue [35], interferers may be explicitly specified to be present in certain frequencies. This enables assessment of the performance of the various types of

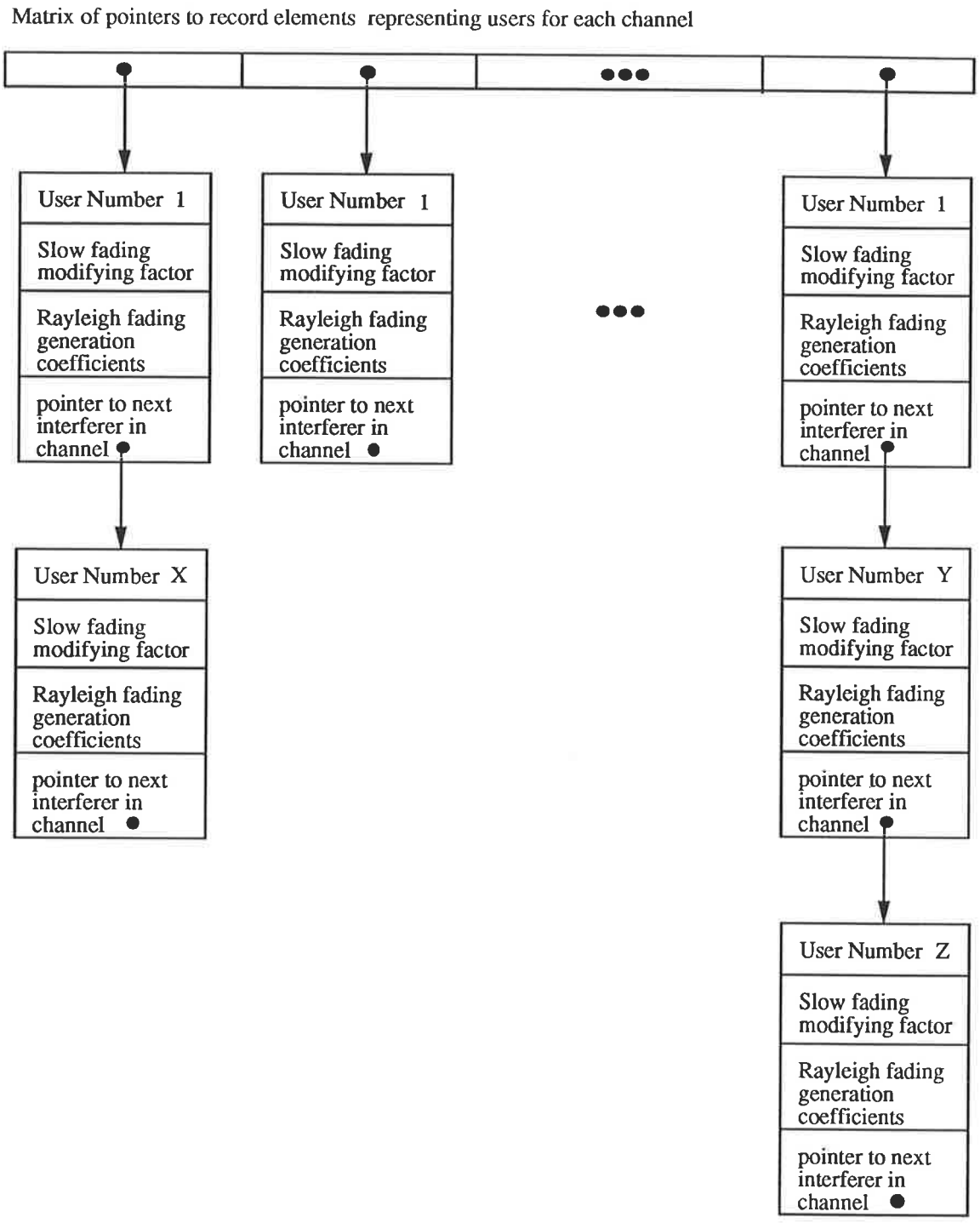

Figure 3.2: Structure of linked lists of records used to hold information for users in each frequency channel.

receivers under identical conditions. Alternatively, the number of interferers may be specified and their positions allocated at random from a uniform distribution over the area. In this case, if frame synchronism exists, the user sequences are chosen from a one-coincidence set in such a way as to minimize the cross-correlation. This results in no interference for all practical numbers of users. If chip or no synchronism is specified, the frequency hopping address vectors are chosen from a one-coincidence address set with a shift that is a random variable uniformly distributed over the hopping sequence period. A search is conducted to find all frequency clashes with the sequence of the target user. When a clash is detected, the parameters relating to that particular interferer are generated in an identical fashion to those of the target user, except that the interferer is only present in one frequency channel. The interferer record is then inserted into a linked list stemming from the appropriate frequency record of the target user. As many interferers as necessary may be chained together in the list representing a particular frequency channel.

The procedure for initializing the uplink simulations may be summarized as follows:

1. If random assignment of users is being used, generate position (uniform distribution over area), speed (uniform distribution over 10–110 km/hr) and hopping sequence of each user, and generate overlaps in whole chips and fractions of a chip between the target user's hopping sequence and those of the other users.

2. If multiple cells are being modelled, generate shadow fading variables for transmissions received from users in other cells (assuming power control means that shadow fading is set to 1.0 for the target user's home cell).

3. Check for clashes between the hopping sequences of the target user and all other users. If the hopping sequences are allowed to be entirely asynchronous (as opposed to chip synchronous, where the sequences are randomly shifted by an integral number of chips), adjacent channel interference will occur as well as the co-channel interference. Adjacent channel interference is taken as

occurring when another user is present in a channel immediately next to that of the target user, for some fraction of the target user's chip period.

4. If a clash occurs, the shadow fading coefficient is adjusted in proportion to the fractional chip overlap and whether it is co-channel or adjacent channel interference. An entry describing the interferer's state (*ie* user number, adjusted shadow fading, Rayleigh fading variables) , is generated in the linked list for that frequency. For the isolated cell, chip synchronous simulation with interferers specified to be in particular arrangements, only this last step is performed.

Similarly, downlink initialization follows a similar sequence:

1. If random assignment of users is being used, allocate the hopping sequence of each user, and generate overlaps in whole chips and fractions of a chip between the hopping sequence of the central base station (communicating with the target user) and transmissions from other base stations. The hopping sequences within a cell are frame synchronous, hence no interference comes from within the central cell (for less users than the total number of channels in the band).

2. If multiple cells are being modelled, generate shadow fading variables for transmissions received from all base stations.

3. Check for clashes between the hopping sequences of the target user and all other users. As the hopping sequences from foreign base stations are asynchronous with respect to the target user's sequence, adjacent channel interference will occur as well as co-channel interference. Only the first adjacent channels on each side are considered to provide significant interference.

4. If a clash occurs, the shadow fading coefficient is adjusted in proportion to the fractional chip overlap and whether it is co-channel or adjacent channel interference. An entry describing the interferer's state (*ie* user number, adjusted

shadow fading, Rayleigh fading variables) , is generated in the linked list for that frequency.

The coefficients for each frequency for the target user and interferers are used to generate a set of initial values for the signals received during an assumed previous frame. Once all the preliminary variables have been set, the simulation proceeds to model the reception of successive codewords until enough errors have been counted or the maximum number of codewords sent. This process is illustrated by the flow chart in figure 3.3.

The message bits or symbols are generated from the appropriate uniformly distributed symbol set by a pseudo-random number generator with good correlation properties. The ISML random number generator was used for most simulations, because of its proven lack of bias and long sequence length [62].

The message bits are then encoded into the appropriate code bits for transmission. The code bits are used to specify the differential coding between the previous transmission and the current one at the particular frequency in the cycle. This corresponds to a 0 or π radians phase shift of the carrier, or alternatively as used here, a ± 1 multiplication of the complex envelope. New values for the inphase and quadrature components of the complex envelope at the particular frequency are generated for the target signal, and multiplied by the appropriate slow fading coefficient. The linked list of interferers is then followed, with each interferer envelope being updated and multiplied by the slow fading modifier and by ± 1 randomly to simulate the data encoding, before being added to the sum. The inphase and quadrature components of the total complex fading envelope are scaled by the signal to noise ratio and then have zero-mean Gaussian noise added. This noise is simple to generate by a number of methods. Again, for convenience and to ensure uncorrelated samples and lack of bias in the samples, the IMSL software library was used, generating values by the inverse cumulative distribution method. (This is not necessary: a more portable package could have been produced by writing the relevant uniform and Gaussian random variate generation routines. Algorithms for such procedures

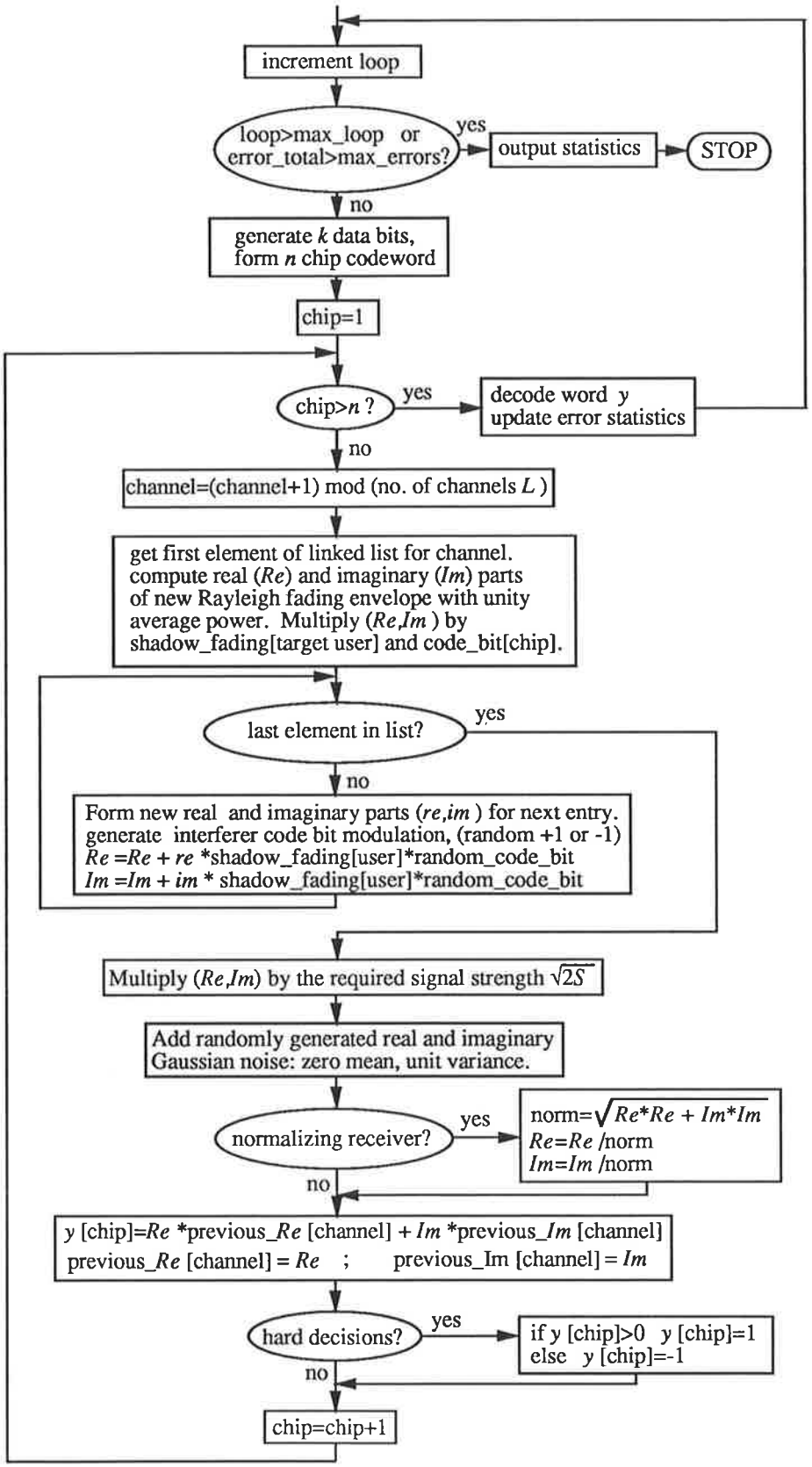

Figure 3.3: Flow chart of the main body of the program, executed after initialization of all variables.

with good randomness properties are well known, for example [63,64].)

Finally, the complex envelope is multiplied by the delayed envelope from the previous frame in a quadratic detector. This consists simply of multiplying the two in-phase components together and the two quadrature components together, and then summing the two products. This output is then stored in a register until all the chips necessary to form a unit of the inner most decoding cycle have been received, and a decision made on the contents of all the registers. Each time a code bit is transmitted, the frequency channel is incremented around the frequency hopping cycle by one channel. Note that the number of channels need not necessarily equal a particular coding cycle length.

3.3 Simulation of Fast Fading

The most widely used model for fast fading on an urban radio channel at UHF is that of Clarke [7], discussed in section 1.1.1. Many other models have also been proposed, using such random variable distributions as the Suzuki, Weibull, and Nakagami-m distributions [65] to model the variability of the received signal. Aulin [66] has also produced a three-dimensional extension to Clarke's plane model. While these models appear to offer improved fits to much of the measured data [67,65], none of them can claim to adequately represent the channel in all circumstances. It seems unlikely that a single model can match the great diversity of fading which is exhibited around cities and suburban areas. The Rayleigh fast-fading, lognormal shadow-fading model has been shown to be a good fit to much measured data [5,67,68] and is of an easily manipulated analytic form. The Weibull and Nakagami-m distributions are more complicated exponential distributions, and the Suzuki distribution is an integral form which requires numerical evaluation. Thus analytically, the Rayleigh distribution is a good choice for the distribution of the envelope of the fast fading. It tends to give the worst case results but is also fairly accurate in many real life situations.

As with analytical models, there have been a large number of methods developed for simulation of the urban mobile UHF radio channel on computers. These can be very detailed, including the effects of Doppler shift, frequency selective fading due to time delay spread, wide coherence bandwidths, specular components and much more. One approach has been to model streetscapes and to compute the effects of the summation of the scattered reflections as the vehicle moves down the street. Such models as these [69,70,71] can be made to give very similar results to real situations, at the cost of much complexity.

What is surprising about many of these simulations is that while they often succeed in matching their models to measured data with a high degree of precision, in a significant number of cases there is often not much difference between their results and those given by a simple Rayleigh fading model [65,68]. It would appear therefore that the Rayleigh fading model, while not strictly accurate for much of the time, is correct often enough to make it very useful and can be thought of as a worst case model. The use of the Rayleigh model for both simulation and analysis enables a comparison between the two methods of deriving results. Hence the approach taken has been to use the Rayleigh distribution to describe the fast fading behaviour, with a lognormal distribution for the local area mean as discussed in section 1.1.1.

3.3.1 Generation of Rayleigh Fading Coefficients

On an individual radio channel in a band, fading may be characterised as being fast or slow, and frequency selective or non-selective. All analyses of the system so far have considered cases of slow fading, with the complex envelope not changing between adjacent DPSK pulses. However, for the mobile channel, fast fading should be considered, as the complex envelope can change significantly over a hopping sequence period. In particular, when the magnitude of the fading envelope is small, phase excursions can be very large. The severity of this effect increases with maximum Doppler shift and leads to an irreducible error rate for conventional DPSK

transmission whereby no increase in transmitted power will improve the bit error rate. Hence the simulation is designed to take account of this correlation between successive fading coefficients.

The frequency selectivity of the channel is the next issue to be discussed. Measured frequency channels exhibit a coherence bandwidth of between 50kHz and 1MHz. Strictly speaking, a simulation should be able to account for the correlation between frequency channels in a frequency hopping system, or alternatively model frequency selective fading within the individual channel if required. However, the computational load to simulate fast fading with accurate correlation across a large number of frequency channels as well as in time, is very large and would be difficult to run in a realistic time on any supermini type computer.

It is observed in [9] that the channels can be considered essentially independent if the average channel separation is greater than the coherence bandwidth, *i.e.*

$$B_c < W/L$$

where B_c is the coherence bandwidth, W is the total bandwidth available for hopping, and L is the number of frequency channels in one user's cycle. Similarly, if the individual channels have an IF filter main lobe bandwidth of $2/\tau$, where τ is the chip period, frequency selective fading within the band will not occur if

$$2/\tau < B_c$$

If the two conditions are met simultaneously, the situation is one where each channel experiences independent fades, flat across each channel. These assumptions will be made for the majority of the simulation results in this thesis, and are identical to those found in most analyses in the literature. Apart from the results of chapter 2, more information on the degrading effects of wide coherence bandwidths on the probability of error may be obtained from [24,55,32], as it was not considered further here. (It is found that the method used to generate the samples of the complex fading envelope may be adapted to produce correlated fading by a suitable choice of parameters. This can be used to produce correlated fading between frequency channels if desired.) The case of frequency selective fading within a channel is

looked at in [9], wherein it is concluded that for normal values of delay spread and coherence bandwidth, a slight degradation of the pulse will occur, causing the peak output from the matched filter or correlator to be diminished. The degradation in peak output is likely to be less than 3 dB with 90% confidence. However, to model the pulse smearing caused by this fading would require far too many samples per waveform to be practical over the large number of frequency channels that a system hops over.

Therefore the requirement is for a method of generating complex envelope fading coefficients with independent statistics, with Rayleigh distributed magnitude and uniformly distributed phase, suitably correlated in time.

A direct method is to generate the Rayleigh coefficients (or the individual Gaussian quadrature components) independently. These may be correlated by digital filtering. Unfortunately, the digital filter would require a very large number of taps in order to produce variables with the correct power spectral density. The computation time would therefore be unrealistic for a large number of channels.

Alternatively, Fourier transform techniques may be used; Fourier transforming the input Gaussian variables, multiplying by the appropriate filter in the frequency domain, and inverse transforming the resultant. Again, the disadvantage of this method is the amount of computation required in the Fourier transforms. One way of alleviating this is to generate a large number of data files once only, and then read the data in as required during each simulation. The drawback of this method is the large amount of disc storage required: for instance, simulating a system hopping over 32 channels with 18 interferers present would require 50 independent Rayleigh fading data files, of adequate length to simulate low probabilities of error. The amount of storage required would easily exceed 50 megabytes, which was not available on the computer systems used for simulation. As the above methods all have disadvantages, they were not used and instead a different approach was used.

Clarke's theory for the generation of a complex fading envelope with Rayleigh distributed magnitude and uniformly distributed phase arises from the considera-

tion of scatterers uniformly distributed in angle around a moving vehicle. Power is assumed to be received from all sources equally, and a omnidirectional antenna on the vehicle such as a vertical whip is assumed. It seems logical therefore to consider a method of generating the fading which mimics this theory. Such a model has been described by Davis [72] and a variant of this method has also been described in [2, chapter 1] for hardware simulation. Consider a set of n scatterers spaced uniformly in angle around a moving vehicle, on which the receiver is mounted. Incoming signals from the base station will be reflected by the scatterers in the immediate vicinity and received at the vehicle. Each component wave from the scatterer will be received with a carrier Doppler shift in keeping with the angle (from 0 to π radians) its direction of arrival subtends with the direction of motion of the vehicle.

Angles with magnitude less than $\pi/2$ contribute a positive Doppler shift, and magnitude greater than $\pi/2$ a negative Doppler shift. The scatterers may be arranged symmetrically such that they are reflected in the x and y axes, where the x axis is in the direction of motion of the vehicle. For each signal with Doppler shift ω_i, there is also one with a Doppler shift of $-\omega_i$.

Assuming the signal $s(t) = \cos\omega_0 t$ was transmitted, the received signal is therefore:

$$\begin{aligned} v(t) &= \sum_{i=1}^{n} [a_i \cos((\omega_0 + \omega_i)t + \alpha_i) + b_i \cos((\omega_0 - \omega_i)t + \beta_i)] \qquad (3.1) \\ &= \left[\sum_{i=1}^{n} a_i \cos(\omega_i t + \alpha_i) + b_i \cos(\omega_i t - \beta_i)\right] \cos\omega_0 t \\ &\quad - \left[\sum_{i=1}^{n} a_i \sin(\omega_i t + \alpha_i) - b_i \sin(\omega_i t - \beta_i)\right] \sin\omega_0 t \end{aligned}$$

Choosing $a_i = b_i$ gives a fading spectrum symmetrical around ω_0, and the two components will be independent [72]. Choosing a_i to all be equal, such that $a_i = 1/2$ will give the best approximation to the Gaussian distribution for the components for the fewest number of scatterers. Hence

$$\begin{aligned} v(t) &= \left[\sum_{i=1}^{n} \cos\theta_i \cos(\omega_i t + \phi_i)\right] \cos\omega_0 t - \left[\sum_{i=1}^{n} \sin\theta_i \cos(\omega_i t + \phi_i)\right] \sin\omega_0 t \\ &= \Re\left[e^{j\omega_0 t} z(t)\right] \end{aligned}$$

where $\phi_i = (\alpha_i - \beta_i)/2$

$\theta_i = (\alpha_i + \beta_i)/2$

$\Re[.]$ denotes real part.

As α_i, β_i are independently and uniformly distributed on $[0, 2\pi)$, then so are ϕ_i, θ_i.

It is convenient to deal with the complex fading envelope $z(t)$.

$$z(t) = \sum_{i=1}^{n} e^{j\theta_i} \cos(\omega_i t + \phi_i) \tag{3.2}$$

By the above analysis it is clear that there is no distinction between positive and negative Doppler frequencies, and only positive Doppler frequencies need be considered. Hence assuming a uniform scatterer distribution, these frequencies are:

$$\omega_i = \omega_D \cos\left[(2i-1)\pi/4n\right] \qquad \text{radian/s} \tag{3.3}$$

where $w_D = 2\pi f_0 v/c$ is the maximum Doppler shift in radian/s

v is vehicle speed in m/s

$c = 3 \times 10^8$ m/s is the speed of light

f_0 is the carrier frequency (in range 900–920MHz)

The phase θ_i is the phase of a component phasor corresponding to the frequencies $\pm\omega_i$ in the sum. Since the phase angle of the complex envelope is uniformly distributed, θ_i is chosen to be uniformly distributed. As $\cos(\omega_i t + \phi_i)$ becomes negative periodically, it is only necessary to choose θ_i in the range $[0, \pi)$. Therefore

$$\{\theta_i\} = \text{some permutation of } \frac{(2i-1)\pi}{2n} \qquad i = 1 \ldots n$$

As the Doppler frequencies are not linearly related, the phase angles ϕ_i may be chosen arbitrarily, such as $\phi_i = 0$. However, if more than one signal is desired, the cross-correlation between the fading envelopes must be minimised.

Consider two fading envelopes:

$$\begin{aligned} z_1(t) &= \sum_{i=1}^{n} e^{j\theta_{1i}} \cos(\omega_i t + \phi_{1i}) \\ z_2(t) &= \sum_{i=1}^{n} e^{j\theta_{2i}} \cos(\omega_i t + \phi_{2i}) \end{aligned}$$

The cross-correlation is given by

$$\begin{aligned} R_{z_1 z_2}(\tau) &= < z_1(t) z_2^*(t+\tau) > \\ &= < \sum_{i=1}^{n} e^{j\theta_{1i}} \cos(\omega_i t + \phi_{1i}) \sum_{k=1}^{n} e^{j\theta_{2k}} \cos(\omega_k (t+\tau) + \phi_{2k}) > \\ &= < \sum_{i=1}^{n} e^{j(\theta_{1i}-\theta_{2i})} \cos(\omega_i t + \phi_{1i}) \cos(\omega_i (t+\tau) + \phi_{2i}) > \\ &= < \frac{1}{2} \sum_{i=1}^{n} e^{j(\theta_{1i}-\theta_{2i})} (\cos(2\omega_i t + \phi_{1i} + \phi_{2i}) + \cos(\omega_i \tau + \phi_{1i} - \phi_{2i}) > \\ &= \frac{1}{2} \sum_{i=1}^{n} e^{j(\theta_{1i}-\theta_{2i})} \cos(\omega_i \tau + \phi_{1i} - \phi_{2i}) \end{aligned} \tag{3.4}$$

The cross-correlation cannot be made zero for all τ. It is possible however to set the correlation to zero at $\tau = 0$. A solution which fulfills this condition is [72]

$$\theta_{1i} - \theta_{2i} = \text{some permutation of } \frac{(2i-1)\pi}{2n} \tag{3.5}$$

$$\phi_{1i} - \phi_{2i} = \frac{k\pi}{n} \quad \text{for some } 0 \leq k < n \tag{3.6}$$

This relationship between the phases is really only of importance in the downlink simulations where more than one user is present on a particular channel, as the maximum Doppler frequencies for each user will be equal. For uplink simulations where each user's maximum Doppler frequency is different, there is no restriction on the phases. To avoid initial correlation between two users who randomly have close Doppler frequencies, the phases $\{\theta, \phi\}$ for each user and channel were allocated as a random permutation as previously described.

So far the scaling of the fading envelope has been ignored. The autocovariance is

$$R_{zz}(\tau) = \frac{1}{2} \sum_{i=1}^{n} \cos \omega_i \tau \tag{3.7}$$

with mean power

$$R_{zz}(0) = \frac{1}{2} \sum_{i=1}^{n} \cos(0) = n/2 \tag{3.8}$$

Hence for a complex envelope $z_a(t)$ with unit average power, it is necessary to multiply $z(t)$ by $\sqrt{2/n}$.

$$z_a(t) = \sqrt{2/n}\, z(t) \tag{3.9}$$

An approximately Rayleigh distributed variable r can be extracted by

$$r(t) = |z_a(t)|$$

with the probability density function

$$p(r) = \frac{r}{\sigma^2} \exp(-\frac{r^2}{2b})$$

and $\mathbf{E}[r^2] = 2b = 1$

$\mathbf{E}[r] = \sqrt{b\pi/2} = 0.8862$

It was initially stated that the point of this method of generating the fading envelope was to impart the correct correlation properties to consecutive samples, *ie* to produce a fading spectrum consistent with that predicted by Clarke's model. The correlation desired for the complex fading envelope is given as (section 1.1.1)

$$R_{zz}(\tau) = J_0(\omega_D \tau) \tag{3.10}$$

The autocorrelation of the normalized complex fading envelope is

$$R_{z_a z_a}(\tau) = \frac{1}{n} \sum_{i=1}^{n} \cos(\omega_i \tau) \tag{3.11}$$

$$= \frac{1}{n} \sum_{i=1}^{n} \cos\left(\omega_D \tau \cos\left[(2i-1)\pi/4n\right]\right) \tag{3.12}$$

By noting that

$$J_0(x) = \frac{2}{\pi} \int_0^{\pi/2} \cos(x \cos\alpha) d\alpha$$

it has been shown that [2, chapter 1]

$$R_{z_a z_a}(\tau) \approx J_0(\omega_D \tau)$$

to 8 significant digits for $\omega_D \tau \leq 15$, provided that more than eight scatterers are used.

3.3.2 Computation Procedure

The requirement is for values of the complex fading envelope at time intervals Δ, one frequency hopping cycle apart. Now

$$z(t) = \sum_{i=1}^{n} e^{j\theta_i} \cos(\omega_i t + \phi_i)$$

$$
\begin{aligned}
&= \frac{1}{2}\sum_{i=1}^{n} e^{j\theta_i}[e^{j(\omega_i t+\phi_i)} + e^{-j(\omega_i t+\phi_i)}] \\
&= \frac{1}{2}\sum_{i=1}^{n} e^{j(\theta_i+\phi_i)}e^{j\omega_i t} + \frac{1}{2}\sum_{i=1}^{n} e^{j(\theta_i-\phi_i)}e^{-j\omega_i t}
\end{aligned}
$$

At time intervals Δ,

$$
\begin{aligned}
z_k = z(k\Delta) &= \frac{1}{2}\sum_{i=1}^{n} e^{j(\theta_i+\phi_i)}e^{j\omega_i k\Delta} + \frac{1}{2}\sum_{i=1}^{n} e^{j(\theta_i-\phi_i)}e^{-j\omega_i k\Delta} \\
z_{k+1} = z((k+1)\Delta) &= \frac{1}{2}\sum_{i=1}^{n} e^{j(\theta_i+\phi_i)}e^{j\omega_i k\Delta}e^{j\omega_i\Delta} \\
&\quad + \frac{1}{2}\sum_{i=1}^{n} e^{j(\theta_i-\phi_i)}e^{-j\omega_i k\Delta}e^{-j\omega_i\Delta}
\end{aligned}
$$

Let

$$
p_{ik} = \begin{cases} e^{j(\theta_i+\phi_i)}e^{j\omega_i k\Delta} & i = 1,\ldots,n \\ 0 & i = 0 \\ e^{j(\theta_i-\phi_i)}e^{-j\omega_i k\Delta} & i = -n,\ldots,-1 \end{cases} \tag{3.13}
$$

Then

$$
\begin{aligned}
z_k &= \frac{1}{2}\sum_{i=-n}^{n} p_{ik} \\
z_{k+1} &= \frac{1}{2}\sum_{i=-n}^{n} p_{ik}e^{j\omega_i\Delta}
\end{aligned}
$$

Hence to obtain the current value of the complex envelope, it is simple just to multiply the previously computed values p_{ik} for each Doppler component (scatterer) by an incremental value representing phase shift with elapsed time. The real and imaginary parts of the envelope are desired and may be obtained by additions of the exponents of the exponential terms followed by conversion to real and imaginary parts. However, this involves calls to *sin* and *cos* functions, which are comparatively long operations. An alternative method was used. Let

$$
\begin{aligned}
p_{ik} &= p_{ik_1} + jp_{ik_2} \\
a_i &= e^{j\omega_i\Delta} = a_{i_1} + ja_{i_2}
\end{aligned}
$$

Then

$$
\begin{aligned}
z_{k+1} &= \frac{1}{2}\sum_{i=-n}^{n} [p_{ik_1}a_{i_1} - p_{ik_2}a_{i_2} + j(p_{ik_2}a_{i_1} + p_{ik_2}a_{i_1})] \\
&= \frac{1}{2}\sum_{i=-n}^{n} p_{i(k+1)_1} + jp_{i(k+1)_2}
\end{aligned}
$$

At any step in the simulation, only the previous values of the scattering coefficients p_{ik} and the increment value a_i are required to compute the Rayleigh fading coefficients. The values of p_{ik} and a_i are computed at $k = 0$ as

$$p_{i0} = p_{i0_1} + jp_{i0_2} = \begin{cases} \cos(\theta_i + \phi_i) + j\sin(\theta_i + \phi_i) & i = 1, \ldots, n \\ 0 & i = 0 \\ \cos(\theta_i - \phi_i) + j\sin(\theta_i - \phi_i) & i = -n, \ldots, -1 \end{cases}$$

$$a_i = a_{i_1} + ja_{i_2} = \begin{cases} \cos\omega_i\Delta + j\sin\omega_i\Delta & i = 1, \ldots, n \\ 0 & i = 0 \\ \cos\omega_i\Delta - j\sin\omega_i\Delta & i = -n, \ldots, -1 \end{cases}$$

and p_i is then updated each time a new fading envelope is computed. As the value p_{ik} is formed by sums of products, rounding errors will occur with each calculation and gradually accumulate. To ensure that the magnitude of p_{ik} does not vary too greatly from unity, it is necessary to renormalize p_{ik} occasionally. For this reason, p_{ik} was renormalized every 500 iterations by dividing it through by its magnitude. Graphs of the sample densities and distributions for the fading magnitude produced by this procedure are shown in figures 3.4 and 3.5. As can be seen, this procedure generates variables which closely approximate Rayleigh variables, except at the very extremities of the graph. Very high values of envelope magnitude are less likely to happen than for the ideal Rayleigh distribution, and very low values are also less likely. This is not a significant drawback to the use of this technique, as the model diverges very little from the ideal. In practice, studies [68] have shown that fades of more than 40 dB down are very uncommon in the real world, as are very high reinforcement values, both of which are allowed by the Rayleigh model. It therefore appears that the simulated model with a finite number of significant scatterers is more realistic model than the infinite number, uniform angular power density theory of Clarke.

One further point is that a Rician fading density (a less extreme form of fading) may be obtained by adding a constant spectral component at a particular Doppler frequency. Although this has not been tried, it would seem relatively easy to implement if desired.

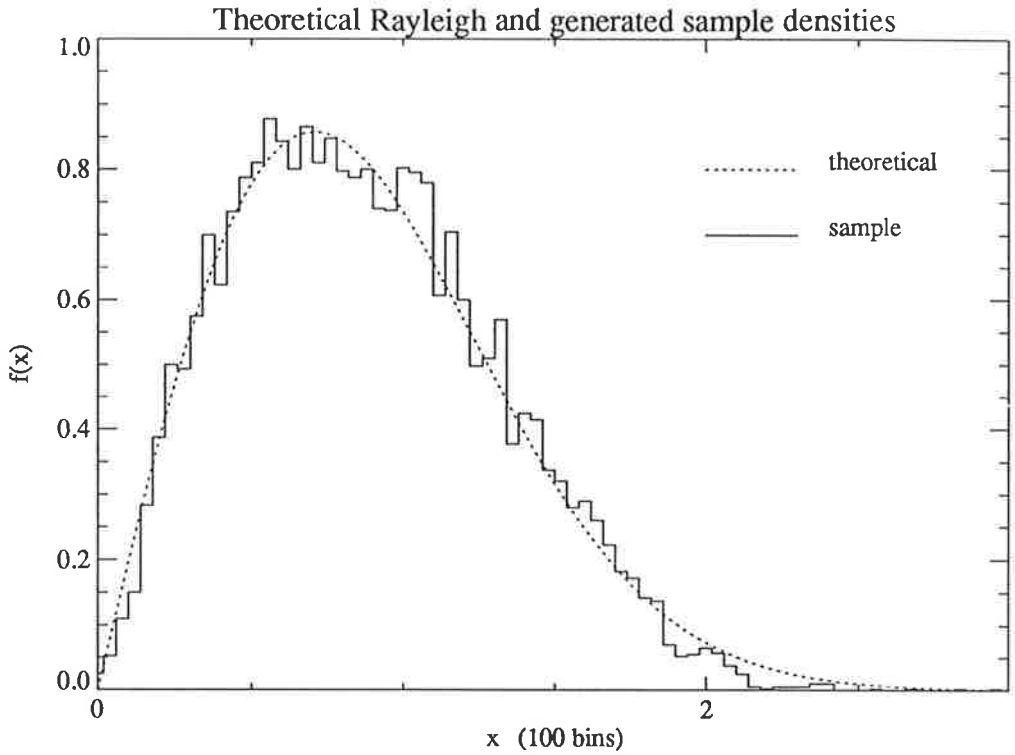

Figure 3.4: Theoretical Rayleigh and generated sample densities, 1000 samples.

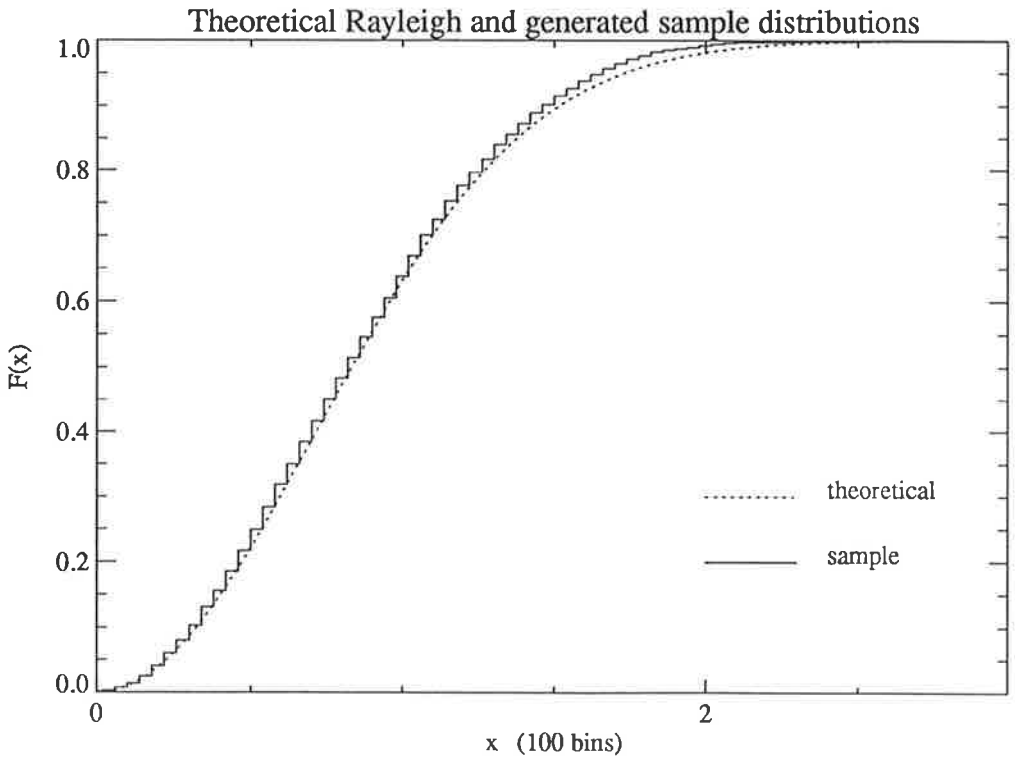

Figure 3.5: Theoretical Rayleigh and generated sample distributions, 1000 samples

Number of scatterers used in model

It is noted that the distribution of the generated fading variables, while closely approximating a Rayleigh distribution for most of its range, fails a chi-square distribution test for equality for reasonable values of n such as 8, 16 and 32. For example, runs of 10000 samples were generated and scaled to have unity mean power for $n = 8, 16, \text{and } 32$.

Using an IMSL [62] routine GFIT to perform a chi-squared test against the theoretical cumulative distribution

$$P(x) = 1 - \exp(-x^2)$$

the results shown in table 3.3.2 are obtained.

n	sample χ_0^2	probability that $\chi^2 > \chi_0^2$
8	177.3	2.4×10^{-6}
16	133.8	1.1×10^{-2}
32	123.4	4.9×10^{-2}

Table 3.1: Results of Chi-squared test for equality of Rayleigh and generated distributions

Using 100 bins for the sample distribution for the χ^2-test, the number of degrees of freedom is 99, and for a 5% chance of rejecting the null hypothesis (*i.e.* distributions are the same) we have $\chi^2_{0.95}(99) = 123.2$. Hence the test would reject the null hypothesis in all cases. However, the steady improvement of the fit of the sample distribution to the Rayleigh distribution with increasing number of scatterers is obvious.

The number of scatterers required to generate samples with accurate correlation was reported to be greater than 8 by Jakes [2]. Davis [72] has suggested that 16 scatterers may be more appropriate. Of course, as the number of scatterers increases, the distribution and correlation statistics become much closer to the ideal. By the same

token, computing time for each variate rises linearly with the number of scatterers. There is also the requirement that any fading variables which are simultaneously generated have minimum cross-correlation. As the number of scatterers increases, so does the number of simultaneous fading variables that may be generated with zero cross-correlation at $\tau = 0$.

A compromise between accuracy and speed of computation must be made. For the simulations of the isolated cell, 16 scatterers were used, with this number being reduced to 8 to produce reasonable run times for the multiple cell system simulations.

3.4 Simulation of Attenuation and Lognormal Fading

Following the model detailed in section 1.1.1, the signal attenuation follows an inverse power law with distance. Lee's model for Philadelphia is chosen as a median case. Once a position for the mobile is read in from a data file or randomly generated from a distribution uniform across the cell area, the slow fading (*ie* the combination of attenuation and shadow fading), can be generated. The cases of uplink and downlink will be treated separately.

For the uplink, power control is assumed, such that the effects of slow fading are annulled by increasing the transmitted power. Thus the local mean (mean of the fast fading envelope) at the user's base station will always be the desired value, specified by E_b/N_0. The power attenuation a_h with distance to this home base station can be computed from:

$$a_h = 112.8 + 36.8 \log r_h \qquad \text{dB} \tag{3.14}$$

where r_h is the distance from the mobile to its corresponding base station in kilometres. The values for base station and mobile receiver antenna heights h_B, h_R and carrier frequency f assumed are the defaults for Lee's model:

$$h_B = 30\text{m}$$

$$h_R = 3\text{m}$$
$$f = 900\text{MHz}$$

The attenuation is then subtracted from the initial signal to noise ratio to form the area mean (in dB)

$$m_{d_h} = P_t - a \qquad \text{dB} \tag{3.15}$$

where the subscript h denotes the user's home cell (that in which his current base station is located). This area mean serves as the mean of the local area mean, which is a log-normally distributed variable, or equivalently a Gaussian variable in dB. The standard deviation σ of this corresponding Gaussian variable lies between 6 and 12 dB, generally found to be increasing with the degree of urbanization [65]. Then a Gaussian variable is generated as $x_h \sim N(0,1)$ by the inverse cumulative distribution method using a standard IMSL [62] software routine (GGNML). To get a variable with the correct variance and mean for the shadow fading, form the Gaussian variable in dB:

$$\bar{s}_{d_h} = \sigma x_h + m_{d_h} \tag{3.16}$$

This value when converted from dB then becomes the mean of the fast-fading distribution.

The slow fading is compensated for by increasing the transmitted power to $P_t + a_h + \sigma x_h$ and hence the signal is received at the home base station with the desired E_b/N_0. Hence all mobile units in an isolated cell will be received at their base station with equal mean power.

However, surrounding cells will receive interference. The attenuation to a base station in a foreign cell at a distance r_f may be calculated as

$$a_f = 112.8 + 36.8 \log r_f \qquad \text{dB} \tag{3.17}$$

Hence the area mean power at the base station in the foreign cell due to the interferer will have a mean value

$$m_{d_f} = P_t + a_h + \sigma x_h - a_f \tag{3.18}$$

This received area mean power is then subject to slow fading, and hence another value of $x_f \approx N(0,1)$ is generated and the local area mean value of the shadow fading at the base station results (in dB).

$$\bar{s}_{d_f} = \sigma x_f + m_{d_f} \qquad \text{dB} \tag{3.19}$$

This value is used as the mean of the signal envelope (*ie* the mean of the fast fading)

$$\bar{s}_i = 10^{\bar{s}_{d_f}/20} \tag{3.20}$$

For the case where the target user is located within the central cell of a cluster, all transmissions from users within that cell will be received with a power P_t dB. Transmissions from outside the central cell will be received with a power $P_t + 36.8\log(r_h - r_f) + 2\sigma x$ where x is a random variable, distributed $\sim N(0,1)$.

Letting the signal amplitude $A = \sqrt{2S} = 10^{P_t/20}$, the slow fading can be accounted for as a factor 10^{κ} multiplying A, where

$$\kappa = \begin{cases} 0 & \text{for the central cell} \\ \frac{1}{20}[36.8\log(r_h - r_f) + 2\sigma x] & \text{for surrounding cells.} \end{cases} \tag{3.21}$$

On the downlink (base to mobile transmission), it is assumed that no power control is in existence, and thus there is no compensation for the slow fading on the home base station link. This can be modelled in the following way:

1. Compute the distance r_h from the central base station to the target mobile user (in the central cell).

2. Compute the distance r_f from the interfering user's own base station to the target mobile user.

3. Taking the the area mean to be specified by the value of P_t, given by the E_b/N_0 being simulated, the factor κ such that 10^{κ} multiplies the factor $A = 10^{P_t/20}$ is

$$\kappa = \frac{1}{20}[36.8\log(r_h - r_f) + 2\sigma x] \tag{3.22}$$

When asynchronous hopping sequence transmission is considered, the slow fading coefficient is multiplied by chip overlap ϵ for cochannel interference and by $\epsilon \sin[\pi\epsilon\Delta f\tau] / [\pi\epsilon\Delta f\tau]$ for adjacent channel interference (these factors are easily derived from the filter characteristics, as shown in [23]).

The slow fading values of a user is not changed during the simulation run and applies to all channels of that user. There are two reasons for this. The first is that the distance travelled by the mobile is short in the time span of the simulation for error rates around $P_b = 10^{-3}$, and no appreciable variation in the shadow fading would occur. Secondly, the extra complexity needed to properly account for the gradual changes in shadow fading would lead to longer run times which are not desirable.

3.5 Accuracy of the Simulation

The accuracy of a Monte Carlo simulation, assuming that the pseudorandom variables used to model random quantities do not bias the results during the simulation period, can be increased by running the simulation for a longer time. However, it is not a linear relationship, and some measure is required to decide for how long the simulation should be run.

For a simulation that counts binary errors which can be written as the probability that a detected value exceeds a certain threshold, and if independent error events are assumed to happen with a probability of error given by p, then the estimate of error probability for a run of N samples is given by

$$\hat{p} = 1/N \sum_{i=1}^{N} e_i$$

where $e_i = 1$ if the ith sample was in error, and $e_i = 0$ otherwise. This estimate $\hat{p}$ is binomially distributed but can be approximated by a normal distribution for large N. This enables a confidence interval of level $1 - \alpha$ to be constructed for the probability of error p. From [61], if $\hat{p} \neq 0$ then it can be written as $\hat{p} = 10^{-k}$,

and $N = \eta 10^k$. For all cases of interest, the approximations $N/(N + d_\alpha^2) \approx 1$ and $p(1-p) \approx p$ are reasonable, where d_α is chosen such that

$$\int_{-d_\alpha}^{d_\alpha} \frac{1}{\sqrt{2\pi}} e^{-t^2/2} dt = 1 - \alpha$$

The confidence interval may be derived for p as [61]

$$\Pr[y_+ \leq p \leq y_-] = 1 - \alpha \tag{3.23}$$

where the confidence interval is given by

$$y_\pm = 10^{-k} \left\{ 1 + \frac{d_\alpha^2}{2\eta} \left[1 \pm \sqrt{\frac{4\eta}{d_\alpha^2} + 1} \right] \right\} \tag{3.24}$$

For a 95% confidence interval of about $(2\hat{p}, \hat{p}/2)$, *ie* a factor of 2 on the error rate, the number of samples that should be taken is of the order of $N = 10^{k+1} = 10/p$, or in other words, about 10 errors should be counted. This is the confidence interval on the point; if the situation is such that a smooth curve can be drawn through a number of points, the confidence interval on the collection of points as a whole will be decreased as information from surrounding points is being used to better the estimate at any particular point.

For the simulations of the FH-DPSK system, decisions are either made on a chip-by-chip basis for the case of hard decision coding, or on a per symbol basis where soft decision decoding is used. The above confidence intervals were derived on the basis of independent errors occurring, which is not necessarily the case. In fact for the fast fading case, a burst of errors is more likely to occur when a particularly bad bout of fading is encountered on a number of channels simultaneously, and when a large number of interferers exist. This has the effect of increasing the variance of the sample mean error rate, and hence more samples are required to achieve the same confidence intervals. The number of samples is dependent on the channel conditions and the number of interferers. At low probabilities of error, the error statistics tend to resemble those of the independent case, as bursts of errors become very much less common.

A tradeoff must then be made between speed of execution and accuracy of the result. It was found that at fairly high probabilities of bit error (above 10^{-3}) the

probability of bit error did not always settle down to a fairly stable value quickly, and a value of 10 codeword errors was too early to terminate the simulation. For this reason, the following criteria was used to determine the simulation run length. For the simulations of the isolated cell system, and employing a block code, the simulation run was continued until either 1000 bit errors had been counted (corresponding to around 400–500 codeword errors) or 10^6 codewords had been been received. This effectively meant that the probability of codeword error could be simulated with a reasonable degree of accuracy down to a probability of 10^{-5}. Values below this were counted but are not to be regarded as accurate, although the trend of results can often enable a curve to be drawn through this area.

For the simulations of multiple cells, random allocation of user position and sequence overlap meant that a number of simulation runs were necessary to obtain a reasonable estimate of the average bit error rate for a given number of users and E_b/N_0 ratio. To count 1000 errors would be far too time consuming and hence the criteria for an individual simulation run to terminate was set to be when the number of bit errors reached 100 (corresponding to about 40 codeword errors), or alternatively to the transmission of 100000 codewords. At error rates of around $P_b = 10^{-4}$–10^{-2}, this was sufficient for the sample mean to converge to be reasonably close to the long-term error rate. As the values were further averaged over a number of simulations for the same parameters (with different random seeds), this was deemed to be accurate enough.

3.6 Language Considerations and Run Times

The efficiency of the simulation is dependent on the algorithms and data structures used. As large numbers of users are possible in the system, but the number of interferers to be simulated may vary from being a very small subset to a large one, it is important to realise the interferer representations in a manner which will not lead to large searches through a sparsely populated database. For these situations, dynamically assigned memory is a natural choice. This is realised most conveniently

through the use of pointers and records. Also to be considered is the ease of writing and debugging code. A structured approach with a highly typed language such as Pascal has distinct advantages in readability and the ability to debug quickly and easily.

For these reasons, the simulation program was initially written in Pascal. Running on a VAX 11/780 computer with the 4.2 Berkeley Standard Unix operating system, the program produced results but took a very large amount of CPU time for error rates of around $P_b = 10^{-4}$. Two factors contributed greatly to this situation. The first was that the version of Pascal distributed with this operating system was formatted in accordance with the standard definition of Pascal, and hence had no enhancements designed to speed it up. Chief among the problems was the fact that the standard definition makes no distinction between single and double precision floating point variables, and hence every real type variable is represented as double precision and all operations pertain to this format. Secondly, the lack of a predefined function to raise variable to the power of another variable requires careful arrangement of the existing predefined functions and operations to obtain accurate results. Secondly, as a result of being a UNIX operating system, the Pascal compiler actually was just a front end processor which then utilised the system C compiler for the remainder of the compilation. As a consequence, the Pascal compiler was found to produce slower code than an equivalent C program.

The program was therefore rewritten in C to gain several advantages. C supports all the features such as pointers used in the program, and hence no major rewrites of the algorithm were necessary. In double precision form, the C version ran faster than the Pascal version by about 15%. Using single precision for most real variables, but performing all operations in double precision as per normal C operation led to a further speed increase. It was also found that the compilation could be made to produce code which performed all floating point operations on single precision variables in single precision. Using this option gave a further speed improvement without any significant loss of precision when compared to the purely double precision version. Even after these improvements, the run times on the VAX were still too large to

enable a large number of simulations to be carried out in a practical length of time. Fortunately, access to a SUN 4 computer became available. When running on this computer, the C program ran 22 times faster than the initial Pascal version on the VAX. The longest isolated cell simulations lasted about 5 hours CPU for very low probabilities of error and using 16 scatterers in the model for the fast fading, but average simulations around $P_b = 10^{-3}$ required about 1 hour of CPU time to run. For the multiple cell simulations, run times ranged from a few minutes to up to 45 minutes of CPU time.

Chapter 4

Orthogonally Coded FH-DPSK

In this chapter, the performance of the system using orthogonal Hadamard coding as proposed by Nettleton and Cooper [24] is investigated. This coding scheme encodes a k bit message word into a 2^k bit codeword by the message acting as an index to the appropriate row of the Hadamard matrix, where the Hadamard matrix is specified previously by equation 2.4.

The amount of redundancy introduced by the code increases rapidly with k, hence increasing the bandwidth at a particular frequency slot of a single user. Too much coding redundancy means the users will tend to interfere more in a tone interferer model, as they cannot be separated adequately by choice of hopping patterns. Too little redundancy will result in an unacceptable error rate for comparatively few interferers. Previous work has concentrated on examining system performance with the parameters shown in table 4.1, which were suggested as a reasonable compromise for transmission assuming the AWGN interference model. More coding gain has only a small effect on the system error rate, at the expense of doubling the number of front end components (filters, detectors, etc.) required.

The performance of the various receiver types is examined for these parameter values. It is notable that this coding scheme as proposed transmits one totally useless chip. The first chip of every codeword is identical, which therefore conveys

Quantity	Symbol	Value Assumed
information bit rate	R_b	32 kbit/s
total one-way bandwidth	W	20 MHz
bits per frame	k	5
codeword length	n	32
number of hops in sequence	L	32
chip period	τ	4.88 μs
frequency separation	$f_s = 1/\tau$	204.8 kHz

Table 4.1: Values initially assumed for transmission

no information. It therefore can be discarded to form a simplex code with a fractional improvement in chip signal to noise ratio for a given bit energy to noise ratio.

4.1 White Gaussian Interference Model

This model, described in section 1.4.1, assumes the interferers may be represented as white Gaussian noise. Thus results will be computed for a one-sided Gaussian noise power spectral density N_0. This can be related to the number of interferers as described previously.

4.1.1 Linear Receiver

The system is assumed to use hopping over L frequency channels, each with its own fast fading coefficients. As each channel experiences fading and interference with identical statistics, it is convenient to let the number of channels equal the length of the codeword and hence $L = 2^k$ as used by Nettleton and Cooper. It is assumed that power control is exercised to counteract the effects of shadow fading and attenuation. Instead of the receiver shown previously in figure 1.8, a correlation receiver as shown in figure 4.1 was assumed, as it is more convenient for simulation. Both forms of receiver are ideally equivalent, but Park [73] has shown that the receiver of

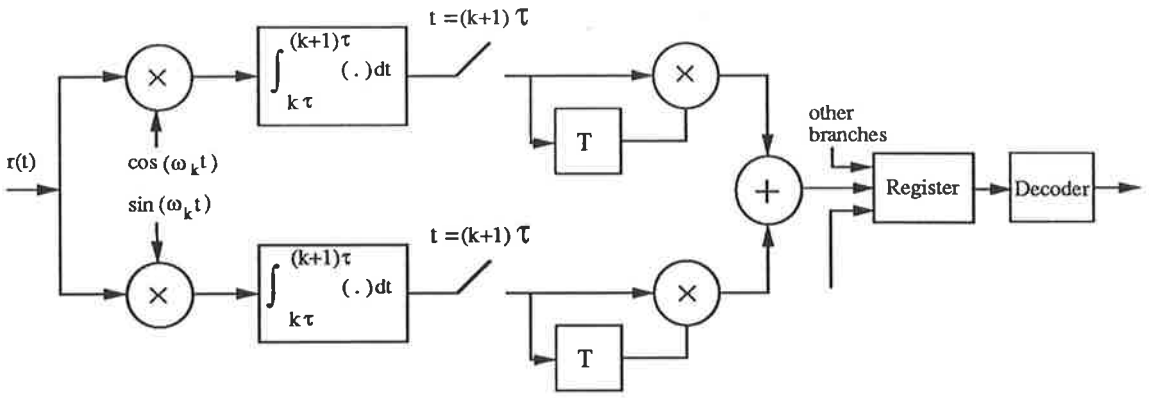

Figure 4.1: Schematic diagram of the linear FH-DPSK correlation receiver

figure 4.1 has better performance in conditions where intersymbol interference is a consideration.

No Fading Case

This case is the simplest to simulate and analytical bounds exist which provide a good check on the simulation results. As addressing has no impact on this model, and multiple cells just result in a increased noise power spectral density, it is sufficient just to know the bit energy/noise ratio E_b/N_0 to simulate the system. The performance which results from a system with no fast fading represents the best possible from that system, such as would be obtained on a direct line of sight communication link with negligible multipath, close to the transmitter.

The system is the same as that treated in chapter 2, except the local oscillator at the correlator receiver is assumed to have an arbitrary phase, and consequently the transmitted signal appears in both the in-phase and quadrature parts of the received signal plus noise. Independent noise samples are generated with a normal $N(0,1)$ distribution for each quadrature component. The magnitudes of the signal components are $(\sqrt{2S}\cos\theta_l)$ and $(\sqrt{2S}\sin\theta_l)$, where θ_l is the phase difference between the local frequency reference signal in the lth chip and the received signal.

For unit variance noise components, the signal amplitude $\sqrt{2S}$ is given by the

relation

$$S = \frac{E_c}{N_0} = \frac{kE_b}{2^k N_0} \tag{4.1}$$

where E_b/N_0 is the bit energy to noise ratio and E_c is the chip energy.

The sampled inphase and quadrature parts of the signal for the lth channel are

$$\begin{aligned} r_{lc} &= \sqrt{2S}\cos\theta_l + n_{lc} \\ r_{ls} &= \sqrt{2S}\sin\theta_l + n_{ls} \end{aligned}$$

These signals are then fed into quadratic detectors as shown in figure 4.1, where they are multiplied by the delayed signals from the previous sequence, and then the two branches are summed. This can be represented by the operation on the complex envelope

$$y_l = \Re\left\{r_l(t)r_l^*(t-T)\right\} \qquad (l-1)\tau \le t \le l\tau \tag{4.2}$$

where $\Re$ denotes real part and $r_l = r_{lc} + jr_{ls}$. The resulting L detector outputs are then combined by the Hadamard transform to produce the correlations of the received signals with each of the codewords. The largest output is then chosen as the best estimate of the transmitted codeword and the corresponding message word is decoded as the number corresponding to the row of the Hadamard matrix, in the range 0–$(2^k - 1)$. The bit errors between the transmitted message word and the received word are counted. The probability of codeword and bit error can then be easily estimated over the simulation run. The results of this simulation are shown by the + symbols in figure 4.2.

The results of Nettleton and Cooper[24], Henry [25] and Yue [27] have all been recomputed from their formulae. These results are plotted on the same graph in figure 4.2, together with results from Yamada and Daikoku for a simulation of the no fading case (taken from a graph in their paper [74]). The results derived from the present simulations are in excellent agreement with other work, lying almost exactly on the results of Yamada and Daikoku. The simulation results can be seen be to bounded by the results of Nettleton and Cooper and those of Henry at low E_b/N_0 and tightly bound by equations 1.31 and 1.30 at high E_b/N_0 values. It shows that the use of the union bound to obtain the probability of error over the L codeword

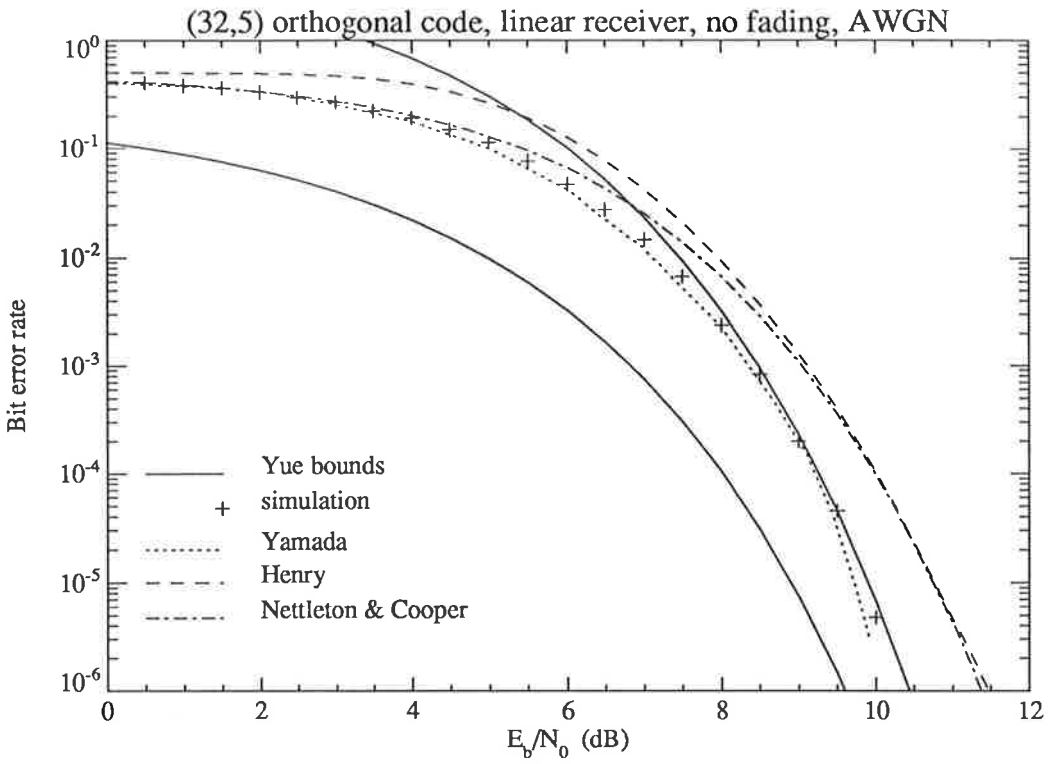

Figure 4.2: Bit error rate of the linear FH-DPSK correlation receiver, hopping over 32 channels, in AWGN and no fading.

comparisons from a pairwise codeword comparison results in a very good estimate of the bit error rate at low probability of error. These results emphasise the accuracy of the simulation as a tool for checking the validity of analytical approximations.

Fading Case

For the case where the signal envelope fades with Rayleigh statistics, Gaussian variables were generated for the inphase and quadrature components of the complex signal envelope for each chip by the method detailed in section 3.3.1. These multiplied the signal amplitude $\sqrt{2S}$, scaled as in the case of no fading, and unit variance zero-mean Gaussian noise was added to complete the signal. To ensure the independence of each of the fading envelopes on different channels, each was computed with a random maximum Doppler shift of the maximum considered (600 rads/s, equivalent to a speed of 115 km/hr at 900 MHz) plus a random shift of 0–14rads/s

due to the channels being located separately within a 20 MHz band. In addition, the oscillator phases θ_n and ϕ_n specified in the fast fading coefficient generation routine (section 3.3.1) were chosen as a random permutation of the set in equations 3.6 and 3.5. This ensures low cross-correlation between fading coefficients in the initial stages of the simulation when two channels are not widely separated in frequency. These conditions satisfy the requirement that the fading on each of the channels be independent.

The results are plotted in figure 4.3, together with results from other authors. The accuracy of the simulation can be seen from the close agreement with the analytic upper bound of Yue (equations 1.30 and 1.32) at low error rates, where the union bound is expected to be tight. Approximations made by Henry in assuming independent combiner outputs and using a union bound based on the pairwise probability of codeword error can be seen to result in slightly worse results. The results of Nettleton and Cooper are very pessimistic at high E_b/N_0 values resulting from their choice of the worst case distribution function for the statistics of the detector outputs, their assumption of independent combiner outputs and their formulation of the probability of bit error.

The fading model adopted in the simulation takes into account the correlation between chips at a particular frequency in adjacent frames. This is in contrast to the analytic bounds derived by Yue, which were derived assuming that the complex fading envelope did not change over the duration of one frame. As the results of the two approaches are very similar at high E_b/N_0 values, this implies that the effect of change in the fading envelope is small for the particular values of parameters being used (*eg* R_b, L, τ, k, n). If this was not the case, the simulation bit error rate curve would lie slightly further to the right, above the analytic bound derived for the case where there is no change in the signal envelope. However, this does not mean that such an assumption is justified in all cases, as the decorrelation increases with hopping sequence length and Doppler shift, and this effect may rapidly become significant in its effect on the bit error rate.

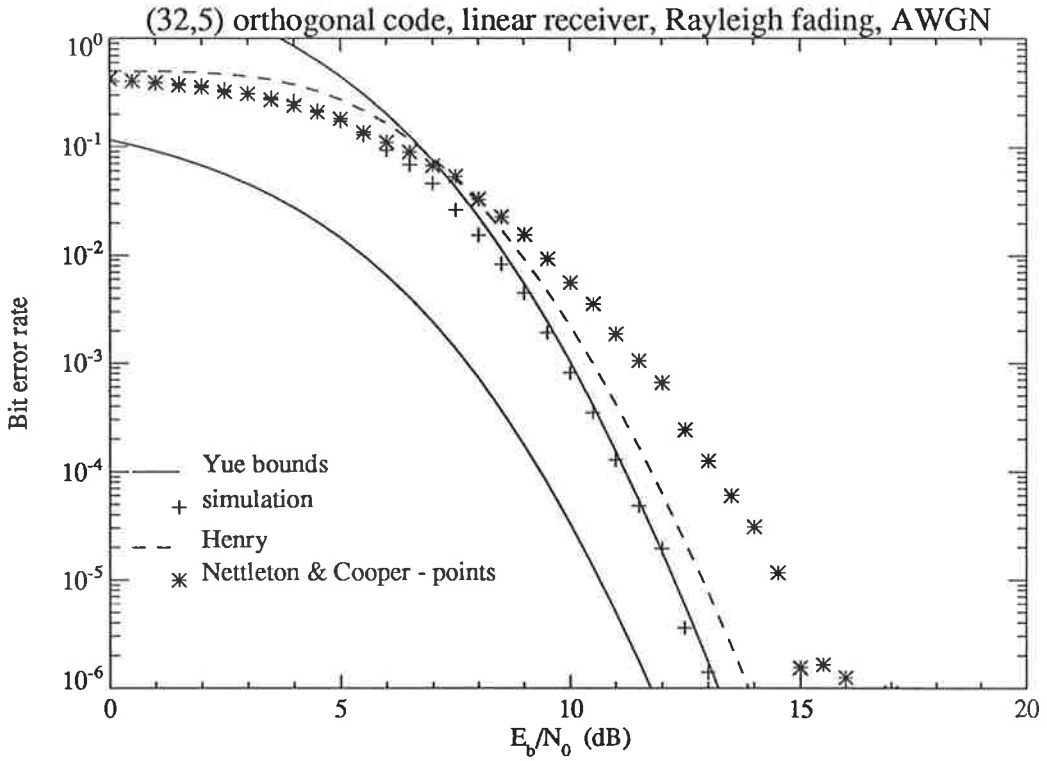

Figure 4.3: Bit error rate of the linear FH-DPSK correlation receiver, hopping over 32 channels, in AWGN and with ideal independent Rayleigh fading.

The effect of correlation between frequency channels due to wide coherence bandwidths has been discussed by [24,55] and in chapter 2. It is possible to directly generate a certain amount of correlation between the fading envelopes at different frequencies, without using the techniques used in the study of diversity systems earlier. From section 3.3.1, the complex fading envelope can be written as

$$z(t) = \sqrt{\frac{2}{n}} \sum_{i=1}^{n} e^{j\theta_i} \cos(\omega_i t + \phi_i) \tag{4.3}$$

$$= \sqrt{\frac{2}{n}} \sum_{i=1}^{n} \cos(\omega_i t + \phi_i)(\cos\theta_i + j \sin\theta_i) \tag{4.4}$$

$$= x(t) + jy(t) \tag{4.5}$$

From the above results, it is obvious that provided the frame period is short enough, the decorrelation in time of two chips at a particular frequency over the frame period may be ignored. A frame of chips at different frequencies may be approximated to be at the same point in time. The desired correlations between the fading components between two frequencies f_1, f_2 separated by Δf, at the same instant in time, are

given by

$$\mathbf{E}[y_1 y_2] = \mathbf{E}[x_1 x_2] = \frac{b_0}{1+(\Delta f/B_c)^2} \tag{4.6}$$

$$\mathbf{E}[x_1 y_2] = -\mathbf{E}[x_2 y_1] = \frac{b_0 \Delta f/B_c}{1+(\Delta f/B_c)^2} \tag{4.7}$$

$$\mathbf{E}[x_1^2] = \mathbf{E}[x_2^2] = \mathbf{E}[y_1^2] = \mathbf{E}[y_2^2] = b_0 \tag{4.8}$$

A solution for the quantities $\theta_{1i}, \theta_{2i}, \phi_{1i}, \phi_{2i}, \omega_{1i}, \omega_{2i}$ such that these correlations are satisfied, seems difficult to obtain, but may be possible. If this is the case, then the fading generation routine could become completely general in terms of specifying correlation in both time and in frequency.

As an example, consider the case where both phases θ_i, ϕ_i are picked from a uniform distribution on $[0, \pi)$ as discussed in section 3.3.1. So the envelopes are not independent, set the maximum Doppler shift and number of scatterers n used in the coefficient generation to be equal for each channel. To ensure that the correct spectra is obtained, the phases θ_i and ϕ_i are generated by taking a random permutation of

$$\{\theta_i\} = \frac{(2i-1)\pi}{2} \qquad i = 1, \ldots, n$$

and $\{\phi_i\} = \{\theta_{n-i}\}$. Thus the θ_i and ϕ_i will appear randomly distributed.

For two fading envelopes $z_1(t)$,.$z_2(t)$ generated this way, with identical Doppler frequencies ω_i, the cross-correlations of components at relative shift $\tau = 0$ given by (where $< . >$ denotes time average)

$$< x_1 x_2 > = < \frac{2}{n} \sum_{i=1}^{n} \cos(\omega_i t + \phi_{1i}) \cos(\omega_i t + \phi_{2i}) \cos\theta_{1i} \cos\theta_{2i} > \tag{4.9}$$

$$= \frac{1}{n} \sum_{i=1}^{n} \cos(\phi_{1i} - \phi_{2i}) \cos\theta_{1i} \cos\theta_{2i} \tag{4.10}$$

If it is assumed that $\theta_{1i}, \theta_{2i}, \phi_{1i}, \phi_{2i}$ are independent, uniformly distributed on $[0, \pi)$ (which is approximately true due to the random permutations taken for signals 1 and 2), we can take the expectation of the autocorrelation over these variables

$$\mathbf{E} < x_1 x_2 > = \frac{1}{n} \sum_{i=1}^{n} \mathbf{E}[\cos(\phi_{1i} - \phi_{2i})] \mathbf{E}[\cos\theta_{1i}] \mathbf{E}[\cos\theta_{2i}] \tag{4.11}$$

Now let $\psi = \phi_{1i} - \phi_{2i}$. Then the density function of ψ is

$$p(\psi) = \begin{cases} \frac{1}{\pi}(1 - \psi/\pi) & 0 \le \psi \le \pi \\ \frac{1}{\pi}(1 + \psi/\pi) & -\pi \le \psi \le 0 \end{cases} \tag{4.12}$$

and the expectation

$$\mathbf{E}[\cos\psi] = 4/\pi^2 \tag{4.13}$$

and

$$\mathbf{E}[\cos\theta_{\{1,2\}i}] = 0 \tag{4.14}$$

Hence $\mathbf{E} < x_1 x_2 >= 0$

Similarly,

$$< y_1 y_2 >= \frac{1}{n}\sum_{i=1}^{n} \cos(\phi_{1i} - \phi_{2i}) \sin\theta_{1i} \sin\theta_{2i} \tag{4.15}$$

and

$$\begin{aligned} \mathbf{E} < y_1 y_2 > &= \frac{1}{n}\sum_{i=1}^{n} \mathbf{E}[\cos\psi]\mathbf{E}^2[\sin\theta_{1i}] \\ &= \frac{4}{\pi^2}\left[\frac{2}{\pi}\right]^2 \\ &= \frac{16}{\pi^4} \end{aligned} \tag{4.16}$$

$$\mathbf{E} < x_1 y_2 >= \frac{1}{n}\sum_{i=1}^{n} \mathbf{E}[\cos(\phi_{1i} - \phi_{2i})]\mathbf{E}[\cos\theta_{1i}]\mathbf{E}[\sin\theta_{2i}] = 0 \tag{4.17}$$

and

$$\mathbf{E} < x_2 y_1 >= 0 \tag{4.18}$$

Correlation then exists between the two imaginary parts of the complex envelope.

The above situation was tested by simulation. Although this is not the exact correlation that would be required to simulate wide coherence bandwidths, it does give some idea of the effect of correlated fading coefficients on the probability of bit and frame error. The results are shown for case of transmission in additive white Gaussian noise in figure 4.4, and should be compared with those of figure 4.3. An increase in the error rate of the order of 2 is noted at medium to low probabilities of error over the case of independent fading.

4.1.2 Hard Decision Receiver

The hard decision receiver is identical to that of figure 4.1, except that instead of a continuous (or finely quantized) value being recorded in the register following

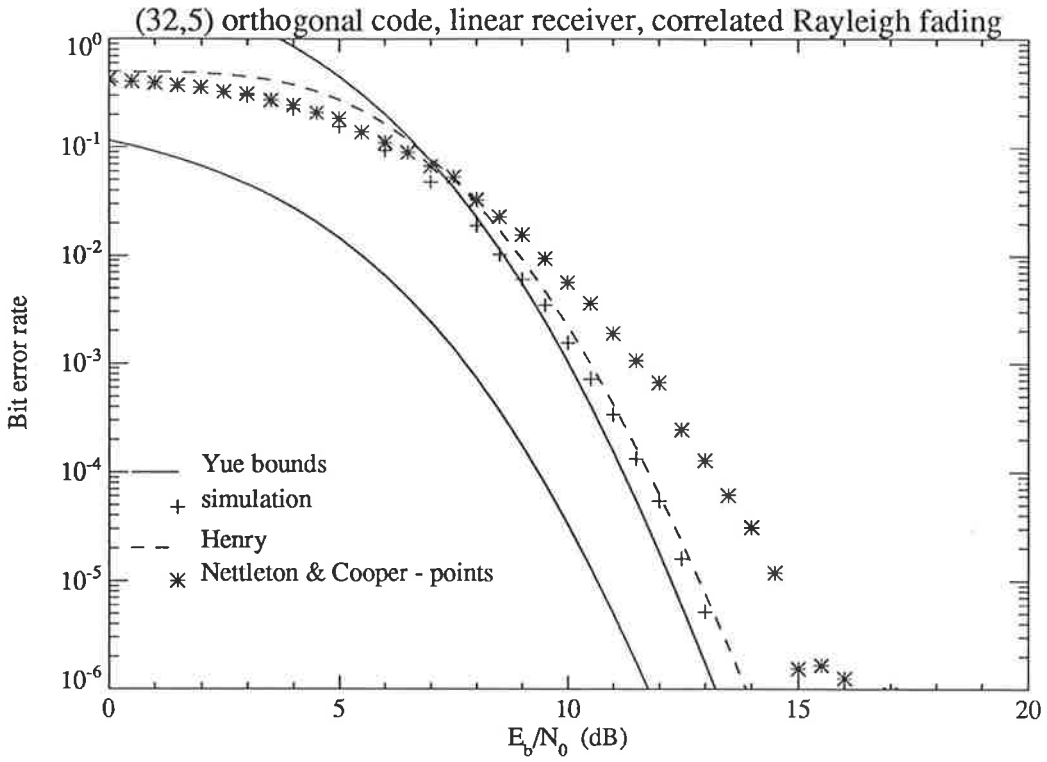

Figure 4.4: Bit error rate of the linear FH-DPSK correlation receiver, hopping over 32 channels, in AWGN and correlated Rayleigh fading.

detection, hard decisions are made on each chip, before decoding.

No Fading Case

Frequency hopping systems have been proposed for mobile radio to counteract the serious problem of frequency selective fading. The performance of a hard decision receiver when no fading occurs on the link is identical to that of single channel per carrier, frequency division multiplexed (FDM) systems with equivalent coding. It serves as a lower bound to the bit error rate possible for this receiver in fast fading, without spatial diversity.

For (32,5) Hadamard code, the bit error rate of the hard decision receiver in AWGN is shown together with that of the linear receiver in figure 4.5. It can be seen to require about 1.4 dB more E_b/N_0 to achieve a bit error rate of 10^{-3}. The normalizing receiver, discussed in a following section, has performance lying between

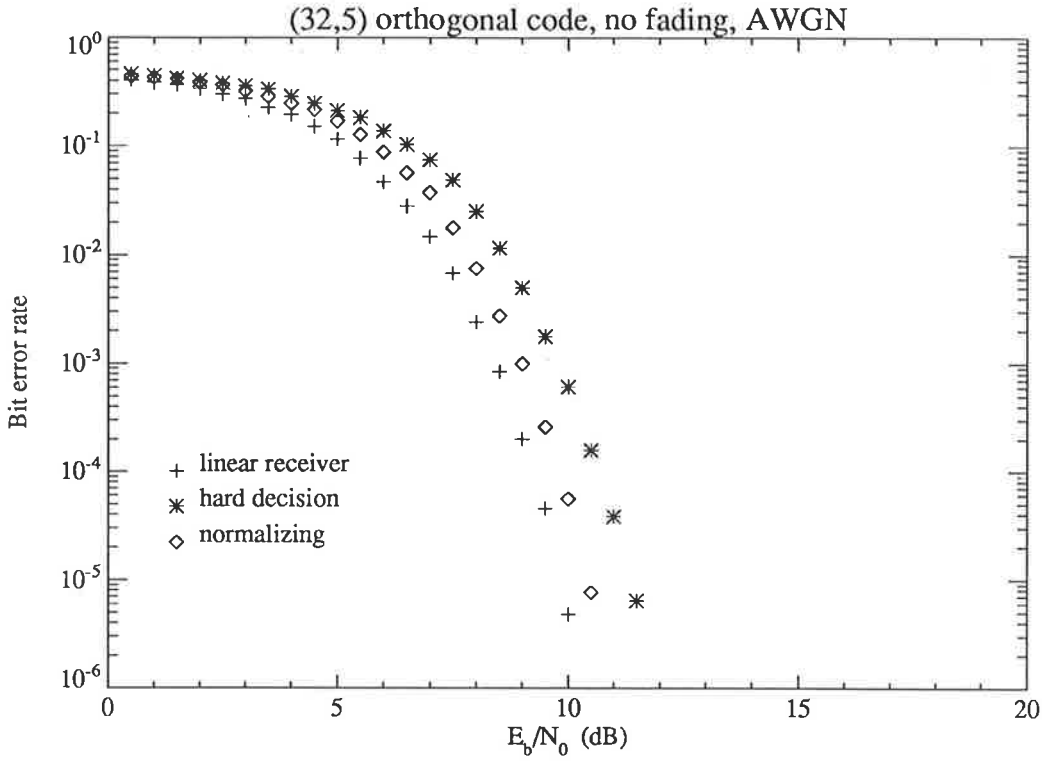

Figure 4.5: Bit error rate of (32,5) orthogonal coding, for linear, hard decision and normalizing receivers, hopping over 32 channels, in AWGN with no fading.

these two receivers, and achieves $P_b = 10^{-3}$ with approximately 0.7 dB more E_b/N_0 than the linear receiver. Under the AWGN interference model, these curves would correspond to 91, 78 and 66 users in an isolated cell for the linear, normalizing and hard decision receivers respectively, and these numbers form an upper bound for the Rayleigh fading situation under the AWGN interference model.

As it is a "best case" condition which occurs rarely in practice, the no fading condition is not considered further. Instead, this thesis will concentrate on the system behaviour when fast Rayleigh fading is present, as this fading is the major channel degradation which frequency hopping has some potential to alleviate.

Fading Case

The performance of the receiver in fading conditions is simplified by the assumption that each channel is independent and thus may be treated separately. For each

channel, a decision is made on a fading signal received in additive white Gaussian noise. Voelcker's result for the DPSK on a Rayleigh fading channel is

$$P_c = \frac{\Gamma(1-\varepsilon)+1}{2(1+\Gamma)} \tag{4.19}$$

where Γ is the signal to noise ratio, defined as

$$\Gamma = \sigma_s^2/\sigma_n^2 \tag{4.20}$$

and σ_s^2 is the variance of either of the inphase or quadrature signal components and σ_n^2 is the variance of the inphase and quadrature noise components.

For the received signal in the lth chip

$$\begin{aligned} r(t) &= \sqrt{2S}\alpha_l \cos(\omega_l t + \phi_l) + n_c \cos\omega_l t + n_s \sin\omega_l t \\ &= \sqrt{2S}(\alpha_l \cos\phi_l \cos\omega_l t + \alpha_l \sin\phi_l \sin\omega_l t) + n_c \cos\omega_l t + n_s \sin\omega_l t \\ &= \sqrt{2S}(z_c \cos\omega_l t + z_s \sin\omega_l t) + n_c \cos\omega_l t + n_s \sin\omega_l t \end{aligned}$$

and hence for ϕ_l uniformly distributed on $[0, 2\pi)$ and power control ensuring that $\mathbf{E}[\alpha_l^2] = 1$,

$$\begin{aligned} \sigma_s^2 &= \mathbf{E}[2Sz_c^2] \\ &= 2S\mathbf{E}[\alpha_l^2]\mathbf{E}[\cos^2\phi_l] \\ &= S \\ \sigma_n^2 &= (I+N_0)/\tau \end{aligned}$$

where $I = S(J-1)/W$ is the equivalent white Gaussian noise one-sided power spectral density of the interference. For N_0 negligible with respect to I, which is the case at normal signal levels,

$$\sigma_n^2 = I/\tau = \frac{S(J-1)}{W\tau}$$

and hence

$$\Gamma = \frac{W\tau}{(J-1)} = \frac{E_c}{I} \tag{4.21}$$

The chip error probability is therefore

$$P_c = \frac{(1-\varepsilon)(E_c/I)+1}{2(1+E_c/I)} \tag{4.22}$$

For a $(2^k, k)$ orthogonal code, an upper bound on codeword error can be derived as [75]

$$P_w \leq (2^k - 1)\left[\frac{1}{2}\binom{2^{k-1}}{2^{k-2}} P_c^{2^{k-2}}(1-P_c)^{2^{k-2}} + \sum_{l=2^{k-2}+1}^{2^{k-1}} \binom{2^{k-1}}{l} P_c^l (1-P_c)^{2^{k-1}-l}\right] \tag{4.23}$$

The bit error rate is strictly bounded by $P_b \leq P_w$, but an approximate asymptote for high E_b/N_0 is given by

$$P_b \approx \frac{2^{k-1}}{2^k - 1} P_w \tag{4.24}$$

The system was simulated and the results are compared to those of the linear receiver and the normalizing receiver in figure 4.6, in which the hard decision bit error rate asymptote is also plotted.

The results show a marked degradation in bit error rate from that of the linear receiver. This is to be expected, as the hard decision receiver is not using all the information presented to it, and the linear receiver is maximum likelihood optimal for a fading DPSK signal in AWGN with no interference (discussed in the next chapter). The difference in performance amounts to several dB at a bit error rate of 10^{-3}, and represents a substantial decrease in the number of users that can be supported in the system over that the linear receiver could support. The results are validated by the hard decision bit error rate approaching the asymptote at high E_b/N_0 as predicted, although the bound is very loose at low E_b/N_0.

It is of interest to determine the system performance using a code with less redundancy, as it is possible that the hardware cost for the 32 channel system would be too great. Alternatively, a concatenated scheme with the same overall code rate may be envisaged, with the inner code a Hadamard code, and a Reed-Solomon code as the outer code. In this fashion, longer overall code lengths can be constructed.

For the $(16, 4)$ Hadamard orthogonal coding scheme, similar trends in receiver performance are found to those for the $32, 5)$ code, linear receiver being about 4.5 dB better than the hard decision receiver at a bit error rate of $P_b = 10^{-3}$. The results are shown in figure 4.7. The smaller amount of coding redundancy and diversity

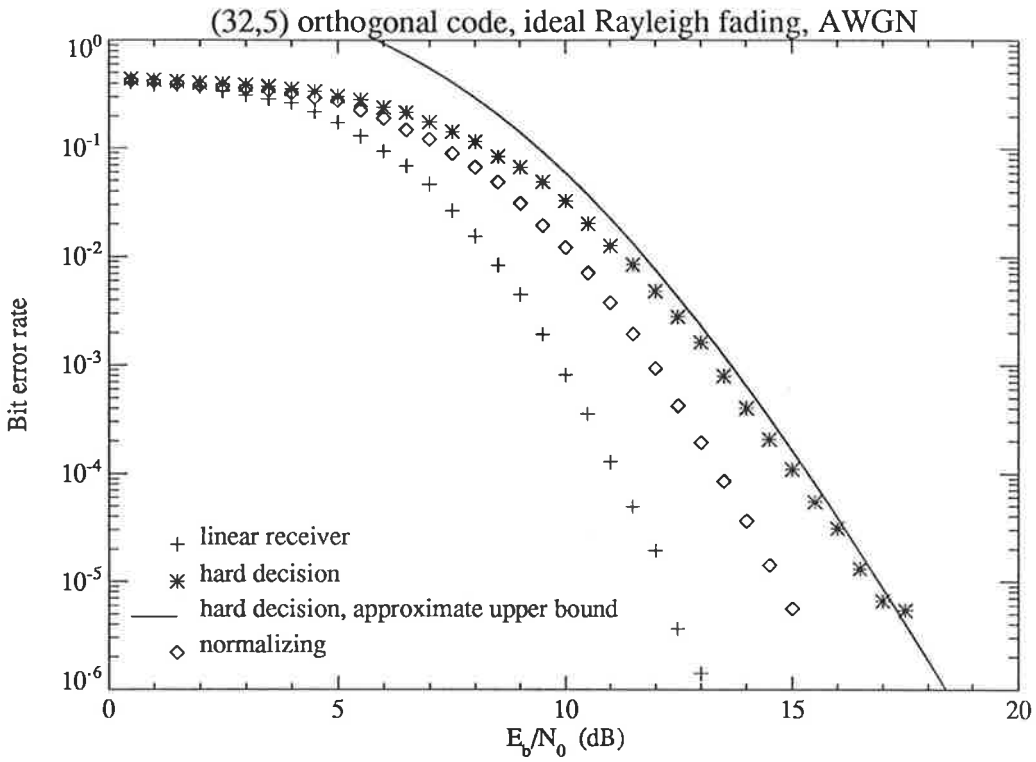

Figure 4.6: Bit error rate performance of three receiver types for (32,5) orthogonal coding, with unit power Rayleigh fading and AWGN.

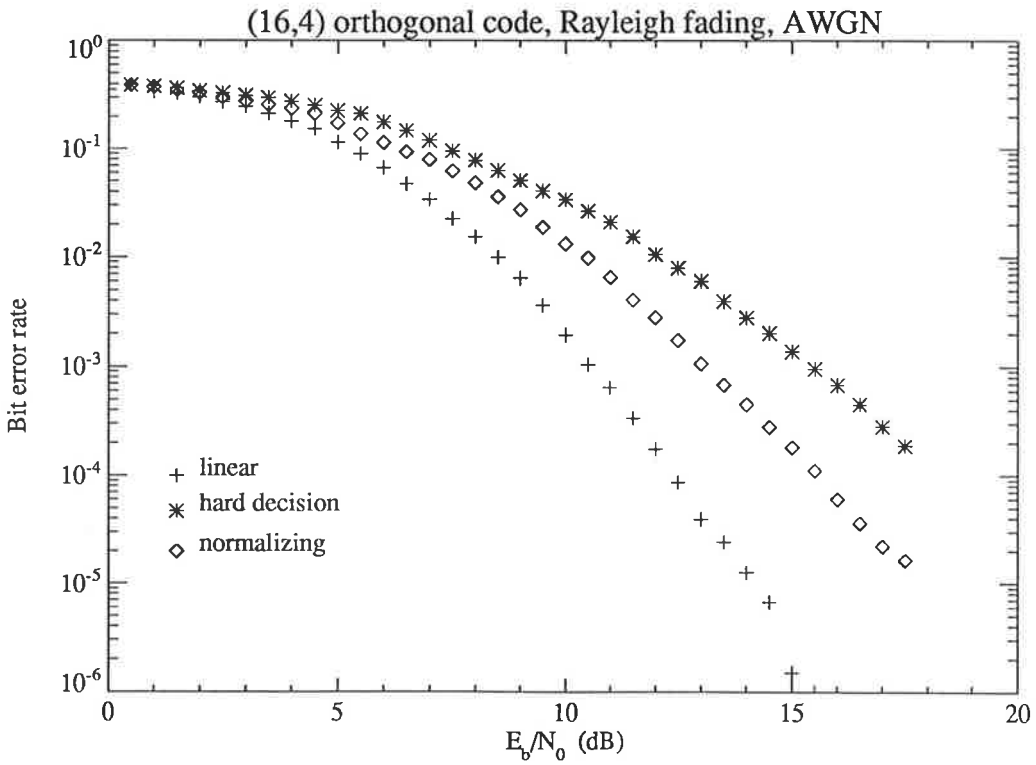

Figure 4.7: Bit error rate performance of three receiver types for (16,4) orthogonal coding, with unit power Rayleigh fading and AWGN.

against fading leads to a higher error rate at a given E_b/N_0, as expected.

4.1.3 Normalizing Receiver

This receiver is shown in figure 4.8. It is equivalent to the receiver of figure 1.8 with ideal hard limiting and bandpass filtering inserted after the matched IF bandpass filter and before the quadratic detector. The magnitude of the complex envelope on each channel is normalized, retaining only the phase on which to make a decision. In fading and additive white Gaussian noise, large changes in phase between one frame and the next are more likely when the envelope magnitude is small. The linear receiver implicitly uses this information, effectively weighting the quadratic detector output by the magnitude of the envelope for that channel. The normalizing receiver therefore discards some information pertaining to the reliability of the faded received signal in AWGN.

However, it does retain a continuous phase measurement, unlike the hard decision receiver, and thus can be expected to give performance in between the linear receiver and the hard decision receiver. This is quite easily pictured. The normal behaviour of the received signal on a particular channel will be to undergo a phase shift of either 0 or π radians between frames. A large deviation from either of these two values indicates that some combination of fading and noise is affecting the signal severely. As this deviation approaches $\pi/2$ radians, the contribution from that channel will approach zero. The phase measurement is therefore in proportion to the reliability of the channel, although it is not a simple linear relationship.

Fading Case

The non-linearity of this receiver and the complexity of the analysis due to the dimensionality of the signal combining resulted in accurate analytical results being too difficult to obtain for this type of receiver. On the other hand, it is a simple matter to alter the simulation program for the linear receiver to include the normalizing

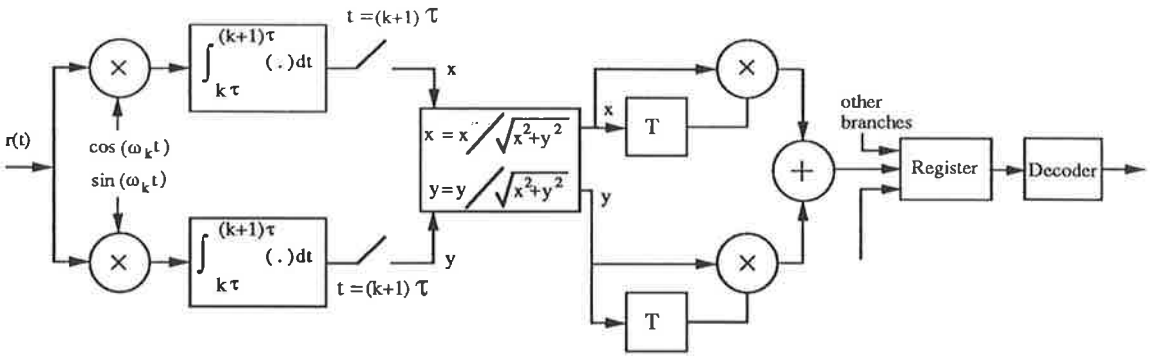

Figure 4.8: Normalizing receiver

operation. Results for simulations of the (32,5) and (16,4) Hadamard orthogonal codes are shown in figures 4.6 and 4.7 respectively.

As predicted, the performance of this receiver is poorer than that of the linear receiver, correspondingly requiring E_b/N_0 to be 2 dB higher to achieve $P_b = 10^{-3}$ for the (32,5) code, and 2.5 db more for the (16,4) code. However, the performance of the normalizing receiver for the (32,5) code is around 1.5 dB better than that of the hard decision receiver at $P_b = 10^{-3}$, and about 2.0 dB better for the (16,4) code.

4.1.4 Usage under the AWGN Interference Model

From the results given in previous sections, the number of users possible at in an isolated cell can be determined for the three receiver types. From equation 4.21 and the fact that $E_c = kE_b/2^k$,

$$\frac{E_b}{I} = \frac{WE_b}{S(J-1)} = \frac{WT}{(J-1)} = \frac{W}{R_b(J-1)} \tag{4.25}$$

Hence

$$J = \frac{W}{R_b(E_b/I)} + 1 \tag{4.26}$$

The numbers of users that can be supported in fast Rayleigh fading at an average bit error rate of $P_b = 10^{-3}$ for the (32,5) and (16,4) Hadamard codes are given in table 4.2.

Values at $P_b = 10^{-3}$	Hadamard code (32,5) E_b/N_0 dB	(32,5) No. Users	(16,4) E_b/N_0 dB	(16,4) No. Users
linear rec.	9.8	66	10.6	55
normalizing rec.	12	40	13.15	31
hard decision rec.	13.3	30	15.5	17

Table 4.2: Number of users that could be supported at an average $P_b = 10^{-3}$ in an isolated cell, for the different receiver types and assuming Rayleigh fading and AWGN

4.2 Performance with Tone Interferers

For this interference model, chip synchronism between user hopping sequences and orthogonal tones are assumed. Interferers are modelled as a series of fading tones with random data modulation, as discussed previously in section 1.4.2.

Simulation is used here as a comparative guide to the merits of the various receivers. Only a small number of all the different combinations of user interference patterns can be examined in a realistic timescale. However, for the linear and hard decision receiver, analytical or analytical/numerical solutions can be derived for the random addressing case. The comparative performance of the normalizing receiver may then be estimated for the area of interest, around a bit error rate of 10^{-3}, by observing the difference in performance from the other receivers for interferer configurations which result in bit error rates around that level.

The performance of the various receivers in fading conditions were assessed for different bit energy to noise ratios, and a number of different interferer patterns. Interferers were inserted into frequencies in a particular order to produce the desired patterns, with each new pattern in a sequence being formed by the addition of an interferer to the previous pattern. Figures 4.9 and 4.10 show the performances of the receivers with a signal corrupted by a certain sequence of interferer patterns, which will be collectively referred to as "pattern 1", for bit energy to thermal noise E_b/N_0

ratios of 17 and 28 dB (*ie* $E_c/N_0 = 9$ and 20 dB). In these interferer patterns, only one interferer, of equal average power to the wanted signal, is present in a particular time chip. As expected, the bit error rate increases with increasing numbers of interferers. It is also clear that the system is influenced by noise up to reasonably high levels of E_b/N_0.

The linear receiver is seen to perform poorly in the presence of even small numbers of strong tone interferers. The hard decision receiver shows a large improvement over the linear receiver, especially in the presence of a small number of interferers. This is to be expected, as the effect of the interference is limited to the particular chip in which it is present, and hence for a small number of chip errors, the code distance will ensure that the correct codeword is recovered. As the thermal noise or the number of interferers increases, the effectiveness of the hard decision decoder decreases. These results are in accord with those published previously by Yue [26,35], where the hard decision decoding performance is superior to that of the linear receiver.

A major gain in performance is noted for the normalizing receiver. This receiver exhibits superior performance for large numbers of interferers present, with over an order of magnitude improvement over the hard decision receiver at bit error rates of at or below 10^{-3}. A curious fact is that the normalizing receiver performs better than both other receivers even when every channel has an interferer present with average power equal to that of the wanted signal. This effectively means that when analyzing the normalizing receiver, the interferers on each channel are not well represented as Gaussian noise with samples independent from frame to frame. (Otherwise the bit error rate would equal the Gaussian noise case with $E_b/N_0 = 0$ dB). Although the randomness of the data will cause the phase of a single interfering signal to vary by 0 or π radians randomly from frame to frame, the magnitude will only change slightly. For the case of one interferer per chip, the normalizing receiver is obviously able to exploit this structure to produce a lower error rate than for the other receiver types. This effect would decrease in magnitude as the number of interferers per chip became larger, and approximated Gaussian noise more closely.

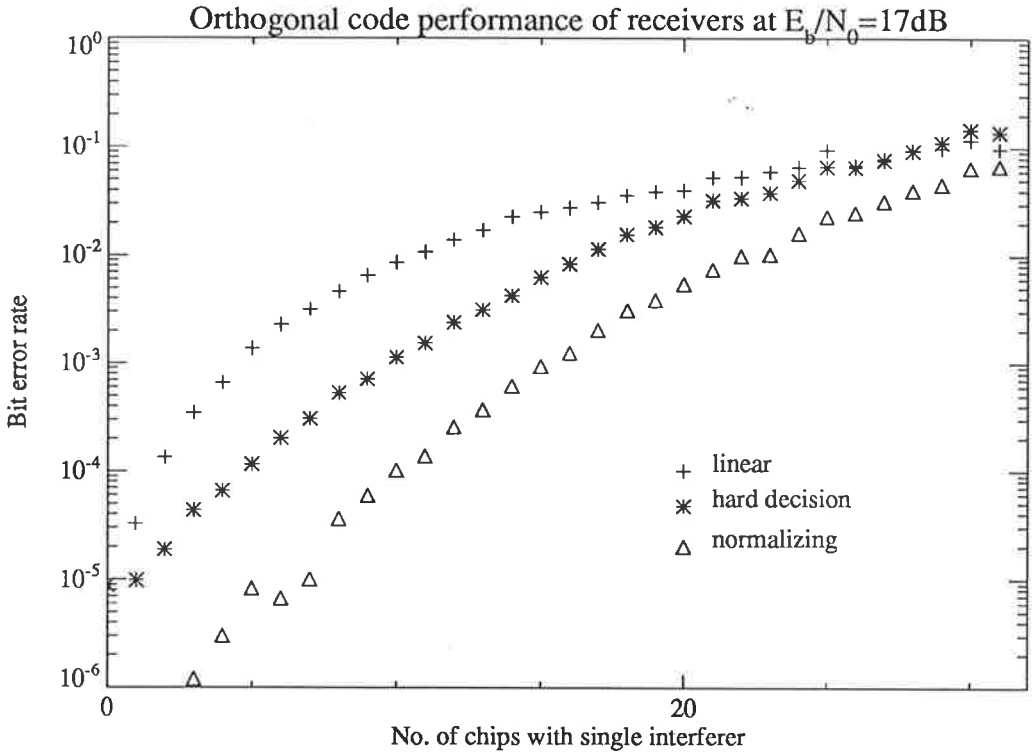

Figure 4.9: Bit error rate of three receiver types for (32,5) orthogonal coding and fading tone interferers, unit power Rayleigh fading, $E_b/N_0 = 17$ dB.

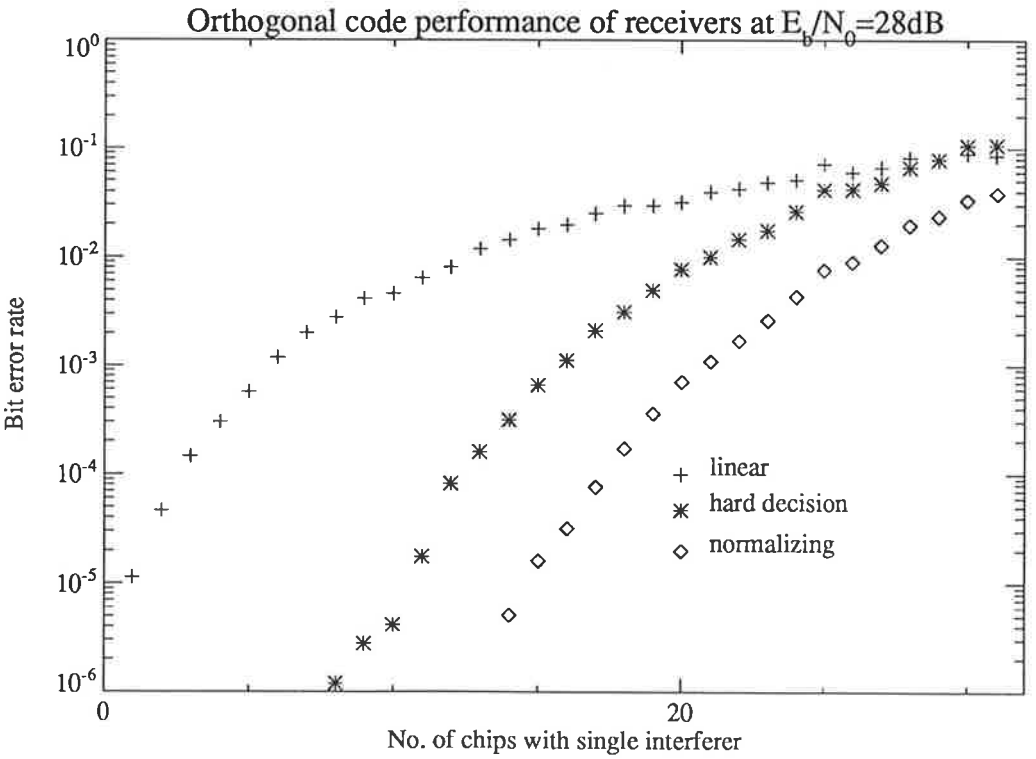

Figure 4.10: Bit error rate of three receiver types for (32,5) orthogonal coding, unit power Rayleigh fading, $E_b/N_0 = 28$ dB.

4.3 Effect of Interference Patterns

One of the quoted advantages of a spread spectrum system is the ability to degrade gracefully. By this, it is meant that the bit error rate of the system degrades for all users gradually as more users are added, increasing the mutual interference. Conversely, it is expected that every user should communicate with almost the same error rate. While the chance of this condition being met is to a large extent determined by the addressing algorithm, it is reasonable to desire that two users subject to the same number of interferers would suffer the same error rate. Unfortunately, the system as presently proposed does not meet this criterion.

Use of a hopping sequence length equal to the codeword length results in a sensitivity of the receiver performance to the interferer locations within the hopping sequence, notably for the hard decision and normalizing receiver. This is not an obvious result. Normal coding practice on a fading or burst noise channel is to interleave the data over a large time frame such that the bits in the de-interleaved stream may be viewed as having independent statistics, and thus the distribution of errors is closer to a random distribution, more easily handled by the majority of decoding schemes. This technique allows the decoder to decode accordingly with no knowledge of the error locations, but requires a large memory and can introduce substantial delay.

With frequency hopping systems, independence of the code bits is achieved through the independence of the frequency channels, and hence there is no need to interleave over time unless the channels happen to be correlated due to a wide coherence bandwidth. It has been shown that [76] that several hundred kilohertz of spread bandwidth used with frequency hopping gives performance equivalent to several hundreds of bits of interleaving. However, this analysis ignores the presence of cyclic interferers which may be present in the frequency hopping cycle in a multiple access situation.

If the code used has a weight structure which exhibits a range of steps, then

the sensitivity to large tone interferers at particular points in the codeword will be different among all the codewords. However, in the case of the Hadamard (or Walsh) orthogonal code, the codewords are regularly structured by their method of formation. All codewords have the same Hamming distance from any other codeword. This leads to a situation where all codewords exhibit an increased error rate when large interferers occur in particular locations within the codeword. This can be shown clearly by the graphs of the codeword error rate for two different series of interferer patterns (patterns 1 and 2), shown in figures 4.11, 4.12 and 4.13. The linear receiver codeword error rate is not significantly disturbed by the effect of the interferer pattern, but the hard decision and normalizing receivers are affected severely.

The comparative performance of the different receiver types for pattern 2 is graphed in figures 4.14–4.17. As shown previously for interferer pattern 1, the differences in performance of the receiver types are maintained, with the normalizing receiver being far superior to both the linear and hard decision receiver at both high and low E_b/N_0 values when one or more tone interferers are present.

In addition to the effect of interferer patterns on codeword error rate, the mapping from the data to codeword is of importance. Under certain mappings, the codeword most likely to be chosen in error will result in the same number of bits being wrong, irrespective of what codeword was transmitted. This can lead to a further deterioration in the bit error rate for certain users, and hence increase the difference in performance between users with the same number of interferers. To illustrate this, the bit error rate graphs corresponding to those previously given for codeword error are shown in figures 4.18, 4.19 and 4.20.

At the high E_b/N_0 value of 28 dB, the bit error rate for pattern 2 is almost identical to the codeword error rate, especially where about half the chips are subject to interference. This implies that a majority of the codeword errors are causing 5-bit errors to occur in the decoded message. Pattern 1, on the other hand, exhibits behaviour which is similar to the case of fading transmission in additive white Gaus-

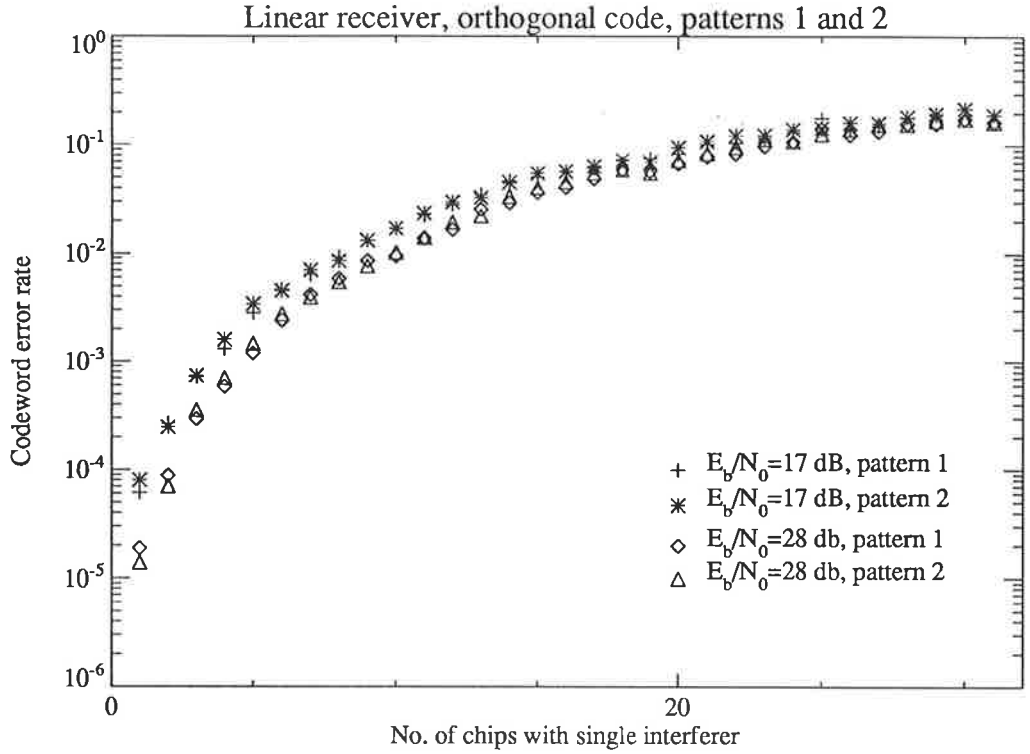

Figure 4.11: Codeword error rate of linear receiver for (32,5) orthogonal coding, with fading tone interferers, unity power Rayleigh fading and two interferer patterns.

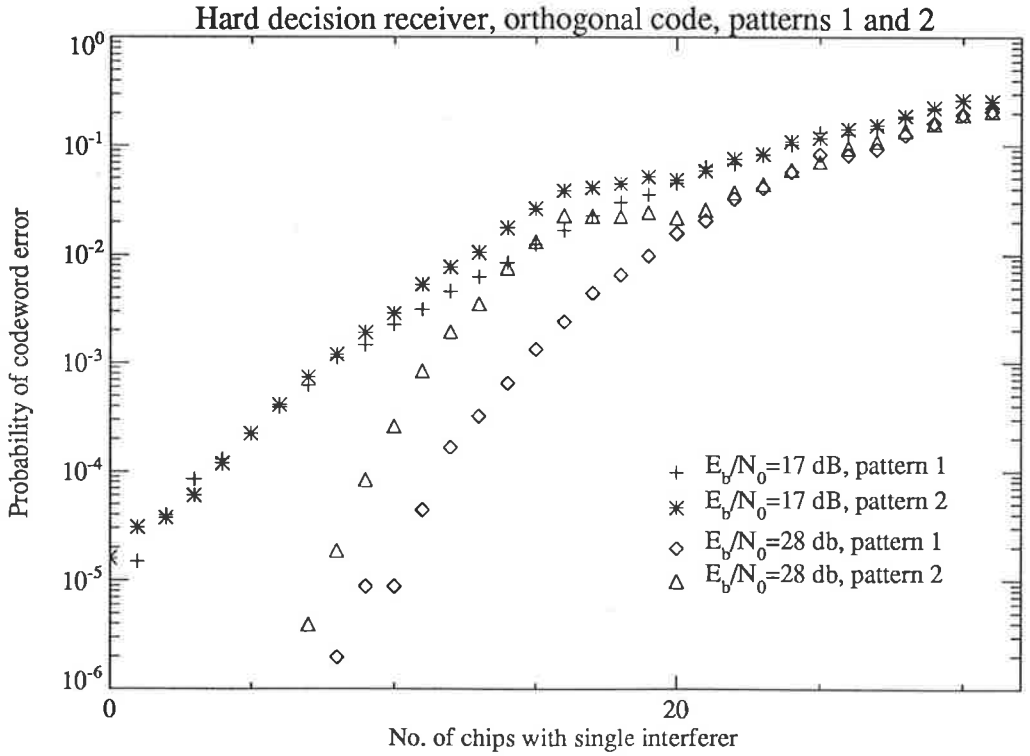

Figure 4.12: Codeword error rate of hard decision receiver for (32,5) orthogonal coding, with unity power Rayleigh fading and two interferer patterns.

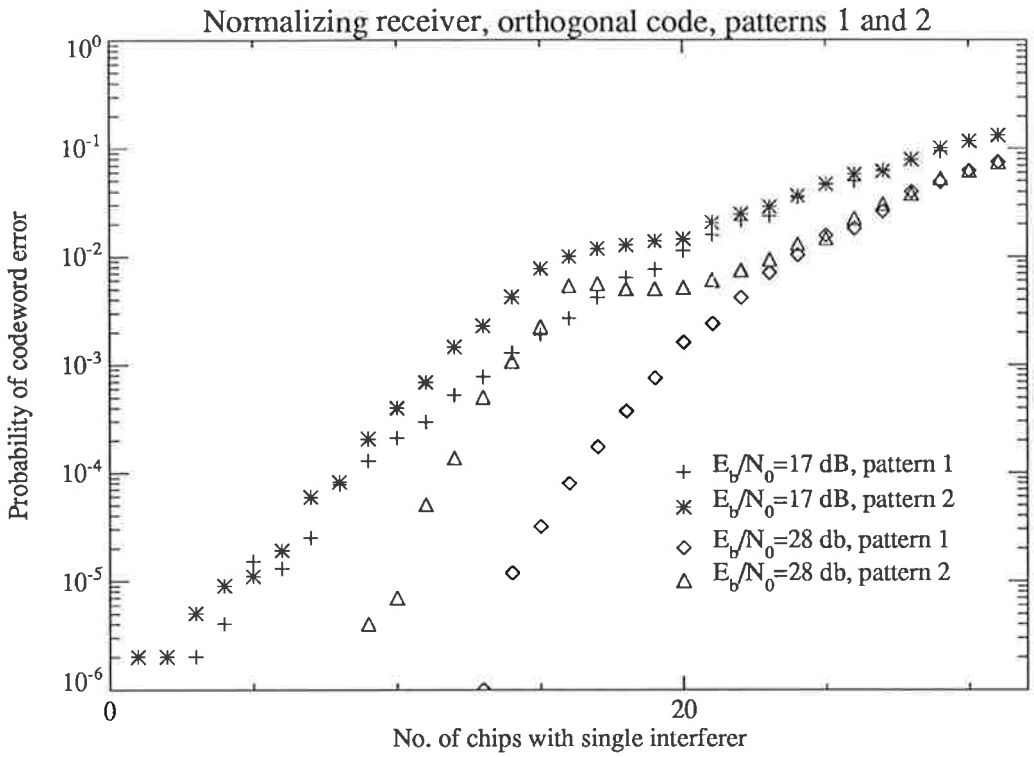

Figure 4.13: Codeword error rate of normalizing receiver for (32,5) orthogonal coding, with unit power Rayleigh fading and two interferer patterns.

sian noise, where the average bit error rate $P_b = 2^{k-1}/(2^k - 1)P_w$, and P_w is the codeword error rate.

The choice of these two patterns is not random. While simulating different interferer patterns with the same number of interferers and interfered chips, it soon became apparent that widely different codeword and bit error rates resulted from different arrangements. After investigating the causes of this problem, two patterns were chosen to exemplify the range of values which could be obtained. The worst case is arranged by successively placing interferers into locations which cause a high probability of a codeword error occurring. This turns out to correspond to the positions of the -1 elements of any of the allowable codewords (how this occurs will be demonstrated shortly). Therefore, a worst case pattern (pattern 2) could be chosen, and corresponds to the last row of the Hadamard matrix when constructed as shown in the introduction to this chapter. (Any of the patterns corresponding to the -1 positions may be chosen, but the last row of the Hadamard matrix was

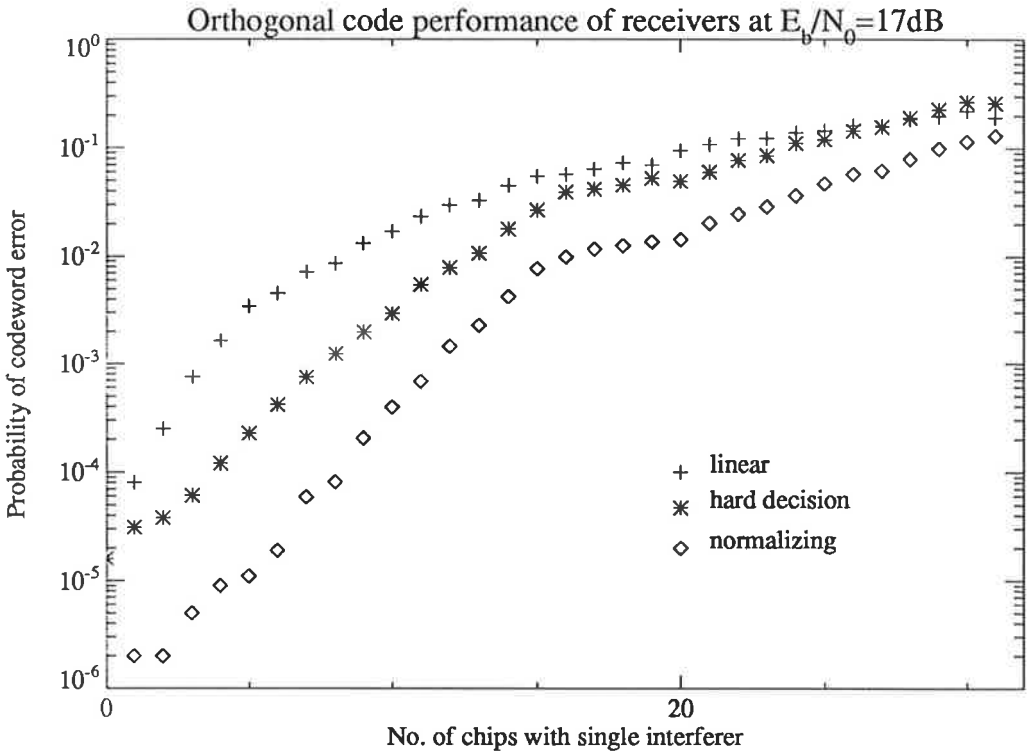

Figure 4.14: Codeword error rate of receivers for (32,5) orthogonal coding and fading tone interferers in pattern 2, unity power Rayleigh fading, $E_b/N_0 = 17$ dB.

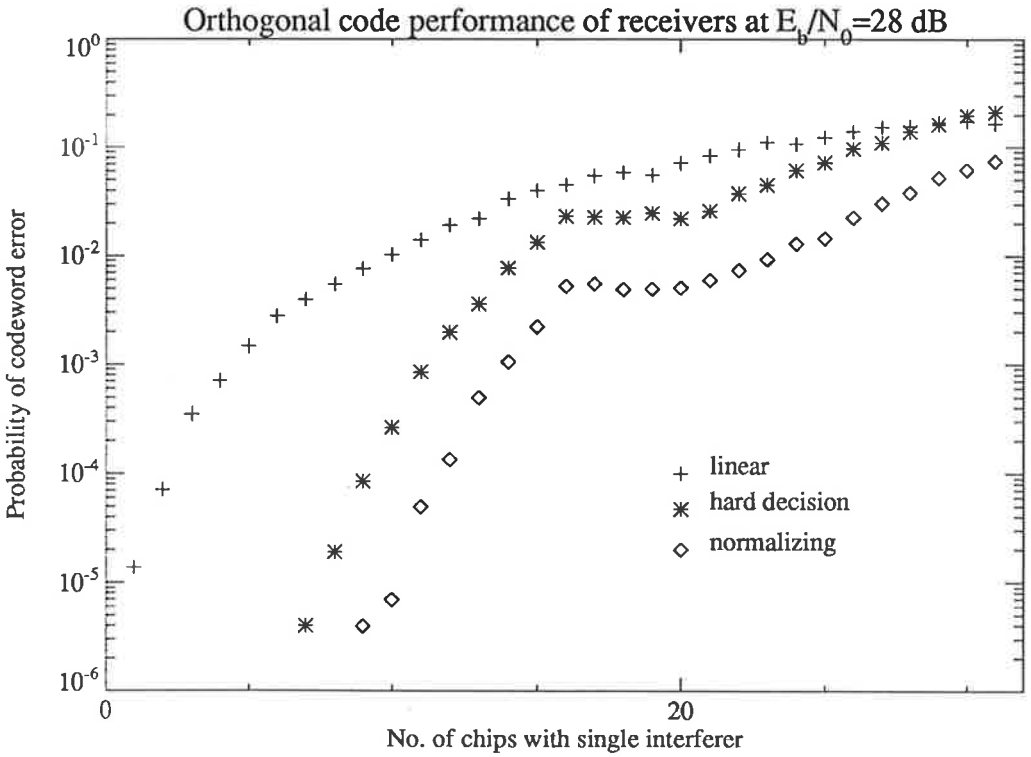

Figure 4.15: Codeword error rate of receivers for (32,5) orthogonal coding and fading tone interferers in pattern 2, unity power Rayleigh fading, $E_b/N_0 = 28$ dB.

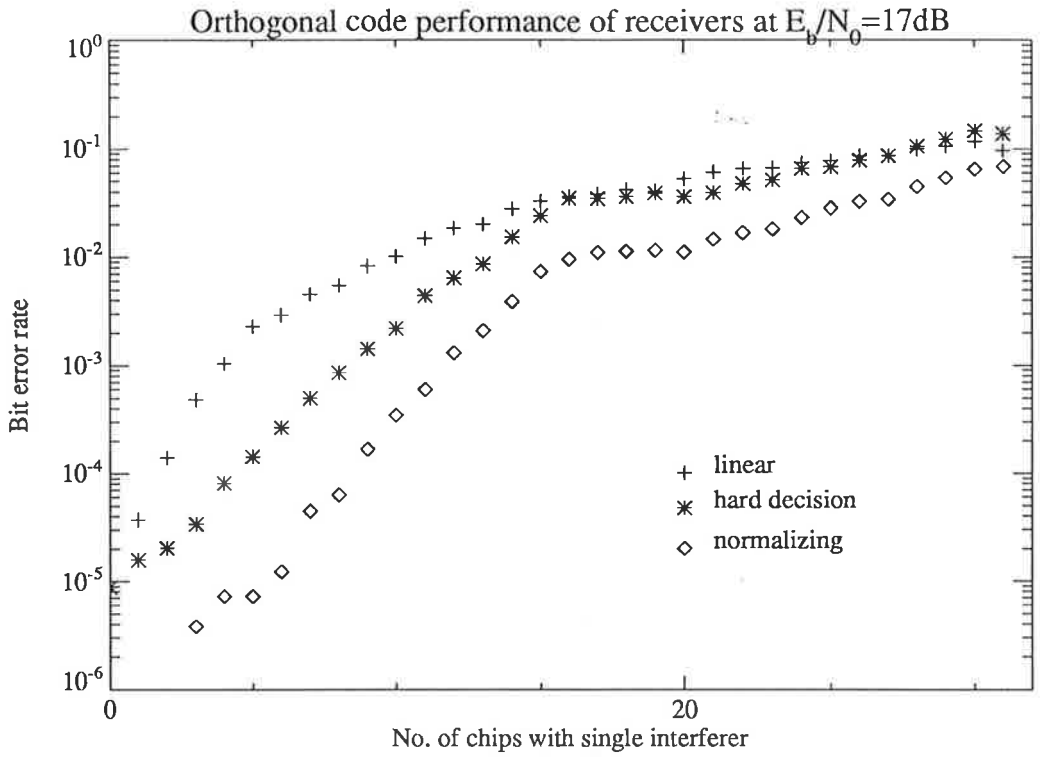

Figure 4.16: Bit error rate of receivers for (32,5) orthogonal coding and fading tone interferers in pattern 2, unity power Rayleigh fading, $E_b/N_0 = 17$ dB.

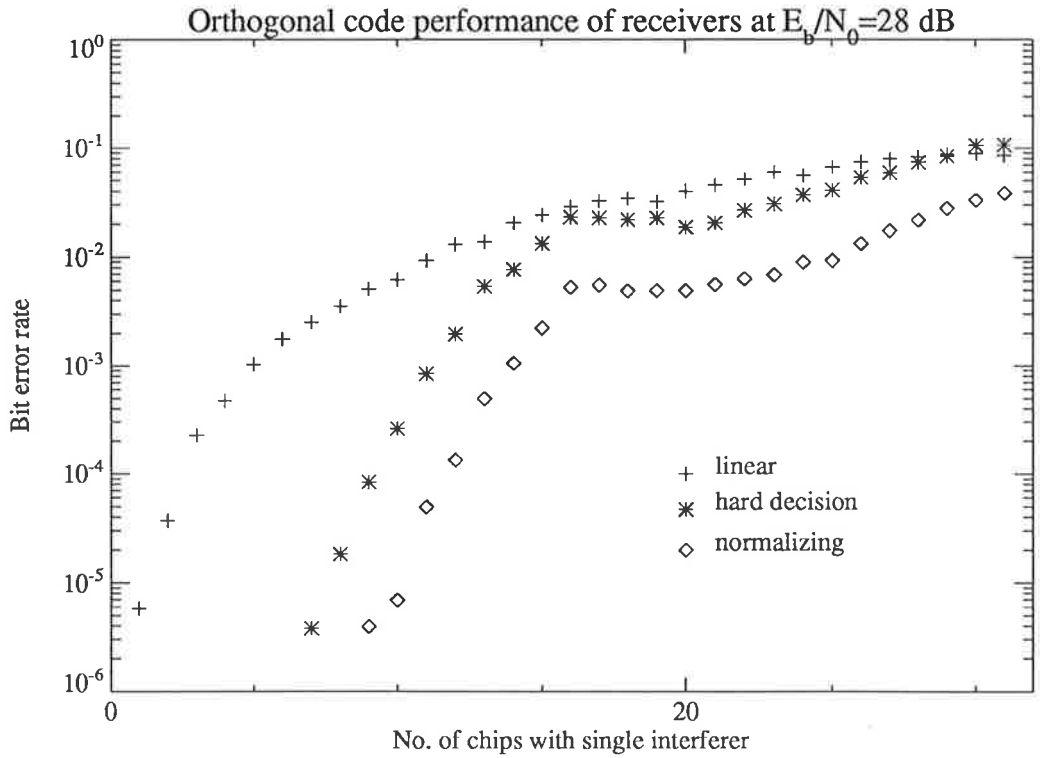

Figure 4.17: Bit error rate of receiver types for (32,5) orthogonal coding and fading tone interferers in pattern 2, unity power Rayleigh fading, $E_b/N_0 = 28$ dB.

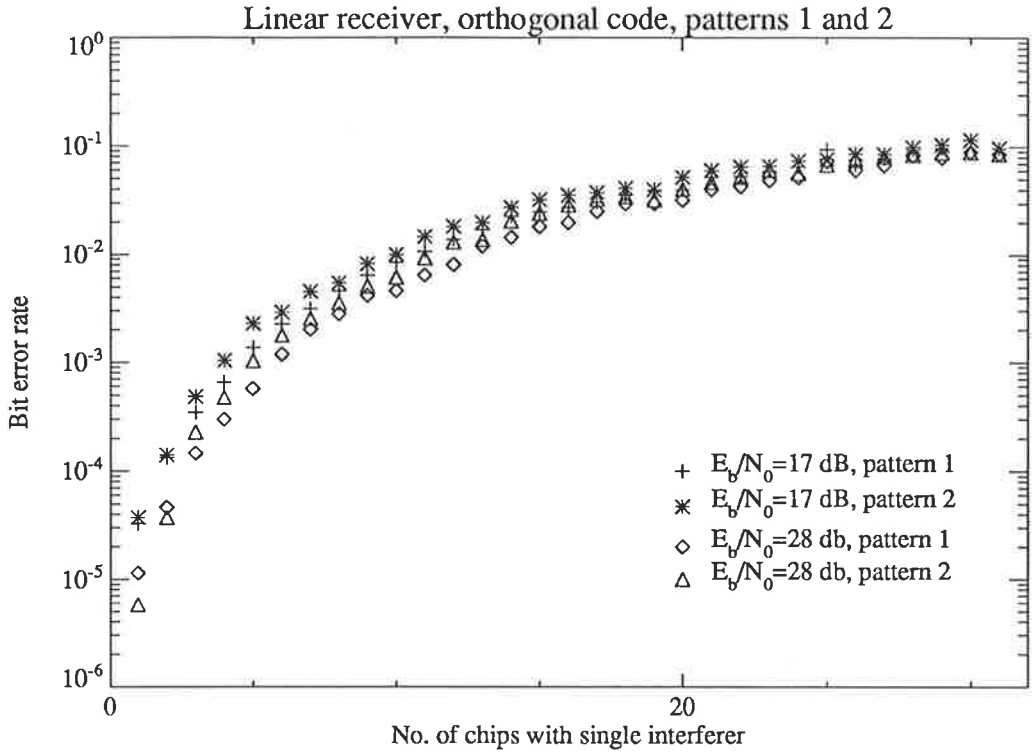

Figure 4.18: Bit error rate of linear receiver for (32,5) orthogonal coding and fading tone interferers, with unit power Rayleigh fading, two interferer patterns.

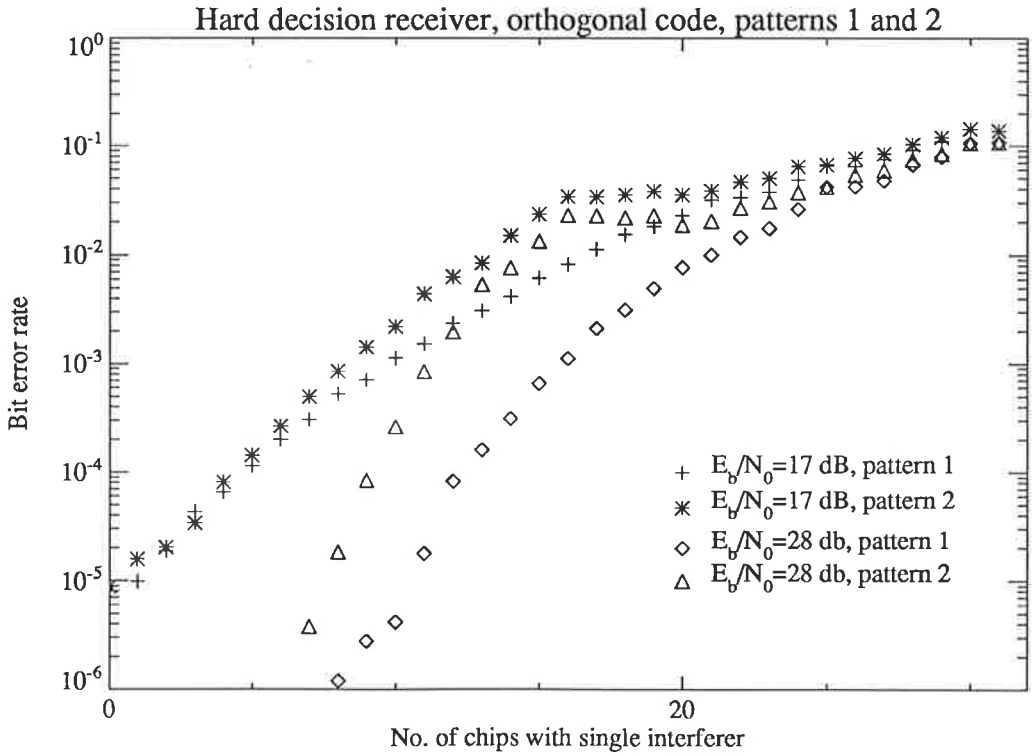

Figure 4.19: Bit error rate of hard decision receiver for (32,5) orthogonal coding, with unit power Rayleigh fading, two interferer patterns.

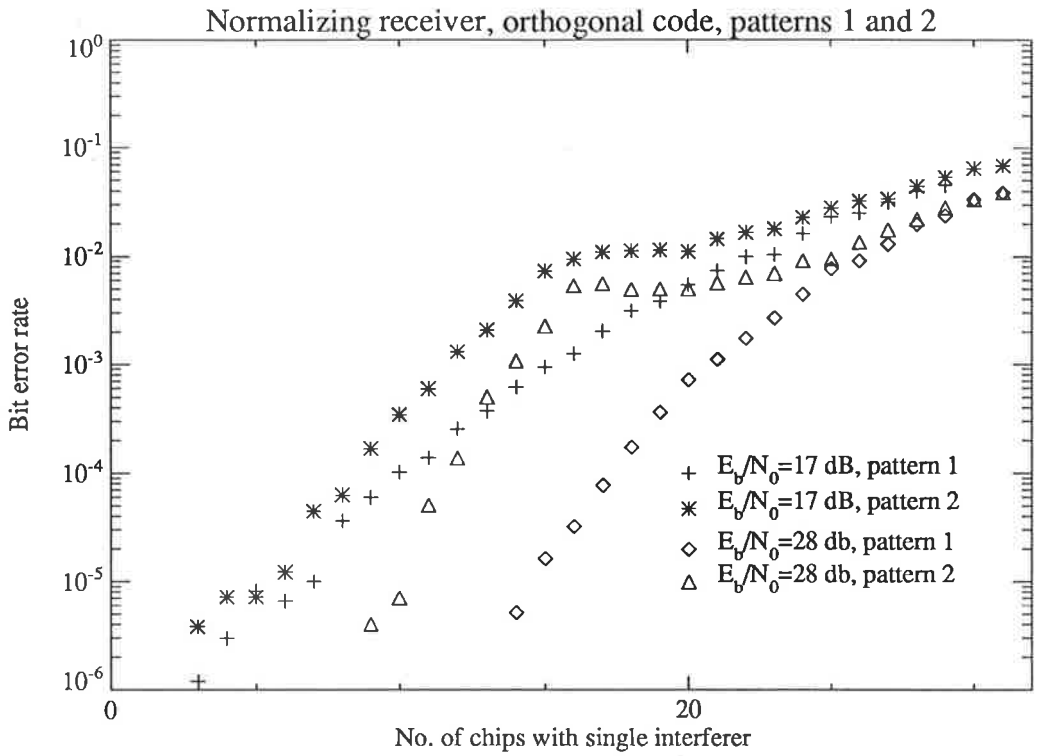

Figure 4.20: Bit error rate of normalizing receiver for (32,5) orthogonal coding, with unit power Rayleigh fading and two interferer patterns.

chosen to illustrate a further property of mapping data to codewords, which will be discussed later.) As the number of interferers increased from 1 to 16, they were randomly placed into one of these remaining slots dictated by the -1 code bit. When all 16 of these slots had been filled, the interferers were placed randomly into all the remaining slots until these were full, with the last to be filled being the very first channel. This channel transmits no information when the number of channels is equal to the number of chips in the codeword of the orthogonal code.

An interferer pattern that reflected the best possible performance was also required. At any stage, the way to assure this is to choose a pattern which has the maximum Hamming distance from the vectors with entries corresponding to the -1 code bits of each of the codewords. To obtain this optimum pattern would require extensive computer searching through all the possible patterns as each new interferer pattern was added, and would take an enormous amount of time to do for all 32 positions. Instead, it was observed that the structure of the Hadamard matrix

incorporates a large amount of repetition in it, with factors of two being prevalent in relating sub-matrices. For this reason, a pattern was devised such that no power of two relationship or symmetry was embodied in the structure when up to 16 interferers were present. Spacing between interferers was arranged such that the number of odd and even chip separations was roughly equal, and the number of chips in each half of the codeword was approximately the same at all stages of filling the chips with interferers. The order of insertion of interferers into the two patterns is shown in table 4.3.

Channel number	Interferer Number	
	pattern 1	pattern 2
1	32	32
2	19	16
3	17	12
4	1	20
5	25	2
6	14	23
7	8	28
8	22	5
9	30	4
10	9	30
11	5	26
12	11	10
13	26	22
14	20	6
15	28	14
16	3	27
17	12	3
18	10	19
19	2	18
20	23	11
21	31	31
22	29	1
23	21	13
24	4	24
25	6	25
26	13	7
27	7	8
28	16	21
29	24	9
30	18	29
31	27	17
32	15	15

Table 4.3: Order in which interferers are inserted, one to each channel.

That the two patterns are well chosen can be seen from the fact that pattern 1 produces codeword errors which result in bit errors which span the entire range from 1 to 5, and have an average bit error rate close to the theoretical average of $P_b = (2^{k-1}/(2^k - 1))P_w$ where P_w is the codeword error rate. Pattern 2 has a far worse error rate that rises steeply with increasing numbers of interferers, and produces 5 bit errors for every codeword error consistently.

Thus not only is there the potential for a user to have a poor codeword error rate due to a bad interferer pattern, but the number of bit errors per codeword error for these patterns can be quite high. Conversely, patterns may be found which have a high codeword error rate, but consistently produce 1 bit error per codeword. This means that for a similar level of interference, the bit error rates for different users may vary by a large amount, and hence all users will not experience the same level of service. Why this occurs is due to the structure of the code, and is best shown by a set of simple examples.

Example

Consider the (8,3) code formed by three data bits acting as an index to the appropriate row of the 8×8 Hadamard matrix, which is to be transmitted. It is assumed that three interferers are present in separate frequencies of the hopping pattern. The number of interferers which will contribute to a pairwise comparison of two codewords can be ascertained. For simplicity, it is assumed that a hard decision receiver is used.

Row A is transmitted and the received row correlated with rows B, where $B = 1 \ldots L$, including A. In checking whether an error has occurred, a series of pairwise comparisons is conducted between the correct output from A and the other outputs. Only those elements $H[A, j] \neq H[B, j]$ are counted in a pairwise comparison. Define the matrix C such that element C_{ij} is the number of interferers which affect the result when the combiner output for transmitted row i is compared with that for row j.

Firstly consider interferers present in the second, third and fifth columns of the

received codewords. It is assumed that the power in the interferers is comparable to that of the wanted signal in those chips, and that noise of far lower power is present in all chips. It is obvious that those chips with strong interferers present will be more likely to be in error in a hard decision receiver. In a normalizing receiver, the more strong interferers present in a pairwise comparison, the more likely that a codeword error is likely to be made.

$$\begin{array}{c} \text{Data} \\ \begin{pmatrix} 000 \\ 001 \\ 010 \\ 011 \\ 100 \\ 101 \\ 110 \\ 111 \end{pmatrix} \end{array} \Rightarrow \begin{array}{c} \text{H} \\ \begin{pmatrix} 1 & 1 & 1 & 1 & 1 & 1 & 1 & 1 \\ 1 & -1 & 1 & -1 & 1 & -1 & 1 & -1 \\ 1 & 1 & -1 & -1 & 1 & 1 & -1 & -1 \\ 1 & -1 & -1 & 1 & 1 & -1 & -1 & 1 \\ 1 & 1 & 1 & 1 & -1 & -1 & -1 & -1 \\ 1 & -1 & 1 & -1 & -1 & 1 & -1 & 1 \\ 1 & 1 & -1 & -1 & -1 & -1 & 1 & 1 \\ 1 & -1 & -1 & 1 & -1 & 1 & 1 & -1 \end{pmatrix} \end{array}$$

Then matrix C is

$$C = \begin{pmatrix} 0 & 1 & 1 & 2 & 1 & 2 & 2 & 3 \\ 1 & 0 & 2 & 1 & 2 & 1 & 3 & 2 \\ 1 & 2 & 0 & 1 & 2 & 3 & 1 & 2 \\ 2 & 1 & 1 & 0 & 3 & 2 & 2 & 1 \\ 1 & 2 & 2 & 3 & 0 & 1 & 1 & 2 \\ 2 & 1 & 3 & 2 & 1 & 0 & 2 & 1 \\ 2 & 3 & 1 & 2 & 1 & 2 & 0 & 1 \\ 3 & 2 & 2 & 1 & 2 & 1 & 1 & 0 \end{pmatrix}$$

This matrix shows that if the interferers are in the stated positions, every transmitted codeword will have on reception a larger probability of being mistaken for one particular codeword than any other. Irrespective of what codeword was transmitted, the full effect of all three interferers is certain to be felt in one pairwise comparison, leading to a much higher probability of error for that comparison, and hence for the overall probability codeword error probability.

The mapping of data to the codeword is clearly seen to be of importance here. The most likely codeword to be chosen in error will result in all three data bits being incorrect, which is the worst case that could be arranged.

So what happens if the interferer pattern is changed? Take another interferer

pattern, such as interferers present in the second, fourth and sixth columns.

$$C = \begin{pmatrix} 0 & 3 & 1 & 2 & 1 & 2 & 2 & 1 \\ 3 & 0 & 2 & 1 & 2 & 1 & 1 & 2 \\ 1 & 2 & 0 & 3 & 2 & 1 & 1 & 2 \\ 2 & 1 & 3 & 0 & 1 & 2 & 2 & 1 \\ 1 & 2 & 2 & 1 & 0 & 3 & 1 & 2 \\ 2 & 1 & 1 & 2 & 3 & 0 & 2 & 1 \\ 2 & 1 & 1 & 2 & 1 & 2 & 0 & 3 \\ 1 & 2 & 2 & 1 & 2 & 1 & 3 & 0 \end{pmatrix}$$

Again, at least one pairwise comparison will feel the full effect of the interferers for any codeword transmitted, and hence a higher codeword error rate will result. The bit error rate will equal one third of the codeword error rate, as the most likely codeword error will always result in one bit error.

Both of the previous patterns of interferers have been distinguished by the fact that they correspond to a subset of the -1 locations of a codeword. Now a pattern will be tried which bears no relation to this criterion, interferers in the third, fifth and seventh elements of the codeword.

$$C = \begin{pmatrix} 0 & 0 & 2 & 2 & 2 & 2 & 2 & 2 \\ 0 & 0 & 2 & 2 & 2 & 2 & 2 & 2 \\ 2 & 2 & 0 & 0 & 2 & 2 & 2 & 2 \\ 2 & 2 & 0 & 0 & 2 & 2 & 2 & 2 \\ 2 & 2 & 2 & 2 & 0 & 0 & 2 & 2 \\ 2 & 2 & 2 & 2 & 0 & 0 & 2 & 2 \\ 2 & 2 & 2 & 2 & 2 & 2 & 0 & 0 \\ 2 & 2 & 2 & 2 & 2 & 2 & 0 & 0 \end{pmatrix}$$

In this situation, the probability of a codeword being in error is reduced, as there are at most only two interferers in each codeword comparison. Instead of one particular codeword being more likely to be picked if errors exist, there are six other possible codewords that could be the ones picked. If the noise level is low compared to the signal and interference levels, such that the probability of a chip error due to noise alone is very low (this being the usual case), the effect will be a lower codeword error rate.

Given that this situation exists, what can be done about it? The obvious solution is to try to randomise the interferer pattern over time. This can be done by mapping the bits of the codewords onto the frequency channels in an order which changes

with time, such as from cycle to cycle. At the receiving end, the inverse transform must be carried out to reorder the code bits correctly prior to decoding. This may raise problems when synchronisation is lost and must be reestablished. To enable this to be done reasonably quickly, the number of different permutations of the code bits must be limited to be fairly small. The choice of the best permutations to use is also not obvious.

One method possible for achieving a limited amount of randomness of the interferer patterns is to rotate the codeword through a larger frequency set than the codeword length. As long as the hopping sequence length L and the codeword length n are relatively prime, this will ensure that the interferers effectively cycle through L different patterns in the codewords. When using a longer sequence length, the variance of the number of interferers within the sequence over all the users should decrease, and bit error rates of the users should be more tightly clustered around the mean. However, using longer sequences also has a disadvantage in that the frame period increases, and thus the irreducible error rate of the DPSK modulation will be higher due to decreased correlation between chips at a particular frequency.

This rotation scheme was simulated for the patterns 1 and 2. For efficiency reasons, the (31,5) simplex code was used instead of the (32,5) orthogonal code, and a channel set of 32 frequencies was used for each user. This means that any interferer present will appear in all 31 chips of the codeword successively. The contrasting situation where an interferer will always appear in the same chip of the codeword is obtained by using a set of 31 channels. The results for the codeword error rate of the hard decision and normalizing receivers are shown in figures 4.21–4.24.

It is clear that this method does substantially reduce the difference between patterns 1 and 2 which represent one of the best and one of the worst cases respectively. Pattern 1 is shown to give very slightly worse error rates, while the error rates for pattern 2, while still exhibiting a pronounced "hump" for moderate numbers of interfering chips, are far lower than for the case where interferers are stationary within the same codeword chips. Also shown is the relative bit error rate performance of the

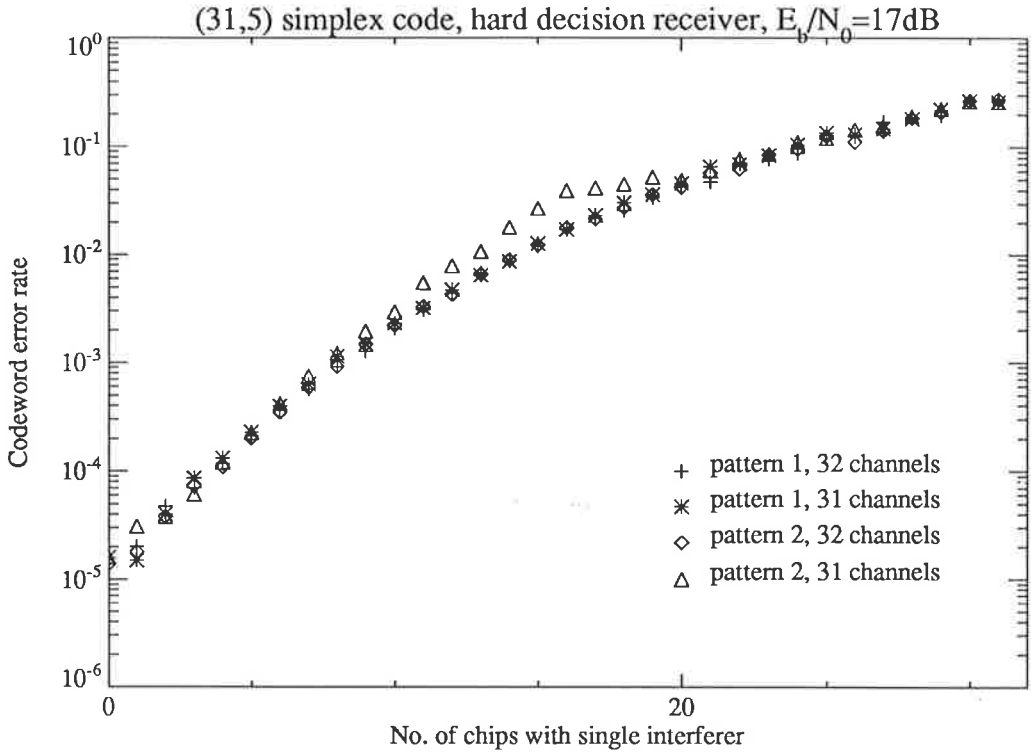

Figure 4.21: Codeword error rate of hard decision receiver for (31,5) simplex coding, Rayleigh fading, $E_b/N_0 = 17$ dB, interferer patterns 1&2, using 31 and 32 channels.

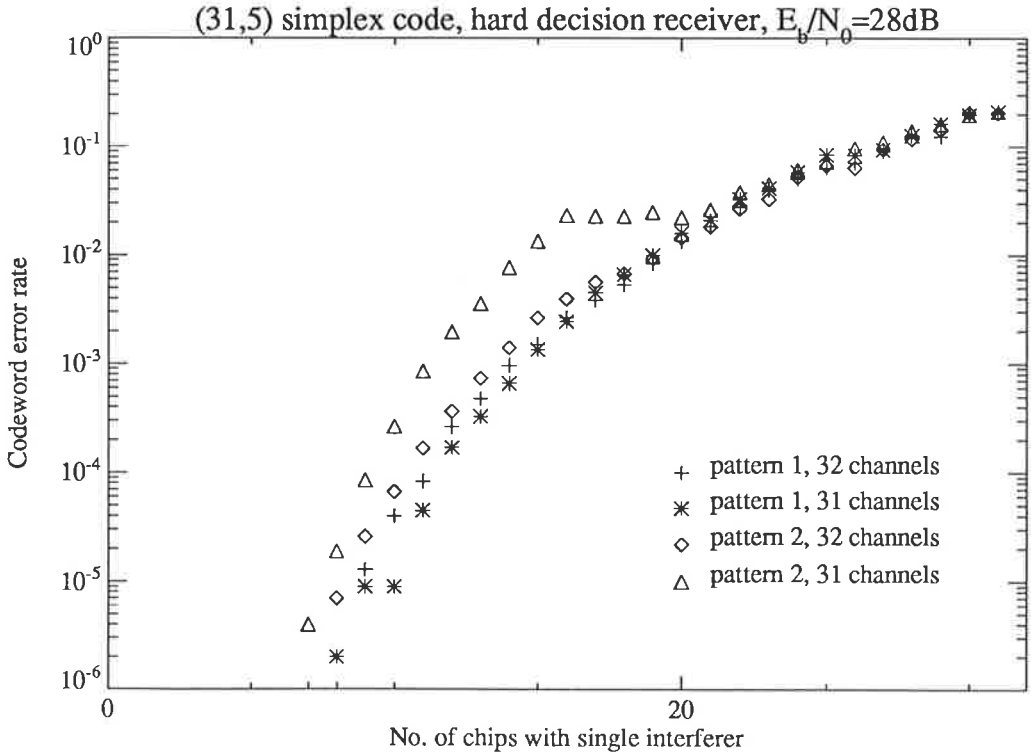

Figure 4.22: Codeword error rate of hard decision receiver for (31,5) simplex coding, Rayleigh fading, $E_b/N_0 = 28$ dB, interferer patterns 1&2, using 31 and 32 channels.

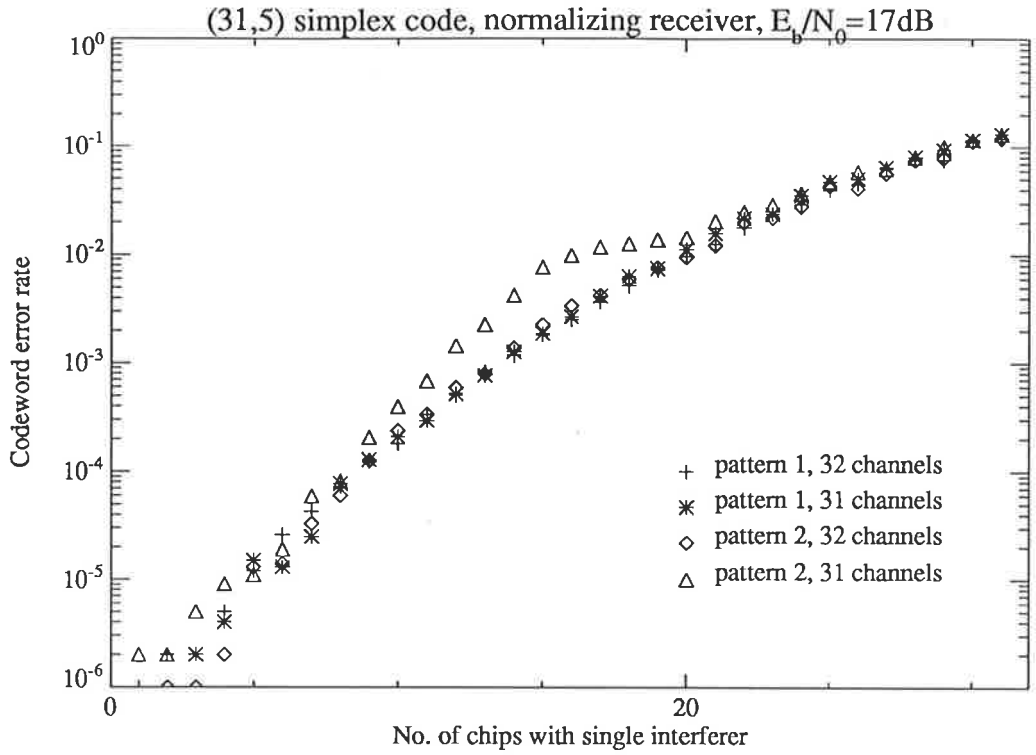

Figure 4.23: Codeword error rate of normalizing receiver for (31,5) simplex coding, Rayleigh fading, $E_b/N_0 = 17$ dB, interferer patterns 1&2, using 31 and 32 channels.

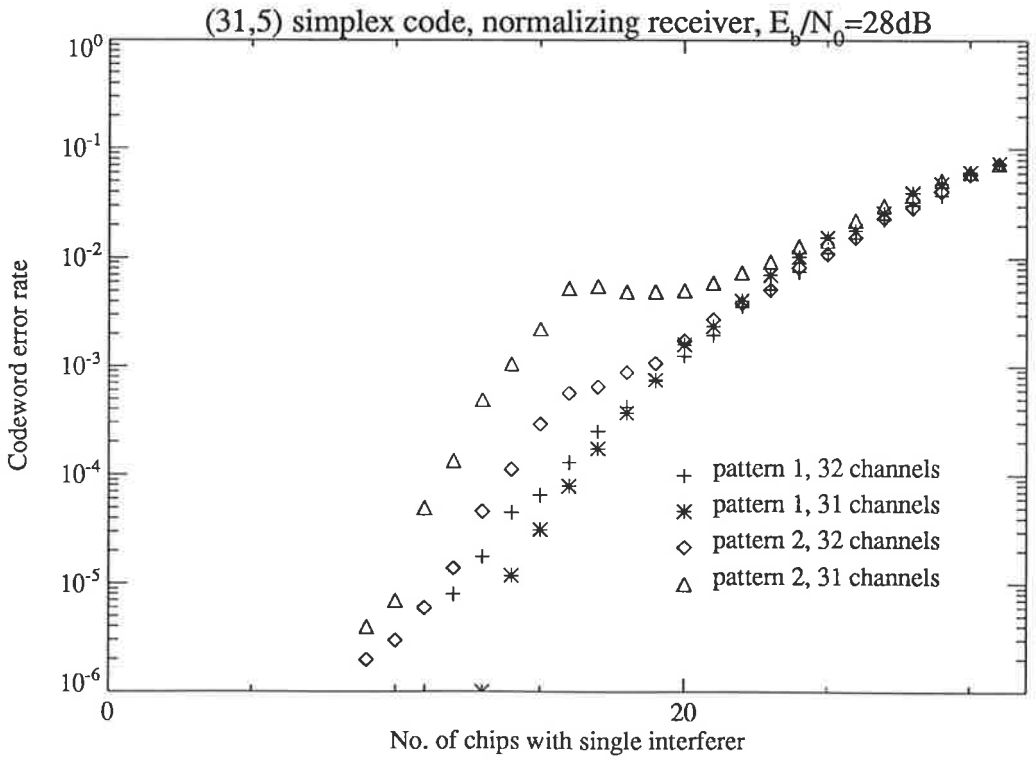

Figure 4.24: Codeword error rate of normalizing receiver for (31,5) simplex coding, Rayleigh fading, $E_b/N_0 = 28$ dB, interferer patterns 1&2, using 31 and 32 channels.

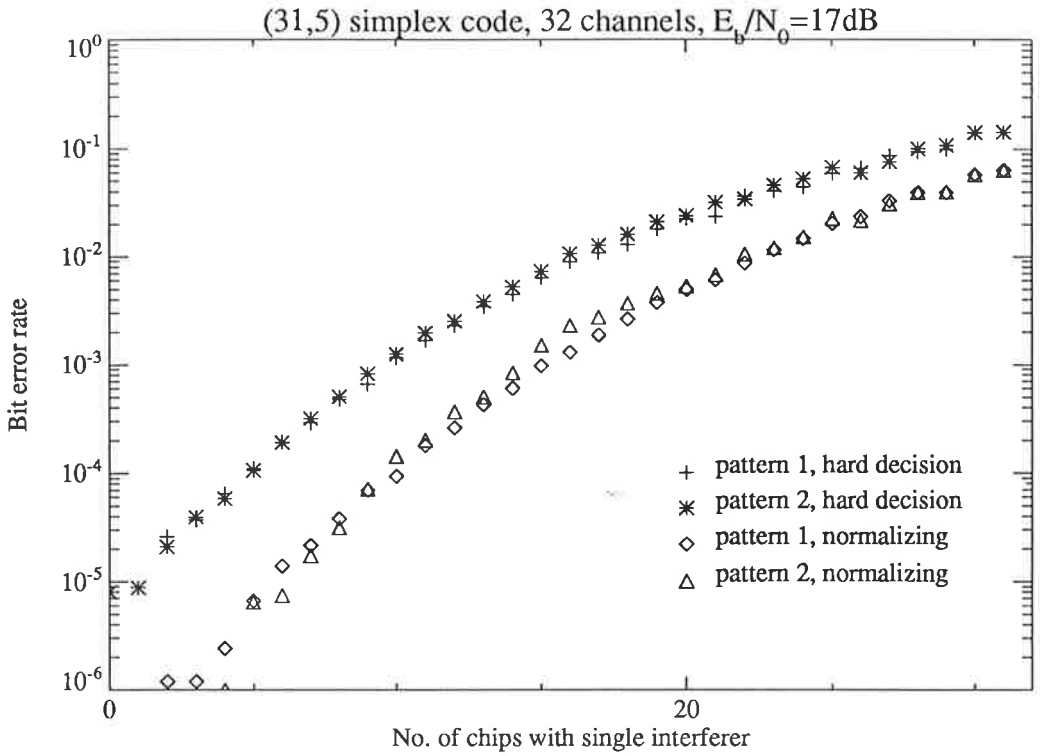

Figure 4.25: Bit error rates of receivers for (31,5) simplex coding, Rayleigh fading, $E_b/N_0 =$ 17 dB, 32 channels, interferer patterns 1&2.

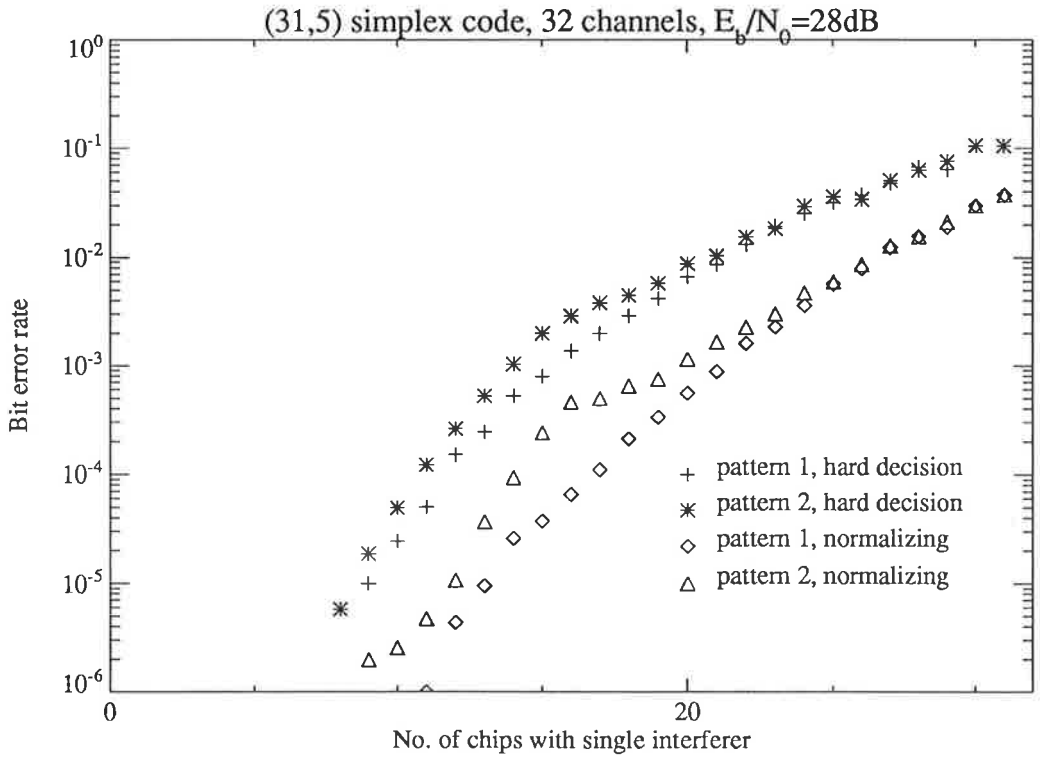

Figure 4.26: Bit error rates of receivers for (31,5) simplex coding, Rayleigh fading, $E_b/N_0 =$ 28 dB, 32 channels, interferer patterns 1&2.

two receivers at E_b/N_0 of 17 dB and 28 dB. The difference in performance between the two receivers is maintained at a value similar to that previously noted.

In this rotation scheme, some patterns will still be a problem, such as the pattern 101010... in the simplex code (where the 1's represent an interfered frequency channel), which will have a higher codeword error rate every second codeword. For example, for the hard decision receiver with 16 interfered channels and $E_b/N_0 = 28$ dB, this interferer pattern has a codeword error rate of about 2.3×10^{-2} when 31 channels are used, and 1.0×10^{-2} when a set of 32 channels are used. This is consistent, as the error rate for 32 channels is expected to be around half the error rate for when 31 channels are used. However, the probability of this particular pattern occurring is fairly remote. It is possible with this approach to arrange the patterns with the most amount of uniform repetition in them (such as 101010...) to correspond to the least number of bits in error, given that that codeword error is made: a form of Gray coding.

To avoid the complexity of this Gray coding approach, or if a codeword-to-channel permuting process is not being used, another mapping approach would be to have the average number of information bit errors per wrong codeword to be about half the number of bits per data word for all interferer patterns. No optimal procedure could be found for mapping the data to the codeword. It is likely that an exhaustive search of all possibilities by computer would be necessary. For the Hadamard matrix as shown previously, it has been found that any structure present in the Hadamard matrix should not be present in the corresponding data matrix. In the example given previously, the mapping progresses uniformly down the rows of the Hadamard matrix, with higher order data bits referring to alternate rows. This factor of two relationship can be seen to be reflected in the Hadamard matrix. In fact, any structure which incorporates a factor of two in the mapping appears to result in a poor mapping. For example, for the Hadamard matrix as defined above,

the mappings

$$\begin{pmatrix} 000 \\ 001 \\ 011 \\ 010 \\ 110 \\ 111 \\ 101 \\ 100 \end{pmatrix} \qquad \begin{pmatrix} 010 \\ 011 \\ 001 \\ 000 \\ 111 \\ 110 \\ 100 \\ 101 \end{pmatrix}$$

are not optimum, as for interferers in positions (2,4,5) and (2,3,5) respectively, the most likely codeword error will always produce three bit errors. The first and second columns of the each pattern exhibit a factor of two relationship in the blocks of 1s and 0s. Mappings such as

$$\begin{pmatrix} 000 \\ 001 \\ 010 \\ 100 \\ 111 \\ 011 \\ 110 \\ 101 \end{pmatrix}$$

which are designed to avoid symmetry and two-fold element structures, perform well for a large number of interferer patterns, although this was not exhaustively tested. Thus it is feasible that such mappings with good properties may exist, but they are difficult to find, and the difficulty is increased as the codeword length increases. Moreover, the importance of the optimality of such data-to-codeword mappings is diminished if a codeword-to-channel permuting process is used, as the different interferer patterns in the codewords will ensure that a variety of bit errors will occur overall.

4.4 Isolated Cell Uplink Simulation with Random Allocation of User Hopping Sequences

It has been demonstrated in previous sections that the performance of the normalizing receiver is far better than that of the hard decision and linear receivers when

the number of tone interferers present in each chip is constrained to be one or zero. Before any conclusions may be drawn from this result, it is necessary to determine whether the normalizing receiver outperforms the hard decision receiver when an arbitrary subset of the total number of interferers may be present in each chip. (The linear receiver performs so poorly in the presence of tone interferers that it is not considered).

As there are are an enormous number of ways in which even a small number of interferers may be distributed throughout a user's hopping cycle, it is feasible only to take a few samples of the possible interferer patterns. This was achieved by assigning to each user a hopping sequence with a random time shift (as happens in practice) and using the resulting pattern of interferers in the target user's hopping cycle as the condition for simulation. By performing enough such simulations, a representative spread of situations likely to occur in practice may be achieved.

The simulations assumed the same parameters used in the previous simulations, with the exception that (31,5) simplex coding was used, as it requires one less bit per codeword to be transmitted than the (32,5) orthogonal code and gives a slightly greater number of channels ($q = 100$ instead of 96) within the 20 MHz bandwidth. The E_b/N_0 value was reduced by 0.18 dB to make the chip energy equal to that used in the orthogonal code simulations previously performed. Power control was assumed on the uplink, and therefore user position and shadow fading were ignored, with the Rayleigh fading, which multiplied the transmitted signals, having an average power of unity. As before, chip synchronism between user hopping sequences was assumed, ensuring that results could be compared with those already obtained.

For a given number of users in the cell, each user was allocated a hopping sequence from a one-coincidence set (section 1.3) with a random time shift corresponding to an integral number of chips, distributed uniformly over the entire hopping cycle. This meant that the number of interferers that could be present in a hopping cycle was less than or equal to the total number of active users, and that every permutation of positioning these interferers within a set of channels was possible. The

values of users per cell were chosen to be those values predicted to give $P_b \approx 10^{-3}$ for a certain E_b/N_0 ratio and random addressing (this is discussed in more detail in section 6.3). To average out the effects of bad user patterns within the codeword, a set of 32 channels was assumed for each user.

The resulting system was simulated and the error statistics collected. For a particular combination of E_b/N_0 ratio and number of users, 50 simulations were executed with different initial random seeds, (50 being chosen as a compromise between accuracy and total run time). For these simulations, the sample mean $\bar{P}_b$ and sample variance V_{P_b} were calculated for the bit error rate. In addition, the median bit error rate $\hat{P}_b$ was determined.

The results are given in table 4.4 and illustrated in figures 4.27, 4.28. The normalizing receiver can be seen to maintain its superiority over the hard decision receiver. When the normalizing receiver is experiencing an error rate in the range 10^{-4}–10^{-3}, the corresponding hard decision receiver error rate will be 6–8 times larger, with the factor increasing with E_b/N_0. This is in agreement with the restricted cases where a maximum of one interferer per chip is allowed. The spread of the results is reflected in the sample variances. From the limited number of points, it appears that the variance, as a proportion of the mean value, increases as the number of users and E_b/N_0 increase. A possible reason for this is that in an interference-limited system (noise has little effect), bad interferer patterns which cause high error rates can occur even when the majority of interferer patterns will cause low error rates. At lower E_b/N_0, the system error rate is influenced far more by noise, and therefore the effect of interferer patterns is of less importance, leading to a more tightly bunched set of samples. As the number of users increases, the probability of a specified bad pattern occurring increases, and so too does the possible severity of the interference. These factors are responsible for the larger spread of bit error rate samples.

The median bit error rate is also of interest. It is noted from the graphs of results (figures 4.27, 4.28) that the spread of results sometimes extends quite a long way below the mean. In such cases where the distribution may have a large area

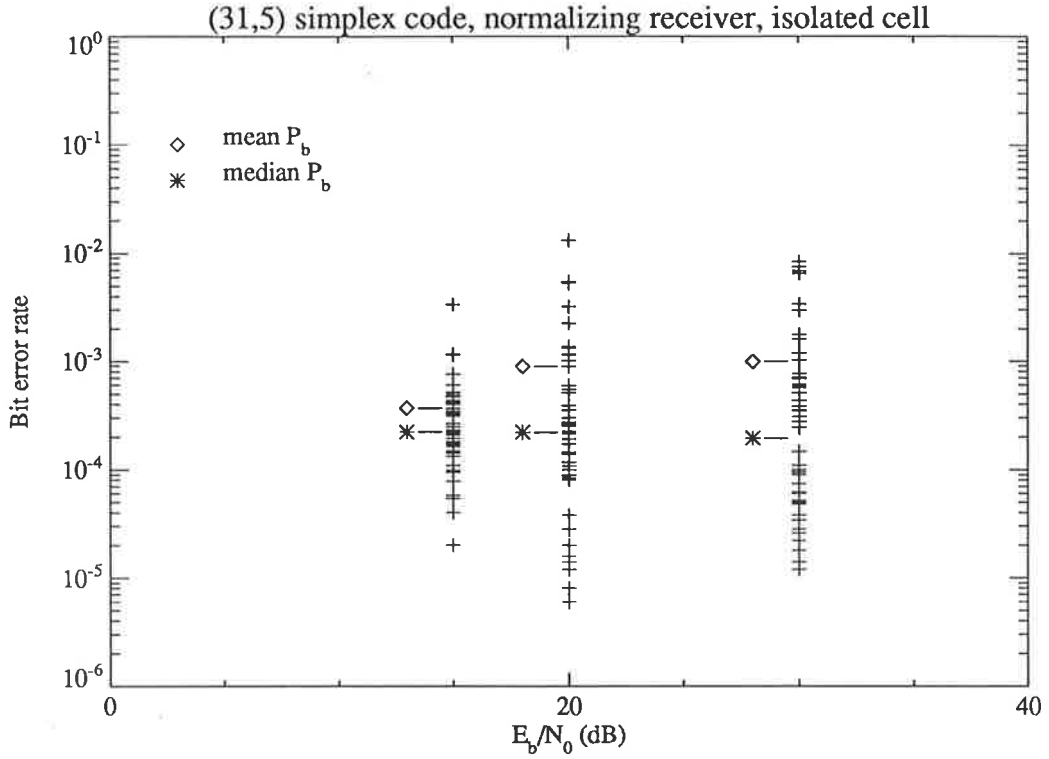

Figure 4.27: Sample bit error rates of 50 uplink simulations for the normalizing receiver, with (E_b/N_0, no. of users) being (15,30), (20,60) and (30,75).

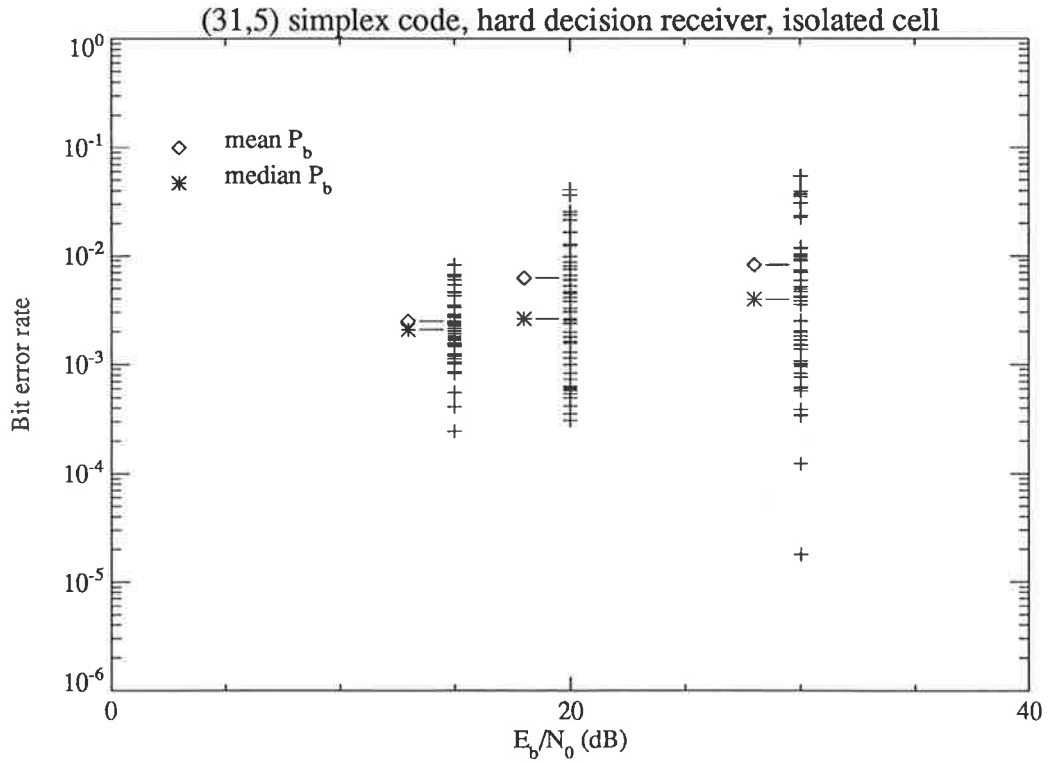

Figure 4.28: Sample bit error rates of 50 uplink simulations for the hard decision receiver, with (E_b/N_0, no. of users) being (15,30), (20,60) and (30,75).

	E_b/N_0 (dB)	No. Users	$\bar{P}_b$	$\hat{P}_b$	V_{P_b}
Normalizing receiver	15	30	3.7×10^{-4}	2.2×10^{-4}	2.6×10^{-7}
	20	60	9.0×10^{-4}	2.2×10^{-4}	4.8×10^{-6}
	30	75	9.9×10^{-4}	2.0×10^{-4}	4.0×10^{-6}
Hard decision receiver	15	30	2.5×10^{-3}	2.1×10^{-3}	3.0×10^{-6}
	20	60	6.2×10^{-3}	2.6×10^{-3}	8.0×10^{-5}
	30	75	8.2×10^{-3}	4.0×10^{-3}	1.4×10^{-4}

Table 4.4: Error rate statistics for user numbers estimated to give $P_b = 10^{-3}$ for normalizing receiver and random addressing.

in the tails of the distribution, the median is often taken as a more robust measure of centre of the distribution. The median position is an estimate of the error rate below which the error rates of 50% of all users will fall. In this instance, the median value $\hat{P}_b$ lies consistently below the mean value $\bar{P}_b$, indicating that a small number of large values of P_b are inflating $\bar{P}_b$ to a value greater than that experienced by a majority of users. This suggests that the median has more practical significance than an average error rate taken over all users. The difference between the median $\hat{P}_b$ values for the hard decision and normalizing receivers is approximately an order of magnitude, again emphasising the better performance of the latter.

On the basis of these results, the difference in performance between the normalizing and hard decision receivers can thus accepted as being generally true in practice for the values of E_b/N_0 and number of users being considered. This will be used to estimate the number of users possible in a isolated cell system in a later chapter.

4.5 Multiple Cell Simulation of the Uplink

For the multiple cell simulation of the uplink, a cluster of one central hexagonal cell and six surrounding cells was modelled. A cell corner radius of eight kilometers was used. Power control was assumed within each of the cells to overcome attenuation and shadow fading, and for transmissions received from foreign cells, shadow fading

was incorporated as described in section 3.4. For a given number of users in each cell, each user was allocated a one-coincidence hopping sequence with a random time shift, uniform over the hopping sequence.

Both chip synchronous and entirely asynchronous systems were studied. In the former, hopping sequences of all users are aligned at chip boundaries, thus leading to total or nil overlap of chips and no adjacent channel interference. In the second system, a continuous time overlap of the user hopping sequences exists, and hence cochannel and adjacent channel interference can exist for fractions of a chip. In this latter case, only the immediately adjacent channels on each side were modelled, as contributions from further channels decrease rapidly in significance and to take account of them would increase run times considerably. Again as for the isolated cell, 50 simulations were run for each combination of E_b/N_0 and number of users.

The mean and median bit error rates are shown in figure 4.29, and all results are tabulated in Appendix B. Similar trends in results are noted to the isolated cell simulations. The normalizing receiver always outperforms the hard decision receiver, with the hard decision receiver bit error rate being 3–8 times the corresponding normalizing receiver bit error rate when the latter is in the range 10^{-3}–10^{-4}. A larger spread of recorded bit error rates, as a proportion of the mean, is observed for larger numbers of users and higher E_b/N_0. The median bit error rates are again always below the sample mean bit error rates, the median often being about half the mean in the vicinity of $P_b = 10^{-3}$.

When interference is constrained to be chip synchronous, the bit error rates recorded are 2–3 times higher than the corresponding result when interference is allowed to be asynchronous. It would appear that the effects of adjacent channel interference and increased numbers of co-channel interferers, overlapping for fractions of a chip in the asynchronous case, are not severe enough to equal the interference from a smaller number of co-channel interferers, each overlapping for a complete chip. This justifies the approach of modelling the interference as chip synchronous in the isolated cell to give a worst case scenario (proposed by Yue [26]).

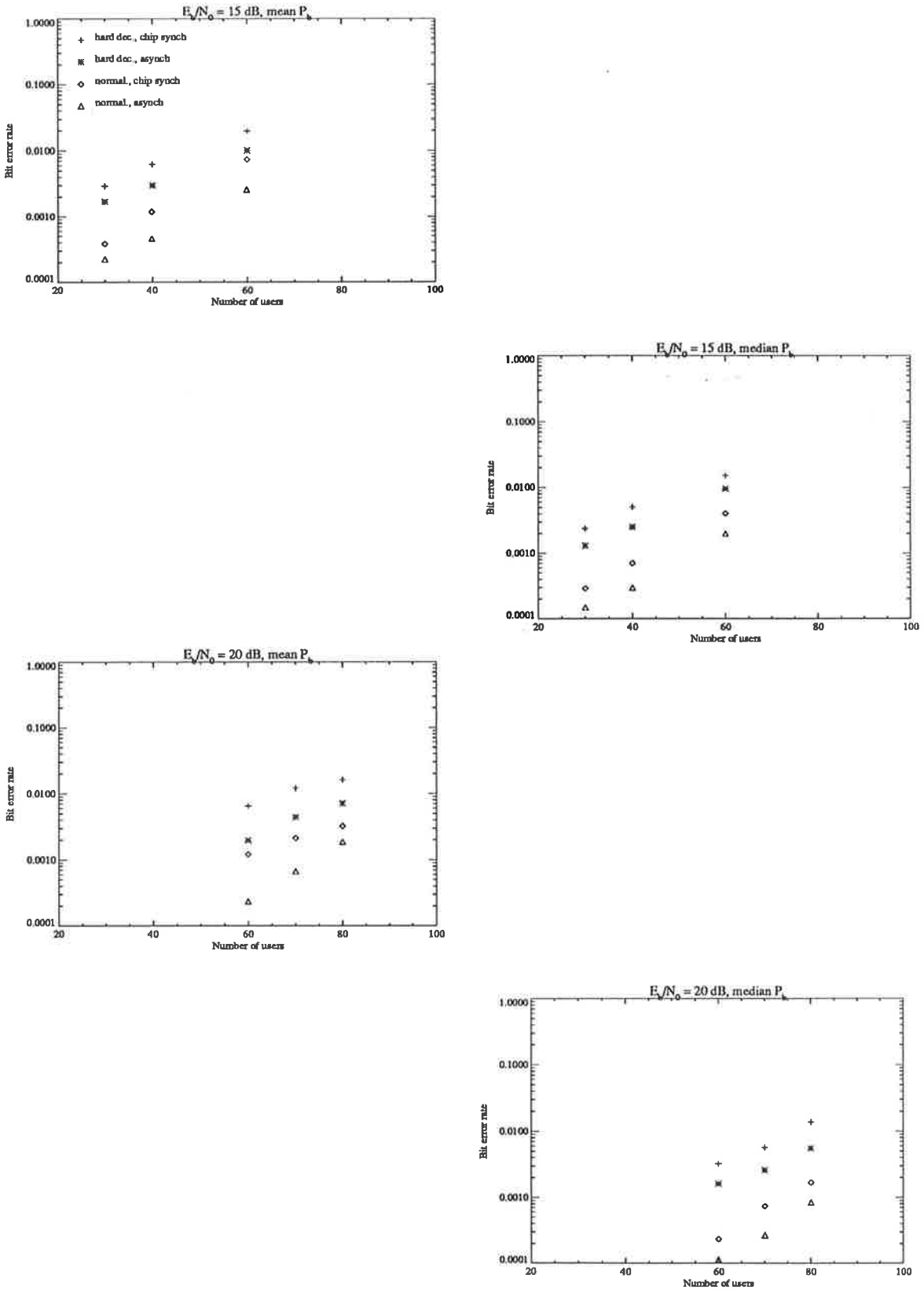

Figure 4.29: Sample mean and median bit error rates of 50 uplink simulations, for $E_b/N_0 =$ 15 and 20 dB

This is in contrast to the FH-MFSK scheme with adjacent channel interference examined by Agusti *et al* [44], where it was found that the presence of asynchronous users and the resulting adjacent channel interference substantially degraded the performance of the system over the chip synchronous case. The poor performance of FH-MFSK can be explained by an increased number of false alarms in incorrect chips being recorded as a result of interference being above threshold in the adjacent channel as well as the correct channel. A net increase in the number of signals above threshold which form valid codeword sequences increases the error rate of the FH-MFSK system.

In areas where many more than seven cells exist, it may be difficult to achieve a high E_b/N_0 value in a cell due to interference (assumed here to be Gaussian) from those cells outside the first surrounding ring. However, if an E_b/N_0 of 20–30 dB is available, the results for these multiple cell uplink simulations indicate that up to 70–80 users per cell should be feasible in a power control situation. These results are superior to those for the FH-MFSK system obtained by Agusti *et al*, given in section 1.6, although further improvements in the FH-MFSK system capacity are obtained through using addressing knowledge in the decoding process.

4.6 Multiple Cell Simulation of Downlink

For downlink simulations, transmissions from a particular base station are frame synchronous. As no power control is used, signals from the target user's current base station are assumed to be received with a certain specified area mean E_b/N_0 ratio, which is then subject to lognormal fading to form the local mean. Rayleigh fading and Gaussian noise then affect each channel independently. The signals from a foreign base station (which do not interfere among themselves) are assumed to arrive with a random time shift uniformly and continuously distributed over the hopping sequence period, thus forming asynchronous interference. If it is assumed that each base station transmits equal power, then these signals from foreign cells are received with area means that suffer extra attenuation due to any excess dis-

tance from the mobile to the foreign base stations over the distance to the home base. The procedure used to calculate the slow fading modifier was described in section 3.4. The transmissions from foreign base station also suffer Rayleigh fading independently on each channel.

As a complete characterisation of the system is beyond the scope of this work, a limited number of simulations were performed to observe the trend of the results. Both hard limiting and normalizing receivers were simulated, with 50 simulations being performed for E_b/N_0 ratios of 15 and 20 dB, and the number of users fixed at 60 per cell. The radius to the cell corners from the central base station was 8 km, with the mobile unit being located in a cell corner, equidistant from its base station and two others. This has been found to be the worst position for interference when no power control is employed [25,77]. The results are given in table 4.5, and illustrated in figures 4.30 and 4.31. Where no errors occurred during the 10^5 codewords transmitted during a simulation, the codeword error rate was set to 10^{-5} as an estimated worst case and the corresponding bit error rate estimated to be 5.2×10^{-6}.

Receiver	E_b/N_0 (dB)	No. Users	$\bar{P}_b$	$\hat{P}_b$	V_{P_b}
Hard	15	60	6.8×10^{-2}	1.6×10^{-4}	1.7×10^{-2}
decision	20	60	2.9×10^{-2}	$< 5.2 \times 10^{-6}$	6.6×10^{-3}
Normalizing	15	60	6.1×10^{-2}	1.5×10^{-5}	1.5×10^{-2}
	20	60	2.4×10^{-2}	$< 5.2 \times 10^{-6}$	5.9×10^{-3}

Table 4.5: Error rate statistics for simulations of downlink, 7 cells, 60 users per cell, normalizing and hard decision receivers.

The figures show that shadow fading seriously degrades the quality of the received signal. For the mobile in the cell corner, significant levels of tone interference were found to be received only from the two closest surrounding cells, the bases of which are at the same distance from the mobile unit as it's own current base station. Although the majority of users in this position will not experience an unacceptable error rate even when area mean E_b/N_0 is as low as 15 dB (as indicated by the median $\hat{P}_b$), a significant proportion of users will. This results in the large spread in

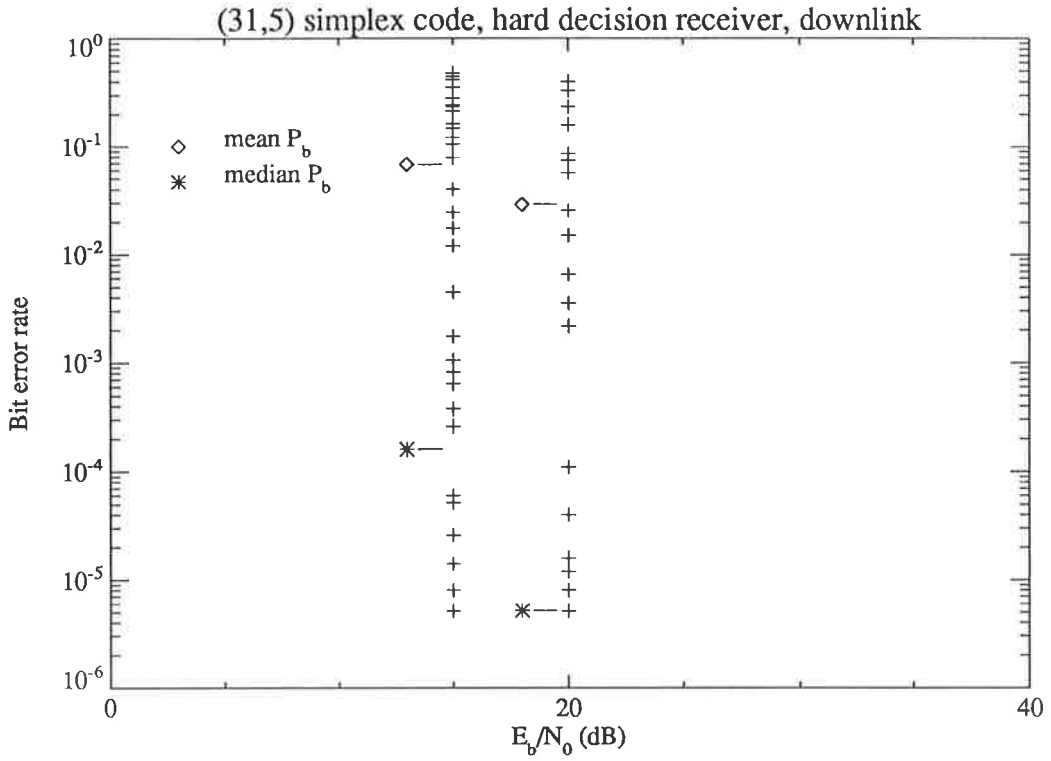

Figure 4.30: Sample bit error rates of 50 downlink simulations for the hard decision receiver, with 60 users and $E_b/N_0 = 15, 20$ dB.

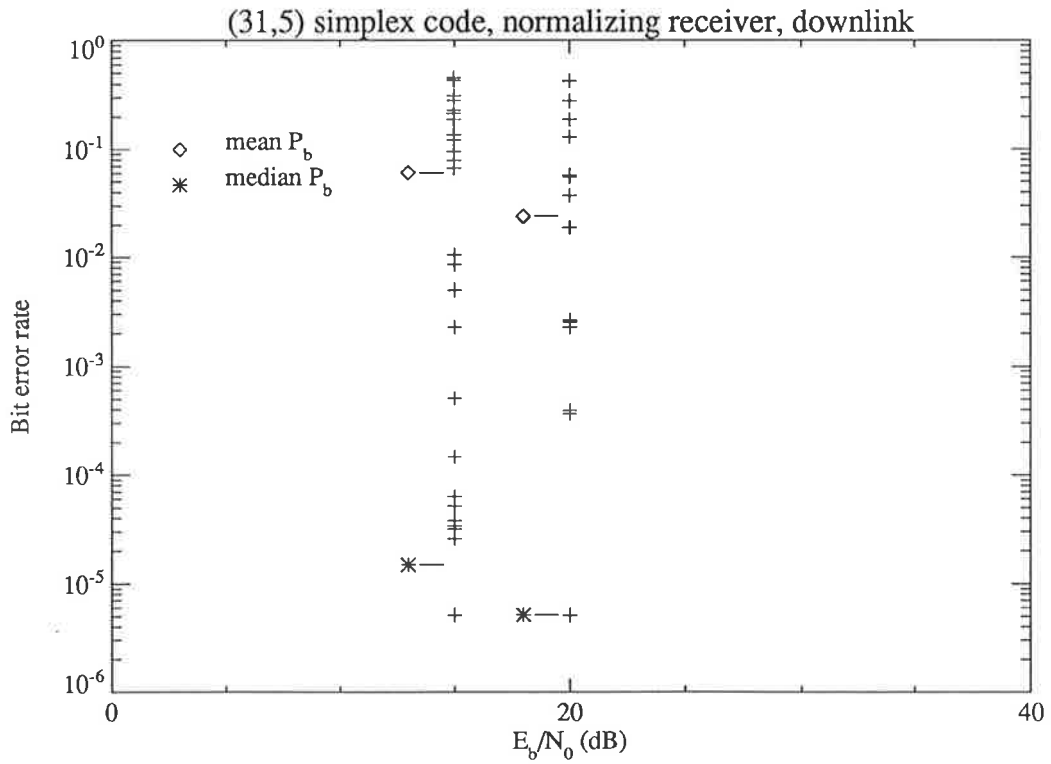

Figure 4.31: Sample bit error rates of 50 downlink simulations for the normalizing receiver, with 60 users and $E_b/N_0 = 15, 20$ dB.

recorded values, reflected in the sample variance. (Note that for both E_b/N_0, many simulations recorded no errors and are set to the minimum bit error of 5.2×10^{-6}, shown as one point on the graphs).

For the limited number of samples taken, it was found that in all cases where the error rate was unacceptable, an interfering base station was being received with a much stronger signal. This indicates that a hand-off strategy would generally be an appropriate solution to the poor signal reception. In practice, situations may arise where signals from all surrounding bases are received with inadequate strength due to shadowing, but this is a problem no matter what modulation or multiple access scheme is used. Given that in all but exceptional circumstances, handoff protocols will result in acceptable bit error rates for all downlink users, the system capacity is therefore limited by the number of active uplink users that may use the system at a specified bit error rate.

To check that this applies, further work is required to establish the downlink performance at mobile locations closer to the centre of the cell, where more surrounding cells may contribute significant levels of interference, although at a much lower level than that found at the corners.

Chapter 5

An Optimum Linear Receiver

The optimum receiver delivers the best possible performance for a given set of conditions. It is thus of interest to determine this receiver as a benchmark against which others may be measured. In this chapter, the optimum linear receiver to operate with the Nettleton and Cooper type orthogonal Hadamard coding is derived. Transmission through a Rayleigh fading environment with background white Gaussian noise is initially assumed, and the results extended to the more general case of Gaussian interferers being present. In the event of the magnitude and location of the interference being known at the receiver, this information may be used to obtain a lower bit error rate. The treatment is adapted from that of Wozencraft and Jacobs [78] for FSK with envelope detection, extended further for the case where interferers are known to exist in certain chips.

5.1 Optimum Receiver for Rayleigh Fading

In this section, no interferers are assumed to be present, but the theory will be developed to allow for extension to that case in the next section. Uplink transmission with power control is assumed. For convenience, the number of channels is assumed to be equal to the number of chips in a codeword, although this is not necessary.

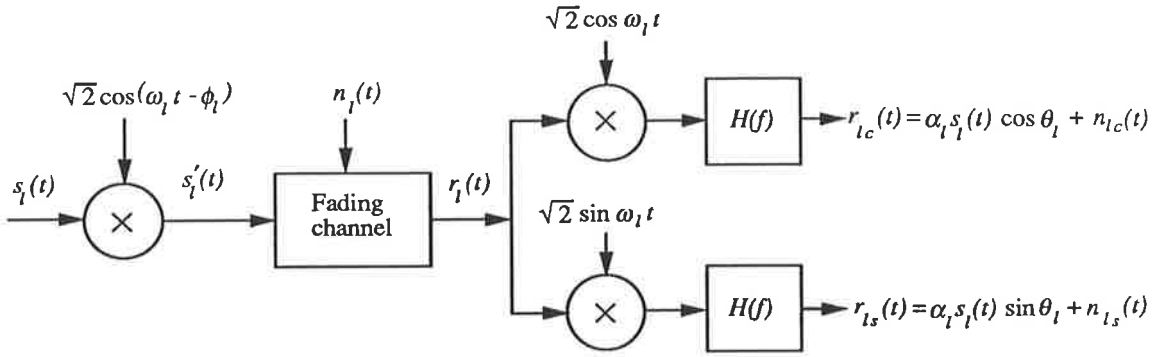

Figure 5.1: Schematic diagram of a transmission and reception on a single channel.

Without loss of generality, it may be assumed that the transmitted signal on each channel is composed of two parts, the first being a reference and the second being the message encoded by differential phase shift keying. In sequential operation, the previously transmitted signal serves as a reference for the current transmission. Over two frame periods $0 \leq t \leq 2T$, the transmitted RF signal given that the kth message is sent can therefore be written as

$$s'_k(t) = \sum_{l=0}^{L-1} \left[\sqrt{2S}\mathrm{rect}_\tau(t - l\tau)\cos(\omega_l t - \phi_l) + h_{kl}\sqrt{2S}\mathrm{rect}_\tau(t - T - l\tau)\cos(\omega_l t - \phi_l)\right] \tag{5.1}$$

where the differential encoding is specified by the element h_{kl} of the Hadamard matrix, and ϕ_l is a random phase constant uniformly distributed on $[0, 2\pi)$.

The received message is corrupted by Rayleigh fading and additive white Gaussian noise.

$$\begin{aligned} r(t) \;=\; & \sum_{l=0}^{L-1} [\alpha_l\sqrt{2S}\mathrm{rect}_\tau(t - l\tau)\cos(\omega_l t - \theta_l) \\ & + h_{kl}\alpha_l\sqrt{2S}\mathrm{rect}_\tau(t - T - l\tau)\cos(\omega_l t - \theta_l) + n_l(t)] \qquad 0 \leq t \leq 2T \end{aligned} \tag{5.2}$$

where $n_l(t)$ is assumed to be additive white Gaussian noise with one-sided power spectral density of N_{0_l}. The α_l are independent Rayleigh variables with power control implying $\mathbf{E}[\alpha_l^2] = 2b_l = 1$, and θ_l are independent random variables, uniformly distributed on $[0, 2\pi)$.

It is assumed that the transmitted signal is bandlimited such that the in-phase and quadrature components may be recovered with no loss of energy and with

minimum noise by the arrangement in figure 5.1. After multiplication of the received IF signal plus noise by $\sqrt{2}\cos\omega_l t$ and $\sqrt{2}\sin\omega_l t$ in each branch respectively, the resultants are lowpass filtered to produce

$$r_{l_c}(t) = (\alpha_l \cos\theta_l) s_{kl}(t) + n_{l_c}(t) \tag{5.3}$$

$$r_{l_s}(t) = (\alpha_l \sin\theta_l) s_{kl}(t) + n_{l_s}(t) \tag{5.4}$$

where $n_{l_c}(t)$ and $n_{l_s}(t)$ are zero mean Gaussian noise processes, and $s_{kl}(t)$ is the equivalent baseband transmitted waveform for the kth message

$$s_{kl}(t) = \sqrt{S}\mathrm{rect}_\tau(t - l\tau) + h_{kl}\sqrt{S}\mathrm{rect}_\tau(t - T - l\tau) \tag{5.5}$$

For convenience, renumber the quadrature (sine) demodulator outputs

$$r_l(t) = \begin{cases} s_{kl}(t)\alpha_l \cos\theta_l + n_{l_c}(t) & l = 0, \ldots, L-1 \\ s_{k(l-L)}(t)\alpha_{l-L} \sin\theta_{l-L} + n_{(l-L)_s}(t) & l = L, \ldots, 2L-1 \end{cases} \tag{5.6}$$

Define

$$z_l \triangleq \begin{cases} \alpha_l \cos\theta_l & l = 0, \ldots, L-1 \\ \alpha_{l-L} \sin\theta_{l-L} & l = L, \ldots, 2L-1 \end{cases} \tag{5.7}$$

which implies z_l are independent Gaussian random variables with zero mean and variances $\mathbf{E}[z_l^2] = b_l$ for $l = 0, \ldots, 2L-1$.

It is convenient to write $s_{kl}(t)$ in terms of an appropriate orthonormal basis set for each of the $l = 0, \ldots, L-1$ channels.

$$s_{kl}(t) = \sum_{j=1}^{2} s_{klj}\varphi_{jl}(t) \tag{5.8}$$

where the orthonormal functions $\varphi_{jl}(t)$ are defined as

$$\varphi_{1l}(t) = \frac{1}{\sqrt{\tau}}\mathrm{rect}_\tau(t - l\tau) \tag{5.9}$$

$$\varphi_{2l}(t) = \frac{1}{\sqrt{\tau}}\mathrm{rect}_\tau(t - T - l\tau) \tag{5.10}$$

(An alternative set of basis functions such as

$$\varphi_{1l}(t) = \frac{1}{\sqrt{2\tau}}\mathrm{rect}_\tau(t - l\tau) + \frac{1}{\sqrt{2\tau}}\mathrm{rect}_\tau(t - T - l\tau)$$

$$\varphi_{2l}(t) = \frac{1}{\sqrt{2\tau}}\mathrm{rect}_\tau(t - l\tau) - \frac{1}{\sqrt{2\tau}}\mathrm{rect}_\tau(t - T - l\tau)$$

can be found, but this representation is not convenient for later analysis.)

The lth demodulator output for the kth message transmitted may then be represented in vector notation as

$$\boldsymbol{r}_l = z_l \boldsymbol{s}_{kl} + \boldsymbol{n}_l \qquad l = 0, 1, \ldots, 2L-1 \tag{5.11}$$

where each vector has two components.

Additive white Gaussian noise is represented by the components $\boldsymbol{n}_l$ which are zero-mean Gaussian variables with variances $N_{0_l}/2$ when projected onto the orthonormal basis. (In a situation where there is only background Gaussian noise and no interference, the variances would all equal $N_0/2$. However, allowing them to differ accommodates the possibility of interferers being present in some chips.)

The vector of random variables representing all of the demodulator outputs is

$$\boldsymbol{r} = (\boldsymbol{r}_0, \boldsymbol{r}_1, \ldots, \boldsymbol{r}_{2L-1}) \tag{5.12}$$

with an actual sample value being

$$\boldsymbol{\rho} = (\boldsymbol{\rho}_0, \boldsymbol{\rho}_1, \ldots, \boldsymbol{\rho}_{2L-1}) \tag{5.13}$$

where each component is a 2 element vector.

When $\boldsymbol{r} = \boldsymbol{\rho}$, the optimum receiver sets the estimated message $\hat{m} = m_i$ for which $\Pr[m_i | \boldsymbol{r} = \boldsymbol{\rho}]$ is a maximum. Assuming all messages m_i are equally likely,

$$\Pr[m_i | \boldsymbol{r} = \boldsymbol{\rho}] = \frac{\Pr[m_i] p_{\boldsymbol{r}}(\boldsymbol{\rho} | m_i)}{p_{\boldsymbol{r}}(\boldsymbol{\rho})} \propto p_{\boldsymbol{r}}(\boldsymbol{\rho} | m_i) \tag{5.14}$$

The noise vectors $\{\boldsymbol{n}_l\}$ are statistically independent, with probability density function

$$p_{\boldsymbol{n}_l}(\boldsymbol{x}) = \frac{1}{\pi N_{0_l}} e^{-|\boldsymbol{x}|^2 / N_{0_l}} \tag{5.15}$$

Conditional on the $\{N_{0_l}\}$ (perhaps known through side information)

$$p_{\boldsymbol{r}}(\boldsymbol{\rho} | m_i, \{z_l\}, \{N_{0_l}\}) = \prod_{l=0}^{2L-1} p_{\boldsymbol{n}_l}(\boldsymbol{\rho}_l - z_l \boldsymbol{s}_{il}) \tag{5.16}$$

Averaging over $\{z_l\}$ to get $p_{\boldsymbol{r}}(\boldsymbol{\rho}|m_i, \{N_{0_l}\})$

$$p_{\boldsymbol{r}}(\boldsymbol{\rho}|m_i, \{N_{0_l}\}) = \mathbf{E}_{z_l}\left[p_{\mathbf{r}}(\boldsymbol{\rho}|m_i, \{z_l\}, \{N_{0_l}\})\right] \tag{5.17}$$

$$= \prod_{l=0}^{2L-1} \mathbf{E}_{z_l}\left[\frac{1}{N_{0_l}\pi}\exp\left(-\frac{1}{N_{0_l}}|\boldsymbol{\rho}_l - z_l\boldsymbol{s}_{il}|^2\right)\right] \tag{5.18}$$

through independence of the z_l. Now

$$|\boldsymbol{\rho} - z_l\boldsymbol{s}_{il}|^2 = |\boldsymbol{\rho}_l|^2 - 2z_l(\boldsymbol{\rho}_l \cdot \boldsymbol{s}_{il}) + z_l^2|\boldsymbol{s}_{il}|^2 \tag{5.19}$$

$$= |\boldsymbol{\rho}_l|^2 + |\boldsymbol{s}_{il}|^2\left(z_l - \frac{\boldsymbol{\rho}_l \cdot \boldsymbol{s}_{il}}{|\boldsymbol{s}_{il}|^2}\right)^2 - \frac{(\boldsymbol{\rho}_l \cdot \boldsymbol{s}_{il})^2}{|\boldsymbol{s}_{il}|^2} \tag{5.20}$$

Letting $|\boldsymbol{s}_{il}|^2 = E_i$ (the symbol energy contained in the two time chips at the lth frequency), then

$$|\boldsymbol{\rho}_l - z_l\boldsymbol{s}_{il}|^2 = |\boldsymbol{\rho}_l|^2 + E_i\left(z_l - \frac{\boldsymbol{\rho}_l \cdot \boldsymbol{s}_{il}}{E_i}\right)^2 - \frac{(\boldsymbol{\rho}_l \cdot \boldsymbol{s}_{il})^2}{E_i} \tag{5.21}$$

$$= |\boldsymbol{\rho}_l|^2 + E_i(z_l - \rho_{li})^2 - E_i\rho_{li}^2 \tag{5.22}$$

where

$$\rho_{li} \triangleq \frac{\boldsymbol{\rho}_l \cdot \boldsymbol{s}_{il}}{E_i} \tag{5.23}$$

Hence (dropping terms in $|\boldsymbol{\rho}_l|^2$ as they are independent of the message m_i)

$$p_{\boldsymbol{r}}(\boldsymbol{\rho}|m_i, \{N_{0_l}\}) \equiv \prod_{l=0}^{2L-1} \frac{1}{N_{0_l}\pi}\mathbf{E}_{z_l}\left[\exp\left(-\frac{E_i}{N_{0_l}}(z_l - \rho_{li})^2\right)\right]\exp\left(\rho_{li}^2\frac{E_i}{N_{0_l}}\right) \tag{5.24}$$

From [78, page 522], the following Lemma is required:

Lemma For a Gaussian random variable x, with mean m_x and variance σ_x^2, with w any complex constant such that $\Re(w) < 1/(2\sigma_x^2)$, then

$$\mathbf{E}_x\left[e^{wx^2}\right] = \frac{\exp\left(wm_x^2/(1-2w\sigma_x^2)\right)}{\sqrt{1-2w\sigma_x^2}} \tag{5.25}$$

Hence putting $w = -E_i/N_{0_l}$, $m_x = -\rho_{li}$ and $\sigma_x^2 = b_l$

$$\mathbf{E}_{z_l}\left[\exp\left(-\frac{E_i}{N_{0_l}}(z_l - \rho_{li})^2\right)\right] = \frac{1}{\sqrt{1+2b_l(E_i/N_{0_l})}}\exp\left[-\frac{(E_i/N_{0_l})\rho_{li}^2}{1+2b_l(E_i/N_{0_l})}\right] \tag{5.26}$$

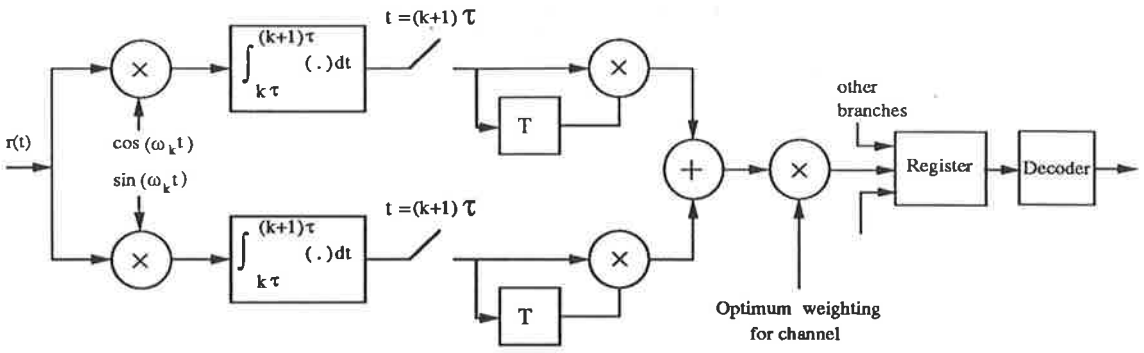

Figure 5.2: Schematic diagram of the optimum FH-DPSK receiver

Then

$$\begin{aligned} p_{\boldsymbol{r}}(\boldsymbol{\rho}_l|m_i,\{N_{0_l}\}) &\propto \prod_{l=0}^{2L-1} \frac{1}{N_{0_l}\pi\sqrt{1+2b_l(E_i/N_0)}} \exp\left[-\frac{(E_i/N_0)\rho_{li}^2}{1+2b_l(E_i/N_0)}\right] \exp\left[\rho_{li}^2\frac{E_i}{N_{0_l}}\right] \\ &= \prod_{l=0}^{2L-1} \frac{1}{N_{0_l}\pi\sqrt{1+2b_l(E_i/N_0)}} \exp\left[\rho_{li}^2\frac{2b_l(E_i/N_0)^2}{1+2b_l(E_i/N_0)}\right] \\ &= \prod_{l=0}^{2L-1} \frac{1}{N_{0_l}\pi\sqrt{1+2b_l(E_i/N_0)}} \exp\left[(\boldsymbol{\rho}_l\cdot\boldsymbol{s}_{li})^2\frac{2b_l/N_0^2}{1+2b_l(E_i/N_0)}\right] \quad (5.27) \end{aligned}$$

This is the decision variable which must be maximised.

For the case where there are no interferers, with equal fading statistics on each channel and equal energy signals, the following quantities are

$$\begin{aligned} N_{0_l} &= N_0 \qquad l=0,\ldots,2L-1 \\ b_l &= b \qquad l=0,\ldots,2L-1 \\ E_i &= E_s = 2E_c \quad \text{where } E_c \text{ is the chip energy for all signals} \end{aligned}$$

Then as $\ln(x)$ is a monotonically increasing function

$$p_{\boldsymbol{r}}(\boldsymbol{\rho}_l|m_i,\{N_0\}) \propto \prod_{i=0}^{2L-1} \exp(\boldsymbol{\rho}_l\cdot\boldsymbol{s}_{il})^2 \quad (5.28)$$

$$\equiv \sum_{l=0}^{2L-1} (\boldsymbol{\rho}_l\cdot\boldsymbol{s}_{il})^2 \quad (5.29)$$

Consider now a correlation receiver of the type shown in figure 5.2. The receiver forms the following quantities over each chip period τ

$$X_{l1} = \int_{(l-1)\tau}^{l\tau} r_l(t)\,dt \qquad l=0,\ldots,L-1 \quad (5.30)$$

$$X_{l2} = \int_{(l-1)\tau+T}^{(l\tau)+T} r_l(t)\,dt \qquad l = 0,\ldots,L-1 \tag{5.31}$$

$$Y_{l1} = \int_{(l-1)\tau}^{l\tau} r_{(l+L)}(t)\,dt \qquad l = 0,\ldots,L-1 \tag{5.32}$$

$$Y_{l2} = \int_{(l-1)\tau+T}^{(l\tau)+T} r_{(l+L)}(t)\,dt \qquad l = 0,\ldots,L-1 \tag{5.33}$$

$$\tag{5.34}$$

Then

$$\sum_{l=0}^{2L-1} (\boldsymbol{\rho}_l \cdot \boldsymbol{s}_{il})^2 = V \sum_{l=0}^{L-1} (X_{l1} + h_{il}X_{l2})^2 + (Y_{l1} + h_{il}Y_{l2})^2 \tag{5.35}$$

where V is a gain constant. The best strategy is therefore to choose m_i such that

$$\sum_{l=0}^{L-1} (X_{l1} + h_{il}X_{l2})^2 + (Y_{l1} + h_{il}Y_{l2})^2 = \sum_{l=0}^{L-1} X_{l1}^2 + X_{l2}^2 + Y_{l1}^2 + Y_{l2}^2 + 2h_{il}(X_{1l}X_{2l} + Y_{1l}Y_{2l}) \tag{5.36}$$

is maximum.

Discarding terms which are independent of i, the best strategy is then to pick the $\hat{m} = m_i$ such that

$$\sum_{l=0}^{L-1} h_{il}(X_{1l}X_{2l} + Y_{1l}Y_{2l})$$

is maximum.

This corresponds to the linear receiver, with each combiner input being equally weighted. This proves that the linear receiver is the optimum receiver in a fading environment, with white Gaussian noise and no tone interference.

5.2 Optimum Receiver in Fading Tone Interference

Consider the case where the fading on each channel is independent and identically distributed. Interferers are present in some channels, and are assumed to fade with Rayleigh amplitude and phase distributed randomly on $[0, 2\pi)$. The interferers are assumed to be phase modulated by random data, and thus each chip is randomly modulated by ± 1. The assumption is thus made that an interferer can be included

with the noise on each channel by representing it as a Gaussian random variable, with zero mean and variance $N_{0_l}/2$ in the lth time chip. Each message m_i is transmitted with the same energy $E_i = E_s = 2E_c$ and fading takes place with the Rayleigh variables α_l such that $\mathbf{E}[\alpha_l^2] = 2b_l$.

$$\begin{aligned} p_{\boldsymbol{r}}(\boldsymbol{\rho}|m_i, \{N_{0_l}\}) &= \prod_{l=0}^{2L-1} \frac{1}{N_{0_l}\pi\sqrt{1+2b_l(E_s/N_{0_l})}} \exp\left((\boldsymbol{\rho}_l \cdot \boldsymbol{s}_{il})^2 \frac{2b_l/N_{0_l}^2}{1+2b_l(E_s/N_{0_l})}\right) \\ &\equiv \sum_{l=0}^{2L-1} \left[\ln\left(\frac{1}{N_{0_l}\pi\sqrt{1+2b_l(E_s/N_{0_l})}}\right) + (\boldsymbol{\rho}_l \cdot \boldsymbol{s}_{il})^2 \frac{2b_l/N_{0_l}^2}{1+2b_l(E_s/N_{0_l})}\right] \end{aligned}$$

Dispensing with terms of the sum that are independent of i

$$p_{\boldsymbol{r}}(\boldsymbol{\rho}|m_i, \{N_{0_l}\}) \equiv \sum_{l=0}^{2L-1} (\boldsymbol{\rho}_l \cdot \boldsymbol{s}_{il})^2 \frac{2b_l/N_{0_l}^2}{1+2b_l(E_s/N_{0_l})} \tag{5.37}$$

Now substituting for $(\boldsymbol{\rho}_l \cdot \boldsymbol{s}_{il})^2$ from equation 5.35

$$\begin{aligned} p_{\boldsymbol{r}}(\boldsymbol{\rho}_l|m_i, \{N_{0_l}\}) &= \sum_{l=0}^{L-1} V\left[(X_{l1} + h_{il}X_{l2})^2 + (Y_{l1} + hilY_{l2})^2\right] \frac{2b_l/N_{0_l}}{1+2b_l(E_s/N_{0_l})} \\ &\equiv \sum_{l=0}^{L-1} h_{il}(X_{l1}X_{l2} + Y_{l1}Y_{l2}) \frac{2b_l/N_{0_l}^2}{1+2b_l(E_s/N_{0_l})} \end{aligned} \tag{5.38}$$

Hence the appropriate strategy is to weight the output of the product detector for each chip by the factor

$$\frac{2b_l/N_{0_l}^2}{1+2b_l(E_s/N_{0_l})}$$

For the case where the average power of the fading is unity ($\mathbf{E}[\alpha_l^2] = 2b_l = 1$), the factor becomes

$$\frac{1/N_{0_l}^2}{1+(E_s/N_{0_l})}$$

The weighted outputs are then summed to produce the codeword and a decision made by choosing the largest output.

Now what is required is a link between the presence of an interferer and the noise density N_{0_l}. Consider the signal representation over the orthonormal basis set used previously. The signal vectors defined on the orthonormal basis are then

$$\boldsymbol{s}_{l_1} = (\sqrt{E_s/2}, \sqrt{E_s/2}) = (\sqrt{E_c}, \sqrt{E_c}) \tag{5.39}$$

$$\boldsymbol{s}_{l_2} = (\sqrt{E_s/2}, -\sqrt{E_s/2}) = (\sqrt{E_c}, -\sqrt{E_c}) \tag{5.40}$$

This representation allows the interference power to be equally split into each dimension irrespective of the modulation of the interferer, and thus be lumped in with the noise.

Assuming that signal s_1 was transmitted, the received signal on the lth channel in the presence of noise alone can be written as

$$r_l = (z_l\sqrt{E_c} + n_{l1}, z_l\sqrt{E_c} + n_{l2}) \tag{5.41}$$

where z_l is a zero-mean Gaussian random variable random variable with $\mathbf{E}[z_l^2] = b_l$ as before. Let $b_l = 1/2$ which corresponds to a power control situation, removing attenuation and lognormal (shadow) fading variation.
The n_{l1}, n_{l2} are zero mean Gaussian random variables with variance $N_0/2$ projected onto the orthonormal basis.

Introducing an interferer i_l into this channel:

$$r_l = (z_l\sqrt{E_c} + i_{l1} + n_{l1},\ z_l\sqrt{E_c} + i_{l2} + n_{l2}) \tag{5.42}$$

Now the interferer i_l is assumed to be of identical average power to the target signal. In this case

$$\begin{aligned} < z_l^2 E_c > &= < z_l^2 > E_c \\ &= E_c/2 \\ &= < i_l^2 > \qquad (5.43) \\ < n_{l1}^2 > &= < n_{l2}^2 >= N_0/2 \qquad (5.44) \end{aligned}$$

If $i_{l1} = v_l\sqrt{E_c}$ (where v_l is a Gaussian variable) then by the independence of the data, $i_{l2} = \pm v_l\sqrt{E_c}$ with equal probability and the autocorrelation $R_{i_{l1},i_{l2}}(T) = 0$. This approach has been justified by studies of the performance of (hard decision, no diversity) DPSK in Rayleigh fading by Wu *et al* [79], and by Sevy [80]. Hence we can form two new Gaussian quantities with identical and independent distributions as

$$\begin{aligned} n'_{l1} &= i_{l1} + n_{l1} \qquad (5.45) \\ n'_{l2} &= i_{l2} + n_{l2} \qquad (5.46) \end{aligned}$$

where

$$< n_{l1}'^2 > = < n_{l2}'^2 > = < i_{l1}^2 > + < n_{l1}^2 > \quad (5.47)$$

$$= (E_c + N_0)/2 \quad (5.48)$$

Now the equivalent one-sided noise density is N_{0_l} with equivalent variance on the orthonormal basis functions of $N_{0_l}/2$, and hence $N_{0_l}/2 = (E_c + N_0)/2$

The weighting function for the lth product detector output, given a single interferer is present, is

$$\frac{1/N_{0_l}^2}{1 + E_s/N_{0_l}} = \frac{1/(E_c + N_0)^2}{1 + 2E_c/(E_c + N_0)}$$

$$= [(N_0 + E_c)(N_0 + 3E_c)]^{-1} \quad (5.49)$$

$$\simeq 1/(3E_c^2) \qquad \text{for high signal to noise ratios} \quad (5.50)$$

For j interferers, where $0 \leq j \leq J - 1$, the weighting function is

$$\frac{1/(jE_c + N_0)^2}{1 + 2E_c/(jE_c + N_0)} \quad (5.51)$$

The ratio of weights for a chip with j interferers to a chip with no interferers is

$$\frac{\text{weight } (j \text{ interferers})}{\text{weight (no interferer)}} = \frac{N_0(N_0 + 2E_c)}{(jE_c + N_0)(N_0 + (j+2)E_c)} \quad (5.52)$$

For high signal to noise ratios $E_c >> N_0$

$$\frac{\text{weight } (j \text{ interferers})}{\text{weight (no interferer)}} \simeq \frac{2N_0E_c}{jE_c(j+2)E_c} \quad (5.53)$$

$$\simeq \frac{2N_0}{j(j+2)E_c} \quad (5.54)$$

Hence if a certain number of interferers are known to be present in a particular time chip, the weighting of that chip can be adjusted to give the optimum result. Surprisingly, this may actually be possible in practice. On the link from mobile to base, power control exists. The base station will have to track the optimum sample instants for the transmission of each user independently. With this timing information, the base station will be able to determine which chips of a wanted signal are being interfered with strongly, and make an estimation of the weight function for

those chips. Analysis of the received signal over a long time period may give information on whether interference is present in a channel. For the downlink, it is unlikely that the mobile unit would be sophisticated enough to distinguish the interference, but frame synchronism within a cell should lessen interference considerably.

The performance of the optimum receiver has been simulated with the tone interferer patterns previously used for examining the linear, hard decision and normalizing receiver, although the simplex (31,5) code was used instead of the orthogonal code (resulting in less computation). Results are shown for patterns 1, 2 and a third pattern. The results show a vast improvement over the bit error rate of the other re-

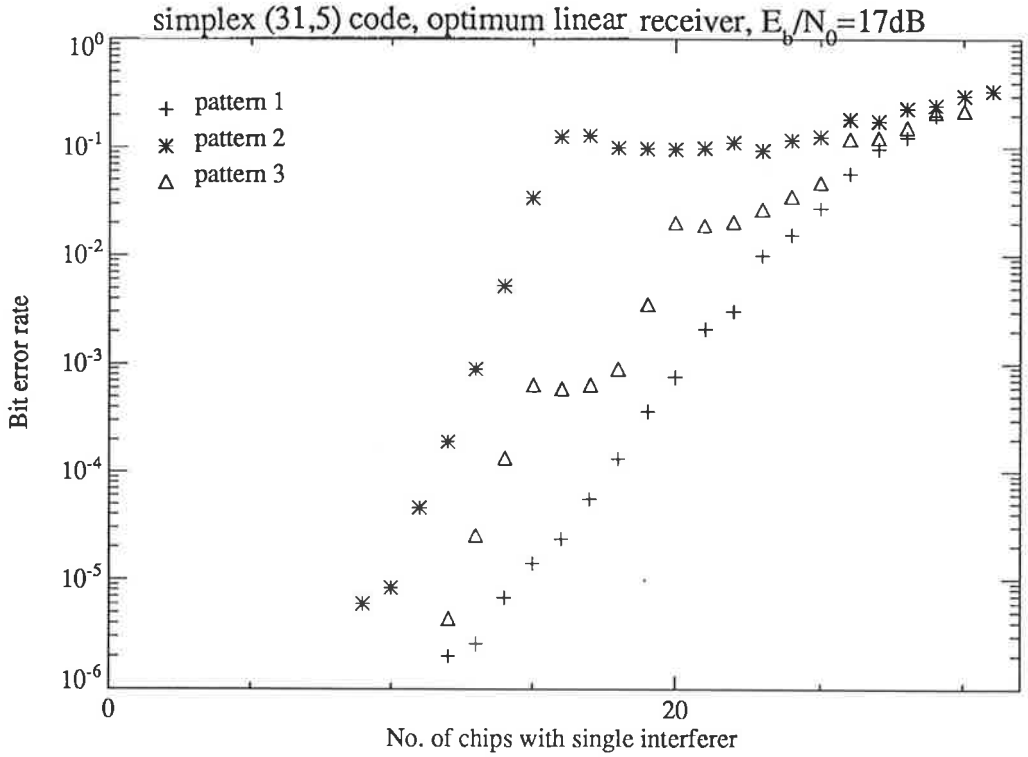

Figure 5.3: Bit error rate of (31,5) simplex code, optimum linear receiver, with ideal Rayleigh fading and tone interferers, $E_b/N_0 = 17$ dB

ceivers for small numbers of interferers. As the number of interfered chips increases, advantage of this receiver over the normalizing receiver becomes smaller and eventually disappears. The effect of bad interferer patterns can be clearly seen to affect the optimum linear receiver, in contrast to the linear receiver examined earlier which had no weighting on the detector outputs. Again, to avoid these repetitive bad pat-

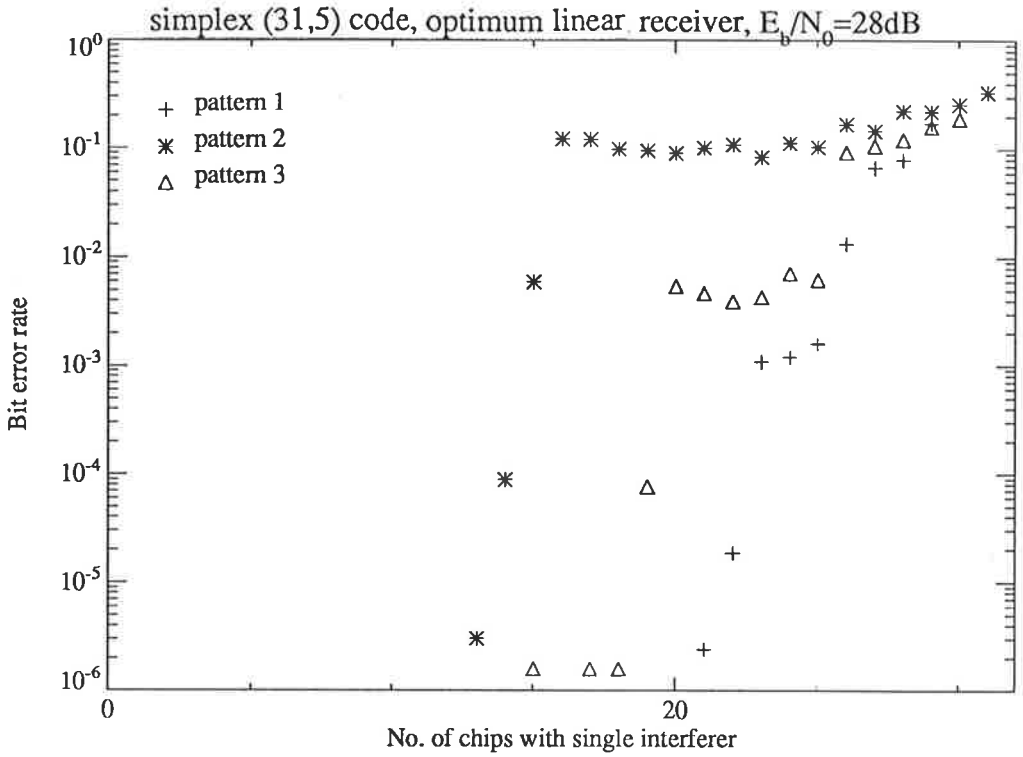

Figure 5.4: Bit error rate of (31,5) simplex code, optimum linear receiver, with ideal Rayleigh fading and tone interferers, $E_b/N_0 = 28$ dB

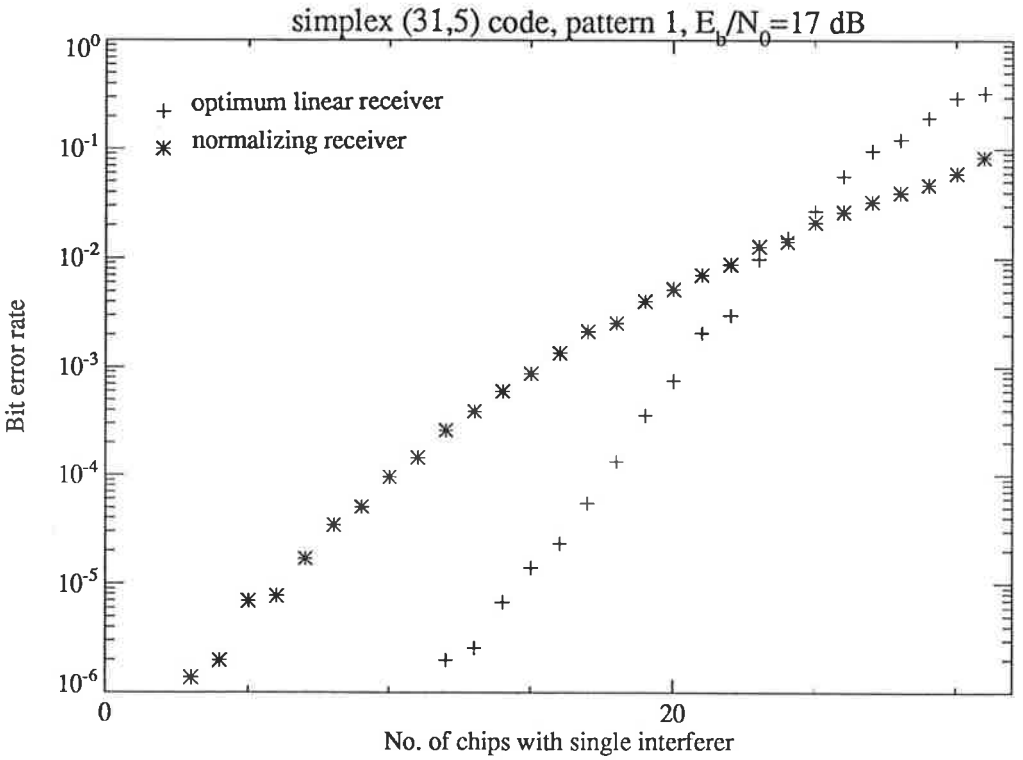

Figure 5.5: Bit error rate of (31,5) simplex code for interferer pattern 1, different receivers, with ideal Rayleigh fading and tone interferers, $E_b/N_0 = 17$ dB

terns, a cyclic codeword-to-channel mapping process must be used, as described in the preceding chapter.

For small numbers of interfered chips, the optimum linear receiver has a clear performance advantage over the normalizing receiver. However, when large numbers of chips are subject to interference, the normalizing receiver exhibits better performance than the optimum linear receiver (although still resulting in too high an error rate). This may result from the assumption in the derivation of the of the optimum linear receiver that the signal plus noise samples are independent. In fact, as the magnitude of the signal component varies only slightly during the period T, these samples are not independent, although uncorrelated. The normalizing receiver is able to exploit this structure to produce better results when many channels suffer interference. In specifying only an optimum linear receiver, this leaves open the question of whether an optimum non-linear receiver may be derived.

Chapter 6

Other Coding Schemes

The ability of a frequency hopping scheme to cope with interference is inextricably linked to the type of coding used and the nature of the interference, a fact well demonstrated in a tutorial treatment by Viterbi [81]. Previous authors have all assumed the (32,5) orthogonal Hadamard code was being used and not investigated the possibility of using more suitable codes for the FH-DPSK system. This chapter examines how some of the more commonly used block codes perform with the different receiver structures. Estimates of the number of users possible in an isolated cell under a random addressing assumption, for the hard decision and normalizing receivers, are also presented. Simulations for the simplex coding case indicate that these estimates are reasonable.

Although insufficient time was available to thoroughly research the application of convolutional codes and concatenated schemes to the FH-DPSK system, some initial investigations were made into these important methods of error control. The preliminary results are presented in appendix C, and appear to be quite promising.

6.1 Biorthogonal Coding Schemes

The orthogonal and simplex codes used previously have considerable redundancy, with an effective $31/5 = 6.2$ chips transmitted for every message bit. This redundancy gives considerable protection against interference but the shorter chip period results in wider channel bandwidths. If the bandwidth required by each user is reduced by using less redundancy, the number of channel slots in the total bandwidth will be increased and the mutual interference for a given number of users will be reduced. The bit error rate of the system will be determined by this trade-off between redundancy versus number of channels available in the total bandwidth.

It is logical then to examine a scheme which has a slightly lower code rate, providing less protection against random noise and interference but allowing more frequency slots to be used because of the lower transmitted symbol rate. This may therefore allow more users under the tone interferer model and the random addressing assumption.

An obvious extension of the orthogonal coding scheme is a biorthogonal coding scheme. This can be derived simply from an orthogonal scheme by simply adding the complements of the existing orthogonal codeword set. This doubles the number of codewords of a particular length, or alternatively halves the length of a codeword necessary to transmit a certain number k of information bits. For example, the set of $2^k = 8$ codewords for $k = 3$ have length $2^{k-1} = 4$ and can be specified as

$$\begin{array}{c} \text{Data} \\ \left(\begin{array}{c} 000 \\ 001 \\ 010 \\ 011 \\ 111 \\ 110 \\ 101 \\ 100 \end{array}\right) \end{array} \Rightarrow \begin{array}{c} \text{Codewords} \\ \left(\begin{array}{cccc} 1 & 1 & 1 & 1 \\ 1 & -1 & 1 & -1 \\ 1 & 1 & -1 & -1 \\ 1 & -1 & -1 & 1 \\ -1 & -1 & -1 & -1 \\ -1 & 1 & -1 & 1 \\ -1 & -1 & 1 & 1 \\ -1 & 1 & 1 & -1 \end{array}\right) \end{array} \tag{6.1}$$

where the mapping from the data to the codeword is designed to minimise three-bit errors by mapping complementary message words to complementary codewords. For the same reasons as previously given for the orthogonal code, the biorthogonal code

also suffers from the sensitivity to particular patterns of interferers. The solution is the same as for the orthogonal code: rotation through a larger frequency set or a repeated sequence of mappings from the codewords to the frequency channels.

Decoding of the code utilises the same approach as for the orthogonal Hadamard code. A set of half of the codewords corresponding to the orthogonal codewords can be used to correlate with the received signal, with the complementary codewords not required. The greatest magnitude of correlation and the polarity determines which codeword is the most likely to have been transmitted. As the decoding is a linear transformation (via the Hadamard transform) which is easily performed, the same choices of receiver exist for the biorthogonal code as for the orthogonal code.

The bit error rate of the (32,6) biorthogonal code in the presence of Rayleigh fading and additive white Gaussian noise is shown in figure 6.1, and is slightly better than that of the (32,5) orthogonal code. As the number of nearest neighbours is increased by a factor of two for codewords of the same length, the probability of codeword error is approximately doubled over that of the orthogonal code at a given chip signal to noise ratio. However, as the biorthogonal code has a larger chip energy for a specified E_b/N_0 than the orthogonal code of the same codeword length, the biorthogonal code shows a net decrease in the probability of error. The number of users under the AWGN approximation can be computed from equation 4.26 as 72, 45 and 32 users for the linear, normalizing and hard decision receivers respectively. This represents a small increase on the numbers for the simplex and orthogonal codes.

The performance with tone interferers is also similar to that of the orthogonal code, and is shown in figures 6.2–6.6. There is little difference in the performance for orthogonal and biorthogonal coding for the same number of tone interferers at $E_b/N_0 = 15$ dB and above, with the separation in performance between the three receiver types being maintained at the same level as for the orthogonal coding. The number of channels available for hopping for the (32,6) biorthogonal code is given

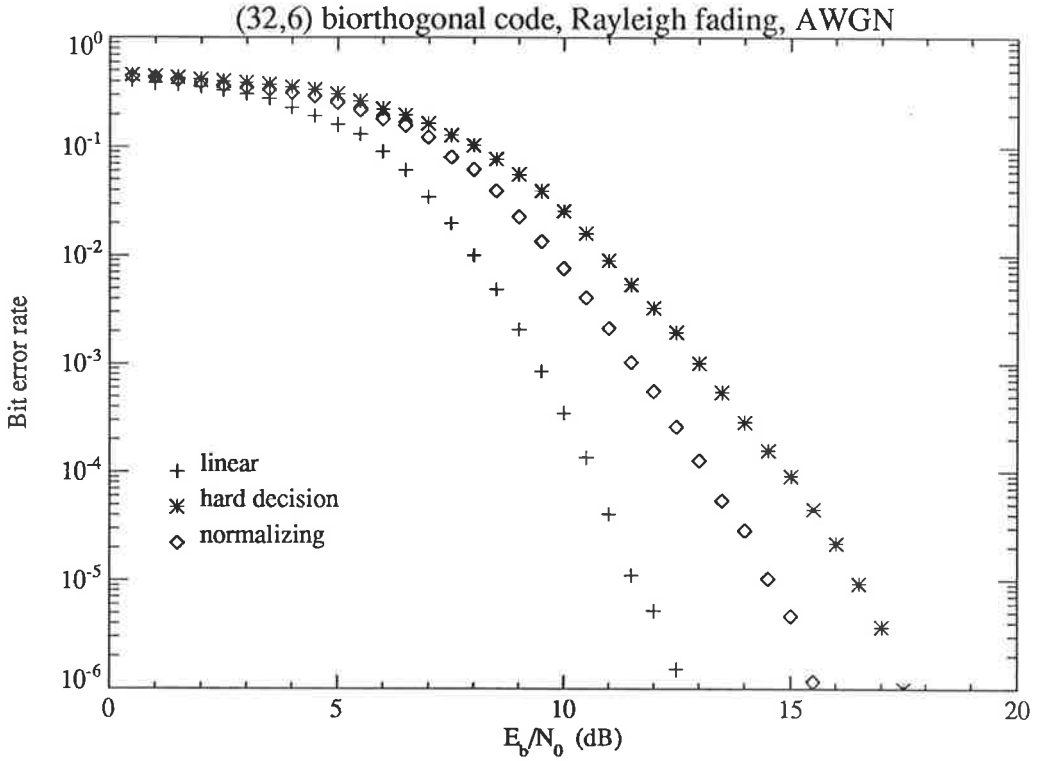

Figure 6.1: Bit error rate of the (32,6) biorthogonal code, with ideal Rayleigh fading and additive white Gaussian noise.

as

$$q = \frac{Wk}{R_b 2^{k-1}} = 117$$

which is an increase of 20% over the orthogonal code. The closeness of performance for the biorthogonal and orthogonal codes, coupled with an increase in the number of channels available for hopping due to the higher code rate, should result in the biorthogonal code being able to support a higher number of users at an error rate of 10^{-3}. This is in fact shown in a forthcoming section.

6.2 Golay Coding Scheme

The opposite extreme to the (32,5) orthogonal code is a high-rate code which provides minimum redundancy but a large number of channels. To investigate what sort of error rates are achievable from high rate codes subject to a few tone inter-

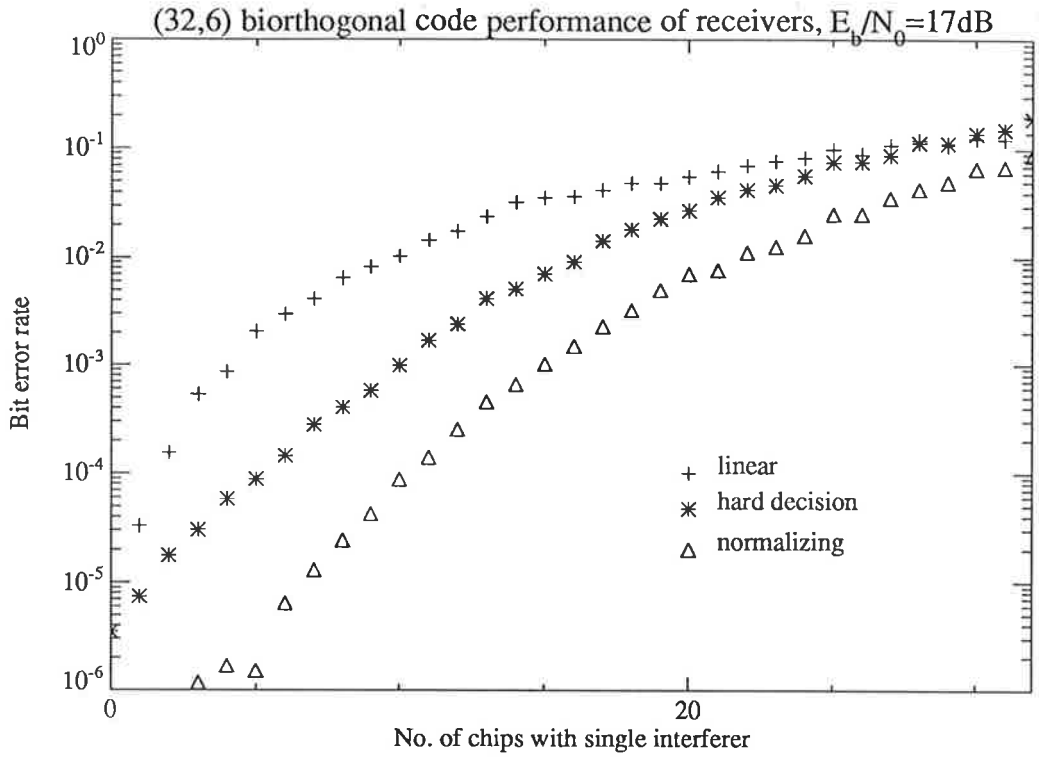

Figure 6.2: Bit error rate of (32,6) biorthogonal code, with ideal Rayleigh fading, fading tone interferers, $E_b/N_0 = 17$ dB.

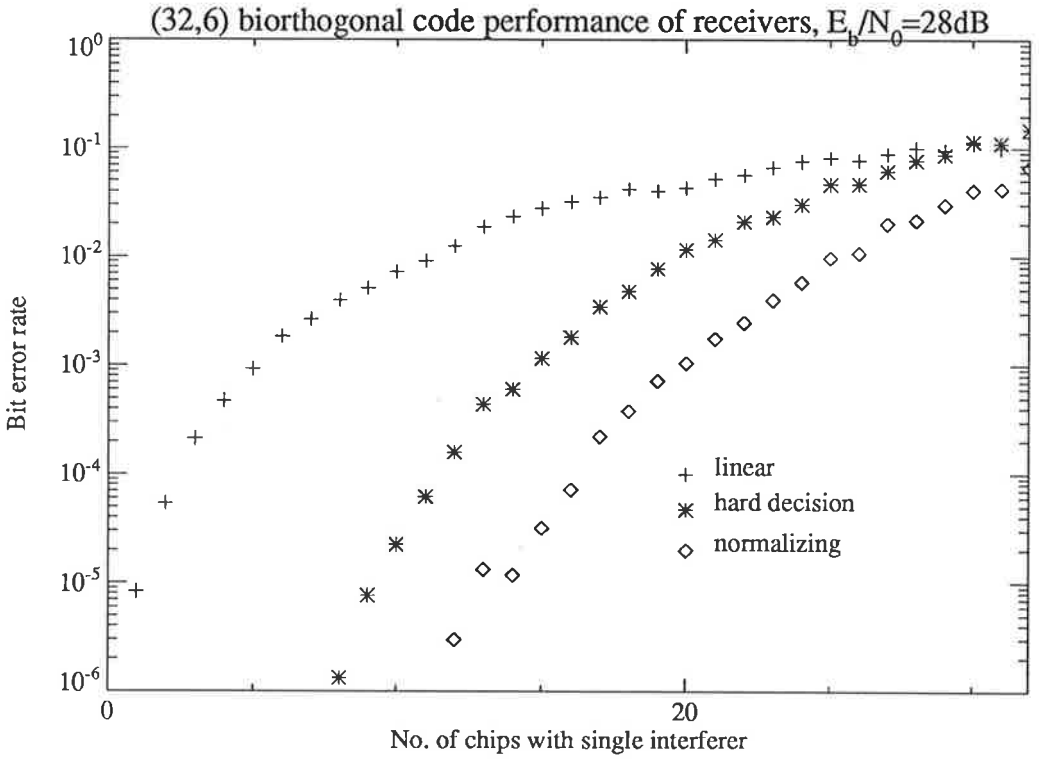

Figure 6.3: Bit error rate of (32,6) biorthogonal code, with ideal Rayleigh fading, fading tone interferers, $E_b/N_0 = 28$ dB.

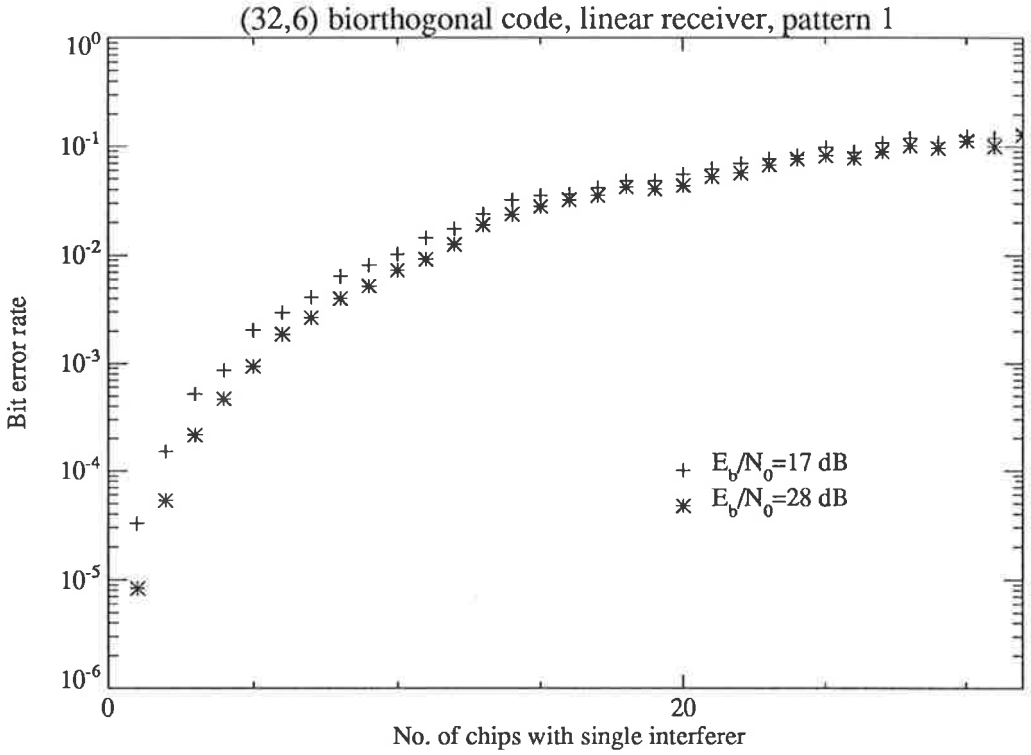

Figure 6.4: Bit error rate of (32,6) biorthogonal code, linear receiver, with ideal Rayleigh fading and fading tone interferers.

ferers, the (23,12) Golay code was used. This code, encoding 12 message bits into 23 code bits, is a so-called "perfect" code and can correct all patterns of 3 errors in the codeword and no others, thus achieving the maximum efficiency possible for the codeword length and code rate. It is not proposed to cover the theory of the Golay code here: texts on coding such as [82] or [83] cover the subject of coding in depth. This investigation serves a dual purpose. It is very easy to analytically compute the probability of codeword error for hard decision decoding of the Golay code, and hence the simulation results for a known interferer configuration may be assessed against theoretical results.

A hard decision encoding/decoding package was written for the Golay code, using a systematic feedback encoder and decoding by a look-up table indexed by syndrome (method based on a hardware implementation in [84]). The performance of the FH-DPSK system was assessed by simulation and by analysis. The parameters of the Golay coded scheme are set out in table 6.2. It was assumed to hop over 23

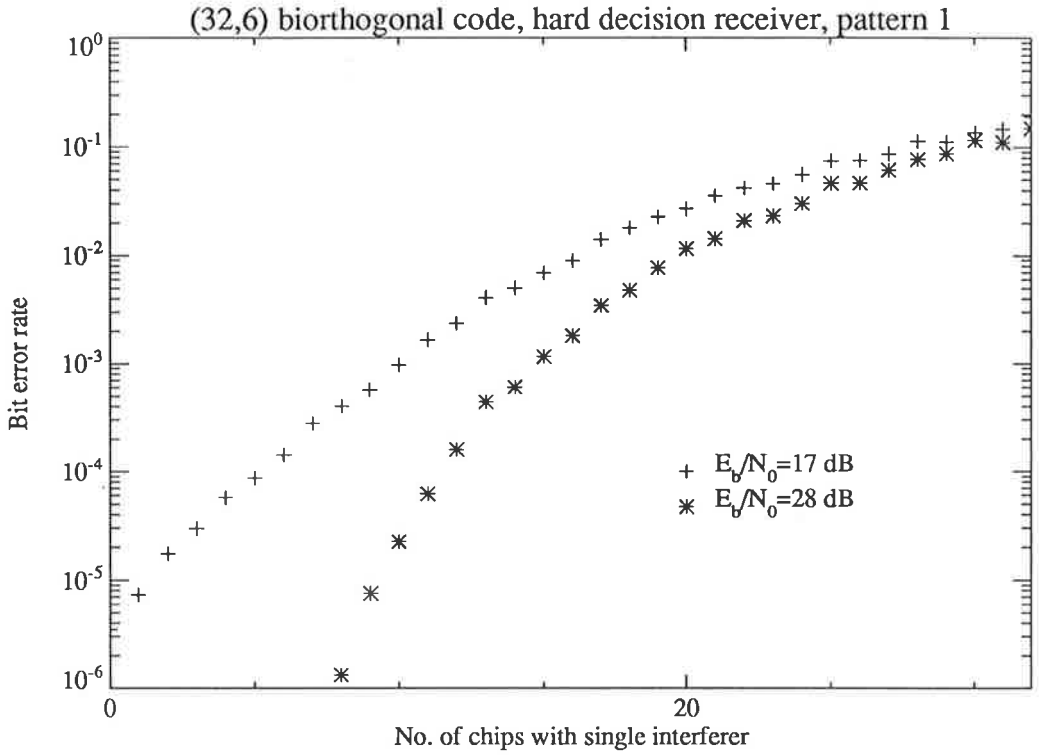

Figure 6.5: Bit error rate of (32,6) biorthogonal code, hard decision receiver, with ideal Rayleigh fading and fading tone interferers.

frequencies, thus assuring the independence of each chip in the codeword.

Note that it is possible to cycle through more frequencies than the actual number of chips in a codeword, as suggested for the case of the orthogonal coding scheme. However, the Golay code has a weight structure which results in a series of groups of codewords at particular Hamming distances from any given codeword. These groups are different for every codeword. An interferer pattern which badly affects one particular codeword by increasing the probability of erroneously choosing a codeword at the minimum distance, for another transmitted codeword may correspond to a pattern which perturbs the codeword in the direction of a codeword at maximum distance and is unlikely to cause an error. This structure seems to be less sensitive to particular interferer patterns, and no significant difference in bit error rate performance was noted for the Golay code for various patterns of interferers tried. In addition, choosing a larger set of frequencies to hop through will increase the frame period, and thus decrease the correlation between chips at the same frequency in

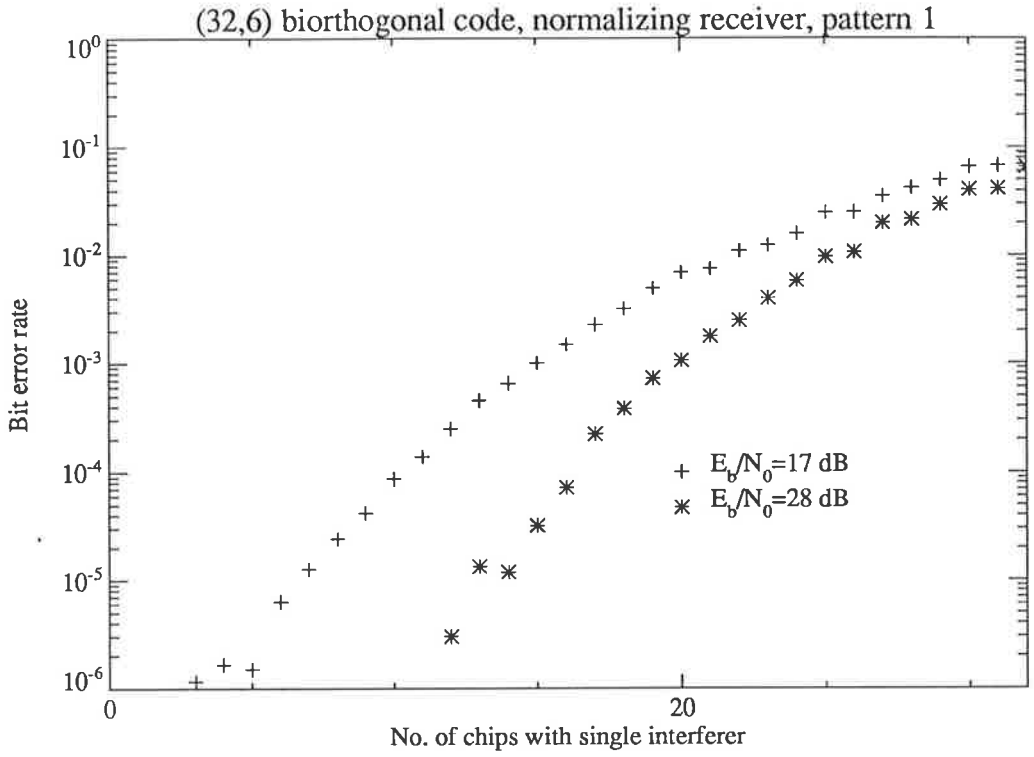

Figure 6.6: Bit error rate of (32,6) biorthogonal code, normalizing receiver, with ideal Rayleigh fading and fading tone interferers.

adjacent frames. This will show up as an increased irreducible error rate.

6.2.1 Analysis and Results

For this analysis, a receiver such as that in figure 6.7 is assumed, with hard decisions (± 1) being made on each chip at the output of the quadratic detector, on sampling.

Consider a frequency hopping signal transmitted over $L = 2^k$ frequencies as:

$$s(t) = d(t)\sqrt{2S}\text{rect}_\tau(t - l\tau)\cos(2\pi f_l t - \phi_l) \qquad l = 0, 1, \ldots, L-1 \qquad (6.2)$$

where all symbols have the meanings previously defined in other chapters.

The data is differentially encoded onto the signal with the mth word of k bits mapping to a corresponding n bit codeword. For example, if the codeword was

Parameter	Value
Total available bandwidth W	20 MHz
Information rate R_b	32×10^3 bits/s
Code rate	12/23
Channel bandwidth	$32 \times 10^3 \times 23/12 = 61.3$ kHz
Number of channels available	326
Frame period T	375 μs
Chip period τ	16.3 μs

Table 6.1: Parameter values used for the (23,12) Golay coded FH-DPSK scheme

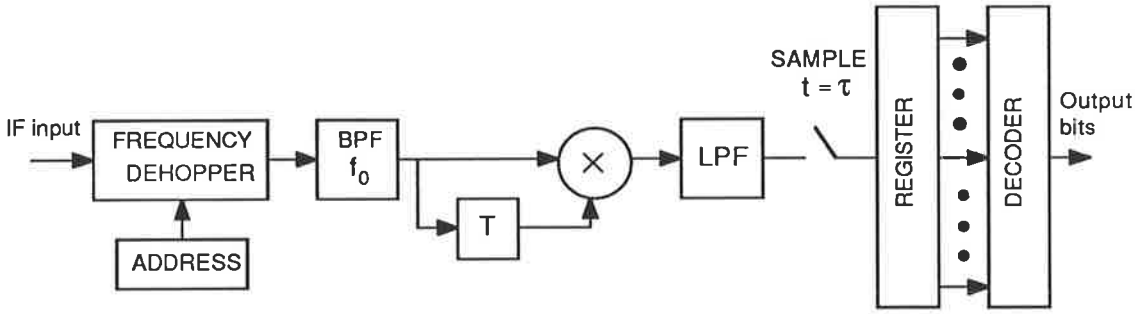

Figure 6.7: Alternative form of the matched filter type receiver.

mapped to the first n frequencies of the L channels for the mth frame under consideration, such that $\boldsymbol{c}_m = (c_{m0}, c_{m1}, \ldots, c_{m(n-1)})$ mapped to channels $0, \ldots, n-1$, the differential encoding would be:

$$d_m(t) = \sum_{l=0}^{n-1} d_{ml} \mathrm{rect}_\tau(t - l\tau) \qquad \text{where} \quad d_{ml} = d_{(m-1)l} c_{ml} \tag{6.3}$$

At this point, there is no restriction on the type of coding that can be applied.

It is assumed that there are J users active in the system with chip synchronism of hopping sequences and power control. After fading through L independent Rayleigh channels with additive white Gaussian noise, the received signal at the output of the matched bandpass filter for the lth time chip around time of the peak output can therefore be written as [35]

$$\begin{aligned} r_l(t) &= d_{ml}\sqrt{2S}\beta(t)\alpha_l \cos(2\pi f_l t - \theta_l) \\ &\quad + \sum_{j=1}^{J-1} \sqrt{2S}\beta(t)\left[\xi_{jl}\cos(2\pi f_l t) + \eta_{jl}\sin(2\pi f_l t)\right] \\ &\quad + n_{l_c}\cos(2\pi f_l t) + n_{l_s}\sin(2\pi f_l t) \end{aligned} \tag{6.4}$$

where θ_l is a phase angle uniformly distributed on $[0, 2\pi)$

α_l is a Rayleigh distributed random variable such that $\mathbf{E}[\alpha_l^2] = 1$

n_{l_c}, n_{l_s} are i.i.d. zero mean Gaussian variables with variance N_0/τ

$\beta(t)$ is the amplitude function resulting from the matched filter, assumed unity at sample time

and ξ_{jl} and η_{jl} are i.i.d. zero mean Gaussian random variables with variance $\gamma_{jl}/2$. The distribution of γ_{jl} is determined by the addressing strategy used, but will not be of importance in this section as γ_{jl} will be set to specific values.

For any frequency, interferers in each frame are assumed independent, as although their magnitudes change only slightly from one frame to the next, the random data ensures no correlation. It is then possible to write the sum of the interferers plus noise for the inphase and quadrature parts in any time chip l as independent Gaussian random variables ξ_l and η_l with zero mean and variance equal to

$$\mathbf{E}\left[\xi_l^2\right] = \left(N_0/\tau + S\sum_{j=1}^{J-1}\gamma_{jl}\right) \tag{6.5}$$

Note also that the signal component of the received waveform in the lth time chip can be written as

$$\begin{aligned} &d_{ml}\sqrt{2S}\beta(t)\alpha_l\cos(2\pi f_l t - \theta_l) = \\ &\qquad d_{ml}\sqrt{2S}\beta(t)\left[z_{lc}\cos(2\pi f_l t) + z_{ls}\sin(2\pi f_l t)\right] \end{aligned} \tag{6.6}$$

where z_{lc}, z_{ls} are i.i.d. zero mean Gaussian random variables with variance $1/2$.

The received signal is applied to a quadratic detector and the output hard-limited to either $+1$ or -1. Using the result due to Voelcker [58], the corresponding hard decision chip error probability for DPSK with Rayleigh fading in the presence of

white Gaussian noise is:

$$P_c = \frac{\Gamma(1-\varepsilon)+1}{2(\Gamma+1)} \tag{6.7}$$

where Γ is the ratio of signal variance to noise variance of either quadrature component of the envelope, and ε is the correlation component over the pulse length.

Now

$$\Gamma = \frac{\mathbf{E}\left[z_c^2(2S)\right]}{\left(N_0/\tau + S\sum_{j=1}^{J-1}\gamma_{jl}\right)} = \frac{1}{\left(N_0/E_c + \sum_{j=1}^{J-1}\gamma_{jl}\right)} \tag{6.8}$$

The correlation coefficient is [2]

$$\varepsilon = J_o(\omega_D T) \tag{6.9}$$

where J_o is the Bessel function of the first kind, order zero.

ω_D is the maximum Doppler frequency in rads/s, taken to be about 600 rads/s, equivalent to a vehicle speed of around 115 km/hr.

T is the frame period.

Hence after substituting the appropriate quantities and a small amount of rearrangement, the probability of a making a hard decision error on a chip is

$$P_c = \frac{(1-\varepsilon)+\left(N_0/E_c + \sum_{j=1}^{J-1}\gamma_{jl}\right)}{2\left(1+N_0/E_c + \sum_{j=1}^{J-1}\gamma_{jl}\right)} \tag{6.10}$$

Yue [35] derived a similar formula by considering the characteristic function of the detector, but did not include the decorrelation between chips at the same frequency but separated by a sequence period. His formula therefore lacks the $(1-\varepsilon)$ term in the numerator, and does not account for the irreducible error rate.

Consider only the case where one or zero interferers may be in any particular chip. Then with hard decision decoding on each chip, we have

$$\Pr(\text{chip in error}|\text{interferer present}) = p_1$$

$$\Pr(\text{chip in error}|\text{no interferer present}) = p_0$$

Then for (23,12) Golay coding, with j interferers distributed one to each chip (where $j \leq 23$)

$$\begin{aligned}\Pr(\text{frame error}|j \text{ interferers}) &= 1 - \Pr(0 \text{ chip errors}|j \text{ interferers}) \\ &\quad - \Pr(1 \text{ chip error}|j \text{ interferers}) \\ &\quad - \Pr(2 \text{ chip errors}|j \text{ interferers}) \\ &\quad - \Pr(3 \text{ chip errors}|j \text{ interferers}) \qquad (6.11) \\ &= \sum_{l=4}^{23} \Pr(l \text{ chip errors}|j \text{ interferers}) \qquad (6.12)\end{aligned}$$

The conditional probabilities can be evaluated by the following formulae using the number of terms appropriate for the number of interferers.

$$\Pr(0 \text{ chip errors}|j \text{ int.}) = (1-p_1)^j(1-p_0)^{23-j} \qquad (j \geq 0) \qquad (6.13)$$

$$\begin{aligned}\Pr(1 \text{ chip error}|j \text{ int.}) &= \binom{j}{1} p_1^1(1-p_1)^{j-1}(1-p_0)^{23-j} \qquad (j \geq 1) \\ &\quad + (1-p_1)^j \binom{23-j}{1} p_0(1-p_0)^{22-j} \qquad (6.14)\end{aligned}$$

$$\begin{aligned}\Pr(2 \text{ chip errors}|j \text{ int.}) &= \binom{j}{2} p_1^2(1-p_1)^{j-2}(1-p_0)^{23-j} \qquad (j \geq 2) \\ &\quad + \binom{j}{1} p_1^1(1-p_1)^{j-1} \binom{23-j}{1} p_0(1-p_0)^{22-j} \qquad (j \geq 1) \\ &\quad + (1-p_1)^j \binom{23-j}{2} p_0^2(1-p_0)^{21-j} \qquad (6.15)\end{aligned}$$

$$\begin{aligned}\Pr(3 \text{ chip errors}|j \text{ int.}) &= \binom{j}{3} p_1^3(1-p_1)^{j-3}(1-p_0)^{23-j} \qquad (j \geq 3) \\ &\quad + \binom{j}{2} p_1^2(1-p_1)^{j-2} \binom{23-j}{1} p_0(1-p_0)^{22-j} \qquad (j \geq 2) \\ &\quad + \binom{j}{1} p_1^1(1-p_1)^{j-1} \binom{23-j}{2} p_0^2(1-p_0)^{21-j} \qquad (j \geq 1) \\ &\quad + (1-p_1)^j \binom{23-j}{3} p_0^3(1-p_0)^{20-j} \qquad (6.16)\end{aligned}$$

Using equation 6.10, the quantities p_0, p_1 may be evaluated. The value of ω_D used in the simulation was around 600 radians/second, and with the frame period T specified earlier, $\varepsilon = J_0(0.2356) = 0.9862$.

The results for simulation and analysis at two different signal to noise ratios are summarised in tables 6.2.1 and 6.2.1.

Number of chips with single interferer	Pr(codeword error)		
	calculated	simulation	calculated (Yue's formula)
0	1.17×10^{-4}	1.00×10^{-4}	4.93×10^{-6}
1	5.42×10^{-4}	6.10×10^{-4}	4.68×10^{-5}
2	2.13×10^{-3}	2.02×10^{-3}	3.64×10^{-4}
3	6.95×10^{-3}	6.75×10^{-3}	2.18×10^{-3}

Table 6.2: Calculated and simulation values for the (23,12) Golay code with single interferers in several chips, $E_c/N_0 = 20$ dB

Number of chips with single interferer	Pr(codeword error)		
	calculated	simulation	calculated (Yue's formula)
0	4.96×10^{-2}	4.13×10^{-2}	3.68×10^{-2}
1	7.17×10^{-2}	6.49×10^{-2}	5.57×10^{-2}
2	9.98×10^{-2}	8.60×10^{-2}	8.05×10^{-2}
3	1.34×10^{-1}	1.23×10^{-1}	1.12×10^{-1}

Table 6.3: Calculated and simulation values for the (23,12) Golay code with single interferers in several chips, $E_c/N_0 = 9$ dB

The results show that the correlation term becomes significant at high signal to noise ratios and for few interferers. The simulation results are a very good match to the predictions calculated using the formulae derived above, validating the simulation approach for estimating receiver performance. Yue's formula which assumes perfect correlation between adjacent DPSK chips is shown to consistently underestimate the codeword error rate, by orders of magnitude at high signal to noise ratios and few interferers. The simulation results also validate the modelling of interferers as large independent Gaussian random variables in the inphase and quadrature stream for the case where a hard decision is made on each decoder output. Hence

if the interference pattern distribution is known, the probability of codeword error may be calculated and the bit error rate found.

It would appear that the Golay code is not a suitable code for use with the FH-DPSK system. As the number of interferers increases, the bit error rate increases rapidly. With a chip energy to noise power spectral density ratio of 20 dB, the system is unable to maintain a codeword error rate of 10^{-3} if more than one interferer is present. It will be seen later that this leads to poor results for this system under a random addressing assumption.

It is noted that soft decision decoding of the Golay code is possible by using other techniques. In particular, the Chase algorithm [83] may be used, where the least reliable codeword bits are progressively replaced by their complement and decoded, until the most likely solution is found. This can lead to further gains in performance, but is not examined here, as it is not amenable to analysis.

6.3 Performance of Coding Schemes under Random Addressing

To compare the performances of the various coding schemes for the model where interferers are assumed to appear as fading tones with random ± 1 modulation in each time chip, it is necessary to take the effect of the addressing scheme into account. The probability of an interferer pattern occurring is a function of the way the hopping sequences are generated and allocated. Unfortunately, the "one-coincidence" addressing schemes, which have the lowest cross-correlation properties for a random time shift, are difficult to incorporate into analysis. As an interferer may use a particular frequency only once, and may only interfere with the wanted user's signal in at most one frequency, the probability of an interferer being present in a chip is dependent on the previous chips. This then requires enumeration of all the possible patterns that the interferers may take, and subsequent evaluation for

the probability of error.

This has been achieved for the FH-MFSK system [51], where the probability of error can be evaluated based on the probability of receiving valid patterns of chips with energy above a threshold. An error is made when the number of chips in a valid but erroneous pattern is greater than (or equal to) the number of chips detected in the correct pattern. Now consider the FH-DPSK system. This type of analysis used for the FH-MFSK system cannot be applied to the linear or normalizing receiver as the decisions are not made on a chip by chip basis. Secondly, the method of [51] enumerates the possibilities of interferer signals being in frequency channels other than that of the wanted signal with an energy greater than a threshold value. It does not take account of interferers being present in the same frequencies as the wanted signal, as the probability that an interferer will cause the wanted signal to be below threshold is assumed to be very small. It also relies on the fact the every user can interfere with the wanted signal in at least one chip, as the frequency transmitted at any chip is determined by the data.

For the FH-DPSK systems, the number of frequencies that a user can transmit on is a function of the sequence length and the number of frequency channels in the available bandwidth. In addition, the error probability is determined by the number of users transmitting in each time/frequency chip and the interferer arrangement within the codeword. The determination of probability of error becomes a very large enumeration problem, whereby the conditional probability of error and the probability of occurrence must be evaluated for every interferer pattern, and combined to obtain the overall error rate.

To estimate the number of users that may use the system at any time, a random addressing approach [35] is used to upper bound the probability of error. The random allocation of addresses covers all possible sequences. As the sequences with low cross-correlation properties will have a lower error rate than those chosen randomly, the error rate for the randomly allocated sequences will form an upper bound on the probability of error for the "one-coincidence" addressing schemes.

This approach has been used for FH-MFSK schemes, where simulation has confirmed that the allocation of hopping addresses on a random basis leads to results which approach those of the "one-coincidence" addressing as the total available bandwidth and the number of users increases [22]. However, these results are not entirely valid for the case of FH-DPSK, as the number of users able to interfere with the wanted signal is the subset of users who have one or more of the frequencies in their hopping set in common with the target user's set. Those users in this subset have an increased chance of a clash with the target user, inversely proportional to the sequence length, and proportional to the number of frequencies which are common to both the target user and the interferer sequences. It is therefore unknown how tight the random addressing bound is for the FH-DPSK case.

Under the tone interferer model from section 1.4.2, the effect of the jth interferer on the wanted signal can be modelled as

$$i_j(t) = \sum_{l=0}^{L-1} \sqrt{2S}\mathrm{rect}_\tau(t - l\tau)\left[\xi_{jl}\cos(2\pi f_l t) + \eta_{jl}\sin(2\pi f_l t)\right] \tag{6.17}$$

where ξ_{jl} and η_{jl} are i.i.d. zero mean Gaussian random variables with variance $\gamma_{jl}/2$ such that

$$\gamma_{jl} = \begin{cases} 1 & \text{if the } j\text{th interferer is present in the } l\text{th chip} \\ 0 & \text{otherwise} \end{cases} \tag{6.18}$$

The distribution of γ_{jl} is determined by the addressing technique, but for reasons given above, hopping sequences are allocated by a memoryless process. At any frequency, the probability of next hopping to a particular frequency is uniformly $\mu = 1/q$, where q is the total number of available hopping channels. The number of channels available in a bandwidth W Hz, assuming an information bit rate R_b and a code rate $C = k/n$, is $q = W/(R_b/C)$. For the purposes of comparison, the values of $W = 20$ MHz and $R_b = 32$ kilobits/second were used. In a system where the user hopping sequences are constrained to be chip synchronous, the distribution of γ is given by

$$p_\gamma(x) = \delta(x)(1-\mu) + \delta(1-x)\mu \tag{6.19}$$

for every user. As the γ_{jl} are identically and independently distributed for each user

and each channel, the total number of interferers present in a chip is distributed binomially.

6.3.1 Hard Decision Decoding Performance

It is assumed that the signals and receiver used are as defined in section 6.2.1, with the exception that any hard decision block code may be thought to be encoding the message bits.

For J users active in the system, the probability of a making a hard decision error on a chip is

$$P_c = \frac{(1-\varepsilon) + \left(N_0/E_c + \sum_{j=1}^{J-1} \gamma_{jl}\right)}{2\left(1 + N_0/E_c + \sum_{j=1}^{J-1} \gamma_{jl}\right)} \tag{6.20}$$

where all symbols have the previously defined meanings.

Assuming that frequency hopping sequences are allocated by random addressing, each γ_{jl} will be distributed as equation 6.19. For (J-1) interferers, using hard decisions on each chip, the probability of chip error can be obtained from the identical and independently distributed binomial probability distributions for the γ_{jl} as:

$$P_c = \sum_{j=1}^{J-1} \binom{J-1}{j} \mu^j (1-\mu)^{J-1-j} \frac{(1-\varepsilon) + (j + N_0/E_c)}{(1 + j + N_0/E_c)} \tag{6.21}$$

The upper bound on codeword error rate for a given chip error rate for an orthogonal code is given by [75,35] and is expected to be tight for codeword error rates around and below the region $P_w \approx 10^{-3}$.

$$P_w \leq (2^k - 1)\left[\frac{1}{2}\binom{2^{k-1}}{2^{k-2}} P_c^{2^{k-2}} (1-P_c)^{2^{k-2}} + \sum_{l=(2^{k-2}+1)}^{2^{k-1}} \binom{2^{k-1}}{l} P_c^l (1-P_c)^{2^{k-1}-l}\right] \tag{6.22}$$

The mean bit error rate is then asymptotic to $P_b = P_w 2^{k-1}/(2^k - 1)$.

From the above equations, the probability of bit error versus number of users can be computed for a given E_b/N_0 for the orthogonal code. This is shown graphically in figure 6.8. By dropping the useless bit transmitted at the start of every orthogonal

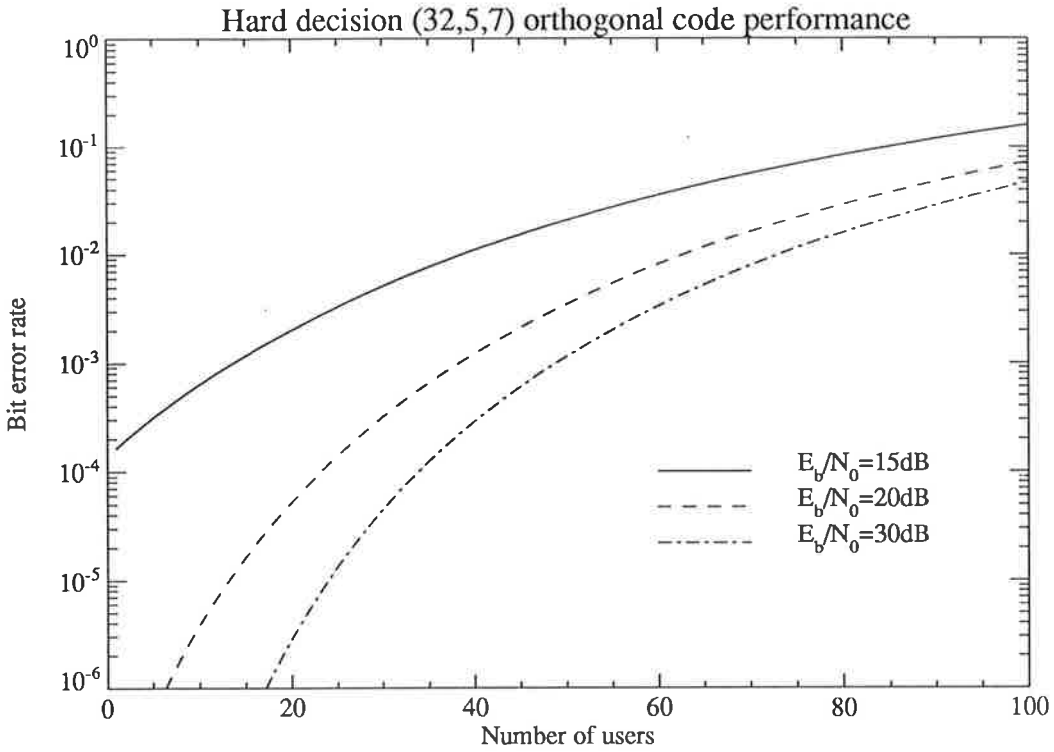

Figure 6.8: Bit error rate versus number of active users, for (32,5) orthogonal coding, hard decision decoding and random addressing.

codeword, the simplex code thus formed can also be assessed: for a given chip error rate, the bit error rate is identical to the orthogonal code, but the chip error rate is smaller due to the increased number of channels available for hopping and the fractional increase in chip signal to noise ratio for a given E_b/N_0. Two more users than for the orthogonal code may be present in the system at an average bit error rate of 10^{-3}.

For the biorthogonal code, defined in a previous section, a similar relation can be derived. Any codeword has the property of being at the same Hamming distance $d_1 = d_{min}$ from any other codeword except one, which is at twice the distance $d_2 = 2d_{min} = n$. One extra information bit can thus be transmitted with no increase in bandwidth over the orthogonal code. For this (n, k) bi-orthogonal code, the probability of a codeword error can be obtained from the union bound, (choosing randomly when both the correct and incorrect codewords compared have the same

number of chips in error)

$$\begin{aligned} P_w &\leq (2^k - 2)\Pr(\text{error in codeword at distance } d_1) \\ &\quad + \Pr(\text{error in codeword at distance } d_2) \\ &= (2^k - 2)\left[\Pr(\text{more than } 2^{k-3} \text{ errors in } 2^{k-2} \text{ chips})\right. \\ &\quad \left. + (1/2)\Pr(2^{k-3} \text{ errors in } 2^{k-2} \text{ chips})\right] \\ &\quad + \left[\Pr(\text{more than } 2^{k-2} \text{ errors in } 2^{k-1} \text{ chips})\right. \\ &\quad \left. + (1/2)\Pr(2^{k-2} \text{ errors in } 2^{k-1} \text{ chips})\right] \\ &= (2^k - 2)P_{d_1} + P_{d_2} \end{aligned} \tag{6.23}$$

where

$$\begin{aligned} P_{d_1} &= \sum_{l=2^{k-3}+1}^{2^{k-2}} \binom{2^{k-2}}{l} P_c^l (1 - P_c)^{2^{k-2}-l} \\ &\quad + \tfrac{1}{2}\binom{2^{k-2}}{2^{k-3}} P_c^{2^{k-3}} (1 - P_c)^{2^{k-3}} \end{aligned} \tag{6.24}$$

$$\begin{aligned} P_{d_2} &= \sum_{l=2^{k-2}+1}^{2^{k-1}} \binom{2^{k-1}}{l} P_c^l (1 - P_c)^{2^{k-1}-l} \\ &\quad + \tfrac{1}{2}\binom{2^{k-1}}{2^{k-2}} P_c^{2^{k-2}} (1 - P_c)^{2^{k-2}} \end{aligned} \tag{6.25}$$

The bit error probability is then bounded by

$$P_b < (1/k) \sum_{d=d_{min}}^{n} B_d P_d \tag{6.26}$$

where B_d is the total number of all bit errors that occur in all block error events involving codewords at distance d from a codeword

P_d is the probability of wrongly choosing a codeword at a distance d

Assume the complementary information words are mapped to the complementary codewords to minimise the probability that a codeword error will cause all information bits to be in error. Then

$$B_{d_1} = \sum_{i=1}^{k-1} \binom{k}{i} i \tag{6.27}$$

$$B_{d_2} = k \tag{6.28}$$

The results for this code are given in figure 6.9. Due to the increased number of channels being available, and the codeword error rate being only slightly worse than that of the Hadamard code, the biorthogonal code allows a few more users to use the system at a bit error rate of 10^{-3}.

Results for other block coding schemes can also be obtained in a straightforward manner. Given a binary (n, k, t) block code (hard decision decoding) with k information bits encoded per block of n channel symbols and an error correction capacity of t channel symbols, for a given channel symbol (chip) error probability P_c the information bit error probability is approximately given by [85]

$$P_b = \frac{d_{min}}{n} \sum_{i=t+1}^{d_{min}} \binom{n}{i} P_c^i (1-P_c)^{n-i} + \frac{1}{n} \sum_{i=d_{min}+1}^{n} i \binom{n}{i} P_c^i (1-P_c)^{n-i} \qquad (6.29)$$

where $d_{min} = 2t + 1$ is the minimum Hamming distance.

The above approximation has been shown [85] to be very accurate for the (23,12) Golay code. Applying it to the FH-DPSK Golay encoded system, discussed in a previous section, is straightforward. Results are shown in figure 6.10. It is apparent that the increased number of channels available to the Golay coded system is not sufficient to overcome its reduced redundancy compared to the Hadamard system.

In order to see the effect of code rate on the system, the performance of primitive binary BCH codes [82] was computed using equations 6.21 and 6.29. Only those codes which resulted in chip periods of approximately five microseconds or greater are of interest, as systems with chip periods shorter than this will experience severe problems with time delay spread. In addition, only code lengths of up to 127 symbols were examined, as the longer code lengths will have very long sequence periods and thus the DPSK irreducible error rate will be unacceptable. (The hardware requirements for such long codes using n independent channels would probably prohibit their use). For each code, the correlation coefficient ε was computed for a sequence length equal to the codeword length, and the maximum Doppler frequency was set to 600 radians/second for all cases. The number of active users that may use an isolated cell at a bit error rate not exceeding $P_b = 10^{-3}$ for the different length and rate codes are summarised in table 6.3.1.

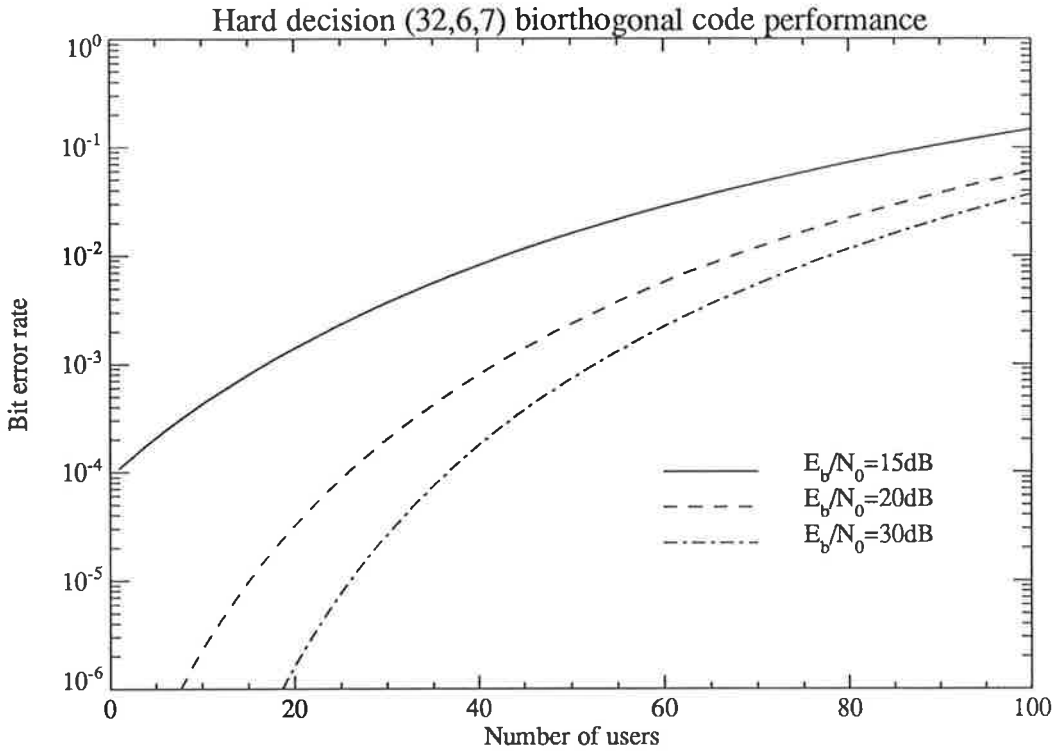

Figure 6.9: Bit error rate versus number of active users, for (32,6) biorthogonal coding, hard decision decoding and random addressing.

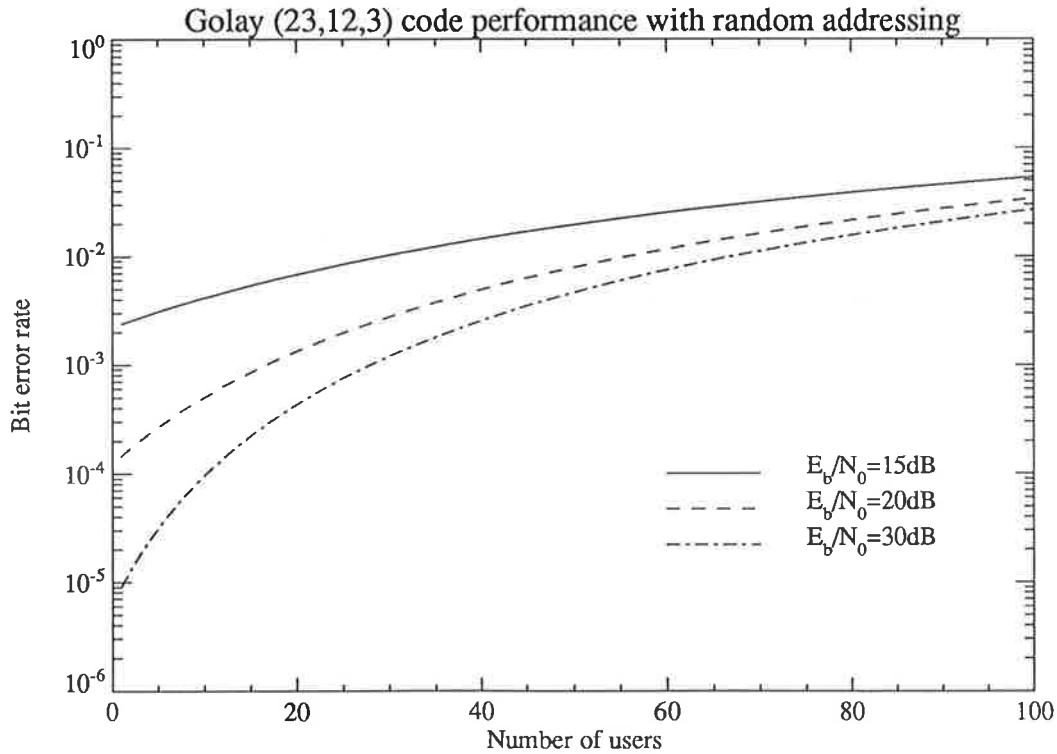

Figure 6.10: Bit error rate versus number of active users, for (23,12,3) Golay coding with hard decision decoding and random addressing.

n	k	t	code rate k/n	chip period $k/(Rn)$ (μs)	No. of users at $P_b \leq 10^{-3}$ 15	20	30
7	4	1	0.571	17.9	0	3	14
15	11	1	0.733	22.9	0	0	2
15	7	2	0.467	14.6	0	9	20
15	5	3	0.333	10.4	0	21	32
31	16	3	0.516	16.1	0	1	12
31	11	5	0.354	11.1	1	28	39
31	6	7	0.193	6.0	5	30	40
63	24	7	0.380	11.9	0	3	14
63	18	10	0.285	8.9	4	30	41
63	16	11	0.254	7.9	9	35	45
63	10	13	0.159	5.0	6	31	41
63	7	15	0.111	3.5	3	27	37
127	29	21	0.228	7.1	0	24	35
127	22	23	0.173	5.4	5	30	41

It is noted that the $(127, 22, 23)$ code requires more channels than would be available at the frequency spacing of $1/\tau$ in a total bandwidth of 20 MHz, which would lead to more correlation between fading on adjacent channels and hence a higher error rate. This compromise between code rate and number of channels in the total bandwidth leads to an optimum rate for the code. This is clearly seen for the length 63 codes, where the user capacity increases as the code rate decreases, until a maximum is reached for a code rate of 0.254, whereupon the number of users possible in the system decreases with decreasing code rate. The same behaviour is exhibited for length 127 codes. Codes with chip periods of less than 5 microseconds are not optimum, so the effect of time delay spread can be assumed to be reasonably small. Indeed it is possible to double the chip period, halving the channel bandwidth, and have two frequencies transmitted simultaneously (as proposed by Timor [42] for FH-MFSK), to mitigate the effect of frequency selective fading within a channel. As the sequence period is not increased, there is no increase in the irreducible error rate.

The best three BCH codes, assuming that the n chips are all on different frequencies, are the (63,16,11), (63,10,13) and (31,6,7) codes, and the results for the

best length 63 and 31 codes are plotted in figures 6.11 and 6.12. Under the random addressing assumptions, none of the BCH codes match the bi-orthogonal code performance. The average number of users that each of the above hard decision codes can support at E_b/N_0 ratios of 15, 20 and 30 dB, are summarised in table 6.4.

E_b/N_0 (dB)	Number of users at $P_b = 10^{-3}$					
	orthogonal (32,5)	biorthogonal (32,6)	Golay (23,12,3)	BCH (31,6,7)	BCH (63,10,13)	BCH (63,16,11)
15	13	17	0	5	6	9
20	38	42	17	30	31	35
30	48	52	28	40	41	41

Table 6.4: Number of users possible at $P_b = 10^{-3}$ for hard decision decoding

The number of users which can use the system at an average bit error rate of 10^{-3} for the (31,5) simplex code is midway between that of the orthogonal and biorthogonal codes, being 15,40, and 50 for E_b/N_0 of 15,20 and 30 dB respectively. These values were used as the number of users in an isolated cell with addresses allocated from a one-coincidence set for a series of 50 simulations, as described in section 4.4. The results obtained for the mean bit error rate $\bar{P}_b$, the median $\hat{P}_b$, and the sample variance V_{P_b} are given in table 6.5.

E_b/N_0 (dB)	No. Users	$\bar{P}_b$	$\hat{P}_b$	V_{P_b}
15	15	6.0×10^{-4}	4.9×10^{-4}	1.6×10^{-7}
20	40	4.8×10^{-4}	1.9×10^{-4}	7.9×10^{-7}
30	50	7.4×10^{-4}	1.3×10^{-4}	3.6×10^{-6}

Table 6.5: Error rate statistics for those user numbers estimated to give $P_b = 10^{-3}$ on uplink with hard decision receiver and random addressing.

The mean bit error rate is consistently just below the $P_b = 10^{-3}$ predicted by the random addressing model. While the number of samples taken is not large, it does provide an indication that the random addressing leads to a reasonably close approximation and is within an order of magnitude as an upper bound on mean bit

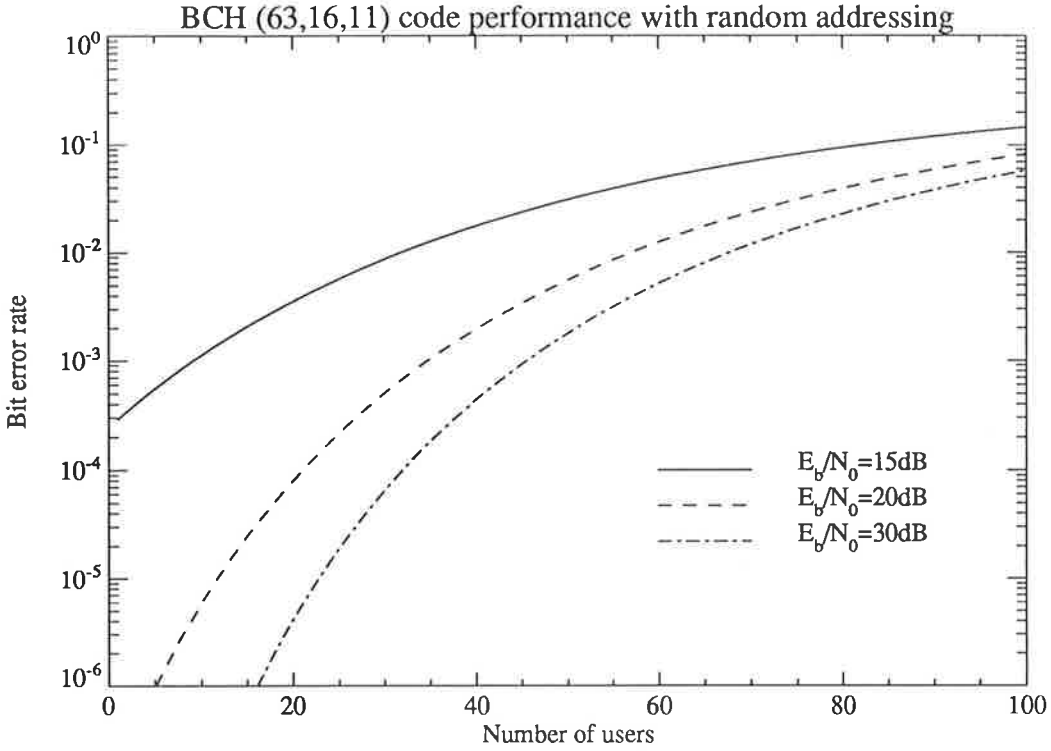

Figure 6.11: Bit error rate versus number of active users, for (63,16,11) BCH coding with random addressing.

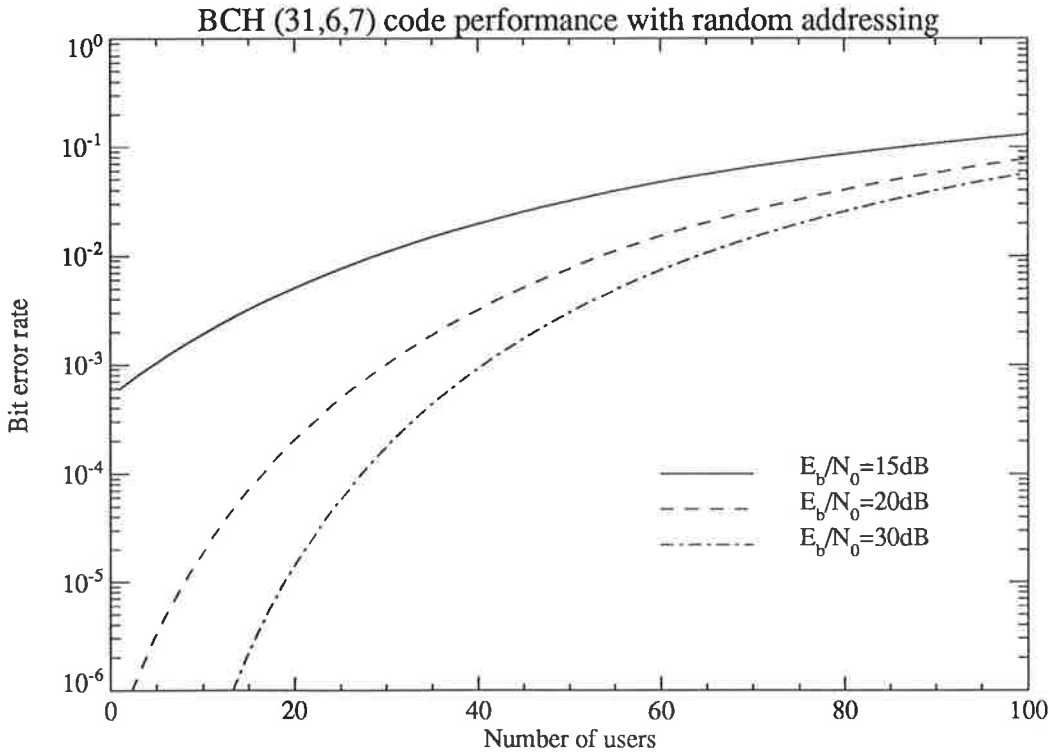

Figure 6.12: Bit error rate versus number of active users, for (31,6,7) BCH coding with random addressing.

error rate.

The difference between the mean and median sample bit error rates again raises the question of what is the appropriate quantity to be measured: despite the convenience of an analytic formulation for the mean, it would perhaps be more logical to take the median, or perhaps a particular percentile of the distribution, as the point of comparison. A common practice in telecommunications is to specify a service in terms of a given probability of success, where success is measured in terms of a quantity not exceeding a threshold. Thus a service area for mobile radio may be dimensioned on the basis that users at 90 percent of locations in the service area will experience a bit error rate below a maximum of 10^{-3}. Unfortunately, to establish such a detailed profile of bit error rate as a proportion of users is a time-consuming problem, especially if the mathematics is intractable and the distribution must be estimated from simulation, and as such was not pursued further.

6.3.2 Estimation of Normalizing Receiver Performance

As no method of analysing the performance of the non-linear normalizing receiver exists, apart from direct simulation, it is not possible to produce a formula like that derived for the hard decision receiver. It is therefore necessary to estimate the performance, based on the behaviour of the normalizing receiver compared to the hard decision receiver, for conditions which result in bit error rates close to 10^{-3}.

Results for the normalizing receiver show that the probability of codeword error at error rates of 10^{-3}–10^{-2} is consistently less than that of the hard decision receiver. The difference in error rate is lower with high background noise levels, and is also dependent on the actual arrangement of interferers within the received signal. The benefit of the normalizing receiver is greatest when only single interferers are located within a chip. This is to be expected, for as the number of interferers per chip increases, the total interference per chip becomes more truly Gaussian, and the magnitude of the interference from frame to frame at a particular frequency will

vary instead of remaining roughly constant as in the case of a single interferer.

Consider the isolated cell simulations where the interference is limited to one interferer per chip. Results for the orthogonal and biorthogonal codes indicate a decrease by a factor of 4–10 (greater at high E_b/N_0) in the probability of codeword error over the hard decision case for a given number of tone interferers, in the region of interest such that $P_b \approx 10^{-3}$. The factors 4,7, and 10, for $E_b/N_0 = 15$,20 and 30 dB respectively, were applied to the probability of codeword error in the random addressing case. This enabled an estimate to be made of the increased number of users possible for the normalizing receiver with the simplex and biorthogonal codes. (table 6.6).

E_b/N_0 (dB)	No. of users at $P_b = 10^{-3}$	
	(31,5) simplex	(32,6) biorthogonal
15	29	31
20	60	63
30	75	78

Table 6.6: Estimate of number of users at $P_b = 10^{-3}$ for (31,5) simplex and (32,6) biorthogonal codes using the normalizing receiver.

The estimated numbers of users have been used as the basis for a series of simulations. These have been previously described and the results given in section 4.4. As in the case of the hard decision receiver, the mean bit error rates are close to that predicted by random addressing. It would appear that the estimation employed is a reasonable approximation.

These figures represent an increase on the number of users which Yue's post-detection soft-limiting receiver was able to provide. Further gains could be expected by using the true optimum receiver, which assumes an estimate of the chip position of the interferers could be obtained. Another point is that the use of chip synchronism between user hopping sequences has been shown in the multiple cell simulations to

give a worst case estimate. Thus the figures given above are conservative estimates of the number of users that may use the system at an average bit error rate of 10^{-3}.

A final important point is that no account is taken of user voice activity. All analysis has assumed that users continue to transmit on a channel during the silent periods in a conversation. As a speaker is silent for roughly 50% of the conversation, only transmitting when necessary would reduce the interference seen in the network. This would allow a further increase in the user capacity. Of course, the problem of acquiring synchronization every transmission and the overheads involved must be examined.

6.4 Comparison of Usage with FDM systems

It is of interest to compute the number of users in a digital FDM system (each user is assigned a single channel in a cell) and compare it to that supported in the FH-DPSK scheme with equivalent operational parameters. In a multiple cell FDM system, the number of users will be markedly reduced from the single cell case due to the effects of co-channel interference and channel assignment strategies.

The same parameter values will be assumed for the FDM system as for the FH-DPSK system: an information bit rate R_b of 32 kbits/second and a total one-way bandwidth W of 20 MHz. The modulation is assumed to be binary DPSK. (It is noted that higher order modulation schemes, *eg* QPSK, have been considered for the mobile channel in FDM schemes, and these schemes require less bandwidth to achieve the same bit rate as the binary schemes. However, if the error rate of these schemes is higher for a given SNR, this leads to larger re-use distances and/or increased redundancy in the channel coding, which diminishes their advantage.)

The average number of users per cell U which may be accomodated in each cell for a code rate C is given by the relation

$$U = \frac{WCf_t}{R_b f_r} \tag{6.30}$$

where f_t is the trunking efficiency, a factor which holds the call blocking probability to a specified level (*eg* 2%). The re-use factor f_r denotes the number of cells which share the total available bandwidth before channels are re-used in other cells.

For omnidirectional base stations, Yue [86] states that a re-use factor of 12 is necessary for FDM systems. Calculations are made for this factor, and also for a smaller re-use factor of 7. In addition, error correction coding is likely to be used, and so figures are given for a code rate of 1/2 as well as for $C = 1$. Trunking efficiency factors of 100% and 80% are assumed. The results are presented in table 6.4.

Re-use factor	Code Rate	Trunking Efficiency	No. of Users
12	1.0	1.0	52
12	1.0	0.8	41
12	0.5	1.0	26
12	0.5	0.8	21
7	1.0	1.0	89
7	1.0	0.8	71
7	0.5	1.0	44
7	0.5	0.8	35

Table 6.7: Number of users supported in a multi-cell FDM system for a range of re-use factor, code rate and trunking efficiency.

A wide range of user numbers is obtained for the FDM systems, dependent on the operational parameters. The best results exceed the performance of the FH-DPSK system, which is estimated in section 4.5 to support about 70–80 users per cell. However, under less ideal assumptions, the FDM system performance is inferior to that of the FH-DPSK system. These results are promising for FH-DPSK systems and reinforce the need for further work to fully characterise the performance of such systems.

Chapter 7

Conclusions

The FH-DPSK system has been analysed and simulated to provide a more complete picture of the performance that such a system could attain. Previously published research on this topic has assumed different transmission parameters and conditions when analysing receivers, making comparisons of performance very difficult. The work presented in this thesis has attempted to present results for a uniform set of basic assumptions for each receiver modelled, so that valid judgements on the relative performances may be made.

In chapter 2, previous results from [24] for the performance of an orthogonally coded FH-DPSK system using the linear receiver in correlated fading and white Gaussian noise have been extended to investigate the use of spatial diversity techniques. The use of maximal ratio combining, equal gain combining and selection diversity (well characterised in single channel FM transmission) leads to greatly improved performance both in uncorrelated and correlated Rayleigh fading. Better results are obtained from these schemes than from an alternative diversity scheme proposed in [24], although the level of complexity is much greater. These results apply for transmission in a Rayleigh fading and AWGN environment. While the modelling of multiple user interference as AWGN is not viewed as a very good approximation to the real situation, these results are applicable to downlink trans-

mission in an isolated cell where synchronization at the base station ensures that no interference exists between all the signals to users. In this circumstance, spatial diversity, and in particular the combining methods, may be of use in decreasing the frequency with which the combination of wideband fast fading and shadow fading causes the signal power to fall to a level where the bit error rate becomes unacceptable. It is likely that similar gains from diversity would be forthcoming for the alternative receivers examined in the remainder of the thesis, but the appropriate form and implementation remain to be determined.

In chapter 4, the performance of three different receivers for the orthogonally coded system proposed by Cooper and Nettleton was assessed by simulation. In additive white Gaussian noise, and both with and without independent Rayleigh fading on each channel, the results for the linear and hard decision receivers match those predicted from analysis, validating the accuracy of the simulation. The performance of a non-linear "normalizing" receiver was also investigated for these conditions, and found to be slightly inferior to the linear receiver, but superior to the hard decision receiver. The de-correlation between the successive samples of the complex fading envelope at a particular frequency, modelled accurately in the simulation program, was found to have negligible effect for the sequence periods assumed by previous authors, whose analytic predictions had assumed 100% correlation. However, this de-correlation effect, which leads to an irreducible error rate, was found to be significant when longer sequence periods were later considered, and should be taken into account under these circumstances.

The main argument against the AWGN interference argument is that it does not adequately represent the cyclical presence of a large amplitude interferer within the frequency hopping sequence. By using the tone interference model originated by Yue [26,35], this repetitive interference may be accounted for. The interference from other users is modelled as a series of independent Gaussian tone interferers in individual channels of the target user's frequency hopping sequence, each randomly modulated (corresponding to random data). Under these conditions, the linear receiver of [24] is no longer optimal. Instead, the "hard decision" receiver, which

makes hard decisions on each transmitted code bit in the individual channels before decoding, was predicted by Yue [35] to provide improved performance.

While this behaviour was verified by simulation in chapter 4, the best receiver under conditions of tone interference was the normalizing receiver. Results for this receiver indicate a considerable performance improvement over the hard decision receiver in all conditions. A decrease of up to an order of magnitude in bit error rate may be realized in going from a hard decision receiver to a normalizing receiver for bit error rates around 10^{-3}. This gain in performance is dependent on the number of channels subject to interference, and the ratio of bit energy to noise power spectral density.

The systems examined in the literature all assume that the number of channels in a hopping sequence is equal to the codeword length, commonly 32 chips. Simulation revealed that when a moderate number of interferers were present in discrete channels of the hopping cycle, the use of the Hadamard orthogonal code resulted in a very wide spread of bit error rates depending on where the interferers were located within the codewords. This disparity in bit error rates between users subject to the same number of interferers is due to the structure of the code, and the solutions proposed to combat the problem rely on changing the mapping from the codeword to the frequency channels over time. A reasonably effective solution has been found in the rotation of the frequencies used to transmit the codewords through a set of channels larger than and relatively prime to the number of code bits in a codeword. Simulation results prove that this technique significantly reduces the spread of error rates experienced by users. The extra hardware necessary is only a small increment on the existing requirement, and would provide a more consistent response for all users. However, the task of synchronization of the hopping sequence at the receiver would become more complex, especially if synchronism is lost after being initially acquired.

A further problem is the consistent number of bit errors which result for any wrong codeword when the codeword error rate is high as a result of the coding

method being sensitive to certain interferer patterns. This effect is entirely dependent on the mapping from data to codewords. While no optimal mapping was found, several mappings which produce a more random spread of errors have been found. The mapping problem decreases in importance if the codeword to channel mapping is permuted over time, but must still be considered if uniform error rates across all users for the same amount of interference is to be achieved (*ie* a "graceful degradation" characteristic is desired).

As a benchmark for performance, the optimum linear receiver for the orthogonally coded system was derived in chapter 5. Simulations show that if large Gaussian tone interferers are present within the frequency hopping cycle and their locations and magnitude can be estimated, this information may be used to significantly lower the mean bit error rate in the area of interest. This translates into an increase in the number of users that may be simultaneously active in the system. Such a proposition should be feasible at the base station, as it has accurate timing knowledge of the incoming mobile signals from within the cell. Measurement of the signal strength over time would also be able to indicate the presence and magnitude of a significant interferer.

To investigate the effect of varying coding redundancy, systems using biorthogonal coding and Golay coding were simulated and compared to the orthogonally coded system. In Rayleigh fading and AWGN, (*eg* downlink transmission in an isolated cell), the biorthogonal code achieved a lower bit error rate for a specified E_b/N_0 than the orthogonal code. When tone interferers were introduced, very little degradation was noted in bit error rate performance compared to the orthogonal code, but the lower coding redundancy enables more channels to be created in the total available one-way bandwidth. The probability of a given number of interferers being present in the codeword is thus less for the biorthogonal than for the orthogonal code.

The (23,12) Golay code performed poorly in the presence of more than a single interferer. This is not surprising, as it was decoded as a hard decision code, and hence could only correct a maximum of 3 incorrect chips within a 23 chip codeword.

However, as the probability of codeword error could be derived exactly for a given number of chip errors, the results from the Golay code were useful in assessing the accuracy of the theory used to predict the probability of a chip error for the hard decision receiver. An improved analytical formulation of the hard decision bit error rate produced results in close agreement with simulation results, and proved more accurate than a previous formula from [35].

Predictions for the number of users that can be active in an isolated cell for an average bit error rate of 10^{-3} were computed for the hard decision receiver from a random addressing approximation. Simulation using one-coincidence frequency hopping addresses indicates that the random addressing approximation results in a fairly tight upper bound. By noting the difference in performance between the hard decision and normalizing receiver when the number of interferers is constrained to be at most one per channel, an estimate was produced for the number of active users possible in an isolated cell with the normalizing receiver.

This estimate was confirmed by simulation. Assuming an information bit rate of 32 kilobits/second, a total one-way bandwidth of 20 MHz and (31,5) simplex coding, up to 75 users (at an E_b/N_0 of 30 dB) may communicate with an average bit error rate of 10^{-3} in an isolated cell, as opposed to 50 for the hard decision receiver. This figure assumes that users hop in synchronism ("chip synchronism"), although their hopping sequences are not aligned for minimum cross-correlation, having a random shift of an integral number of chips. This is a considerable improvement on a figure of 56 users given by Yue [38] for a receiver with soft limiting after the quadratic detectors and before combining by the Hadamard transform.

Further modelling of mobile to base transmission for a cluster of seven hexagonal cells, each with a corner radius of 8 km, indicated that the number of active users per cell for the normalizing receiver under the chip synchronism assumption is of the same order as for the isolated cell. This suggests that for the parameters assumed, the average difference in distance to the base station between the target user in the same cell and the interferers in foreign cells is large enough for attenuation to ensure

that the amount of significant interference contributed by mobiles in foreign cells is small. If the chip synchronism assumption is relaxed such that user sequences are entirely asynchronous, the bit error rate is roughly halved, and the user capacity slightly increased. This implies that there is an overall reduction in the effect of interference under the asynchronous assumption, despite increased numbers of users contributing co-channel and adjacent channel interference for part of a chip. The chip synchronous figures for the number of users possible in the system can therefore be viewed as a worst case.

A small number of simulations of the downlink (base to mobile) in a multiple cell situation with (31,5) simplex coding were performed. With no power control to counter shadow fading, a mobile in the cell corner (8 km radius in this example) will observe a wide signal strength variation from area to area. While the shadow fading alone will generally be insufficient to cause an unacceptable bit error rate at high E_b/N_0 values, it will have a disastrous effect when coupled with strong interference from neighbouring base stations. Bit error rates of 10^{-2}–10^{-1} are not uncommon, even though the median bit error rate over many users may be low, around 10^{-5}–10^{-4}. Such a poor error rate can only be countered effectively by handing over control to the base station with the strongest signals at the mobile. This is effectively the same strategy as used in present FDM schemes.

Several further conclusions may be drawn from the results. Hard decision codes like the BCH codes do not match the performance of those codes able to decoded using a form of soft decision logic (such as the biorthogonal code). Thus although the biorthogonal and simplex codes based on the Hadamard matrix are sensitive to certain interferer patterns, they are still preferable to the other codes considered here. It appears that the $(32, 6)$ biorthogonal code using the normalizing receiver is a slightly better choice than the $(32, 5)$ orthogonal code proposed previously. A reasonable estimate of the number of active users with a mean bit error rate of 10^{-3} in an isolated cell would be of the order of 78 for an E_b/N_0 of 30 dB. This is the estimate from the chip synchronous sequence assumption: while the results show a further gain under asynchronous conditions, real world imperfections in equipment

would probably negate any theoretical gain.

Unlike the FH-MFSK system, performance in asynchronous interference is not seriously degraded from the chip synchronous case but is actually improved. The number of users in a multiple cell scheme has also been found not to be reduced much from the isolated cell case. If a received E_b/N_0 of 20–30 dB is achievable, a value close to the asynchronous synchronous system estimate of 70–80 users per cell may be achievable in practice. This represents a considerable improvement the previous estimates for the FH-DPSK system, and equals or betters some estimates of capacity for a FH-MFSK multiple cell system [45,44]. In addition, depending on the propagation conditions in the service area, the FH-DPSK system may equal or better the performance of digital FDM system.

It has been demonstrated that the FH-DPSK system may be improved through using receivers which, in the absence of knowledge of the interference, use phase alone as a measure of the reliability of the received pulses on a channel. Other codes which can be decoded using soft decision techniques may produce better performance than the block codes considered here. While some preliminary investigations into convolutional and concatenated coding schemes are presented in Appendix C, further work is required to explore the potential of these schemes, variants of which are commonly used in forward error correction on such fading channels as satellite links. The performance of these codes is critically dependent on the burst error distribution, and the interleaving schemes to randomise the errors. As there are a large number of variables required to specify these schemes, (such as the metric weights, truncation lengths, interleaving depths, code rate), many simulation runs are necessary to determine a good combination of factors. Although some initial results were encouraging, there was insufficient time to cover this area and this has been left as further work.

Another avenue for further investigation is the synchronization process and re-acquisition of the signal after loss when using a codeword-to-channel mapping which cycles over time. When high user densities exist, this may prove to be a difficult

and time consuming exercise. The effect of different cell sizes on the interference from multiple cells, and hence the number of users possible per cell, is also worthy of investigation.

As noted in chapter 6, all calculations have been made on the basis of the active users transmitting constantly. As a typical speaker will have silent periods in speech amounting to about 50% of the time, the interference from other users could be reduced further by not transmitting any carrier while the user is not speaking. This would entail a packetizing protocol, and hence the attendant problems of synchronisation would need to be addressed on a packet by packet basis. Provided an efficient scheme could be implemented, still more users could use the system.

While much work is still required to produce an optimized FH-DPSK system, the results presented in this thesis both independently confirm earlier work, and provide new insight into the performance that may be expected from several receivers, for both an isolated cell and multiple cells. Other coding schemes apart from the Hadamard orthogonal code offer improved performance. The picture of the system that emerges is more optimistic than that published in literature, and might perhaps provide a real alternative to conventional FM/FDM systems if the considerations of implementation and economics were favourable.

Appendix A

Glossary and Notation used in this thesis

A.1 Glossary

The following terms are used throughout the thesis:

address sequence the frequency hopping sequence of a particular user

chip the frequency/time unit of a hopping sequence; a single frequency output from a frequency hopping generator. The chip period is the time occupied by a pulse at a single frequency.

code rate the effective number of message symbols sent as a proportion of the number of code symbols

direct sequence a spectrum spreading operation where a pseudo-noise sequence of ± 1, modulated at a much greater rate than the message bit rate, multiplies the carrier to spread the signal over a wide bandwidth

downlink the radio link from base station to mobile unit

DPSK differential phase shift keying

FDM frequency division multiplexing (single channel per carrier systems)

frequency hopping spectrum spreading via hopping the carrier frequency in time

hit a clash between two users' frequency hopping sequences

interferer an intentional, or more commonly in this work, unintentional signal causing interference to reception of the desired signal

MFSK multi-level frequency shift keying

MSK minimum shift keying

target user a user who is assumed to be the partner to the communication

uplink the radio link from mobile unit to base station

UHF the ultra-high frequency band (300–1000 MHz)

A.2 List of Common Symbols

Where possible, the following notation has been used for quantities that are referred to in various parts of the thesis, in order to preserve continuity.

t time (seconds)

S unfaded average signal power seen at the receiver

$r(t)$ the received signal

n_{lc}, n_{ls} inphase and quadrature background noise in the lth time chip

α_l magnitude of complex fading envelope in lth time chip (Rayleigh distributed)

E_c chip energy

E_b bit energy

N_0 one-sided power spectral density of background noise

R_b uncoded message bit rate

C code rate $C = k/n$

n number of code bits (chips) in a code word

k number of information (message) bits encoded into a n bit codeword

L number of frequencies in user hopping sequence

T period of complete frequency hopping sequence in seconds

τ period of one hop (chip) in seconds

J number of users considered to be active in the system

W total bandwidth available for all users on uplink or downlink

B_c coherence bandwidth (Hz)

f_l, ω_l frequency channel of lth hop in Hz and rad/s respectively

ω_D maximum Doppler frequency of the user in rads/s

P_b bit error rate

P_w codeword error rate

Γ signal to noise ratio

γ_{jl} variance of the Gaussian noise due to the jth interferer in the lth time chip

ε correlation coefficient for two chips at same frequency between which DPSK is used

$\rho(.)$ autocorrelation

m_d area mean power as a result of signal attenuation with distance — mean of lognormal (shadow) fading

σ variance of lognormal fading distribution (in dB)

$J_0()$ Bessel function of first kind, order zero

$rect(t)$ rectangular window function, defined as

$$\text{rect}_\tau(t) = \begin{cases} 1 & \text{if } 0 \leq t \leq \tau \\ 0 & \text{otherwise} \end{cases}$$

Appendix B

Results of Multiple Cell Uplink Simulations

The results of the simulations for a mobile located in the corner of a central cell (corner radius 8 km), surrounded by six cells and with power control employed to counteract shadow fading and attenuation, are tabulated in the following tables. Discussion of these results is given in section 4.5.

$E_b/N_0 = 15$ dB	No. Users	$\bar{P}_b$	$\hat{P}_b$	V_{P_b}
Hard decision, chip synch.	30	2.9×10^{-3}	2.4×10^{-3}	4.4×10^{-6}
	40	6.1×10^{-3}	5.0×10^{-3}	2.0×10^{-5}
	60	2.0×10^{-2}	1.5×10^{-2}	2.3×10^{-4}
Hard decision, asynch.	30	1.7×10^{-3}	1.3×10^{-3}	2.3×10^{-6}
	40	3.0×10^{-3}	2.5×10^{-3}	4.8×10^{-6}
	60	1.0×10^{-2}	9.6×10^{-3}	2.4×10^{-5}
Normalizing, chip synch.	30	3.8×10^{-4}	2.9×10^{-4}	1.7×10^{-7}
	40	1.2×10^{-3}	7.1×10^{-4}	3.1×10^{-6}
	60	7.3×10^{-3}	4.0×10^{-3}	7.5×10^{-5}
Normalizing, asynch.	30	2.2×10^{-4}	1.5×10^{-4}	4.6×10^{-8}
	40	4.5×10^{-4}	3.0×10^{-4}	1.6×10^{-7}
	60	2.5×10^{-3}	2.0×10^{-3}	3.9×10^{-6}

Table B.1: Mean, median and variance of the bit error rates recorded from 50 multiple cell uplink simulations with a range of receivers, sequence synchronism and user numbers, $E_b/N_0 = 15$ dB

$E_b/N_0 = 20$ dB	No. Users	$\bar{P}_b$	$\hat{P}_b$	V_{P_b}
Hard decision, chip synch.	60	6.5×10^{-3}	3.2×10^{-3}	7.5×10^{-6}
	70	1.2×10^{-2}	5.7×10^{-3}	2.3×10^{-4}
	80	1.6×10^{-2}	1.4×10^{-2}	1.6×10^{-4}
Hard decision, asynch.	60	2.0×10^{-3}	1.6×10^{-3}	4.0×10^{-6}
	70	4.4×10^{-3}	2.6×10^{-3}	2.7×10^{-5}
	80	7.1×10^{-3}	5.5×10^{-3}	3.4×10^{-5}
Normalizing, chip synch.	60	1.2×10^{-3}	2.4×10^{-4}	1.3×10^{-5}
	70	2.1×10^{-3}	7.4×10^{-4}	1.6×10^{-5}
	80	3.2×10^{-3}	1.7×10^{-3}	1.5×10^{-5}
Normalizing, asynch.	60	2.4×10^{-4}	1.2×10^{-4}	1.2×10^{-7}
	70	6.7×10^{-4}	2.7×10^{-4}	1.3×10^{-6}
	80	1.9×10^{-3}	8.5×10^{-4}	7.8×10^{-6}

Table B.2: Mean, median and variance of the bit error rates recorded from 50 multiple cell uplink simulations with a range of receivers, sequence synchronism and user numbers, $E_b/N_0 = 20$ dB

$E_b/N_0 = 30$ dB	No. Users	$\bar{P}_b$	$\hat{P}_b$	V_{P_b}
Hard decision, chip synch.	70	7.2×10^{-3}	2.1×10^{-3}	1.5×10^{-4}
	80	9.6×10^{-3}	5.3×10^{-3}	1.3×10^{-4}
	90	1.8×10^{-2}	1.2×10^{-2}	3.0×10^{-4}
Hard decision, asynch.	70	1.8×10^{-3}	8.5×10^{-4}	8.1×10^{-6}
	80	4.0×10^{-3}	2.4×10^{-3}	1.8×10^{-5}
	90	7.8×10^{-3}	5.1×10^{-3}	4.5×10^{-5}
Normalizing, chip synch.	70	6.2×10^{-4}	1.1×10^{-4}	1.7×10^{-6}
	80	1.3×10^{-3}	3.8×10^{-4}	5.1×10^{-6}
	90	2.9×10^{-3}	1.3×10^{-3}	1.8×10^{-5}
Normalizing, asynch.	70	2.0×10^{-4}	5.9×10^{-5}	2.0×10^{-7}
	80	6.4×10^{-4}	2.3×10^{-4}	1.0×10^{-6}
	90	1.9×10^{-3}	7.9×10^{-4}	6.9×10^{-6}

Table B.3: Mean, median and variance of the bit error rates recorded from 50 multiple cell uplink simulations with a range of receivers, sequence synchronism and user numbers, $E_b/N_0 = 30$ dB

Appendix C

Convolutional and Concatenated Coding Schemes

This appendix describes some preliminary research undertaken to assess the potential of using convolutional and concatenated coding schemes. As there was not time available to investigate further, these results are presented as supplementary material, intended to indicate the possibilities of this avenue of research. It is assumed that the reader is familiar with the basic concepts of convolutional and Reed-Solomon codes. A good introduction to these may be found in Lin and Costello [82] or Clark and Cain [83].

C.1 Convolutional Coding Schemes

Many communication links subject to fading (such as satellite links) or jamming (military communications links) [87] now use convolutional codes in preference to block coding schemes. The reasons include the large coding gain that may be obtained through soft decision decoding, and the availability of high speed hardware decoders. However, the performance of such schemes is heavily dependent on a random distribution of errors in the received symbols, and they do not cope well with

burst errors. Thus in a single channel system, it is necessary to use interleaving, where the consecutive code symbols over a long time period are re-ordered, transmitted, received and then restored to the original order before decoding. In the fast FH-DPSK scheme, each channel fades or is interfered with independently, and the interference can be viewed as permanently present in the channel for any particular connection. For this situation, there seems to be little advantage in interleaving, as long as the number of channels used is at least as great as the truncation depth of the decoder.

Generally, error correction capability and decoding complexity increases with increasing constraint length (memory) and with decreasing code rate (more code bits to the information bit). For example, a code often used in satellite communications is the optimum rate 1/2, constraint length 7 code, discovered by Odenwalder (given in [82]). Two code bits are output for every information bit input, with a memory of the 6 previous information bits as well as the current information bit being used in the computation. It is usually acknowledged to be the largest rate 1/2 code that may be decoded in reasonable time by the optimum method, Viterbi decoding. This decoding algorithm uses *maximum a posteriori probability* (MAP) to find the optimum path through the trellis of possible encoder states, based on the likelihood of the received symbols and their *a priori* probabilities. (Sequential decoding is used for larger constraint lengths and will not be considered here).

Half rate convolutional codes are often used as the inner code in a two-level coding scheme, where the outer level encodes words of information bits before the convolutional code. By this method, long and powerful codes may be constructed which cope well with random and burst errors.

To obtain an indication of the performance that a convolutional code could deliver, programs to perform half-rate convolutional encoding and Viterbi decoding were written and incorporated into the FH-DPSK simulation, replacing the orthogonal/biorthogonal schemes. The truncation length of the decoder was chosen to be at least five times the constraint length of the code (by which time the alternative

bit streams have converged to the same answer in almost all cases). This left the choice of the constraint length to be decided. The optimal constraint length 3 and 7 codes were used as examples (*ie* (2,1,3) and (2,1,7) codes), with truncation lengths of 20 and 35 respectively.

The values of the metric weights in the Viterbi algorithm depend on whether a hard decision, linear, or normalizing receiver is used. A linear receiver is assumed to to have a front end detection structure similar to that in figure 4.1. The detector output of each channel is assumed to be quantized to 8 uniformly spaced levels (no significant advantage is gained by having more levels [82]). In the situation where Rayleigh fading and tone interference exist, the choice of weights becomes complicated. As for the linear receiver for the orthogonal code, the effect of interference was ignored. The metric weights for each path through the decoding trellis were allocated by assuming that a Gaussian noise distribution exists for a fixed E_b/N_0. Errors are more likely during a fade, when the E_b/N_0 is low, and hence the decision was made to set the metrics initially assuming a mean E_b/N_0 of 4 dB. While this is just an estimation of the threshold, it is justified by the demonstration in [21] that a small signal approximation of the optimum receiver for orthogonal code transmission in Gaussian noise alone leads a receiver which has been proved in this thesis to be the optimum receiver in Rayleigh fading and Gaussian noise. For the hard decision receiver, the detector output for each channel was set to the extreme opposite levels of the linear scale and the corresponding metric weights allocated.

For the correct weights for the normalizing receiver (*ie* using a channel detector as in figure 4.8 and quantizing the output to 8 equally spaced levels), knowledge is required of the probability density function of the sum of outputs of the quadratic detectors for a channel. Although this could be obtained by simulation, no time was available to perform this and it is an area for further work. Instead, the detected output from each channel was linearly quantized and then weighted as per the linear receiver, which assumed a Gaussian noise density. The purpose of this investigation is to get an idea of the possibilities of the normalizing receiver, and hence a non-optimal preliminary weighting is acceptable.

No. of	linear		hard decision		normalizing	
Intfr.	(2,1,3)	(2,1,7)	(2,1,3)	(2,1,7)	(2,1,3)	(2,1,7)
0			1×10^{-3}	1.4×10^{-3}		
1	2.2×10^{-4}	5.7×10^{-5}	2.6×10^{-3}	3.1×10^{-3}	4.8×10^{-4}	5.7×10^{-5}
2	2×10^{-3}	3.6×10^{-4}	7×10^{-3}	4.2×10^{-3}	1.3×10^{-3}	8.2×10^{-4}
3	1.1×10^{-2}	1.7×10^{-3}	1.8×10^{-2}	8.4×10^{-3}	8.4×10^{-3}	1.7×10^{-3}
4	2.0×10^{-2}	4.0×10^{-3}	2.8×10^{-2}	2.2×10^{-2}	8.9×10^{-3}	3.4×10^{-3}
5	4×10^{-2}	1×10^{-2}	4.3×10^{-3}	2.9×10^{-2}	1.7×10^{-2}	6.1×10^{-3}
6	6.3×10^{-2}	1.8×10^{-2}	5.9×10^{-2}	3.8×10^{-2}	3.0×10^{-2}	9.1×10^{-3}
7	1.1×10^{-1}	2.6×10^{-2}	1.1×10^{-1}	4.8×10^{-2}	5.6×10^{-2}	1.5×10^{-2}

Table C.1: Bit error rates for interferers located singly within the frequency channels of the target user, various receivers, 1/2-rate convolutional codes with constraint lengths 3 and 7.

The results for the two constraint length codes for the linear, hard decision and normalizing receivers are given in table C.1. Only one interferer may be present in any chip, and the ratio of bit energy to noise power spectral density used was $E_b/N_0 = 17$ dB. As for the block codes examined in the main body of the thesis, the normalizing receiver is superior to the linear and hard decision receivers when large numbers of interfered channels exist. However, in contrast to the situation for the orthogonal code, the hard decision receiver did not perform well. It did not significantly outperform the linear receiver at any stage, and in fact was worse for most areas of interest. This is a somewhat surprising result when compared to the block coding performance, and indicates that the metric weighting for the linear and normalizing receivers is important in obtaining a good error rate. It also implies that a weighting function on the detector outputs other than a linear scale may improve the performance of the receivers for the orthogonal and biorthogonal codes.

The error rate is better for the longer constraint length code than for the shorter, for the same number of interferers. However, the longer constraint length code hops over almost twice as many channels, and for a set number of users, would have a far higher probability of x interferers appearing somewhere in the sequence. Further

work is required to investigate the optimum constraint lengths to obtain minimum overall error rate.

C.2 Concatenated Codes

One method of synthesising longer code lengths is to use concatenated codes. These schemes have advantages in coping well with both random and burst errors. Typical schemes use Reed-Solomon (RS) codes as an outer code, where the RS code takes several words of information bits and produces a number of parity words. The resulting bit stream is then fed through an inner encoder before being transmitted. (Interleaving is also usually incorporated to randomize bursts of errors that would otherwise seriously degrade the performance of the inner decoder). The received bit stream is first decoded for the inner code before then being passed to the outer decoder. The inner code may be a convolutional or block code, and soft decision decoding is often used to gain maximum coding gain. Further enhancement can be obtained by setting the inner decoder to produce erasures for marginal decisions.

Some preliminary investigations were carried out into this technique. As the RS codes operate over finite fields GF(2^m) and produce $2^m - 1$ codewords with values between 0 and $2^m - 1$, it is a simple matter to use a simplex code of length $2^m - 1$ as the inner code to encode the output of a RS encoder. As an example, to maintain approximately the same overall code rate as the (31,5) simplex code, a (15,4) simplex code can be used as the inner code and a (15,9) RS code used as the outer code. This results in an overall code rate of 0.16 for the concatenated code, equal to 0.16 for the (31,5) simplex code. This RS code has the capacity to correct 3 symbol errors out of a group of 15 transmitted, where the symbols are the 4 bits output from the simplex decoder.

This code was simulated for a number of tone interferers located singly within channels of the target user's hopping sequence. Interleaving of codewords was not employed for the RS encoder, but 16 frequencies were used in the hopping sequence

to average out the effect of interferer positions on the simplex code performance. A bit energy to noise power density ratio of $E_b/N_0 = 17$ dB was assumed. The performance for 4 and 8 interferers is given in table C.2.

P_b	Number of interferers	
	4	8
linear	2.1×10^{-2}	5.2×10^{-3}
hard decision	1.6×10^{-3}	2.3×10^{-3}
normalizing	7.9×10^{-5}	1.7×10^{-3}

Table C.2: Bit error rates for various receivers, for a (15,4) simplex inner code and a (15,9) outer Reed-Solomon code.

Consider the performance of the (31,5) simplex code with a similar proportion of interferers to channels. For 16 interfered channels out of 32 (*cf* 8 out of 16), the bit error rate is typically around 2×10^{-3} for the normalizing receiver. For 8 interfered channels out of 32, the bit error rate is around 4×10^{-5}. The concatenated coding scheme therefore gives performance of the same order as the straight simplex code in this case.

However, more or less parity bits may be included in the RS code, thus giving different performance. Changing the amount of parity in the outer code leads to a different sequence period for the inner code as well as changing the number of channels available in the total bandwidth. As the probability of interferers appearing in the frequency channels being used varies with the change in parity, it becomes difficult to compare the effect of different code rates. Similarly, as the behaviour of the concatenated system is dependent on the burst error statistics of the inner code, simulation of each case is required.

It is possible to use the tone interferer model with the chip synchronous sequence assumption and random addressing to obtain an estimate of the performance of the concatenated scheme with the hard decision receiver for the inner simplex code. Let the inner simplex code be a (n, k) code, where $n = 2^k - 1$. The outer code

Number of Users at $P_b = 10^{-3}$	E_b/N_0 dB 15	20	30
$K = 5$	23	31	34
$K = 7$	26	38	43
$K = 9$	26	41	48
$K = 11$	22	40	48
$K = 13$	11	33	43

Table C.3: Bit error rate for the system with a $(15, 4)$ simplex inner code with hard decisions and a $(15, K)$ Reed-Solomon outer code.

is a Reed-Solomon code, with K information symbols and $N = 2^M - 1$ symbols per codeword. Then the distance of the Reed-Solomon code is $d = 2t + 1$, and it can correct $t = (n - k)/2$ errors. We consider the case where $n = N$ and $k = m$, and n k-bit words of decoded output bits of the simplex decoder are fed to the Reed-Solomon decoder to be decoded into K output words of k bits.

Given a symbol error rate P_s, the information bit error rate for hard decision decoding of the Reed-Solomon code is approximately given by [85]

$$P_b \approx \frac{n+1}{2n^2}\left[d\sum_{i=t+1}^{d}\binom{n}{i}P_s^i(1-P_s)^{n-i} + \sum_{i=d+1}^{n} i\binom{n}{i}P_s^i(1-P_s)^{n-i}\right] \qquad \text{(C.1)}$$

Now the symbol error rate is the codeword error rate P_w of the simplex code. This is given under the random addressing and chip synchronous assumption by equation 6.22. The chip error rate P_c is obtained by equation 6.21, with number of channels q given by $q = WC/R_b$ and $C = (k/n)(K/N)$is the overall code rate. The chip period is then $\tau = C/R_b$, and assuming that $n + 1$ channels are used to average out bad interferer patterns, the frame period $T = (n + 1)\tau$.

Using the above equations, the usage at $P_b = 10^{-3}$ may be evaluated for the inner $(15, 4)$ simplex code and the $(15, K)$ Reed-Solomon outer code. The results are shown in table C.3.

These results assume a random distribution of codeword errors from the inner

decoder, equivalent to infinite interleaving. As such, they represent the best performance that could be achieved for a given codeword error rate, but are in the same range as the results for the $(31, 5)$ simplex hard decision receiver. This offers the possibility of decreasing the number of channels from 32 to 16, with consequent savings in hardware.

As in the case of the orthogonal codes, an estimate of the codeword error rate for the normalizing receiver could be made in the vicinity of $P_w = 10^{-2}$ from the relative performance of the hard decision and normalizing receivers. However, this requires characterization of the performances of the receivers for the shorter code, as they may have a smaller differential in bit error rate than that found for the $(31, 5)$ simplex code. Therefore, no estimate is given here.

It is clear that further work is required to explore what improvements may be obtained from different choices of parameters. Similarly, half-rate convolutional codes are often used as inner codes in concatenated schemes. The promising results for the half-rate code with the normalizing and linear receivers in the previous section indicates that this scheme would also be worthy of further attention.

Bibliography

[1] R. C. Dixon. *Spread Spectrum Systems.* John Wiley, New York, 1976.

[2] William C. Jakes, Jr., editor. *Microwave Mobile Communications.* John Wiley, 1974.

[3] William C.Y. Lee. *Mobile Communications Engineering.* McGraw-Hill, New York, 1982.

[4] IEEE Vehicular Technology Society Committee on Radio Propagation. Coverage prediction for mobile radio systems operating in the 800/900 MHz frequency range. *IEEE Transactions on Vehicular Technology*, 37:3–72, February 1988.

[5] Donald C. Cox and Robert C. Leck. Correlation bandwidth and delay spread multipath propagation statistics for 910-MHz urban mobile radio channels. *IEEE Transactions on Communications*, COM-23(11):1271–1280, November 1975.

[6] Andreas Zogg. Multipath delay spread in a hilly region at 210 MHz. *IEEE Transactions on Communications*, VT-36(4):184–187, November 1987.

[7] R. H. Clarke. A statistical theory of mobile-radio reception. *Bell System Technical Journal*, 47:957–1000, July 1968.

[8] R.H. Moffett. Echo and delay problems in some digital communication systems. *IEEE Communications Magazine*, 25(8):41–47, 1987.

[9] George R. Cooper and Raymond W. Nettleton. A spread-spectrum technique for high capacity mobile radio systems. *IEEE Transactions on Vehicular Technology*, VT-27(4):264–275, November 1978.

[10] M.B. Pursley et al. Error probability for direct-sequence spread-spectrum multiple access communications – Part I: upper and lower bounds. *IEEE Transactions on Communications*, COM-30(5):975–984, May 1982.

[11] E.A. Geraniotis and M.B. Pursley. Error probability for direct-sequence spread-spectrum multiple access communications – Part II: approximations. *IEEE Transactions on Communications*, COM-30(5):985–995, May 1982.

[12] A. M. Brooks. Simulation of digital transmission on narrow-band mobile radio channels. In *IREECON International 85*, Institute of Radio and Electronic Engineers Australia, 1985.

[13] Jhong S. Lee and Leonard E. Miller. Error performance analyses of differential phase-shift-keyed/frequency-hopping spread-spectrum communication system in the partial-band jamming environments. *IEEE Transactions on Communications*, COM-30(5):943–952, May 1982.

[14] Jean-Louis Dornstetter and Didier Verhulst. Cellular efficiency with slow frequency hopping: analysis of the digital SFH900 mobile system. *IEEE Journal on Selected Areas in Communications*, SAC-5(5):835–848, June 1987.

[15] Rudolf Lidl and Harald Niederreiter. *Finite Fields.* Addison-Wesley, Reading, Mass., 1983.

[16] Thomas S. Seay. Hopping patterns for bounded mutual interference in frequency hopping multiple access. In *MILCOM '82*, pages 22.3–1–22.3–6, I.E.E.E., 1982.

[17] R.M. Mersereau and T.S. Seay. Multiple access frequency hopping patterns with low ambiguity. *IEEE Transactions on Aerospace and Electronic Systems*, AES-17(4):571–578, July 1981.

[18] D.V. Sarwate and M.B. Pursley. Hopping patterns for frequency-hopped multiple-access communication. In *International Conference on Communications ICC '78*, I.E.E.E., New York, June 1978.

[19] D.V. Sarwate and M.B. Pursley. New results on frequency hopping patterns for spread-spectrum multiple-access communications. In *International Conference on Communications ICC '80, Seattle*, I.E.E.E., New York, June 1980.

[20] G. Einarsson. Address assignment for a time-frequency-coded spread-spectrum system. *Bell System Technical Journal*, 59(7):1241–1255, September 1980.

[21] Alex W. Lam and Dilip V. Sarwate. Multiple user interference in FHMA-DPSK spread-spectrum communications. *IEEE Transactions on Communications*, COM-34(1):1–12, January 1986.

[22] B. G. Haskell. Computer simulation results on frequency hopped MFSK mobile radio - noiseless case. *IEEE Transactions on Communications*, COM-29(2):125–132, February 1981.

[23] On-Ching Yue. Performance of frequency-hopping multiple access multilevel FSK systems with hard-limited and linear combining. *IEEE Transactions on Communications*, COM-29(11):1687–1694, November 1981.

[24] Raymond W. Nettleton and George R. Cooper. Performance of a frequency-hopped differentially modulated spread-spectrum receiver in a Rayleigh fading channel. *IEEE Transactions on Vehicular Technology*, VT-30(1):14–28, February 1981.

[25] Paul S. Henry. Spectrum efficiency of a frequency-hopped-DPSK spread-spectrum mobile radio system. *IEEE Transactions on Vehicular Technology*, VT-28(4):327–332, November 1979.

[26] On-Ching Yue. Frequency hopping, multiple access, phase-shift-keying performance in a Rayleigh fading environment. *Bell System Technical Journal*, 59(6):861–879, July 1980.

[27] On-Ching Yue. Useful bounds on the performance of a spread-spectrum mobile communication system in various fading environments. In *International Conference on Communications ICC '80, Seattle*, pages 24.6.1–24.6.6, I.E.E.E., New York, June 1980.

[28] R.W. Lucky, J. Salz, and E.J. Weldon. *Principles of Data Communication.* McGraw-Hill, New York, 1968.

[29] On-Ching Yue. Saddle point approximation for the error probability in PAM systems with intersymbol interference. *IEEE Transactions on Communications*, COM-27(10):1604–1609, October 1979.

[30] J.J. Jones. Multichannel FSK and DPSK reception with three-component multipath. *IEEE Transactions on Communications Technology*, COM-16:808–821, December 1968.

[31] J.N. Pierce. Theoretical diversity improvement in frequency shift keying. *Proceedings of the IRE*, 48:903–910, May 1958.

[32] J.N. Pierce and S.Stein. Multiple diversity with nonindependent fading. *Proceedings of the IRE*, 48:89–104, January 1960.

[33] Seymour Stein. Unified analysis of certain coherent and noncoherent binary communications systems. *IEEE Transactions on Information Theory*, IT-10:43–51, January 1964.

[34] J. E. Mazo. Some theoretical observations on spread-spectrum communications. *Bell System Technical Journal*, 58(9):2013–2023, November 1979.

[35] On-Ching Yue. Hard-limited versus linear combining for frequency-hopping multiple-access systems in a Rayleigh fading environment. *IEEE Transactions on Vehicular Technology*, VT-30(1):10–14, February 1981.

[36] Masao Matsumoto and George R. Cooper. Multiple narrow band interferers in an FH-DPSK spread-spectrum communication system. *IEEE Transactions on Vehicular Technology*, VT-30(1):37–42, February 1981.

[37] Masao Matsumoto and George R. Cooper. Performance of a non-linear FH-DPSK spread spectrum receiver with multiple narrow-band interfering signals. *IEEE Transactions on Communications*, COM-30(5), May 1982.

[38] On-Ching Yue. Maximum likelihood combining for non-coherent and differentially coherent frequency-hopping multiple access systems. *IEEE Transactions on Information Theory*, IT-28(4):631–639, July 1982.

[39] Andrew J. Viterbi. A processing satellite transponder for multiple access by low-rate mobile users. In *Proceedings of the Fourth Digital Satellite Conference, Montreal, 1978*, I.E.E.E., New York, 1978.

[40] D. J. Goodman, P. S. Henry, and V. K. Prabhu. Frequency- hopped multilevel FSK for mobile radio. *Bell System Technical Journal*, 59(7):1257–1275, September 1980.

[41] U. Timor. Improved decoding scheme for frequency-hopped multilevel FSK system. *Bell System Technical Journal*, 59(10):1839–1855, December 1980.

[42] Uzi Timor. Multitone frequency-hopped MFSK system for mobile radio. *Bell System Technical Journal*, 61(10):3007–3016, December 1982.

[43] R. Agusti-Comes and G. Junyent-Giralt. Performance of FH-MFSK serial search synchroniser for mobile radio. *Electronics Letters*, 18(9):393–395, April 1982.

[44] Ramón Agustí and Gabriel Junyent. Performance of an FH multilevel FSK for mobile radio in an interference environment. *IEEE Transactions on Communications*, COM-31(6), June 1983.

[45] R. Agusti-Comes, F. Casadevall-Palacio, and G. Junyent-Giralt. Performance of FH-MFSK in the presence of non-synchronous users. *Electronics Letters*, 19(25/26):1077–1079, December 1983.

[46] Ramón Agusti. Multiple tone interferers in an FH-MFSK spread spectrum communication system. *IEEE Transactions on Vehicular Technology*, VT-34(3):136–140, August 1985.

[47] Tsun-Yee Yan and Charles C. Wang. Mathematical models for cochannel interference in FH-MFSK multiple-access systems. *IEEE Transactions on Communications*, COM-32(6):670–678, June 1984.

[48] Rushdi H. Muammar and Someshwar C. Gupta. Spectrum efficiency of a frequency-hopped MFSK spread-spectrum mobile radio system. *IEEE Transactions on Vehicular Technology*, VT-31(2):66–69, May 1982.

[49] Gaetan Niyonizeye, Michel Lecours, and Tuê H. Huynh. Mutual interferences in a binary FH-FSK spread spectrum system for mobile radio. *IEEE Transactions on Vehicular Technology*, VT-34(1):28–34, February 1985.

[50] Mitsuhiko Mizuno. Experimental investigation on the performance of FH-FSK in fading channels. In *Globecom '83 : IEEE Global Telecommunications Conference, San Diego, 1983*, I.E.E.E., New York, November 1983.

[51] L. Molnár and I. Vajda. Decoding error probability of the Einarsson-code for a frequency-hopped multiple access channel. *Problems of Control and Information Theory*, 13(2):109–120, 1984.

[52] Nguyen Quang. An approximate method for estimating the effect of shadow log-normal fading on the performance of frequency-hopped multiple level FSK systems. *Problems of Control and Information Theory*, 14(1):17–23, 1985.

[53] M. Schwartz, W.R. Bennett, and S. Stein. *Communications Systems and Techniques*, pages 395–403. McGraw-Hill, New York, 1966.

[54] D.J.G. Bakewell. Shadow fading induced capacity reduction for an idealized FFH/CDMA cellular mobile radio system. 1987.

[55] R. Viswanathan and S. C. Gupta. Burst error analysis of frequency-hopping systems for mobile communication. In *IEEE International Conference on Communications ICC '82, Philadelphia, 1982*, I.E.E.E., New York, June 1982.

[56] Said M. Elnoubi. Performance of frequency hopped MSK spread spectrum mobile radio system with differential detection. In *IEEE International Con-*

ference on Communications, ICC-82,Philadelphia, 1982, I.E.E.E., New York, June 1982.

[57] Kenkichi Hirade et al. Error-rate performance of digital FM with differential detection in land mobile radio channels. *IEEE Transactions on Vehicular Technology*, VT-28(3):204–212, August 1979.

[58] H. B. Voelcker. Phase-shift keying in fading channels. *IEE Proceedings*, B 107:31–38, January 1960.

[59] K.S. Miller. *Multidimensional Gaussian Distributions*, page 42. Wiley, New York, 1964.

[60] I.S. Gradshteyn and I.M. Rhyzic. *Table of Series, Integrals and Products.* Academic Press, New York, 1980.

[61] Michel Jeruchim. Techniques for estimating the bit error rate in the simulation of digital communications systems. *IEEE Journal on Selected Areas in Communications*, SAC-2(1):153–170, January 1984.

[62] *IMSL Library Reference Manual.* IMSL Inc., ninth edition, 1982.

[63] Milton Abramowitz and Irene Stegun, editors. *Handbook of Mathematical Functions*, chapter 26. Dover Publications, ninth edition, 1972.

[64] Stephen K. Park and Keith W. Miller. Random number generators: good ones are hard to find. *Communications of the ACM*, 31(10):1192–1201, October 1988.

[65] M.F. Ibrahim and J.D. Parsons. Signal strength prediction in built-up areas, Parts 1 and 2. *IEE Proceedings*, 130 Part F(5):377–391, August 1983.

[66] Tor Aulin. A modified model for the fading signal at a mobile radio channel. *IEEE Transactions on Vehicular Technology*, VT-28(3):182–203, August 1979.

[67] J. D. Parsons. Propagation and interference in cellular radio systems. In *IERE International Conference on Land Mobile Radio*, I.E.E., September 1979.

[68] B.R. Davis and R.E. Bogner. Propagation at 500 MHz for mobile radio. *Australian Telecommunications Review*, 18(1):13–32, 1984.

[69] Homayoun Hashemi. Simulation of the urban radio propagation channel. *IEEE Transactions on Vehicular Technology*, VT-28(3):213–225, August 1979.

[70] A.S. Bajwa. UHF wideband statistical model and simulation of mobile radio multipath propagation effects. *IEE Proceedings*, 132 Part F(5):327–333, August 1985.

[71] K.J. Gladstone and J.P. McGeehan. Computer simulation of multipath fading in the land mobile environment. *IEE Proceedings*, 127 Part G(6):323–330, December 1980.

[72] B.R. Davis. *A Fading Simulator.* Technical Report 3/75, Department of Electrical Engineering, University of Adelaide, Adelaide, South Australia, 1975.

[73] J. H. Park. On binary DPSK detection. *IEEE Transactions on Communications*, COM-26(4), April 1978.

[74] Kenji Yamada and Kazuhiro Daikoku. Error performance of frequency-hopped D.P.S.K. system. *Electronics Letters*, 16(8):305–306, April 1980.

[75] A.J. Viterbi and J.K. Omura. *Principles of Digital Communication and Coding.* McGraw-Hill Kogokusha, Tokyo, 1979.

[76] Mitsuhiko Mizuno. Randomization effect of errors by means of frequency-hopping techniques in a fading channel. *IEEE Transactions on Communications*, COM-30:1052–1056, May 1982.

[77] R. Viswanathan and S. C. Gupta. Adjacent cell interference in FH-MFSK cellular mobile radio system. *IEEE Transactions on Vehicular Technology*, VT-32(2):191–200, May 1983.

[78] J. M. Wozencraft and I. M. Jacobs. *Principles of Communication Engineering.* John Wiley, New York, 1965.

[79] Ke Rang Wu et al. Error rate performance of binary DPSK system with multiple co-channel interference in land mobile radio channels. *IEEE Transactions on Vehicular Technology*, VT-33(1):23–31, February 1984.

[80] J.L. Sevy. The effect of limiting on a biphase or quadriphase signal plus interference. *IEEE Transactions on Aerospace and Electronic Systems*, AES-5:387–395, May 1969.

[81] A.J. Viterbi. Spread spectrum communications: myths and realities. *IEEE Communications Society Magazine*, 17(3):11–18, May 1979.

[82] S. Lin and D.J. Costello Jnr. *Error Control Coding: Fundamentals and Applications.* Prentice-Hall, Englewood Cliffs, N.J., 1983.

[83] G.C. Clark and J.B. Cain. *Error Correction Coding for Digital Communications.* Plenum Press, New York, 1981.

[84] I. Morrison. *A System for Burst Error Control in Communications.* Master's thesis, South Australian Institute of Technology, 1986.

[85] Don J. Torrieri. The information-bit error rate for block codes. *IEEE Transactions on Communications*, COM-32(4):474–476, April 1984.

[86] On-Ching Yue. Spread spectrum mobile radio, 1977-1982. *IEEE Transactions on Vehicular Technology*, VT-32(1):98–105, February 1983.

[87] Marvin K. Simon, Jim K. Omura, Robert A. Scholtz, and Barry K. Levitt. *Spread Spectrum Communications, Vols I–III.* Computer Science Press, Rockville, Maryland U.S.A., 1985.

Publications.

Simon Rockliff. "Performance Modelling of a Frequency Hopping Mobile Radio System", In *Proceedings of Australian Symposium on Signal Processing and Applications, 17-19 April 1989*, I.E.E.E., Adelaide, Australia, April 1989.

Simon Rockliff. "Coding for a Frequency Hopping DPSK Mobile Radio System", In *Proceedings of IREECON International 1989*, Melbourne, Institute of Radio and Electronic Engineers Australia, September 1989.